

Copyright

by

Sungjin Bae

2005

**The Dissertation Committee for Sungjin Bae certifies that this is the approved  
version of the following dissertation:**

**SEISMIC PERFORMANCE OF  
FULL-SCALE REINFORCED CONCRETE COLUMNS**

**Committee:**

---

**Oguzhan Bayrak, Supervisor**

---

**James O. Jirsa**

---

**Sharon L. Wood**

---

**Eric Williamson**

---

**Eric B. Becker**

**SEISMIC PERFORMANCE OF  
FULL-SCALE REINFORCED CONCRETE COLUMNS**

by

**Sungjin Bae, B.S., M.S.**

**Dissertation**

Presented to the Faculty of the Graduate School of

The University of Texas at Austin

in Partial Fulfillment

of the Requirements

for the Degree of

**Doctor of Philosophy**

The University of Texas at Austin

December, 2005

**To My Family**

## **Acknowledgements**

The research program presented in this dissertation was carried out at the Phil M. Ferguson Structural Engineering Laboratory at the University of Texas at Austin. I would like to express my most sincere gratitude to Dr. Oguzhan Bayrak for his guidance, support, patience, and encouragement during the course of this research. I would like to thank Dr. James O. Jirsa, Dr. Sharon Wood, Dr. Eric Williamson and Dr. Eric B. Becker for serving on my dissertation committee.

I thank for the devoted effort made by the staff (Mike Bell, Dennis Phillip, Blake Stasney, Eric Schell and Mike Wason) of the Phil M. Ferguson Structural Engineering Laboratory over the years. I would also like to thank the students who worked on the project with me. The work of Alvaro Palma Diaz, Brandon McBee, Eric Methvin and Will Slaughter helped to make this dissertation possible.

This dissertation is dedicated to my family, especially to my wife, Seyoung Lee, for her great support and encouragement. Finally, I also want to thank God for seeing me through.

Austin, Texas, December 2005

Sungjin Bae

# **SEISMIC PERFORMANCE OF FULL-SCALE REINFORCED CONCRETE COLUMNS**

Publication No. \_\_\_\_\_

Sungjin Bae, Ph.D.

The University of Texas at Austin, 2005

Supervisor: Oguzhan Bayrak

The deformation capacity of a concrete column can be expressed by using different ductility parameters such as curvature ductility, displacement ductility or drift capacity. However, little research has been conducted into the relationship among different ductility parameters. The objectives of this research are (1) to investigate the relationship among various ductility parameters by considering the effects of shear span-to-depth ratio and axial load level and (2) to develop methods and procedures that can be used to estimate the deformation capacity of reinforced concrete columns.

Five full-scale reinforced concrete columns were tested at The University of Texas at Austin. Test results indicated that the shear span-to-depth ratio and axial load level were important parameters influencing the relationship among various ductility parameters. Measured plastic hinge lengths of column specimens were also affected by the shear span-to-depth ratio and axial load.

The plastic hinge length of concrete columns was investigated by studying the compressive strain profile of the core concrete. An analytical procedure was used to study

the effect of various parameters on plastic hinge length. Based on the results of the experiments and a parametric study, a new expression that can be used to estimate plastic hinge lengths was proposed.

Two methods that can be used to predict the deformation capacity of reinforced concrete columns were developed. One of these methods can be considered as a state-of-the-art analytical method, which employs various phenomenological models for confinement of concrete, reinforcing bar buckling, reinforcing bar slip and shear deformations. The other method consists of simple expressions derived by studying the lateral load response of columns as influenced by the  $P$ - $\Delta$  effect. The use of the rigorous analytical method provided reasonably accurate estimates for the deformation capacity of over one hundred columns tested by various researchers. The use of simple expressions, on the other hand, traced the lower-bound of the measured drift capacities of these columns. The simple expression is recommended for use in performance-based design of reinforced concrete columns.

## Table of Contents

<b>List of Tables .....</b>	<b>xiv</b>
<b>List of Figures.....</b>	<b>xv</b>
<b>CHAPTER 1 INTRODUCTION.....</b>	<b>1</b>
1.1    Background.....	1
1.2    Problem.....	2
1.3    Research Objectives and Summary .....	5
1.4    Thesis Organization .....	6
<b>CHAPTER 2 REVIEW OF CODE PROVISIONS AND LITERATURE.....</b>	<b>8</b>
2.1    Introduction.....	8
2.2    Code Provisions for Confining Reinforcement Design .....	8
2.2.1    Effect of Confining Reinforcement on Concrete .....	8
2.2.2    ACI 318.....	10
2.2.3    NZS 3101 .....	12
2.2.4    ATC-32 .....	15
2.3    Performance-Based Design Procedures.....	17
2.3.1    Watson et al. (1994).....	17
2.3.2    Wehbe, Saiidi and Sanders (1997).....	18
2.3.3    Sheikh and Khoury (1997).....	19
2.3.4    Saatcioglu and Razvi (2002).....	20
2.4    Confining Reinforcement: Codes and Performance-Based Design Procedures.....	22
2.4.1    Relationship among Various Deformation Capacity Parameters .....	24
2.5    Review of Literature: Simulated Seismic Tests on Columns .....	26
2.5.1    Park, Priestley and Gill (1982).....	26
2.5.2    Watson and Park (1994).....	29

2.5.3	Tanaka and Park (1990).....	31
2.5.4	Azizinamini, Corley and Johal (1992).....	34
2.5.5	Saatcioglu and Ozcebe (1987, 1989) .....	36
2.5.6	Zahn, Park, and Priestley (1986).....	38
2.5.7	Sheikh and Khoury (1993, 1994).....	40
2.5.8	Bayrak and Sheikh (1997, 1999) .....	41
2.6	Examination of Previous Experimental Research.....	43
<b>CHAPTER 3</b>	<b>EXPERIMENTAL PROGRAM .....</b>	<b>45</b>
3.1	Introduction.....	45
3.2	Material Properties of Column Specimens .....	45
3.2.1	Steel.....	45
3.2.2	Concrete .....	48
3.3	Specimens .....	49
3.4	Construction of Column Specimens .....	51
3.4.1	Formwork.....	52
3.4.2	Instrumentation of Reinforcing Bars .....	53
3.4.3	Reinforcing Cages.....	55
3.4.4	Casting and Curing .....	56
3.5	Instrumentation of the Specimens.....	57
3.6	Test Setup.....	61
3.7	Testing.....	64
3.8	Summary .....	64
<b>CHAPTER 4</b>	<b>TEST RESULTS.....</b>	<b>66</b>
4.1	Introduction.....	66
4.2	Test Observations.....	66
4.3	Analysis of Test Data.....	76
4.3.1	Response of Specimens.....	78

4.3.2 Backbone Curves .....	89
4.3.3 Definitions of Ductility Parameters .....	94
4.3.3.1 Curvature and Displacement Ductility Factors .....	94
4.3.3.2 Cumulative Curvature and Displacement Ductility Ratios.....	94
4.3.3.3 Damage Indicators.....	96
4.4 Discussion of Test Results .....	101
4.4.1 Shear Span-to-Depth Ratio ( $L/h$ ) .....	101
4.4.2 Axial Load Level .....	102
4.4.3 Plastic Hinge Length.....	104
4.5 Summary .....	106
<b>CHAPTER 5 PLASTIC HINGE LENGTH .....</b>	<b>108</b>
5.1 Introduction.....	108
5.2 Plastic Hinge Length.....	109
5.3 Previous Research.....	111
5.3.1 Baker (1956) .....	111
5.3.2 Mattock (1964).....	113
5.3.3 Corley (1966).....	115
5.3.4 Mattock (1967).....	115
5.3.5 Park, Priestley and Gill (1982).....	116
5.3.6 Sakai and Sheikh (1989) .....	117
5.3.7 Sheikh (1993, 1994 and 1998).....	117
5.3.8 Mendis (2001).....	117
5.4 Discussion on Previous Research .....	118
5.4.1 Discussion of Current Test Results.....	120
5.5 Plastic Hinge Length: Analytical Approach .....	125
5.5.1 Compressive Strain Profile of Core Concrete.....	125
5.6 Parametric Study on Plastic Hinge Length .....	130
5.6.1 Axial Load Level ( $P/P_o$ ) .....	131

5.6.2	Shear Span-to-Depth Ratio ( $L/h$ ) .....	134
5.6.3	Amount of Longitudinal Reinforcement ( $\rho_l = A_s/A_g$ ) .....	135
5.7	Plastic Hinge Length: A New Expression .....	138
5.8	Plastic Hinge Length: Estimations And Experiments.....	140
5.9	Summary .....	147
<b>CHAPTER 6</b>	<b>BUCKLING BEHAVIOR OF REINFORCING BARS.....</b>	<b>148</b>
6.1	Introduction.....	148
6.2	Buckling Behavior of Longitudinal Reinforcement .....	150
6.3	Experimental Program (Miseses 2002) .....	151
6.4	Proposed Inelastic Buckling Model .....	159
6.4.1	Axial Strain due to Axial Stress.....	161
6.4.2	Axial Strain due to Transverse Deformation .....	163
6.4.2.1	The relationship between axial stress and transverse displacement .....	164
6.4.2.2	The relationship between transverse displacement and axial strain .....	167
6.4.3	Reinforcing Bar Buckling Model: Summary .....	169
6.5	Buckling Length of Longitudinal Reinforcing Bars .....	174
6.5.1	Tie Stiffness ( $k_t$ ).....	175
6.5.2	Required Tie Stiffness ( $k_n$ ) .....	176
6.6	Application of Reinforcing Bar Buckling Model .....	179
6.7	Summary .....	182
<b>CHAPTER 7</b>	<b>DRIFT CAPACITY .....</b>	<b>183</b>
7.1	Introduction.....	183
7.2	Analytical Method .....	186
7.2.1	Flexural Deformations .....	186
7.2.2	Reinforcing Bar Slip .....	187

7.2.3	Shear Deformations .....	188
7.2.4	Lateral Displacement due to P-Δ Effect.....	189
7.2.5	Confined Concrete .....	190
7.2.6	Reinforcing Bars .....	195
7.2.7	Verification of Proposed Analytical Method.....	196
7.2.8	Accuracy of Drift Capacity Estimations .....	198
7.3	Estimation of Drift Capacity: A Simple Method .....	203
7.3.1	Displacement Capacity .....	205
7.3.2	Drift Capacity.....	209
7.3.3	Displacement Ductility .....	210
7.3.4	Deformation Capacity of Columns .....	211
7.3.5	Drift Capacity Estimation: Simplified and Sophisticated Analyses ..	212
7.3.6	Comparison with Column Test Database .....	214
7.3.7	Design Recommendations .....	220
7.4	Summary .....	222
<b>CHAPTER 8</b>	<b>SUMMARY, CONCLUSIONS, AND RECOMMENDATIONS .....</b>	<b>224</b>
8.1	Summary .....	224
8.2	Conclusions.....	225
8.3	Recommendations for Future Study .....	228
<b>APPENDIX A</b>	<b>TEST FRAME .....</b>	<b>230</b>
A.1	Design Considerations .....	230
<b>APPENDIX B</b>	<b>ESTIMATION OF PLASTIC HINGE LENGTH: EXAMPLE .....</b>	<b>242</b>
B.1	Introduction.....	242
B.2	Step (1): Construction of Moment-Curvature Relationship.....	244
B.3	Steps (2) - (3): Construction of Moment and Strain Diagrams along Column Height.....	246

B.4 Steps (4) - (5): Estimation of Location along Column Height Corresponding to Yield Strain of Reinforcing Bar and Plastic Hinge Length .....	247
<b>APPENDIX C COMPUTER PROGRAM SOURCE .....</b>	<b>248</b>
<b>APPENDIX D ANALYTICAL METHOD TO ESTIMATE COLUMN BEHAVIOR: EXAMPLE.....</b>	<b>295</b>
D.1 Introduction.....	295
D.2 Sectional Analysis.....	295
D.3 Analysis of Member Behavior.....	298
<b>APPENDIX E ESTIMATION OF DRIFT CAPACITY: EXAMPLE .....</b>	<b>299</b>
E.1 Application of Equation (7.27) .....	299
<b>REFERENCES.....</b>	<b>302</b>
<b>VITA.....</b>	<b>312</b>

## List of Tables

Table 2.1	Details of Column Specimens (Park et al. 1982).....	28
Table 2.2	Details of Column Specimens (Watson and Park 1994).....	30
Table 2.3	Details of Column Specimens (Tanaka and Park 1990).....	33
Table 2.4	Details of Column Specimens (Azizinamini et al. 1992) .....	35
Table 2.5	Details of Column Specimens (Saatcioglu and Ozcebe 1987, 1989) .....	37
Table 2.6	Details of Column Specimens (Zahn et al. 1986).....	39
Table 2.7	Details of Specimens (Sheikh and Khoury 1993, 1994).....	41
Table 2.8	Details of Specimens (Bayrak and Sheikh 1997, 1999) .....	42
Table 3.1	Material Properties of Reinforcing Steel .....	48
Table 3.2	Concrete Strengths .....	49
Table 3.3	Details of Test Specimens.....	51
Table 4.1	Ductility Parameters of Specimens .....	93
Table 4.2	Section Ductility Parameters.....	100
Table 4.3	Member Ductility Parameters .....	100
Table 4.4	Plastic Hinge Length: Experiments and Estimations.....	105
Table 5.1	Predicted Plastic Hinge Lengths .....	141
Table 6.1	Tensile Properties of Reinforcing Bar Specimens (Mises 2002) .....	151
Table 6.2	Required Spring Stiffness for Different Buckling Modes .....	179
Table 7.1	Summary of Test Specimens .....	185
Table 7.2	Recommended Axial Load Levels for Various Shear Span-to-Depth Ratios .....	221
Table E.1	Factored Axial Load for Column C1 .....	300

## List of Figures

Figure 1.1	Reinforced Concrete Column Tests .....	5
Figure 2.1	Comparison of Design Codes and Performance-Based Design Procedures.....	23
Figure 2.2	Relationship between Curvature and Displacement Ductilities (Park and Paulay 1975) .....	25
Figure 2.3	Behavior of Reinforced Concrete Column .....	25
Figure 2.4	Details of Transverse Reinforcement (Park et al. 1982).....	27
Figure 2.5	Test Setup.....	28
Figure 2.6	Details of Transverse Reinforcement (Tanaka and Park 1990).....	32
Figure 2.7	Details of Transverse Reinforcement (Azizinamini et al. 1992) .....	35
Figure 2.8	Details of Transverse Reinforcement (Saatcioglu and Ozcebe 1987, 1989) .....	37
Figure 2.9	Details of Transverse Reinforcement (Zahn et al. 1986).....	39
Figure 2.10	Details of Transverse Reinforcement (Baryak and Sheikh 1997, 1999) .....	41
Figure 3.1	Stress-Stain Curves for Longitudinal Reinforcing Steel.....	47
Figure 3.2	Stress-Stain Curves for Transverse Reinforcing Steel.....	47
Figure 3.3	Modeling of Column Specimen .....	50
Figure 3.4	Layout of Test Specimens.....	50
Figure 3.5	Nomenclature for Column Specimens .....	51
Figure 3.6	Formwork before Concrete Casting.....	53
Figure 3.7	Location of Strain Gauges .....	54
Figure 3.8	Construction of Column Cage .....	56
Figure 3.9	Locations of Linear Potentiometers, String Potentiometers and Inclinometers.....	58

Figure 3.10 Installation of Linear Potentiometers.....	59
Figure 3.11 Installation of Inclinometers .....	60
Figure 3.12 Test Setup.....	62
Figure 3.13 Specimen Installation.....	63
Figure 3.14 Typical Lateral Displacement History .....	65
Figure 3.15 Definition of Yield Displacement.....	65
Figure 4.1 Specimen S24-1UT .....	67
Figure 4.2 Specimen S24-2UT .....	68
Figure 4.3 Specimen S17-3UT.....	69
Figure 4.4 Specimen S24-4UT .....	70
Figure 4.5 Specimen S24-5UT .....	71
Figure 4.6 Comparison of Failure of All Test Specimens.....	72
Figure 4.7 Hook Length of Transverse Reinforcement Required by Chapter 21 of ACI 318-05 .....	75
Figure 4.8 Opening of Hoops in Specimen S24-1UT .....	75
Figure 4.9 Applied Loads and Deflected Shape of Test Specimen.....	77
Figure 4.10 Lateral Load versus Drift Behavior of Specimen S24-1UT .....	80
Figure 4.11 Lateral Load versus Drift Behavior of Specimen S24-2UT .....	81
Figure 4.12 Lateral Load versus Drift Behavior of Specimen S17-3UT .....	82
Figure 4.13 Lateral Load versus Drift Behavior of Specimen S24-4UT .....	83
Figure 4.14 Lateral Load versus Drift Behavior of Specimen S24-5UT .....	84
Figure 4.15 Moment versus Curvature Behavior of Specimen S24-2UT .....	85
Figure 4.16 Moment versus Curvature Behavior of Specimen S17-3UT .....	86
Figure 4.17 Moment versus Curvature Behavior of Specimen S24-4UT .....	87

Figure 4.18	Moment versus Curvature Behavior of Specimen S24-5UT .....	88
Figure 4.19	Backbone Curves for Moment-Curvature Relationship .....	90
Figure 4.20	Backbone Curves for Lateral Load-Drift Relationship.....	91
Figure 4.21	Normalized Moment-Curvature Backbone Curves .....	92
Figure 4.22	Normalized Lateral Load-Displacement Backbone Curves .....	92
Figure 4.23	Normalized Lateral Load-Drift Backbone Curves.....	93
Figure 4.24	Definitions of Section Ductility Parameters .....	95
Figure 4.25	Definitions of Member Ductility Parameters.....	95
Figure 4.26	Cumulative Ductility Ratios .....	99
Figure 4.27	Damage Indicators .....	99
Figure 4.28	Definition of Plastic Hinge Length (Park and Paulay 1975) .....	104
Figure 5.1	Typical Test Specimens (Baker 1956).....	112
Figure 5.2	Test Beam Specimens (Mattock 1964).....	114
Figure 5.3	Effects of Various Parameters on Plastic Hinge Lengths (Sakai and Sheikh 1989) .....	118
Figure 5.4	Comparison of Various Plastic Hinge Length Estimates.....	120
Figure 5.5	Strain Distribution in Outer Hoops .....	122
Figure 5.6	Strain Distribution in Inner Hoops.....	123
Figure 5.7	Normalized Moment-Curvature Backbone Curves .....	124
Figure 5.8	Normalized Lateral Load-Displacement Backbone Curves .....	124
Figure 5.9	Estimation of Plastic Hinge Length (S24-2UT).....	128
Figure 5.10	Estimated Plastic Hinge Lengths of Tested Column Specimens .....	130
Figure 5.11	Effect of Axial Load on Curvature and Compressive Strain Profiles.....	133
Figure 5.12	Relationship between Plastic Hinge Length and Axial Load .....	133

Figure 5.13 Relationship between Plastic Hinge Length and Shear Span-to-Depth Ratio.....	135
Figure 5.14 Effects of Longitudinal Reinforcement Ratio on Curvature and Compressive Strain Profiles.....	137
Figure 5.15 Effect of Amount of Longitudinal Reinforcement .....	138
Figure 5.16 Plastic Hinge Length: Equation (5.11) versus Analysis .....	139
Figure 5.17 Comparison of Predicted Responses from Various Plastic Hinge Estimations (S24-2UT) .....	143
Figure 5.18 Comparison of Predicted Responses from Various Plastic Hinge Estimations (S17-3UT) .....	144
Figure 5.19 Comparison of Predicted Responses from Various Plastic Hinge Estimations (S24-4UT) .....	145
Figure 5.20 Comparison of Predicted Responses from Various Plastic Hinge Estimations (S24-5UT) .....	146
Figure 6.1 Longitudinal Bar Buckling in Specimen S24-4UT.....	149
Figure 6.2 Buckling Behavior of Bars.....	150
Figure 6.3 Reinforcing Bar Specimen.....	153
Figure 6.4 Test Setup .....	153
Figure 6.5 Stress-Strain Curves of No. 8 Bars (Mieses 2002) .....	155
Figure 6.6 Stress-Strain Curves of No. 10 Bars (Mieses 2002) .....	156
Figure 6.7 Stress-Transverse Displacement Curves of No. 8 Bars (Mieses 2002) .....	157
Figure 6.8 Stress-Transverse Displacement Curves of No. 10 Bars (Mieses 2002) ..	158
Figure 6.9 Deflected Shape of a Reinforcing Bar .....	160
Figure 6.10 Comparison of Stress-Strain Curves for Reinforcing Steel .....	163
Figure 6.11 Axial Stress-Transverse Displacement Estimations .....	165
Figure 6.12 Proposed Model for Axial Stress-Transverse Displacement Response.....	166

Figure 6.13 Proposed Model for Axial Strain-Transverse Displacement Response .....	168
Figure 6.14 Axial Strain-Transverse Displacement Estimations .....	169
Figure 6.15 Analysis of Buckling Response of Bar .....	172
Figure 6.16 Axial Stress-Axial Strain Estimations .....	173
Figure 6.17 Buckling Length of Reinforcing Bars (Dhakal and Maekawa 2002) .....	174
Figure 6.18 Values of $n_b$ and $n_l$ for Typical Reinforcement Arrangements (Dhakal and Maekawa 2002).....	176
Figure 6.19 Estimation of Buckling Length (Dhakal and Maekawa 2002) .....	177
Figure 6.20 Effect of Inclusion of Buckling Behavior on Column Response.....	181
Figure 7.1 Effect of P- $\Delta$ Effect on Column Behavior .....	190
Figure 7.2 Stress-Strain Relationship of Confined Concrete (Razvi and Saatcioglu 1999) .....	194
Figure 7.3 Analytical Procedure.....	197
Figure 7.4 Model Verification.....	199
Figure 7.5 Lateral Load Response: Estimations and Experiments.....	200
Figure 7.6 Sources of Errors in Estimating Deformation Capacity .....	201
Figure 7.7 Lateral Load Response of Reinforced Concrete Columns.....	204
Figure 7.8 Influence of P- $\Delta$ Effect on Lateral Load Response .....	206
Figure 7.9 Effect of Axial Load on Displacement Capacity .....	208
Figure 7.10 Effect of Axial Load on Drift Capacity .....	210
Figure 7.11 Comparison of Estimated Drift Capacities .....	213
Figure 7.12 Comparison with Test Results .....	217
Figure 7.13 Comparison with Test Results ( $A_{sh} \geq A_{sh,ACI}$ ).....	218
Figure 7.14 Comparison with Test Results ( $A_{sh} < A_{sh,ACI}$ ) .....	219

Figure 7.15	Interaction among Drift Capacity, Axial Load and Shear Span-to-Depth Ratio.....	221
Figure A.1	Details and Dimensions of Test Setup.....	231
Figure A.2	Detail of W27×94 Beam .....	232
Figure A.3	Details of Clevis.....	233
Figure A.4	Details of Clevis.....	234
Figure A.5	Details of 3 in. Plate Ear .....	235
Figure A.6	Details of 4 in. Plate Ear .....	236
Figure A.7	Details of Bottom Plate.....	237
Figure A.8	Details of Pin.....	238
Figure A.9	Details of Top Plate .....	239
Figure A.10	Details of Pin Retainer.....	240
Figure A.11	Details of Nylon Spacer .....	241
Figure B.1	Estimation of Plastic Hinge Length: Specimen S24-2UT .....	244
Figure B.2	Details of Column S24-2UT .....	245
Figure B.3	Moment-Curvature Relationship .....	245
Figure B.4	Moment-Compressive Strain Relationship .....	246
Figure B.5	Construction of Moment Diagram and Strain Profile.....	247
Figure D.1	Constitutive Models used for Sectional Analysis .....	296
Figure D.2	Concrete Stress-Strain Relationships (Razvi and Saatcioglu 1999) .....	296
Figure D.3	Stress-Strain Relationship for Longitudinal Reinforcement.....	297
Figure D.4	Moment-Curvature Relationship of Specimen S24-2UT .....	297
Figure D.5	Lateral Load-Displacement Relationship of Specimen S24-2UT .....	298
Figure E.1	Configuration of Example Building.....	299

Figure E.2 Column Details .....	300
Figure E.3 P-M Interaction Curve .....	301
Figure E.4 Drift Capacity-Axial Load Curve .....	301

# CHAPTER 1

## INTRODUCTION

### 1.1 BACKGROUND

It is generally uneconomical to design structures to withstand lateral forces elastically for severe, infrequent earthquakes. An alternative and widely accepted approach is to design structures for a lower force level and detail them to have sufficient energy dissipation capacity to prevent collapse. To ensure a large energy dissipation capacity, it is more desirable to have plastic hinges in the beams than in the columns. The formation of hinges in columns is undesirable, as this may result in the formation of a weak story mechanism. In addition, such mechanisms also result in local damage to critical gravity load bearing elements.

For this reason, most seismic design codes attempt to ensure having hinges in the beams rather than the columns. However, from a practical standpoint, it is not possible to prevent the formation of plastic hinges in the first-story columns of a multistory structure during a strong earthquake. Moreover, recent earthquakes (Northridge 1994; Kobe 1995) and analytical investigations (Mitchell and Paultre 1994; Bayrak 1995) show that the formation of plastic hinges in columns of a framed structure at locations other than the first-story is still possible as a result of higher mode effects. Therefore, columns have to be detailed to accommodate the formation of plastic hinges in order to ensure satisfactory behavior during strong ground motions.

During the last two decades, the deformation capacity of columns has been studied by many researchers to investigate the effect of the amount, arrangement and spacing of confining reinforcement in plastic hinge regions. As a result, many performance-based design procedures (Watson and Park 1994; Wehbe et al. 1997;

(Sheikh and Khoury 1997; Bayrak and Sheikh 1998; Saatcioglu and Razvi 2002) for confining reinforcement in concrete columns have been introduced. Various parameters, such as curvature ductility, displacement ductility, or drift, have been used to define the deformation capacity of a column in these performance-based design procedures. However, the relationship among the parameters to define deformation capacity of a column has not yet been fully studied. It is therefore imperative to investigate the relationship among various parameters to comparatively evaluate these performance-based design procedures.

## 1.2 PROBLEM

As a reinforced concrete column experiences large lateral displacements under cyclic loads while supporting gravity load, severe damage occurs at regions where large inelastic curvatures are observed. The severely damaged region is called the plastic hinge region. Since the inelastic flexural deformations are concentrated in the plastic hinge region, a large curvature capacity is required in this region to withstand large lateral displacement demands.

Based on this, the behavior of concrete columns is commonly analyzed at two different levels: (1) sectional-level behavior, which is a local column response at the plastic hinge region where the inelastic flexural deformations are concentrated, and (2) member-level behavior, which is an overall column response. Similarly, the deformation capacity of a column can also be categorized into two levels: (1) sectional-level deformation capacity, which is commonly expressed as curvature or curvature ductility and (2) member-level deformation capacity, expressed as displacement, displacement ductility, or drift. Therefore, an investigation of the transformation from the sectional-level deformation capacity to the member-level deformation capacity is essential in order to understand the behavior of concrete columns as a whole.

Park and Paulay (1975) derived a relationship between curvature ductility and displacement ductility, as shown in Equation (1.1). This equation indicates that there is a linear relationship between curvature and displacement ductilities of columns. It can be also observed that the plastic hinge length ( $l_p$ ) and the height of a column ( $L$ ) are two important factors influencing this relationship.

$$\mu_\Delta = 1 + 3(\mu_\phi - 1) \frac{l_p}{L} \left( 1 - 0.5 \frac{l_p}{L} \right) \quad (1.1)$$

where

$\mu_\Delta$  = displacement ductility

$\mu_\phi$  = curvature ductility

$l_p$  = equivalent plastic hinge length

$L$  = height of a cantilever column

According to Equation (1.1), the displacement ductility can be improved proportionally with curvature ductility regardless of the level of axial load or the shear span-to-depth ratio of a column. Improving the curvature ductility, in turn, will require increasing the amount of confining reinforcement with proper details. Hence, Equation (1.1) implies that adjusting the amount of confining reinforcement is an efficient way to control both the sectional and member performances of concrete columns. This idea has been widely adopted by most current design codes (ACI 318-05; NZS 3101:1995; ATC-32) and by performance-based design procedures (Watson and Park 1994; Wehbe et al. 1997; Sheikh and Khoury 1997; Bayrak and Sheikh 1998; Saatcioglu and Razvi 2002).

However, Park and Paulay did not consider the effect of axial load in deriving Equation (1.1). Furthermore, little experimental research has been conducted to investigate this relationship. Therefore, an investigation of the

effects of the axial load on the behavior of concrete columns and on the relationship among various deformation capacity parameters is needed.

Analytical methods are frequently used to estimate these deformation capacity parameters. Although these analytical methods have been used in seismic design/evaluation, little research has been done to examine the accuracy of such methods in predicting the deformation capacity parameters of concrete columns. To investigate the accuracy of analytical methods, a state-of-the-art analytical method is developed, which includes a new plastic hinge length expression and a new bar buckling model. A large number of concrete column test results obtained from the UW/PEER column database (<http://maximus.ce.washington.edu/~peera1/>) are used for model verification purposes.

Figure 1.1 shows the section sizes of all concrete columns from the UW/PEER column database. A total of 244 column tests reported in the literature are collected. It can be observed that most of the column specimens obtained from the UW/PEER column database have section sizes between 4 in. and 16 in. There are only a few tests conducted on large-scale concrete columns ( $h \geq 16$  in., where  $h$  is the overall depth or the section size of a concrete column). In order to address this issue, large-scale concrete column specimens with overall column depths of 17.25 in. and 24 in., were constructed and tested under constant axial loads and reversed cyclic lateral displacement excursions in this investigation. Based on the test results, the effects of shear span-to-depth ratio ( $L/h$ , where  $L$  = height of a cantilever column and  $h$  = overall depth of a column), axial load level ( $P/P_o$ , where  $P$  = applied axial compressive force and  $P_o = 0.85f'_cA_g + A_s f_{yl}$  = nominal axial load strength at zero eccentricity), amount of confining reinforcement ( $A_{sh}$ ), and plastic hinge length ( $l_p$ ) on each deformation capacity parameter are studied.

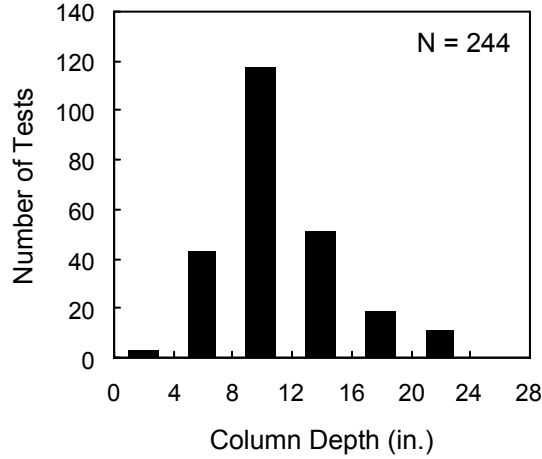


**Figure 1.1 Reinforced Concrete Column Tests**

### 1.3 RESEARCH OBJECTIVES AND SUMMARY

The objective of the current research is to improve our understanding of reinforced concrete column behavior under loads imposed by earthquakes. Five full-scale concrete column specimens were constructed and tested to investigate the relationships among various parameters used to define the deformation capacity of a column. The main test variables are shear span-to-depth ratio ( $L/h$ ), axial load level ( $P/P_o$ ), and amount of confining reinforcement ( $A_{sh}$ ).

The effects of these variables on the sectional and member behavior of columns are investigated experimentally. Based on the test results, the important factors which influence the transition from the sectional deformation capacity to the member deformation capacity are identified.

The effect of axial load on the plastic hinge length ( $l_p$ ) of concrete columns is explored. An analytical approach that can be used to estimate the plastic hinge length is developed. Based on the experimental evidence and results from a parametric study, a new expression for approximating the plastic hinge length is proposed.

In all the column specimens tested in this study, buckling of longitudinal bars was observed. Since buckling behavior of longitudinal bars is not considered in conventional sectional analyses, the column response can be over-predicted with respect to strength and ductility. Bayrak and Sheikh (2001) and Mieses (2002) conducted a large number of reinforcing bar buckling tests. Based on these results, a reinforcing bar buckling model is proposed.

The estimation of the deformation capacity parameters are discussed using two different methods: (1) a state-of-the art analytical method and (2) a simple closed-form expression. The state-of-the-art analytical method is a rigorous method that takes into account constitutive models for concrete confinement and reinforcing bar buckling and deformations due to flexure, shear and bar slip. In addition, the effect of  $P-\Delta$  is considered in the analytical method. In contrast, the closed-form equation derived in this research is a simple tool that can be used to estimate the deformation capacity of reinforced concrete columns.

#### **1.4 THESIS ORGANIZATION**

The effect of confining reinforcement on the deformation capacity of reinforced concrete columns is discussed in Chapter 2. Design code requirements (ACI 318; NZS 3101; ATC-32) and performance-based design requirements for confining reinforcement are also discussed in this chapter. In addition, the definition of deformation capacity parameters and the previous study on the interaction among different deformation capacities are presented. An extensive literature survey on research into the seismic performance of reinforced concrete columns is also included in Chapter 2.

The experimental program conducted on five full-scale concrete columns is described in Chapter 3. Chapter 4 includes the analysis of results obtained in the experimental program described in Chapter 3. Experimental observations on

the effects of the shear span-to-depth ratio ( $L/h$ ) and the level of axial load ( $P/P_o$ ) on the relationships among various deformation capacity parameters are described in this chapter.

Chapter 5 is devoted to an extensive literature survey of the previous research into the plastic hinge length. An analytical procedure that can be used to estimate the plastic hinge length of concrete columns is described, and a new plastic hinge length expression is proposed in this chapter. A bar buckling model developed in this research is presented in Chapter 6.

A state-of-the-art analytical method that can be used to generate the sectional and member responses of concrete columns is presented in Chapter 7. The proposed plastic hinge length expression (Chapter 5) and bar buckling model (Chapter 6) are incorporated into this analytical method. The load-deformation response of the columns tested in this study and those reported in the literature are evaluated using this analytical method. Strengths and weaknesses of the state-of-the art analytical procedure are discussed. A simple expression that can be used to estimate the deformation capacity of reinforced concrete columns is also presented in this chapter.

Finally, the conclusions reached in this research are summarized in Chapter 8. Based on the results obtained in this study, recommendations for future research are included in this chapter.

Appendix A includes drawings for the test setup used in this research and Appendix B provides an example problem illustrating the estimation of plastic hinge length using the analytical approach discussed in Chapter 5. Appendix C describes the computer program presented in Chapter 7, Appendix D provides an example problem that illustrates the computer program presented in Appendix C. Finally, Appendix E illustrates the application of the proposed simple closed-form equation that can be used to estimate the drift capacity of concrete columns.

# **CHAPTER 2**

## **REVIEW OF CODE PROVISIONS AND LITERATURE**

### **2.1 INTRODUCTION**

In seismic design, reinforced concrete columns are detailed to behave in a ductile manner in order to absorb and dissipate the energy transmitted from strong ground motions. Confining concrete is an effective method to provide adequate ductility for reinforced concrete columns.

Various design codes have developed different recommendations for the quantity of confining reinforcement to be used in the potential plastic hinge regions in terms of sectional dimensions, strength of concrete and transverse reinforcement, and axial load level. The current code provisions and previous research into the seismic performance of concrete columns are discussed in this chapter.

### **2.2 CODE PROVISIONS FOR CONFINING REINFORCEMENT DESIGN**

In this section, various code provisions for confining reinforcement design are reviewed. The early research that led to the code development efforts is briefly discussed prior to the review of code provisions for confinement. Following this background research, the ACI 318-05, NZS 3101:1995 and ATC-32 provisions for confining reinforcement are discussed.

#### **2.2.1 Effect of Confining Reinforcement on Concrete**

Richart et al. (1928) found that strength and ductility of concrete significantly increased under triaxial compressive stresses. They reported that the

lateral confining pressure reduced the tendency of internal cracking and volume increase prior to failure.

Richart et al. (1929) further demonstrated that the enhancement of strength and ductility of concrete confined by fluid pressure was similar to that observed for concrete confined by transverse reinforcement.

Based on the work of Richart et al., ACI Committee 105 (1933) reported that the ultimate strength of concentrically loaded reinforced concrete columns confined by spirals could be expressed as follows:

$$\frac{P}{A_c} = C \cdot f'_c \cdot (1 - \rho) + f_y \cdot \rho + k \cdot f_{yh} \cdot \rho_s \quad (2.1)$$

where

$P$  = axial load capacity of column

$A_c$  = cross sectional area of core concrete

$C$  = constant, found to be 0.85

$f'_c$  = compressive strength of concrete cylinders

$\rho$  = ratio of cross sectional area of longitudinal reinforcement to core concrete area

$f_y$  and  $f_{yh}$  = yield strengths of longitudinal reinforcement and spirals, respectively

$k$  = constant, ranging between 1.5 to 2.5 with an average of 2.0

$\rho_s$  = volumetric ratio of spirals to core concrete

With the assumption that spalling of cover concrete should not result in a loss of axial load capacity of a column to ensure a sufficient deformation capacity, Equation (2.1) was further simplified and Equation (2.2) was obtained.

$$\rho_s = 0.43 \left( \frac{A_g}{A_c} - 1 \right) \frac{f'_c}{f_{yh}} \quad (2.2)$$

where

$A_g$  = gross area of column section

$A_c$  = area of core concrete measured out-to-out of transverse reinforcement

$f'_c$  = compressive strength of concrete

$f_{yh}$  = yield strength of transverse reinforcement

### 2.2.2 ACI 318

Equation (2.2) of the ACI Committee 105 (1933) has been used as a basis of the ACI 318 code for confining reinforcement requirements for seismic design since 1971. The current building code requirements (ACI 318-05) for the amount of spiral reinforcement in potential plastic hinge regions of columns are as follows:

For columns with  $P_u > f'_c A_g / 10$ , where  $P_u$  is a factored axial compressive force, the volumetric ratio of spiral reinforcement ( $\rho_s$ ) shall not be less than the values given by:

$$\rho_s = 0.45 \left( \frac{A_g}{A_{ch}} - 1 \right) \frac{f'_c}{f_{yt}} \quad (2.3)$$

$$\rho_s = 0.12 \frac{f'_c}{f_{yt}} \quad (2.4)$$

The total cross sectional area of rectangular hoop reinforcement for confinement ( $A_{sh}$ ) shall not be less than that given by the following two equations:

$$A_{sh} = 0.3sb_c \left( \frac{A_g}{A_{ch}} - 1 \right) \frac{f'_c}{f_{yt}} \quad (2.5)$$

$$A_{sh} = 0.09sb_c \frac{f'_c}{f_{yt}} \quad (2.6)$$

where

$A_g$  = gross area of column section

$A_{ch}$  = area of core concrete measured out-to-out of transverse reinforcement

$f'_c$  = compressive strength of concrete

$f_{yt}$  = yield strength of transverse reinforcement

$s$  = spacing of transverse reinforcement

$b_c$  = cross sectional dimension of column core, measured center-to-center of transverse reinforcement

When  $P_u \leq f'_c A_g / 10$ , columns are designed as flexural members.

Equations (2.3) and (2.5) are slightly modified versions of Equation (2.2), with the same intent that spalling of cover concrete shall not result in a loss of axial load capacity of the column. Since the term  $(A_g/A_{ch} - 1)$  in Equations (2.3) and (2.5) will approach zero for large size columns, Equations (2.4) and (2.6) control for large size columns.

The length of the potential plastic hinge regions is specified as the greatest of the overall depth ( $h$ ) of a column at the joint face, where  $h$  is the larger sectional dimension for a rectangular column or the diameter of a circular column, one-sixth of the clear height of a column, or 18 in. (457 mm). The spacing of transverse reinforcement is required to be less than  $h/4$ ,  $6 \times d_b$ , and  $s_o$ , where  $h$  is the minimum member dimension,  $d_b$  is the diameter of longitudinal

reinforcement, and  $s_o$  is defined as  $4 + (14 - h_x) / 3$ . Here,  $h_x$  is defined as the maximum value of spacing of crossties or legs of overlapping hoops and it has to be kept less than 14 in. The value of  $s_o$  has to be less than 6 in. and need not be taken less than 4 in.

### 2.2.3 NZS 3101

Park and Sampson (1972) and Park and Leslie (1977) conducted analytical research on the moment-curvature response of concrete columns and concluded that the curvature ductility capacities were significantly influenced by axial loads. This conclusion was experimentally examined by Ang et al. (1981) and Park et al. (1982). Based on these investigations, the New Zealand design code adopted modified versions of the ACI code requirements for confining reinforcement to account for the effect of axial loads in 1982 (NZS 3101:1982).

Further experimental and analytical studies of concrete columns have been conducted (Mander et al. 1984; Zahn et al. 1986; Watson and Park 1994; Li et al. 1993). Zahn et al. (1986) proposed design charts to relate the available curvature ductility factor ( $\mu_\phi = \Delta_{ult}/\Delta_y$ ) of reinforced concrete columns to the magnitude of the confining stress applied by transverse reinforcement. Based on the design charts, Watson et al. (1994) proposed design equations for the quantities of confining reinforcement. These equations became the basis of the NZS 3101:1995 code.

For circular columns, the NZS 3101:1995 code requires that the volumetric ratio of spiral reinforcement ( $\rho_s$ ) shall not be less than the values given by Equations (2.7) and (2.8).

$$\rho_s = \frac{(1.3 - \rho_t m)}{2.4} \frac{A_g}{A_c} \frac{f'_c}{f_{yt}} \frac{P}{\Phi f'_c A_g} - 0.0084 \quad (2.7)$$

$$\rho_s = \frac{A_{st}}{110d''} \frac{f_y}{f_{yt}} \frac{1}{d_b} \quad (2.8)$$

For columns with rectangular hoops, NZS 3101:1995 requires that the total cross sectional area of rectangular hoop reinforcement for confinement shall not be less than that given by the following two equations:

$$A_{sh} = \frac{(1.3 - \rho_t m) s_h h''}{3.3} \frac{A_g}{A_c} \frac{f'_c}{f_{yt}} \frac{P}{\phi f'_c A_g} - 0.006 s_h h'' \quad (2.9)$$

$$A_{te} = \frac{\sum A_b f_y}{96 f_{yt}} \frac{s}{d_b} \quad (2.10)$$

where

$$A_g/A_c \geq 1.2 \text{ and } \rho_t m \leq 0.4$$

$A_g$  = gross area of column section

$A_c$  = area of core concrete measured out-to-out of transverse reinforcement

$\rho_t$  =  $A_{st}/A_g$  = longitudinal reinforcement ratio

$A_{st}$  = total area of longitudinal reinforcement

$m$  =  $f_y/(0.85f'_c)$

$f'_c$  = compressive strength of concrete

$f_{yt}$  = yield strength of transverse reinforcement

$d''$  = diameter of core concrete of circular column measured out-to-out of spiral

$d_b$  = diameter of longitudinal bar

$s_h$  = spacing of transverse reinforcement ( $= s$ )

$h''$  = concrete core dimension measured outer-to-outer peripheral hoop

$A_{te}$  = area of one leg of a tie

$\Sigma A_b$  = sum of the areas of the longitudinal bars reliant on the tie

$P$  = design axial load

Equations (2.8) and (2.10) are intended to prevent buckling of longitudinal reinforcement. For this purpose, the spacing of spirals or hoops along the member shall not exceed the smaller of 1/4 of the least lateral dimension of the cross section or 6 times the diameter of the longitudinal bar to be restrained. Equations (2.7) through (2.10) are intended to provide sufficient transverse reinforcement such that a curvature ductility of 20 can be achieved.

Potential plastic hinge regions in columns are considered to be the end regions adjacent to moment resisting connections over a length from the face of the connection as follows:

- (a) Where  $P \leq 0.25\phi f_c' A_g$ , the greater of the longer member cross section dimension in the case of a rectangular cross section or the diameter in the case of a circular cross section, or where the moment exceeds 0.8 of the maximum moment, taking into account dynamic magnification and overstrength actions, at that end of the member.
- (b) Where  $0.25\phi f_c' A_g < P \leq 0.5\phi f_c' A_g$ , the greater of 2.0 times the longer member cross section dimension in the case of a rectangular cross section or 2.0 times the diameter in the case of a circular cross section, or where the moment exceeds 0.7 of the maximum moment, taking into account dynamic magnification and overstrength actions, at that end of the member.
- (c) Where  $0.5\phi f_c' A_g < P \leq 0.7\phi f_c' A_g$ , the greater of 3.0 times larger member cross section dimension in the case of a rectangular cross section or 3.0 times the diameter in the case of a circular cross section, or where the

*moment exceeds 0.6 of the maximum moment, taking into account dynamic magnification and overstrength actions, at that end of the member.*

It is interesting to note that the effect of axial load is considered in determining both the amount of confining reinforcement and the length of the potential plastic hinge region.

#### 2.2.4 ATC-32

The requirements for confining reinforcement in the Caltrans Bridge Design Specifications (1986) were a mixture of the ACI 318 and NZS 3101 codes. Based on experimental and analytical research on concrete columns, the Applied Technology Council (ATC) suggested a modification of the Caltrans Specifications in 1996.

The ATC-32 provisions require the volumetric ratio ( $\rho_s$ ) of spiral or circular hoop reinforcement not be less than the values given by Equations (2.11) and (2.12).

$$\rho_s = 0.16 \frac{f'_{ce}}{f'_{ye}} \left( 0.5 + 1.25 \frac{P_e}{f'_{ce} A_g} \right) + 0.13(\rho_l - 0.01) \quad (2.11)$$

$$\rho_s = 0.0002 n_b \quad (2.12)$$

The total cross sectional area ( $A_{sh}$ ) of tie reinforcement for a rectangular column in the direction perpendicular to core dimension ( $h_c$ ) shall not be less than

$$A_{sh} = 0.12 s_t h_c \frac{f'_{ce}}{f'_{ye}} \left( 0.5 + 1.25 \frac{P_e}{f'_{ce} A_g} \right) + 0.13 s_t h_c (\rho_l - 0.01) \quad (2.13)$$

where

$f'_{ce}$  = expected concrete compressive strength

$f_{ye}$  = expected yield strength of transverse reinforcement  
 $P_e$  = design axial compressive force to a column  
 $A_g$  = gross area of column section  
 $\rho_l$  = longitudinal reinforcement ratio  
 $n_b$  = number of longitudinal bars contained by spiral or circular hoop  
 $s_t$  = spacing of transverse reinforcement  
 $h_c$  = cross sectional dimension of column core measured center-to-center  
of confining reinforcement

Equation (2.12) is intended to provide sufficient lateral reinforcement to prevent longitudinal bar buckling. It is interesting to note that the amount of longitudinal reinforcement is included in Equations (2.11) and (2.13). The analytical study, conducted by ATC, showed that an increase in the amount of longitudinal reinforcement resulted in a proportional decrease in the curvature ductility for typical axial load levels (i.e.,  $P/f_{ce}'A_g \leq 0.4$ ). A curvature ductility of 13 was the minimum level of deformation capacity used in calibrating the ATC-32 requirements for confining reinforcement.

The ATC-32 provisions define the potential plastic hinge region length ( $l_0$ ) as: *the greater of (a) the section dimension in the direction considered or (b) the portion of the column over which the moment exceeds 80 percent of the moment at the critical section.* For axial ratios  $P/f_{ce}'A_g \geq 0.3$ , the potential plastic hinge length is required to be increased by 50 percent. The spacing of transverse reinforcement is required to be less than (1) one-fifth of the least dimension of the cross-section for columns and one-half of the least cross-section dimension for piers, (2)  $6 \times d_b$ , and (3) 8 in.

## 2.3 PERFORMANCE-BASED DESIGN PROCEDURES

In this section, various performance-based design procedures for confining reinforcement are reviewed. These procedures are those proposed by Watson et al. (1994), Sheikh and Khoury (1997), Wehbe et al. (1997), and Saatcioglu and Razvi (2002).

### 2.3.1 Watson et al. (1994)

Based on the design charts developed by Zahn et al. (1986), Watson et al. (1994) proposed the following equations for confining reinforcement:

For rectangular column cross sections,

$$\frac{A_{sh}}{sb_c} = \frac{A_g}{A_c} \frac{(\phi_u / \phi_y - 33\rho_t m + 22)}{111} \frac{f'_c}{f'_{yh}} \frac{P}{\phi f'_c A_g} - 0.006 \quad (2.14)$$

For circular sections where spiral or circular hoop bars are used,

$$\rho_s = 1.4 \frac{A_g}{A_c} \frac{(\phi_u / \phi_y - 33\rho_t m + 22)}{111} \frac{f'_c}{f'_{yh}} \frac{P}{\phi f'_c A_g} - 0.008 \quad (2.15)$$

where

$$A_g/A_c \geq 1.2 \text{ and } \rho_t m \leq 0.4$$

$A_g$  = gross area of column section

$A_c$  = area of core concrete measured out-to-out of transverse reinforcement

$\phi$  = strength reduction factor

$\phi_y$  = yield curvature

$\phi_u$  = ultimate curvature

$\rho_t$  =  $A_{st}/A_g$  = longitudinal reinforcement ratio

$A_{st}$  = total area of longitudinal reinforcement

$m$  =  $f_y/(0.85f'_c)$

- $f'_c$  = compressive strength of concrete  
 $f_y$  = yield strength of longitudinal reinforcement  
 $f_{yt}$  = yield strength of transverse reinforcement

The required amount of confining reinforcement in Equations (2.14) and (2.15) depends on the curvature ductility ( $\phi_u/\phi_y$ ) as well as the axial load level ( $P/\phi f'_c A_g$ ). The flexibility provided by including the curvature ductility demand as a design parameter makes the expressions useful for designing columns in regions of high, moderate and low seismicity.

The proposed equations (Equations (2.14) and (2.15)) give only the transverse reinforcement required for concrete confinement. Watson et al. (1994) stated that the transverse reinforcement provided must also be checked to ensure that it is sufficient to prevent premature buckling of the longitudinal compression bars and to prevent shear failure. The use of  $\phi_u/\phi_y = 20$  and 10 was recommended for ductile and limited ductile behavior of columns, respectively. Equations (2.14) and (2.15) are adopted for the NZS 3101:1995 code.

### 2.3.2 Wehbe, Saiidi and Sanders (1997)

Wehbe et al. (1997) tested four rectangular concrete columns. The column specimens contained 46% to 60% of the confining reinforcement required by the AASHTO provisions (1992), which are similar to the ACI 318-89 code. The applied axial loads were 10% and 20% of  $f'_c A_g$ . The measured displacement ductilities ( $\mu_\Delta$ ) of column specimens were ranged between 5 and 7. An analytical study was also conducted to investigate the relationship between the amount of confining reinforcement and the displacement ductility. Based on the study, the following equation was proposed:

$$\frac{A_{sh}}{s_t h_c} = 0.1\mu_\Delta \sqrt{\frac{f_{c,n}}{f'_{ce}}} \left[ 0.12 \frac{f'_{ce}}{f_{ye}} \left( 0.5 + 1.25 \frac{P}{f'_{ce} A_g} \right) + 0.13 \left( \rho_l \frac{f_y}{f_{s,n}} - 0.01 \right) \right] \quad (2.16)$$

where

$s_t$  = spacing of transverse reinforcement along the axis of the member

$h_c$  = cross sectional dimension of column core measured center-to-center  
of confining reinforcement

$f'_{ce}$  = expected concrete strength

$f_{ye}$  = expected yield strength of transverse reinforcement

$f_y$  = expected yield strength of longitudinal reinforcement

$f_{c,n} = 4$  ksi (or 27.6 MPa)

$f_{s,n} = 60$  ksi (or 414 MPa)

$A_g$  = gross area of column section

$\rho_l$  = longitudinal reinforcement ratio

Equation (2.16) is a modified version of the ATC-32 equation (Equation (2.13)). For the minimum amount of transverse reinforcement in areas of high seismic risk, the use of  $\mu_\Delta = 10$  was recommended.

### 2.3.3 Sheikh and Khoury (1997)

Sheikh and Khoury (1997) employed curvature ductility ( $\mu_\phi$ ) as the performance criterion. The seismic performance of concrete columns was classified to the following three categories: (1) highly ductile columns ( $\mu_\phi \geq 16$ ), (2) moderately ductile columns ( $16 > \mu_\phi \geq 8$ ), and (3) columns displaying low levels of ductility ( $\mu_\phi < 8$ ). The following equation was proposed to relate the amount of transverse reinforcement to axial load level and curvature ductility capacity.

$$A_{sh} = \alpha \cdot \left\{ 1 + 13 \left( \frac{P}{P_o} \right)^5 \right\} \frac{(\mu_\phi)^{1.15}}{29} A_{sh,ACI} \quad (2.17)$$

The constant  $\alpha$  was used to take into account the distribution of transverse and longitudinal steel. According to Sheikh and Khoury (1997),  $\alpha$  is equal to one for tightly knit transverse reinforcement configurations in which effective lateral support to all of the longitudinal bars is provided. For less efficient transverse reinforcement configurations, the  $\alpha$  value is greater than one. They concluded that the ACI 318 requirements for confining reinforcement might not be sufficient even in columns with efficient transverse reinforcement configurations to meet the high curvature ductility demands under moderate-to-high levels of axial loads. They also stated that the ACI code requirements could be relaxed at axial load levels less than  $0.4P_o$ .

Equation (2.17) was modified by Bayrak and Sheikh (1998) for high-strength concrete columns with concrete strengths ranging between 8,000 psi (55 MPa) and 16,000 psi (115 MPa). Bayrak and Sheikh (1998) proposed the following equation.

$$A_{sh} = \alpha \cdot \left\{ 1 + 13 \left( \frac{P}{P_o} \right)^5 \right\} \frac{(\mu_\phi)^{0.82}}{8.12} A_{sh,ACI} \quad (2.18)$$

### 2.3.4 Saatcioglu and Razvi (2002)

Saatcioglu and Razvi (2002) suggested that there was a direct correlation between drift capacity and concrete confinement. They concluded that the shear span-to-depth ratio ( $L/h$ ) of a column did not show a pronounced effect on drift capacity when the  $P-\Delta$  effect was considered. They reported that drift capacity increased by approximately 75% as the shear span-to-depth ratio ( $L/h$ ) increased

from 2.5 to 5.0. They also reported that the amount of longitudinal reinforcement had a minor influence on the drift capacity. Based on these findings, they proposed the following relation.

$$\rho_c = 14 \frac{f'_c}{f_{yh}} \left[ \frac{A_g}{A_c} - 1 \right] \frac{1}{\sqrt{k_2}} \frac{P}{P_o} \delta \quad (2.19)$$

where

$$k_2 = 0.15 \sqrt{\frac{b_c}{s} \cdot \frac{b_c}{s_l}}$$

$$\frac{P}{P_o} \geq 0.2 \text{ and } \frac{A_g}{A_c} - 1 \geq 0.3$$

in which

$\rho_c = A_{sh}/h_{cs}$  = area ratio of transverse reinforcement

$\delta$  = lateral drift ratio, defined as horizontal displacement divided by height

$f'_c$  = compressive concrete strength

$f_{yh}$  = yield strength of transverse reinforcement

$A_g$  = gross area of column section

$A_c$  = area of core concrete measured center-to-center of transverse reinforcement

$P_o$  = nominal concentric compressive capacity of column

$b_c$  = core dimension, center-to-center of perimeter tie

$h_c$  = core dimension perpendicular to transverse reinforcement under consideration (center-to-center of perimeter reinforcement)

$s$  = spacing of transverse reinforcement

$s_l$  = spacing of longitudinal reinforcement, laterally supported by corner of hoop or hook of crosstie

A drift capacity of 2.5% was recommended to ensure ductile performance of concrete columns.

#### **2.4 CONFINING REINFORCEMENT: CODES AND PERFORMANCE-BASED DESIGN PROCEDURES**

Confining reinforcement design provisions of the ACI code are based on the premise of maintaining the axial load carrying capacity of a column after cover spalling takes place. In this way, potential plastic hinge regions are designed to have sufficient deformation capacity. The requirements of the New Zealand code and the ATC-32 design provisions, on the other hand, are calibrated to achieve a certain minimum curvature ductility in the potential plastic hinge regions. In order to compare these various requirements, the amount of the confining reinforcement required by design codes (ACI 318; NZS 3101; ATC 32) and performance-based design procedures (Wehbe et al. 1997; Sheikh and Khoury 1997; Saatcioglu and Razvi 2002) are calculated for a column with square section of  $24 \times 24$  in.<sup>2</sup>, concrete strength of 4,000 psi and Grade 60 reinforcing bars. A comparison of the required amount of confining reinforcement is illustrated in Figure 2.1. This figure clearly illustrates the large variations in the amount of confining reinforcement required by design codes and performance-based design procedures.

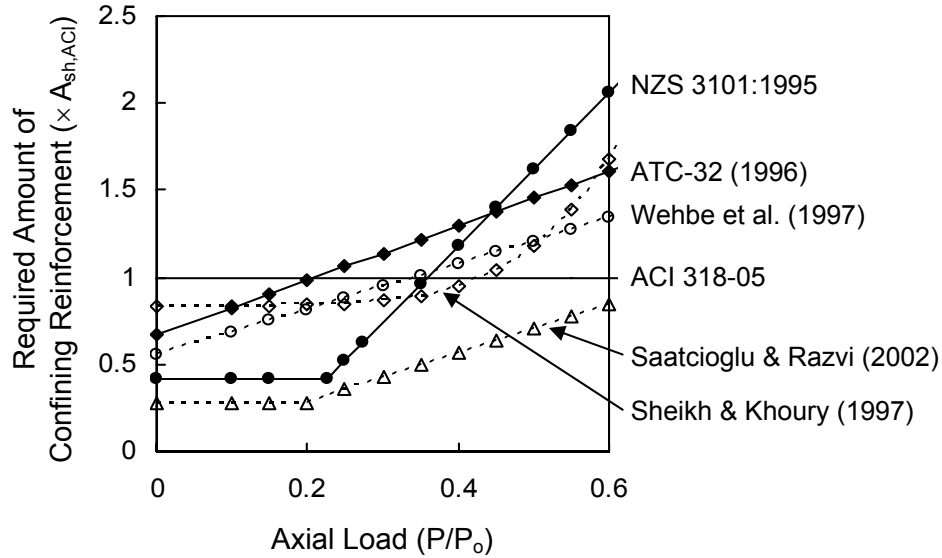


**Figure 2.1 Comparison of Design Codes and Performance-Based Design Procedures**

Performance-based design procedures proposed by Watson et al. (1994), Wehbe et al. (1997), Sheikh and Khoury (1997) and Saatcioglu and Razvi (2002) allow the design of confining reinforcement for a certain level of deformation capacity. To express the deformation capacity, various ductility parameters are used. Wehbe et al. (1997) and Saatcioglu and Razvi (2002) used displacement ductility and drift capacity as design variables to quantify the deformation capacity of a column, respectively. On the other hand, curvature ductility is used by most design codes (NZS3101 and ATC-32) and some performance-based design procedures (Watson et al. 1994; Sheikh and Khoury 1997). It can be observed in Figure 2.1 that larger amounts of confining reinforcement are required when curvature ductility is used as a design parameter for high axial load levels (NZS3101; ATC-32; Sheikh and Khoury 1997).

#### 2.4.1 Relationship among Various Deformation Capacity Parameters

As previously discussed, various parameters are used to express the deformation capacity of a column. Park and Paulay (1975) derived a relationship between the curvature ductility and the displacement ductility based on an assumed curvature profile along the length of a cantilever column.

$$\mu_{\Delta} = 1 + 3(\mu_{\phi} - 1) \frac{l_p}{L} \left( 1 - 0.5 \frac{l_p}{L} \right) \quad (2.20)$$

Equation (2.20) indicates that the length of the plastic hinge ( $l_p$ ) and the height of a column ( $L$ ) influence the relationship between the curvature ductility and the displacement ductility. This means that similar curvature ductilities can correspond to different displacement ductilities depending on the plastic hinge length and the height of a column. By assuming a constant plastic hinge length, a simple linear relationship between curvature and displacement ductilities can be obtained (Figure 2.2). This figure illustrates that displacement ductility can be improved proportionally by increasing curvature ductility.

Equation (2.20) does not account for the effect of axial load and the associated  $P$ - $\Delta$  effect on column response. The behavior of concrete columns can be represented in the form of moment-curvature ( $M$ - $\phi$ ) or lateral load-displacement ( $V$ - $\Delta$ ) response (Figure 2.3). As can be seen in Figure 2.3, the strength degradation in the lateral load-deformation response can be caused by (1) the loss of moment resistance and (2) the  $P$ - $\Delta$  effect. It is important to note that even in the case of a fairly stable sectional response with very little or no post-peak strength reduction, reductions in lateral load capacity can occur due to the  $P$ - $\Delta$  effect. This effect will be exacerbated by high axial loads and at large lateral displacements.

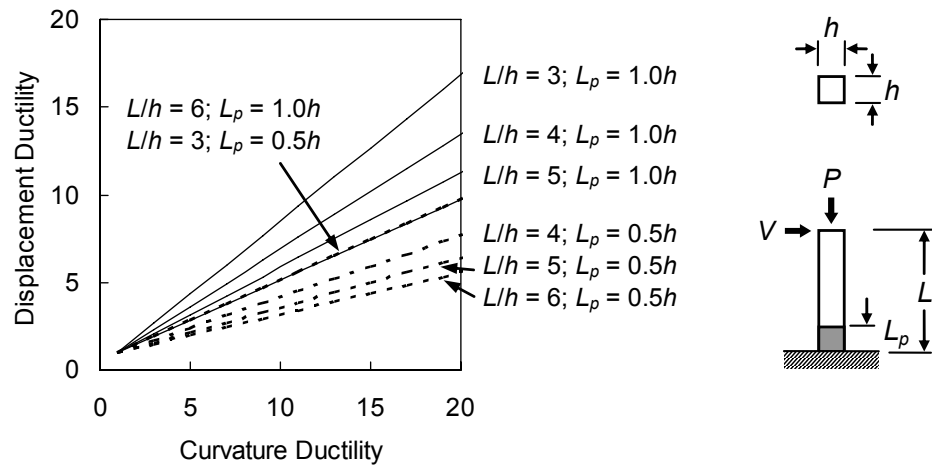


**Figure 2.2 Relationship between Curvature and Displacement Ductilities  
(Park and Paulay 1975)**

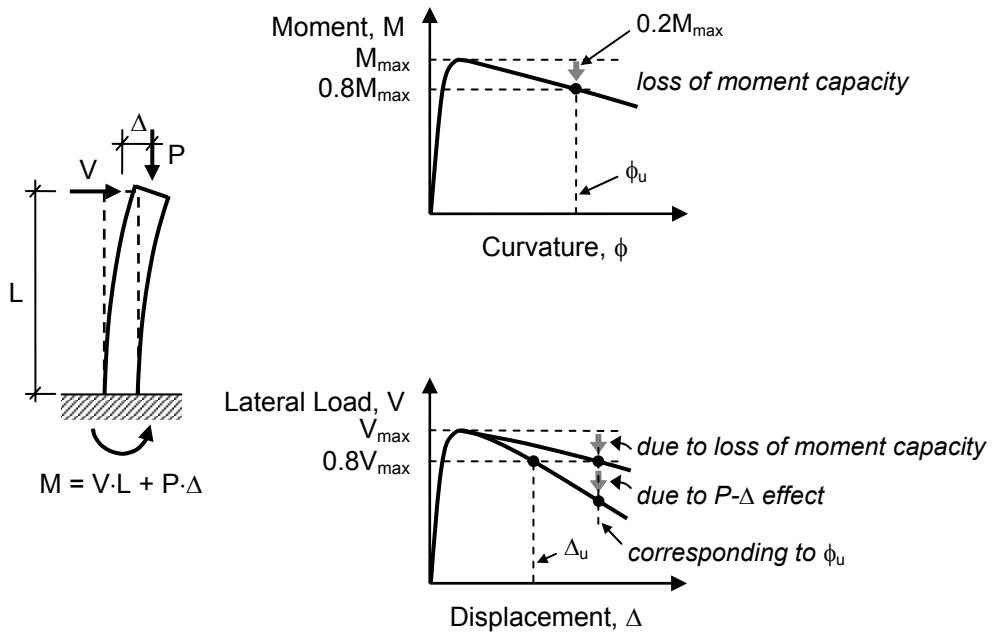


**Figure 2.3 Behavior of Reinforced Concrete Column**

The maximum curvature is typically assessed at a point on the descending branch of a moment-curvature response where the capacity degradation is equal to 20% of the maximum moment ( $0.2M_{max}$  in Figure 2.3) (Watson et al. 1994; Sheikh et al. 1994; Bayrak 1999). Similarly, the maximum tip displacement of a column, typically used in displacement ductility or drift capacity calculation, is measured on the descending branch of a lateral load-displacement response where a 20% drop in lateral load capacity is observed (Figure 2.3) (Saatcioglu and Razvi 2002; Sheikh et al. 1994; Bayrak 1999). Considering the  $P$ - $\Delta$  effect and assuming a constant plastic hinge length, it is possible to appreciate that the relationship between curvature ductility and displacement ductility is typically nonlinear with respect to the axial load. If the plastic hinge lengths of concrete columns are affected by shear span-to-depth ratio or axial load, the relationship between curvature ductility and displacement ductility will be more complicated.

## 2.5 REVIEW OF LITERATURE: SIMULATED SEISMIC TESTS ON COLUMNS

### 2.5.1 Park, Priestley and Gill (1982)

Park et al. (1982) tested four columns. The column specimens had 22-in. (550-mm) square cross sections and they were 4-ft (1.2-m) high with a shear span-to-depth ratio of 2.2. The main objective of this research was to study the performance of tied columns designed according to the draft of New Zealand code (DZ 3101:1978). The main test variables were the level of axial load and the corresponding amount of transverse hoop reinforcement. Details of the test specimens are given in Figure 2.4 and Table 2.1. The amount of transverse reinforcement provided in these columns is also compared with the amount required by the Chapter 21 of the ACI 318-05 code and presented in Table 2.1. Three of four column specimens contained less transverse reinforcement than that required by the ACI 318-05 code ( $0.63 \leq A_{sh}/A_{sh,ACI} \leq 0.89$ ).

All columns demonstrated very ductile behavior. A displacement ductility capacity of at least 6 was observed in all tests. Park et al. (1982) concluded that the requirements of the draft of NZS 3101 code (DZ 3101:1978) were adequate based on the ductile performance displayed by the column specimens. The maximum curvature ductility factor ( $\phi_u/\phi_y$ , in which  $\phi_u$  = maximum measured curvature and  $\phi_y$  = curvature at first yield), measured in each unit within the plastic hinge region, was calculated at  $\mu_\Delta = 6$ . These measured maximum curvature ductility factors ranged between 14 and 21. The maximum curvature values were generally recorded in either the first 100-mm gage length from the stub face or the second 100-mm gage length (Figure 2.5). The concentration of curvature at a short distance away from the central stub was attributed to the significant additional confinement provided by the stub.

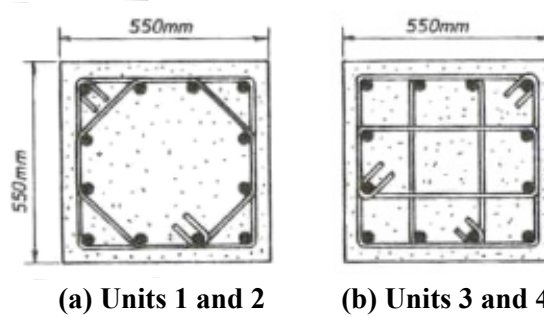


*Figure 2.4 Details of Transverse Reinforcement (Park et al. 1982)*

**Table 2.1 Details of Column Specimens (Park et al. 1982)**

Unit	$f'_c$ (MPa)	Axial Load		Longitudinal Reinforcement		Transverse Reinforcement					$\mu_\phi$
		$P$ (kN)	$\frac{P}{f'_c A_g}$	$f_y$ (MPa)	$\rho_l$ (%)	$d_h$ (mm)	$s_h$ (mm)	$f_{yh}$ (MPa)	$\rho_s^*$ (%)	$\frac{A_{sh}}{A_{sh,ACI}}$	
1	23.1	1,815	0.260	375	1.79	10	80	297	1.5	0.66	21
2	41.4	2,680	0.214	375	1.79	12	75	316	2.3	0.63	20
3	21.4	2,719	0.420	375	1.79	10	75	297	2.0	0.89	14
4	23.5	4,265	0.600	375	1.79	12	62	294	3.5	1.47	16

\*:  $\rho_s$  = volumetric ratio of transverse reinforcement to core concrete

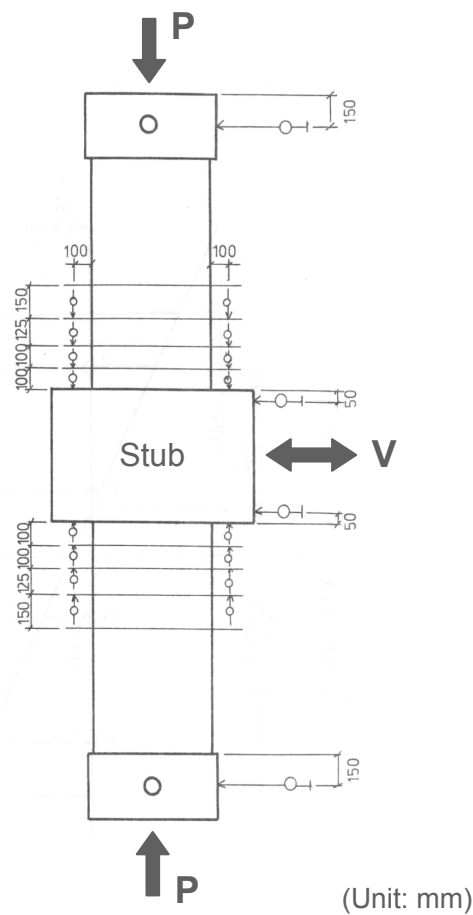


**Figure 2.5 Test Setup**

### 2.5.2 Watson and Park (1994)

Soesianawati et al. (1986) tested four square concrete columns under low axial loads. The column specimens contained smaller quantities of confining reinforcement than those recommended by the NZS3101:1982 code. Watson and Park (1994) further expanded the experimental work of Soesianawati et al. (1986) by testing five more square columns and two octagonal columns under moderate to high axial compression loads. The details of those square column specimens are listed in Table 2.2. The configuration of transverse reinforcement was similar to that shown in Figure 2.4(a) with a concrete cover of 0.5 in. (13 mm). The 16-in. (400-mm) square column specimens had a height of 1.6 m, resulting in a shear span-to-depth ratio of 4.

Units 1 to 4 were tested under low axial load ( $P = 0.1f'_c A_g$  to  $0.3f'_c A_g$ ). Units 1 and 2, with 43% and 46% of the New Zealand code recommended quantity of transverse reinforcement, achieved displacement ductility factors of at least 8 without significant strength degradation. Unit 3, with 30% of the code required quantity of transverse reinforcement, was capable of reaching a displacement ductility factor of 6. Unit 4 with 17% of the code recommended quantity of transverse reinforcement reached a displacement ductility factor of 4 and showed failure of the hoop anchorage, followed by buckling of longitudinal bars.

Units 5 and 6 were subjected to high axial load ( $P = 0.5f'_c A_g$ ). These units which contained 38% and 19% of the confining reinforcement required by the New Zealand code, achieved displacement ductility factors of  $\mu_\Delta = 6.7$  and 5.4, respectively. Buckling of longitudinal bars occurred at the end of test. Units 7, 8 and 9 were subjected to an axial load level of  $P = 0.7f'_c A_g$ . Units 7 and 8, which contained 48% and 34% of the code recommend quantity of confining reinforcement for ductile detailing, achieved  $\mu_\Delta = 6.3$  and 4.0, respectively.

**Table 2.2 Details of Column Specimens (Watson and Park 1994)**

Unit	$f'_c$ (MPa)	Axial Load		Longitudinal Reinforcement		Transverse Reinforcement					$\mu_\phi$
		$P$ (kN)	$\frac{P}{f'_c A_g}$	$f_y$ (MPa)	$\rho_I$ (%)	$d_h$ (mm)	$s_h$ (mm)	$f_{yh}$ (MPa)	$\rho_s$ (%)	$\frac{A_{sh}}{A_{sh,ACI}}$	
1	47	744	0.1	446	1.51	7	85	364	0.84	0.36	24
2	44	2,112	0.3	446	1.51	8	78	360	1.20	0.55	28
3	44	2,112	0.3	446	1.51	7	91	364	0.79	0.36	18
4	40	1,920	0.3	446	1.51	6	94	255	0.56	0.20	14
5	41	3,280	0.5	474	1.51	8	81	372	1.15	0.58	9
6	40	3,200	0.5	474	1.51	6	96	388	0.55	0.29	15
7	42	4,704	0.7	474	1.51	12	96	308	2.16	0.90	12
8	39	4,368	0.7	474	1.51	8	77	372	1.21	0.64	9
9	40	4,480	0.7	474	1.51	12	52	308	3.99	1.75	27

Due to the large spacing of transverse reinforcement outside the plastic hinge regions, the hoops of Unit 7 were not capable of maintaining the strength of the column outside the plastic hinge region. Unit 9 which contained 93% of the code recommended quantity demonstrated excellent performance. No significant degradation of strength was detected when the test ended after completing cycles up to a nominal displacement ductility factor of 10.

Watson and Park (1994) observed that the length of potential plastic hinge regions increased with an increase of the axial load level. As such, they recommended that the length of a potential plastic hinge region can be calculated by using Equation (2.21).

$$\frac{l_c}{h} = 1 + 2.8 \frac{P}{\phi f'_c A_g} \quad (2.21)$$

where

- $l_c$  = length of confined region of column
- $h$  = lateral dimension of rectangular column section
- $\phi$  = strength reduction factor
- $f'_c$  = compressive cylinder strength of concrete
- $A_g$  = gross area of column section

Watson and Park (1994) also conducted analytical research. Combining the results of their experimental and analytical research, they proposed confining reinforcement design expressions, which were discussed in Section 2.2.3.

### 2.5.3 Tanaka and Park (1990)

Two series of column specimens were constructed and tested by Tanaka and Park (1990). The first series of four column specimens (Units 1 to 4) had a total height of 5.9 ft (1.8 m) and square sections of  $16 \times 16$  in.<sup>2</sup> ( $400 \times 400$  mm<sup>2</sup>), resulting in a shear span-to-depth ratio of 4.5. The second series of four column specimens (Units 5 to 8) had a total height of 5.4 ft (1.65 m) and square sections of  $22 \times 22$  in.<sup>2</sup> ( $550 \times 550$  mm<sup>2</sup>), resulting in a shear span-to-depth ratio of 3. The main test variables for the column specimens were the configuration of transverse reinforcement and anchorage details of that reinforcement. Other test variables included the level of applied axial load ( $P/f'_c A_g$ ) and the shear span-to-depth ratio of each column ( $L/h$ ). The mechanical properties of the materials and other details of the column specimens are shown in Figure 2.6 and Table 2.3.

The spacing of the transverse reinforcement in the plastic hinge region of the columns was selected to satisfy the NZS 3101:1982 code for both confinement and shear.

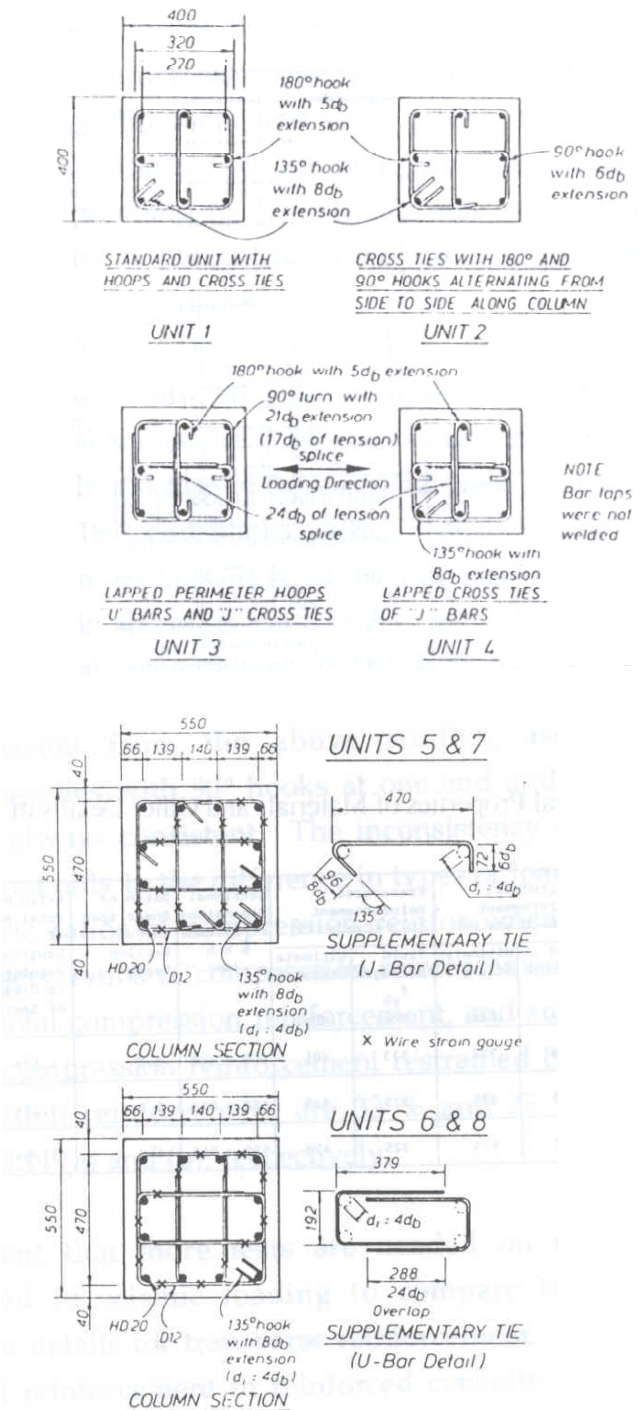


Figure 2.6 Details of Transverse Reinforcement (Tanaka and Park 1990)

**Table 2.3 Details of Column Specimens (Tanaka and Park 1990)**

Unit	$f'_c$ (MPa)	$\frac{P}{f'_c A_g}$	Longitudinal Steel		Transverse Steel				$b \times h$ (mm)	$L/h$
			$f_y$ (MPa)	$\rho_l$ (%)	$s_h$ (mm)	$f_{yh}$ (MPa)	$\rho_s$ (%)	$\frac{A_{sh}}{A_{sh,ACI}}$		
1 to 4	25.6	0.2	474	1.57	80	333	2.55	1.06	400×400	4.0
5 & 6	32.0	0.1	511	1.25	110	325	1.70	0.82	550×550	3.0
7 & 8	32.1	0.3	511	1.25	90	325	2.08	1.00	550×550	3.0

Due to restrictions in tie spacing and bar sizes available, the transverse reinforcement provided in the columns was in excess of the NZS 3101:1982 required quantities by 36% in Units 1 to 4, 17% in Units 5 and 6, and 2% in Units 7 and 8.

Satisfactory behavior was observed for all columns, except Unit 3. The interior cross ties with 90° and 135° (or 180°) end hooks behaved satisfactorily in Unit 2, up to  $\mu_\Delta = 8$ . Beyond that displacement level, the 90° end hooks commenced to open and the effectiveness of those end hooks was reduced gradually. In the case of Unit 3, the 90° bends in the perimeter hoops formed of lapped ‘U’ bars commenced to open at  $\mu_\Delta = 7$ , and in the subsequent cycles of loading the strength of the column rapidly degraded due to significant buckling of the longitudinal bars and ineffective confinement of the core concrete.

The equivalent plastic hinge lengths for column specimens ranged between 0.46 and 0.75 of the overall depth of the column section. Tanaka and Park (1990) observed that the equivalent plastic hinge length increased with increasing axial load level.

#### **2.5.4 Azizinamini, Corley and Johal (1992)**

In order to investigate the effect of transverse reinforcement details, twelve full-scale columns were tested. The experimental variables included the level of axial load, amount and detail of transverse reinforcement. Eleven column specimens had square cross sections and one specimen had a circular cross section. Among eleven square columns, six specimens had typical transverse reinforcement details, while the other five specimens had unusual transverse reinforcement details. Details of these unusual transverse reinforcement configurations can be found elsewhere (Azizinamini et al. 1992). Five columns with these abnormal details are not discussed here, since they are beyond of the scope of this research. The square column specimens had cross sections of  $18 \times 18$  in.<sup>2</sup> and a height of 10.5 ft., resulting in a shear span-to-depth ratio of 7. Figure 2.7 illustrates the reinforcement details of six test specimens which had typical transverse reinforcement details. The details of column specimens are shown in Table 2.4.

All six specimens with typical transverse reinforcement details exhibited good strength and energy dissipation capabilities up to the last loading cycle. The obtained displacement ductilities were in the range of 5 to 8. Test specimens failed by buckling of the longitudinal bars in compression, which coincided with the loss of anchorage of the transverse reinforcement at one or more levels.

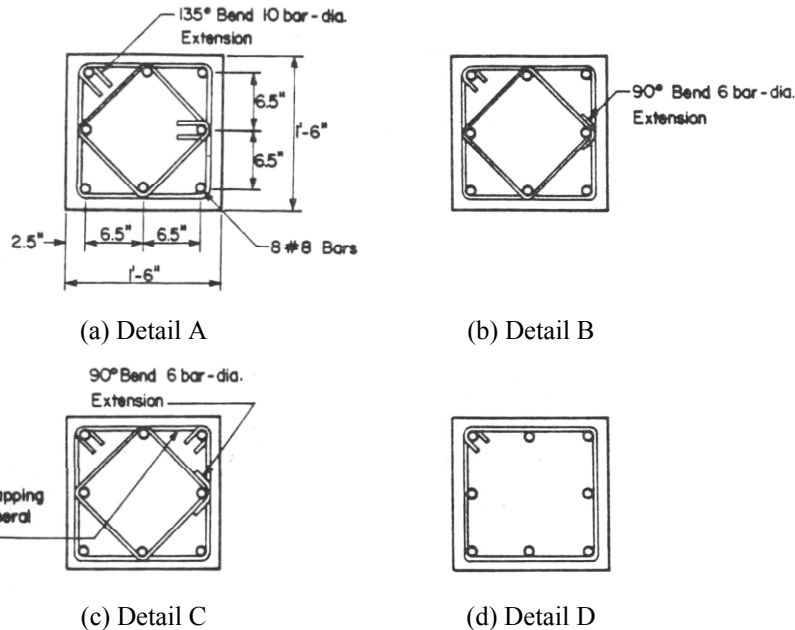


**Figure 2.7 Details of Transverse Reinforcement (Azizinamini et al. 1992)**

**Table 2.4 Details of Column Specimens (Azizinamini et al. 1992)**

Unit	Detail	$f'_c$ (ksi)	Axial Load		Longitudinal Reinforcement		Transverse Reinforcement				$\mu_\Delta$
			$P/P_o$	$P$ (kips)	$\rho_l$ (%)	$f_y$ (ksi)	bar size	$s_h$ (in.)	$\rho_s$ (%)	$\frac{A_{sh}}{A_{sh,ACI}}$	
NC-1	A	5.6	0.3	570	1.95	63.7	No.4	4	2.19	0.94	6
NC-2	B	5.7	0.2	380	1.95	63.7	No.4	4	2.19	0.93	8
NC-3	B	5.8	0.4	780	1.95	63.7	No.4	4	2.19	0.92	5
NC-4	B	5.8	0.3	580	1.95	63.7	No.3	4	1.26	0.47	5
NC-5	C	5.7	0.3	575	1.95	63.7	No.4	4	2.19	0.93	8
NC-6	D	5.0	0.3	520	1.95	63.7	No.4	4	1.29	0.63	5

The amount of confining reinforcement provided in the test specimens ranged between 46% and 97% of the ACI 318-83 requirements. Although the provided confining reinforcement was less than the ACI 318-83 requirements, the observed displacement ductilities of all tested specimens were acceptable. It is interesting to note that comparison of results from specimen NC-1 with those of specimen NC-4 indicated that the use of almost 50 percent less transverse reinforcement in specimen NC-4 resulted in only slightly lower displacement ductility.

#### **2.5.5 Saatcioglu and Ozcebe (1987, 1989)**

Saatcioglu and Ozcebe (1987, 1989) conducted tests on fourteen full-scale reinforced concrete columns. The test parameters included the axial load level, confinement reinforcement, and loading path. Three groups of specimens (U, D, and B) were tested. Each group was labeled according to the loading path imposed. U-specimens were loaded uniaxially in a direction parallel to one of the principal axes of the column section. D-specimens were loaded uniaxially along the diagonal section. B-specimens were loaded simultaneously in two orthogonal directions, following a bi-directional loading path. All specimens had 14-in. (350-mm) square column sections and a height of 3.3 ft (1.0 m), resulting in a shear span-to-depth ratio of 2.86. The details of test specimens are given in Figure 2.8 and Table 2.5.

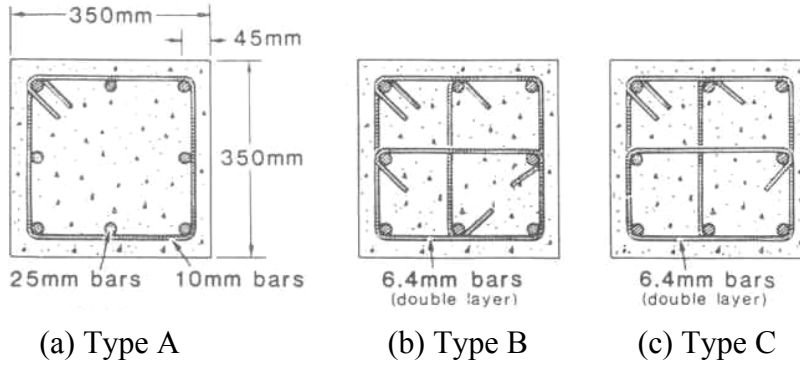


**Figure 2.8 Details of Transverse Reinforcement**

(Saatcioglu and Ozcebe 1987, 1989)

**Table 2.5 Details of Column Specimens (Saatcioglu and Ozcebe 1987, 1989)**

Unit	Detail	$f'_c$ (MPa)	Axial Load		Longitudinal Steel		Transverse Steel			
			$P$ (kN)	$\frac{P}{f'_c A_g}$	$f_y$ (MPa)	$\rho_l$ (%)	$s_h$ (mm)	$f_{yh}$ (MPa)	$\rho_s$ (%)	$\frac{A_{sh}}{A_{sh,ACI}}$
U1	A	43.6	0	0	430	3.27	150	470	0.85	0.51
U2	A	30.2	600	0.16	453	3.27	150	470	0.85	0.73
U3	A	34.8	600	0.14	430	3.27	75	470	1.69	1.27
U4	A	32.0	600	0.15	438	3.27	50	470	2.54	2.07
U5	A	49.3	variable	-0.1~0.1	430	3.27	150	470	0.85	0.45
U6	B	37.3	600	0.11	437	3.27	65	425	1.95	0.97
U7	C	39.0	600	0.11	437	3.27	65	425	1.95	0.93
D1	A	40.3	0	0	453	3.27	150	470	0.85	0.55
D2	A	30.2	600	0.16	453	0.0327	150	470	0.0085	0.73
D3	A	34.8	600	0.14	430	0.0327	75	470	0.0169	1.27
D4	A	43.6	600	0.11	430	0.0327	50	470	0.0254	1.52
D5	A	49.3	variable	-0.1~0.1	430	0.0327	150	470	0.0085	0.45
B1	A	32.0	600	0.15	438	0.0327	50	470	0.0254	2.07
B2	A	39.5	600	0.12	437	0.0327	75	470	0.0169	1.12

It was concluded that ductility of columns improved significantly with the use of a proper transverse reinforcement configuration. A column, where every longitudinal bar was supported by either a hoop or a crosstie, exhibited a better response than a column, where every other longitudinal bar was effectively supported. It was observed that crossties with a 90° hook at one end and a 135° hook at the other end performed as satisfactorily as those with 135° hooks at both ends.

It was also concluded that columns subjected to simultaneously varying bi-directional load reversals showed a different response than those subjected to unidirectional load reversals. The level of damage in one direction adversely affected the column performance in the other directions. If the deformation in one direction was less than the yield deformation, the bi-directional effect on the response in the orthogonal direction was small. However, if post-yield deformations were experienced in both directions, severe strength and stiffness degradations were observed.

#### **2.5.6 Zahn, Park, and Priestley (1986)**

Zahn et al. (1986) conducted an experimental investigation to study the effect of the direction of lateral loading on the behavior of concrete columns. The column specimens had a height of 5.2 ft (1,600 mm) and 16-in. (400-mm) square sections, resulting in a shear span-to-depth ratio of 4. The details of the test specimens are shown in Figure 2.9 and Table 2.6.

The comparison between theoretical and experimental flexural strength of square reinforced concrete columns indicated that there was very little difference between the flexural strengths for bending about a principal axis of the section and for bending about a diagonal axis. The available curvature ductility of the square confined columns for bending about the diagonal axis was found to be no

less than that of the similar columns bending about their principal axis. Hence, Zahn et al. (1986) concluded that the code expressions for confining reinforcement design, originally validated by experimental results from columns tested under uniaxial moments, were conservative for columns subjected to biaxial moments.

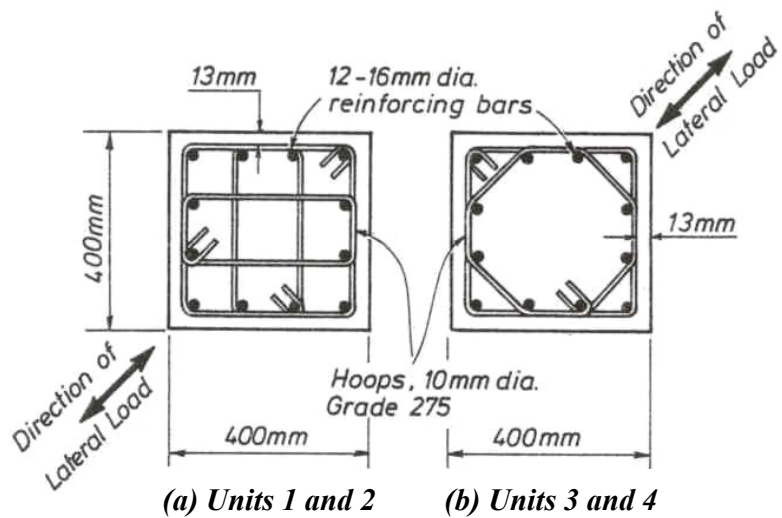


*Figure 2.9 Details of Transverse Reinforcement (Zahn et al. 1986)*

*Table 2.6 Details of Column Specimens (Zahn et al. 1986)*

Unit	$f'_c$ (MPa)	$\frac{P}{f'_c A_g}$	Longitudinal Reinforcement		Transverse Reinforcement					
			$f_y$ (MPa)	$\rho_l$ (%)	$d_h$ (mm)	$s_h$ (mm)	$f_{yh}$ (MPa)	$\rho_s$ (%)	$\frac{A_{sh}}{A_{sh,ACI}}$	
1	36.2	0.23	423	1.51	10	84	318	2.24	1.09	
2	28.8	0.43	423	1.51	10	65	318	2.89	1.77	
3	32.3	0.23	423	1.51	10	72	318	2.14	1.17	
4	27.0	0.42	423	1.51	10	55	318	2.80	1.83	

### **2.5.7 Sheikh and Khoury (1993, 1994)**

Sheikh and Khoury (1993) and Sheikh et al. (1994) conducted experimental research on six large-scale normal-strength concrete and four high-strength concrete column specimens. The concrete columns had a height of 72.5 in. and 12-in. square sections, resulting in a shear span-to-depth ratio of 6. The main test variables were the concrete strength, level of axial load, amount and configuration of transverse reinforcement. The primary objective of the investigation was to evaluate the confinement provisions of the ACI code. Table 2.7 illustrates the details of the specimens tested and the applied axial load levels.

Following are some of the reported conclusions that relate to the current experimental investigation:

- For the same amount of confining reinforcement required by the ACI 318 code, lower strength concrete columns displayed better ductility than comparable columns made with high-strength concrete and tested under similar  $P/f'_c A_g$ . However, for the same level of axial load measured as a fraction of  $P_o$ , high-strength concrete and normal-strength concrete columns behaved similarly in terms of energy-absorption characteristics when the amount of tie steel in the columns was in proportion to the unconfined concrete strength. Conversely, the amount of confining reinforcement required for a certain column performance appeared to be proportional to the concrete strength as long as the applied axial load was measured in terms of  $P_o$  rather than  $f'_c A_g$ .
- Confining reinforcement, designed according to the ACI code, can provide satisfactory behavior only for certain cases. Depending on the reinforcement detailing and axial load level, the code provisions may be unnecessarily conservative or unsafe.

**Table 2.7 Details of Specimens (Sheikh and Khoury 1993, 1994)**

Spec.	$f'_c$ (ksi)	Longitudinal Steel				Transverse Steel					$\frac{P}{f'_c A_g}$
		No. of bars	Size	$\rho_l$ (%)	$f_{yl}$ (ksi)	Size	Spacing (in.)	$\rho_s$ (%)	$f_{yh}$ (ksi)	$\frac{A_{sh}}{A_{sh,ACI}}$	
FS-9	4.70	8	#6	2.44	73.6	#3	3.75	1.68	73.6	1.46	0.76
ES-13	4.72	8	#6	2.44	73.6	#4	4.50	1.69	67.3	1.34	0.76
AS-3	4.81	8	#6	2.44	73.6	#3	4.25	1.68	73.6	1.43	0.60
AS-17	4.54	8	#6	2.44	73.6	#3	4.25	1.68	73.6	1.52	0.77
AS-18	4.75	8	#6	2.44	73.6	#4	4.25	3.06	67.3	2.41	0.77
AS-19	4.68	8	#6	2.44	73.6	#3, 6mm	4.25	1.30	73.6 67.0	1.12	0.47
AS-3H	7.86	8	#6	2.44	73.6	#3	4.25	1.68	73.6	0.88	0.62
AS-18H	7.93	8	#6	2.44	73.6	#4	4.25	3.06	67.3	1.44	0.64
AS-20H	7.78	8	#6	2.44	73.6	#4	3.00	4.30	67.3	2.10	0.64
A-17H	8.57	8	#6	2.44	73.6	#3	4.25	1.68	73.6	0.80	0.65

### 2.5.8 Bayrak and Sheikh (1997, 1999)

Bayrak and Sheikh (1997) and Bayrak (1999) tested twenty four square and rectangular concrete column specimens to investigate the behavior of high-strength concrete columns. The concrete strength used was in the range of 10,000 to 16,000 psi (72 to 112 MPa). Three different column sections were used with a height of 72.5 in. (1,841 mm), resulting in shear span-to-depth ratios of 6, 7.4 and 5.3 (Figure 2.10).

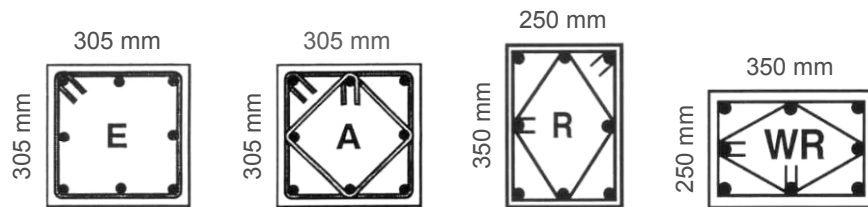


**Figure 2.10 Details of Transverse Reinforcement**  
(Baryak and Sheikh 1997, 1999)

**Table 2.8 Details of Specimens (Bayrak and Sheikh 1997, 1999)**

Spec.	$f'_c$ (MPa)	Longitudinal Steel				Transverse Steel				$\frac{P}{f'_c A_g}$
		No. of bars	Size	$\rho_l$ (%)	$f_{yl}$ (MPa)	Size	Spacing (mm)	$\rho_s$ (%)	$f_{yh}$ (MPa)	
ES-1HT	72.1	8	20M	2.58	454	15M	95	3.15	463	1.13
AS-2HT	71.7	8	20M	2.58	454	10M	90	2.84	542	1.19
AS-3HT	71.8	8	20M	2.58	454	10M	90	2.84	542	1.19
AS-4HT	71.9	8	20M	2.58	454	15M	100	5.12	463	1.83
AS-5HT	101.8	8	20M	2.58	454	10M 15M	90	4.83	542 463	1.08
AS-6HT	101.9	8	20M	2.58	454	15M	76	6.72	463	1.62
AS-7HT	102.0	8	20M	2.58	454	10M	94	2.72	542	0.80
ES-8HT	102.2	8	20M	2.58	454	15M	70	4.29	463	1.08
RS-9HT	71.2	8	20M	2.74	454	10M	80	3.44	542	1.72
RS-10HT	71.1	8	20M	2.74	454	10M	80	3.44	542	1.72
RS-11HT	70.8	8	20M	2.74	454	10M 15M	80	5.43	542 463	2.29
RS-12HT	70.9	8	20M	2.74	454	10M	150	1.83	542	0.92
RS-13HT	112.1	8	20M	2.74	454	10M	70	3.92	465	1.09
RS-14HT	112.1	8	20M	2.74	454	10M	70	3.92	465	1.09
RS-15HT	56.2	8	20M	2.74	454	10M	100	2.75	465	1.49
RS-16HT	56.2	8	20M	2.74	454	10M	150	1.83	465	1.00
RS-17HT	74.1	8	20M	2.74	521	8.0mm	75	1.83	1360*	1.39*
RS-18HT	74.1	8	20M	2.74	521	8.0mm	75	1.83	1360*	1.39*
RS-19HT	74.2	8	20M	2.74	521	11.1mm	75	3.54	1402*	2.67*
RS-20HT	74.2	8	20M	2.74	521	11.1mm	140	1.90	1402*	1.43*
WRS-21HT	91.3	8	20M	2.74	521	10M	70	3.92	465	0.89
WRS-22HT	91.3	8	20M	2.74	521	10M	70	3.92	465	0.89
WRS-23HT	72.2	8	20M	2.74	521	10M	80	3.44	542	1.15
WRS-24HT	72.2	8	20M	2.74	521	10M	80	3.44	542	1.15
										0.49

\*: The maximum average tie strain reached in Specimens RS-17HT, RS-19HT, and RS-20HT was 0.00425. Therefore, the maximum attainable strength of 850 was used in the calculation of  $A_{sh,ACI}$ .

The following are some of the conclusions reported by the authors:

- An increase in axial load reduces a reinforced concrete column's deformability and accelerates strength and stiffness degradation with every load cycle. To compensate for this effect, a larger amount of lateral reinforcement is required. Therefore, the axial load level should be incorporated as an important parameter in the design of confining reinforcement.
- Similar curvature ductility factors can correspond to different displacement ductility factors depending on section geometry and shear span-to-depth ratio. It was observed that the displacement ductility factors decreased with increasing shear span-to-depth ratios ( $L/h$ ). Member ductility parameters were influenced significantly by section geometry and shear span-to-depth ratio, while section ductility parameters were not affected by these factors.

## **2.6 EXAMINATION OF PREVIOUS EXPERIMENTAL RESEARCH**

In this chapter, experimental research on the seismic performance of reinforced concrete columns is summarized. The following are the observations made on the key findings or conclusions reached by the previous researchers:

- Extensive research on reinforced concrete column behavior has been conducted to study the effects of the amount and detailing of confining reinforcement and the level of axial load. However, little attention was given to the relationship among various parameters to define the deformation capacity of a column, such as curvature ductility, displacement ductility, or drift capacity.
- Bayrak (1999) reported that similar curvature ductilities could correspond to different displacement ductilities depending on section geometry and

shear span-to-depth ratio. This observation is consistent with Park and Paulay's relationship (Equation (2.20)). However, Bayrak (1999) made no further attempt to study the relationship among various ductility parameters.

- Tests on large-scale concrete columns have been rarely conducted. The size of column specimens in most research reports ranges between 6 in. and 16 in. Even though Park et al. (1982) and Tanaka and Park (1990) conducted full-scale column tests ( $22 \times 22$  in.<sup>2</sup>), the shear span-to-depth ratio of column specimens were very small ( $2.18 \leq L/h \leq 3$ ). Considering the fact that the shear span-to-depth ratio can affect the deformation capacity of columns and the relationship among ductility parameters, the need to conduct further experimental research on full-scale concrete columns with moderate shear span-to-depth ratios can be appreciated.

# **CHAPTER 3**

## **EXPERIMENTAL PROGRAM**

### **3.1 INTRODUCTION**

Current design codes and performance-based design procedures were presented in the previous chapter. Previous tests reported in the literature were also discussed. Considering the conclusions drawn in Section 2.6, the experimental work was designed to investigate the effects of shear span-to-depth ratio ( $L/h$ ), axial load level ( $P/P_o$ ), and amount of confining reinforcement ( $A_{sh}$ ) on column behavior. A high capacity column tester was designed and constructed at the University of Texas at Austin for this research. The test frame is capable of applying and maintaining axial loads up to 2,000 kips and reversed cyclic moments as large as 4,000 ft-kips. In this chapter, a description of the mechanical properties of the materials used, details, fabrication and instrumentation of the column specimens are presented. In addition, the test setup, loading protocol and testing procedure are described.

### **3.2 MATERIAL PROPERTIES OF COLUMN SPECIMENS**

In order to assess the actual strength of the column specimens, it was necessary to evaluate the stress-strain response of the materials used. Tensile tests for the reinforcing steel and compression tests for the concrete were carried out.

#### **3.2.1 Steel**

Three tensile coupons were tested for each bar size used in this study. Preparation of specimens was performed in accordance with ASTM A 370-03a. A gage length of 8 in. was used, and a clear distance of at least two bar diameters

was left between the gage mark and the testing machine grip. An average of three tests was used to obtain a typical tensile stress-strain response for each bar size.

Grade 60 No. 5, No. 9 and two different types of No. 7 bars were used as longitudinal steel in the columns tested. The stress-strain curves of the longitudinal steel, as obtained from the tension tests, are shown in Figure 3.1.

Two different types of No. 3 and three different types of No. 4 Grade 60 bars were used as transverse reinforcement. The stress-strain curves of transverse reinforcing steel are shown in Figure 3.2. This figure illustrates that the stress-strain curve for No. 3-2 and No. 4-3 bars exhibit an initial linear elastic portion, but they do not exhibit a well-defined yield plateau. According to ASTM A 370-03a, the yield strengths for No. 3-2 and No. 4-3 bars, which lack a well defined yield point, are estimated using the 0.2% offset method. Values of yield stress ( $f_y$ ), yield strain ( $\varepsilon_y$ ), modulus of elasticity ( $E$ ), strain at which the strain hardening starts ( $\varepsilon_{sh}$ ), ultimate stress ( $f_{su}$ ), and strain corresponding to ultimate stress ( $\varepsilon_{su}$ ) for each type of steel are given in Table 3.1.

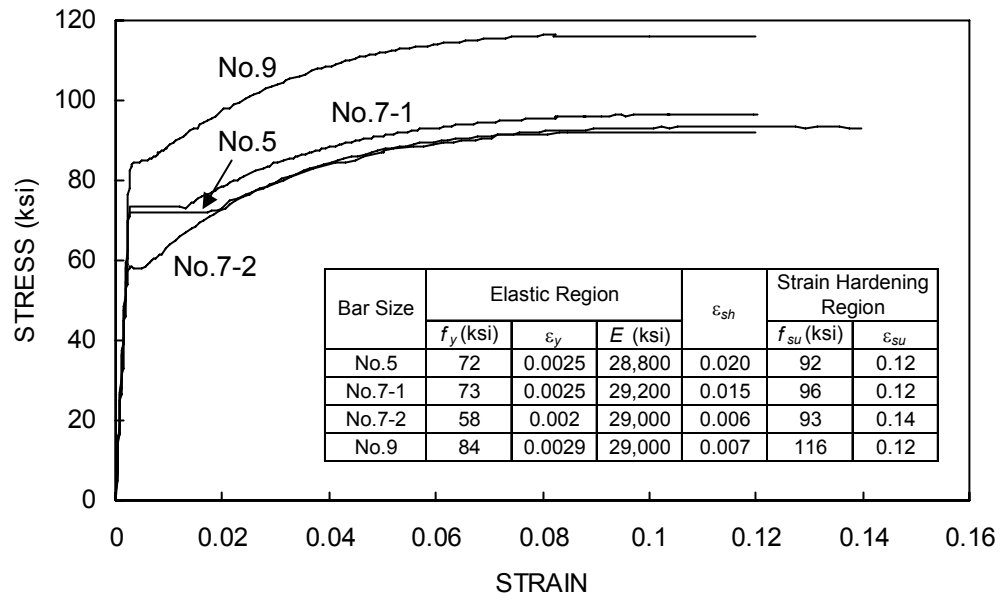


**Figure 3.1 Stress-Stain Curves for Longitudinal Reinforcing Steel**

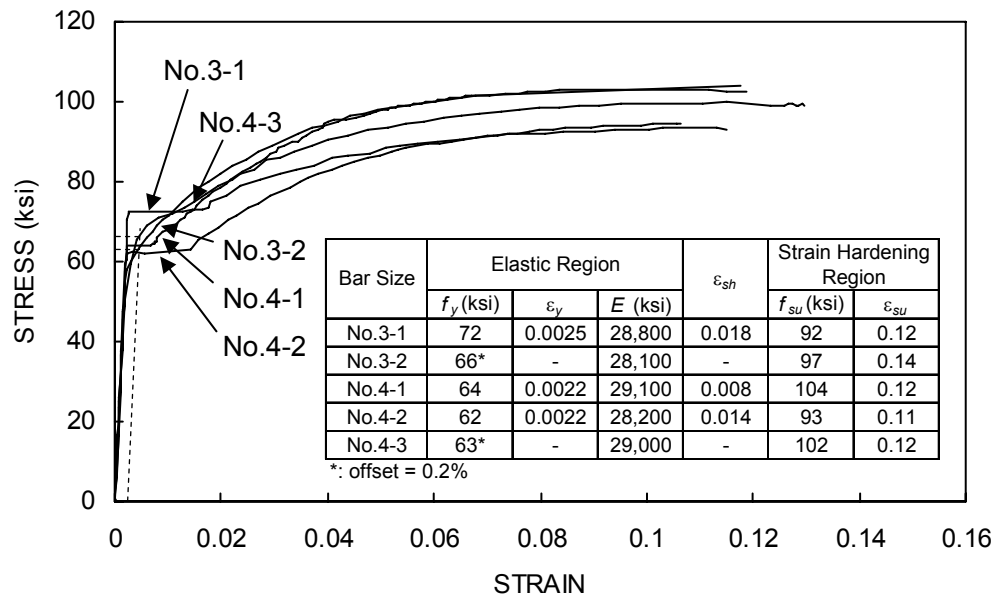


**Figure 3.2 Stress-Stain Curves for Transverse Reinforcing Steel**

**Table 3.1 Material Properties of Reinforcing Steel**

Bar Size	Elastic Region			$\epsilon_{sh}$	Strain Hardening Region	
	$f_y$ (ksi)	$\epsilon_y$	$E$ (ksi)		$f_{su}$ (ksi)	$\epsilon_{su}$
No. 5	72	0.0025	28,800	0.020	92	0.12
No. 7-1	73	0.0025	29,200	0.015	96	0.12
No. 7-2	58	0.0020	29,000	0.006	93	0.14
No. 9	84	0.0029	29,000	0.007	116	0.12
No. 3-1	72	0.0025	28,800	0.018	92	0.12
No. 3-2	66*	-	28,100	-	97	0.14
No. 4-1	64	0.0022	29,100	0.008	104	0.12
No. 4-2	62	0.0022	28,200	0.014	93	0.11
No. 4-3	63*	-	29,000	-	102	0.12

\*: The bars lacked a well-defined yield point ( $f_y$  is calculated using the 0.2% offset method).

### 3.2.2 Concrete

The concrete used in all specimens was delivered by a ready mix supplier in Austin. The specified nominal 28 day strength was 4,000 psi for the first specimen and 6,000 psi for the other specimens. The slump and maximum aggregate size were specified as 6 in. and 3/8 in., respectively. The 6×12-in.<sup>2</sup> concrete cylinders were cured adjacent to the specimens under very similar curing conditions. The concrete strength of each specimen was determined by standard cylinder tests just prior to testing (Table 3.2). Three 6×12-in.<sup>2</sup> (150×305-mm<sup>2</sup>) concrete cylinders were used to determine the compressive strength of concrete used in each test specimen. All cylinder tests were conducted in accordance with ASTM C 39C.

**Table 3.2 Concrete Strengths**

Specimen	Concrete Strength		Age at Test (days)
	$f'_c$ (psi)	$f'_c$ (MPa)	
S24-1UT	4,300	29.6	195
S24-2UT	6,300	43.4	83
S17-3UT	6,300	43.4	114
S24-4UT	5,300	36.5	46
S24-5UT	6,000	41.4	100

### 3.3 SPECIMENS

The column specimens can be visualized as one-half of a column bent in double curvature, as illustrated in Figure 3.3. Four of the test specimens used in this experimental program consisted of  $24 \times 24 \times 103.5\text{-in.}^3$  ( $610 \times 610 \times 2,630\text{-mm}^3$ ) columns and  $38 \times 38 \times 80\text{-in.}^3$  ( $97 \times 97 \times 203\text{-mm}^3$ ) stubs. One specimen (S17-3UT) had a 17.25-in. (440-mm) square cross section. The details of specimens are shown in Figure 3.4. The core size, measured from center-to-center of perimeter hoops, was  $20.6 \times 20.6\text{ in.}^2$  ( $523 \times 523\text{ mm}^2$ ) for all 24-in. (610-mm) square specimens and 15.6 in. (397 mm) for the 17.25-in. (440-mm) square specimen. The details of the specimens tested in this research program and the axial load level applied to each specimen during testing are given in Table 3.3.

Each of the five specimens can be identified by a unique notation. The notation is explained in Figure 3.5. The first letter “S” represents a square cross-section. The following number, “24” or “17”, indicates the size of column sections. The numbers from 1 to 5 show the sequence of the tests. The last two letters, “UT”, are used to indicate that the specimens were constructed and tested at the University of Texas at Austin.

All five specimens were cast horizontally with two specimens in each casting, except the first specimen. This first specimen was used in a pilot test to check the performance of test setup. After testing this specimen, the instrumentation, data acquisition system and test setup were slightly modified.

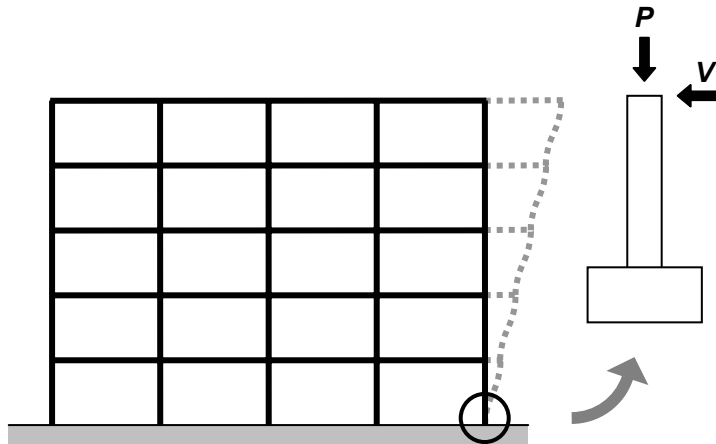


**Figure 3.3 Modeling of Column Specimen**

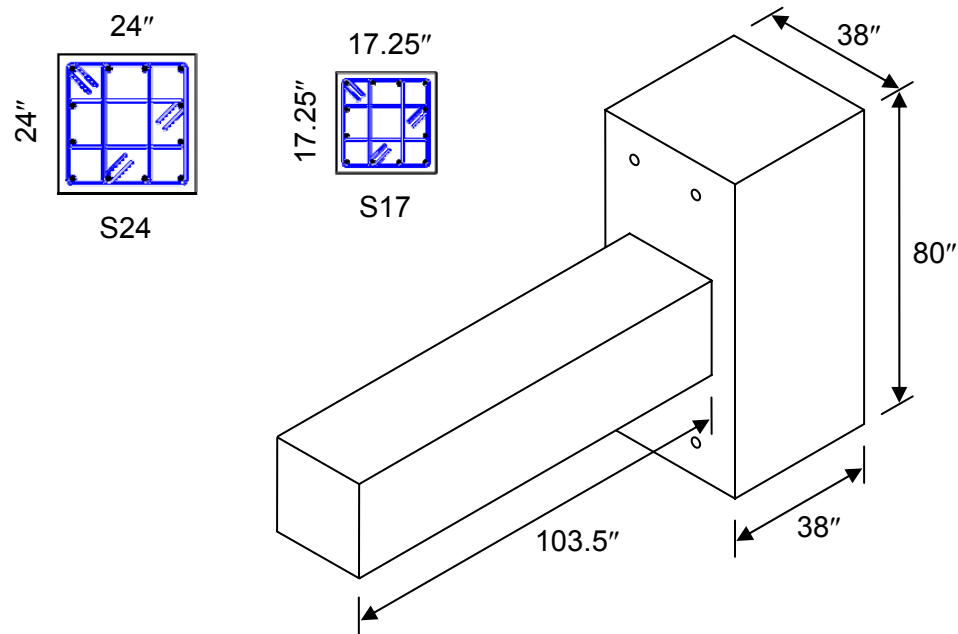


**Figure 3.4 Layout of Test Specimens**

**Table 3.3 Details of Test Specimens**

Spec.	$b \times h$ (in.×in.)	$f'_c$ (ksi)	Longitudinal Steel			Transverse Steel					$\frac{P}{P_o^{**}}$
			ID	$\rho_l$ (%)	$f_{yl}$ (ksi)	ID	$s_h$ (in.)	$\rho_s^*$ (%)	$f_{yh}$ (ksi)	$\frac{A_{sh}}{A_{sh,ACI}}$	
S24-1UT	24×24	4.3	No.9	2.08	84	No.4-1	6	1.28	64	1.04	0.5
S24-2UT	24×24	6.3	No.7-1	1.25	73	No.4-2	3-3/4	2.04	62	1.09	0.5
S17-3UT	17.25×17.25	6.3	No.5	1.25	72	No.3-1	3-3/8	1.76	72	1.12	0.5
S24-4UT	24×24	5.3	No.7-2	1.25	58	No.3-2	6	0.72	66	0.44	0.2
S24-5UT	24×24	6.0	No.7-2	1.25	58	No.4-3	6	1.30	63	0.74	0.2

\*:  $\rho_s$  = volumetric ratio of transverse reinforcement to core concrete

\*\*:  $P_o = 0.85f'_c A_c + f_{yl} A_s$

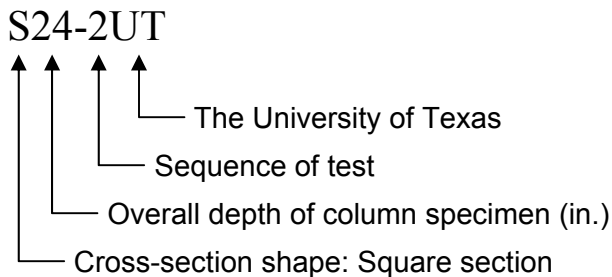


**Figure 3.5 Nomenclature for Column Specimens**

### 3.4 CONSTRUCTION OF COLUMN SPECIMENS

In this section, construction of the test specimens is described. More specifically, the construction of forms, instrumentation of reinforcing bars, assembly of the reinforcing cages, concrete casting, and specimen curing are described.

### 3.4.1 Formwork

The formwork was constructed with 3/4-in. thick plywood and 2×4-in.<sup>2</sup> studs. On the concrete floor, 4×4-in.<sup>2</sup> sections of lumber was placed, leveled, and covered by 3/4-in. thick plywood to provide a flat surface for the formwork. The forms were constructed on the top of this flat surface. Because of the large mass of concrete in each specimen, the column specimens were cast horizontally. For the same reason and in order to keep tight tolerances on specimen dimensions, very stiff formwork was required to prevent any significant movement during concrete casting. To achieve a satisfactory level of stiffness, side panels were horizontally braced with 2×4-in.<sup>2</sup> lumber. All side panels were also attached to neighboring panels by threaded rods.

Before placing the reinforcing cages, the form was cleaned and a light coat of form-release oil was applied to prevent water absorption during curing of the concrete. Thirteen holes were drilled at either end of each form and 7/8-in. diameter threaded rods were installed. These rods were later used to connect a specimen to the testing frame. Before placing concrete, four PVC pipes were placed in the stub forms and one PVC pipe in the column form, as shown in Figure 3.6. The holes made by the PVC pipes were later used as a means of attaching swivel hoist rings to lift and install the specimen to the test frame. During concrete placement, threaded rods passing through these PVC pipes were used to provide lateral restraint to the side panels of the stub forms.

In a similar way, six 1/2-in. diameter threaded rods were installed vertically in the column form near the stub form (Figure 3.6). These rods were later used to mount instrumentation. Rods passing through the concrete core made it possible to measure inelastic strains experienced by the core concrete after cover spalling took place.



*Figure 3.6 Formwork before Concrete Casting*

### 3.4.2 Instrumentation of Reinforcing Bars

Strains in the reinforcing bars were measured through strain gauges installed on longitudinal and transverse reinforcement. A total of 12 strain gauges were attached to longitudinal bars. Strains experienced by tie steel were measured at 21 (or 24) discrete locations, as shown in Figure 3.7.

Strain gauges were installed following the manufacturer's standard strain gauge installation procedure. First, ribs of the reinforcing bars at strain gauge locations were removed by grinding them. Then, the surface was cleaned with M-Preparation Conditioner A and Neutralizer 5A. TML strain gauges (FLA 5-11-3LT) were used. Strain gauges were attached to the prepared steel surface with CN strain gauge adhesive. Finally, M-Coat D was used to cover the strain gauges for waterproofing purposes. After three layers of waterproof coating were applied to the gauge surface, a 1/16-in. thick neoprene rubber was placed on the top to

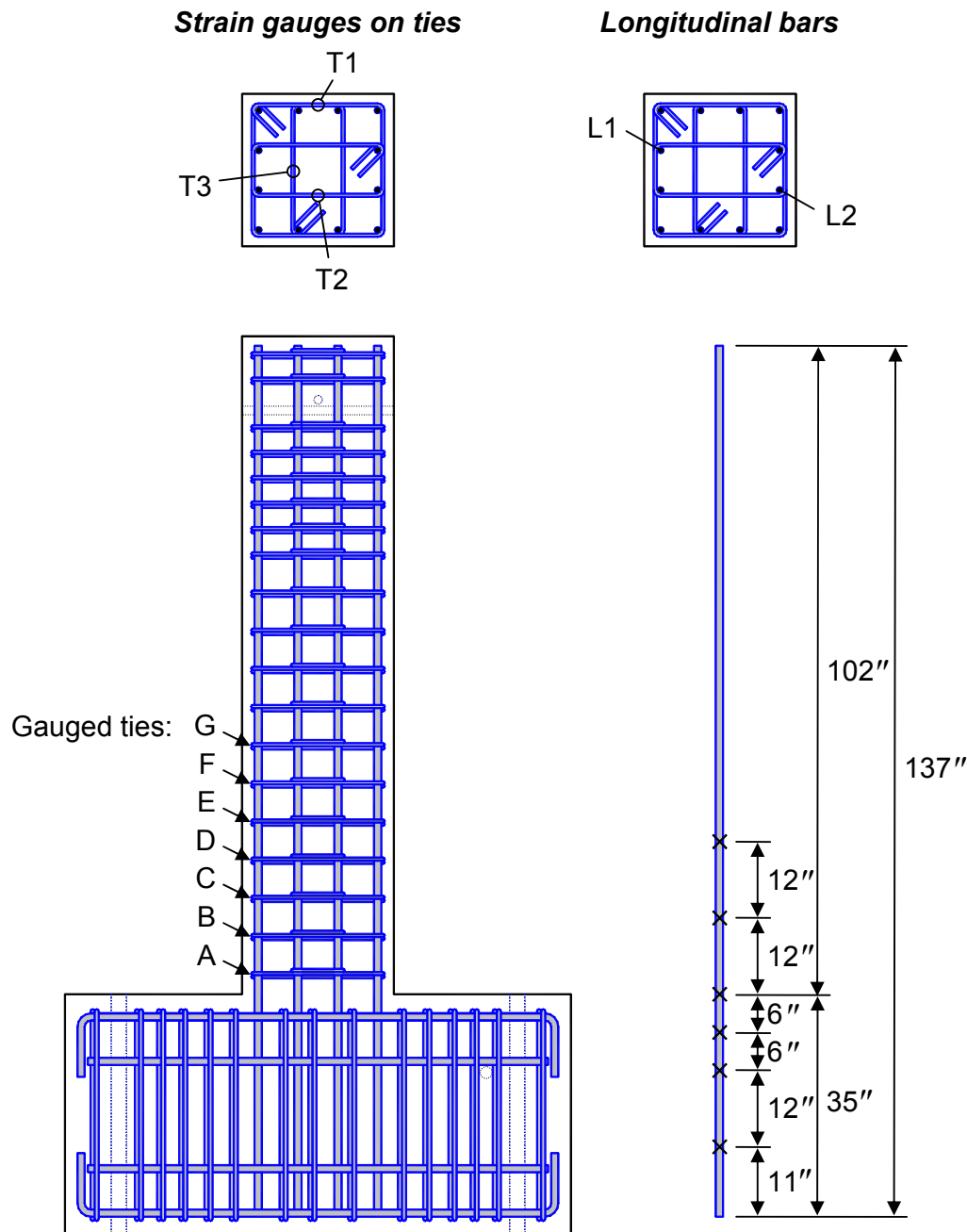


*Figure 3.7 Location of Strain Gauges*

prevent damage to the gauges during concrete placement. Finally, the surface was covered with aluminum tape.

In all specimens, two longitudinal bars were instrumented with six strain gauges (Figure 3.7). The first seven sets of ties in the column near the stub (eight sets of ties for S24-2UT and S24-4UT) were instrumented with 3 strain gauges.

### 3.4.3 Reinforcing Cages

Each reinforcing cage consisted of two parts: a cage for the column and a cage for the stub. They were assembled separately. The stub cage was placed in the form and then the column cage was placed and connected to the stub cage. The reinforcement for the stub cage consisted of No. 9 longitudinal bars and No. 4 stirrups at 4-in. spacing.

Flexural bars used in the column cage were extended through the stub cage. A clear cover of 1.5 in. was used in all test specimens, except S17-3UT, where the cover thickness was reduced to 1 in. The ties were placed at the predetermined spacing within the test regions of the columns, i.e., within 50 in. from the stub's face; after that point spacing was relaxed. Figure 3.8 shows the construction of the column cage.

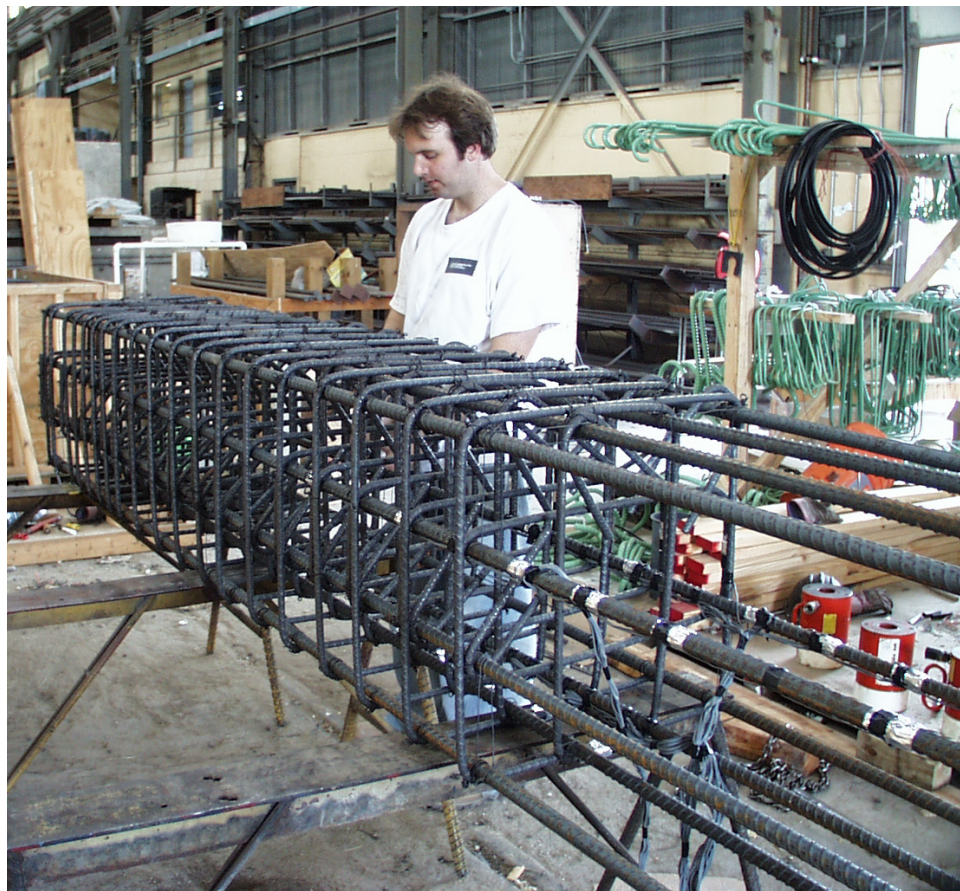


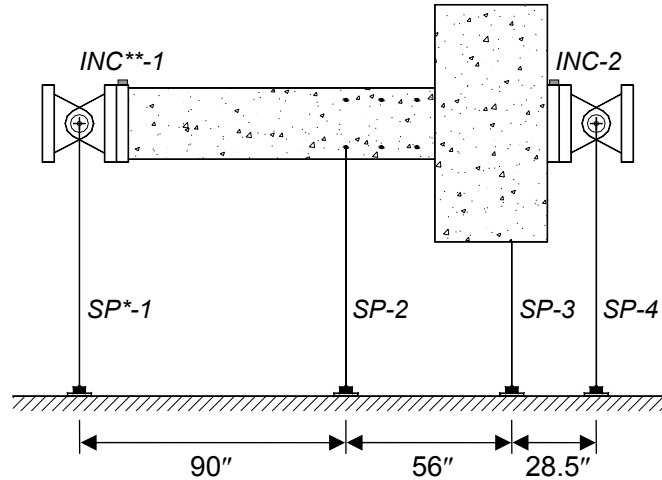
***Figure 3.8 Construction of Column Cage***

#### **3.4.4 Casting and Curing**

All specimens were cast in the horizontal position and rod vibrators were used to consolidate concrete. Twenty 6×12-in.<sup>2</sup> concrete cylinders were cast along with the test specimens for every batch of concrete. After concrete placement, the top surface and sides of the formwork were covered with burlap and plastic sheets to provide a moist curing environment. The forms were removed after 2 weeks. The 6×12-in.<sup>2</sup> concrete cylinders were cured adjacent to the specimens under very similar curing conditions.

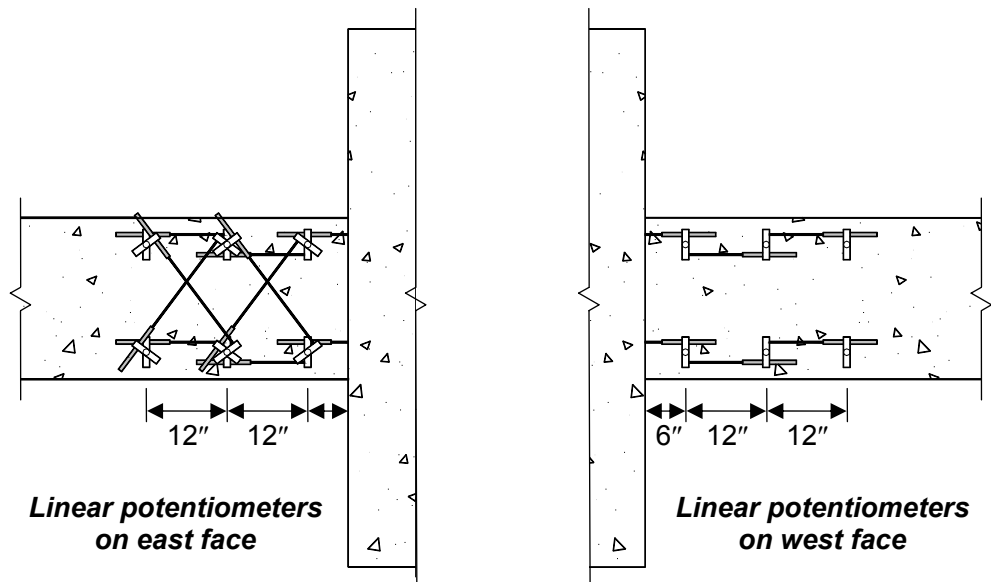
### **3.5 INSTRUMENTATION OF THE SPECIMENS**

Instrumentation of the reinforcing bars was described in detail in Section 3.4.2. The deformations of the concrete core were measured using 16 linear potentiometers. Transverse displacements of test specimens were also measured at four different locations along their lengths using string potentiometers. Two inclinometers were attached at both ends of test specimens to measure the rotations. Therefore, each test specimen was instrumented with a total of 33 (or 37) strain gauges, 16 linear potentiometers, 4 string potentiometers, and 2 inclinometers. Figure 3.9 illustrates locations of the linear potentiometers, string potentiometers, and inclinometers. Figure 3.10 shows the typical linear potentiometer arrangement. Figure 3.11 shows inclinometers attached at both ends of test specimens.



### ***String potentiometers and inclinometers***

(\*: String potentiometer; \*\*: Inclinometer)



Note: The locations of linear potentiometers are described for a specimen with 24-in. square section. These dimensions are scaled down proportionally for specimen S17-3UT.

***Figure 3.9 Locations of Linear Potentiometers, String Potentiometers and Inclinometers***

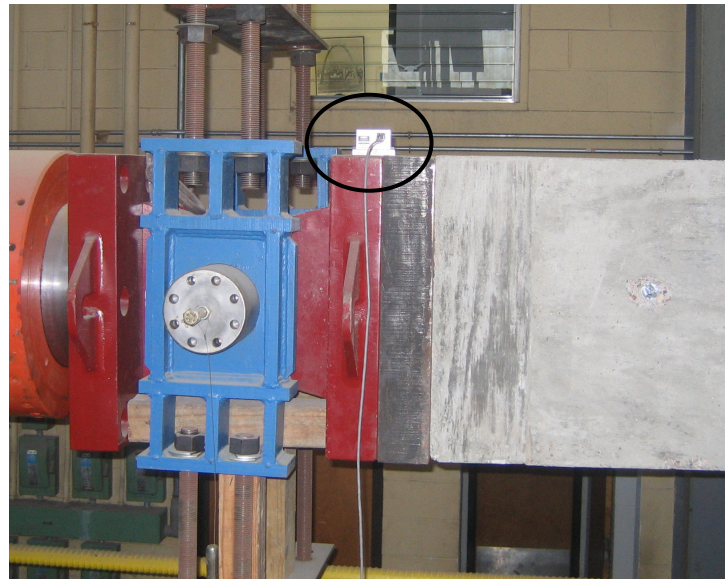


(a) East Face



(b) West Face

*Figure 3.10 Installation of Linear Potentiometers*



(a) Tip of Column Specimen



(b) Bottom of Column Specimen

**Figure 3.11 Installation of Inclinometers**

### **3.6 TEST SETUP**

In order to conduct tests on full-scale columns, a high-capacity test facility was designed and fabricated. Various details and design calculations pertinent to this test setup are included in Appendix A. Over 100,000 pounds of manufactured structural steel was used in the construction of the self-contained high-capacity reaction frame (Figure 3.12). Two 400-kip displacement-controlled ( $\pm 12$  in.) actuators capable of delivering reversed cyclic moments as large as 4,000 ft-kip are used in this test facility. The axial load acting on a column specimen is delivered through a hydraulic ram with a 2-million lb capacity.

Twenty-six high strength threaded rods were cast integrally with each test specimen. These rods were used to mount 4 in.-thick adapter plates. These adapter plates allowed for the installation of a specimen into the test frame. Specimen installation is illustrated in Figure 3.13.

62

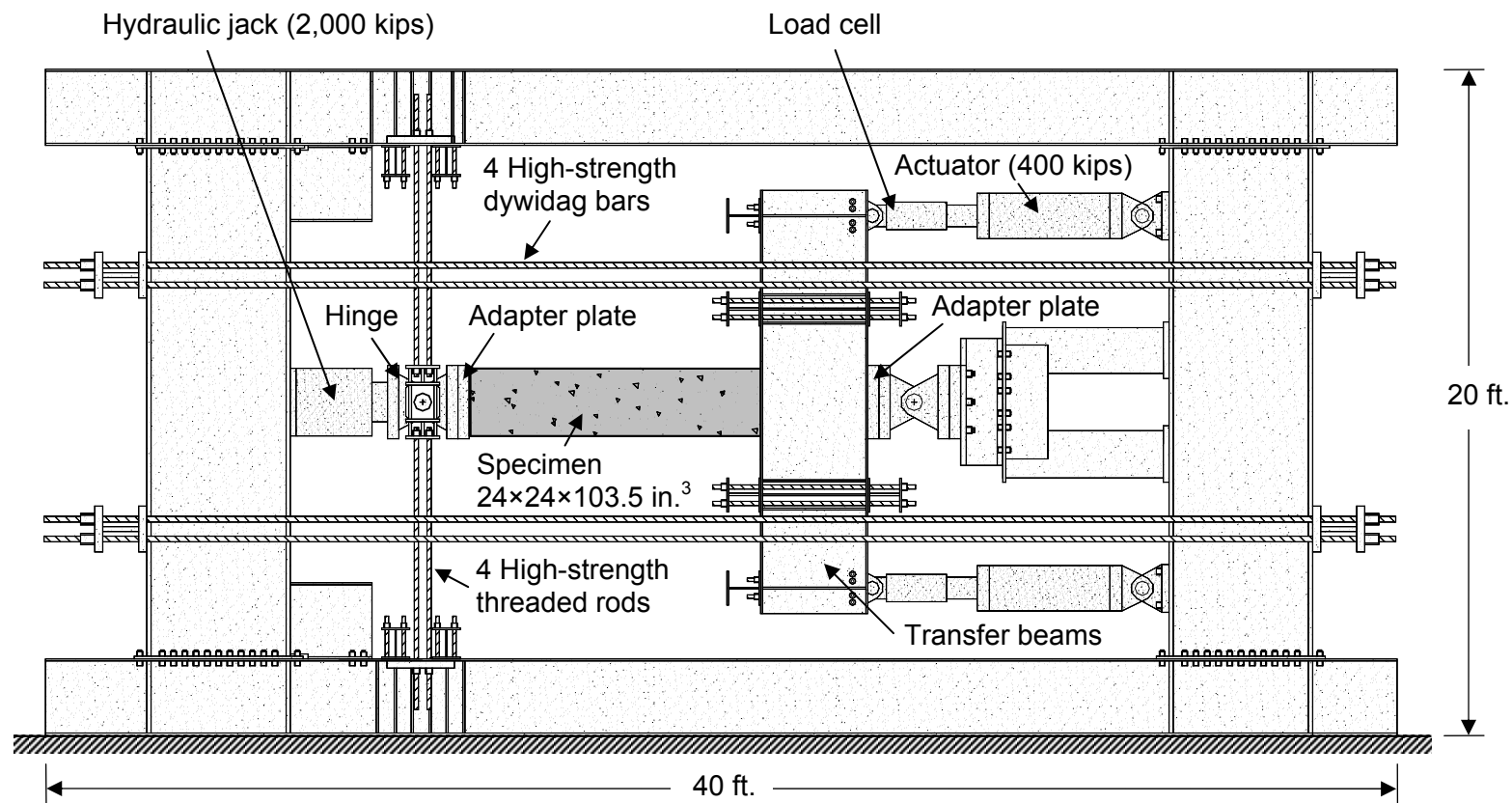
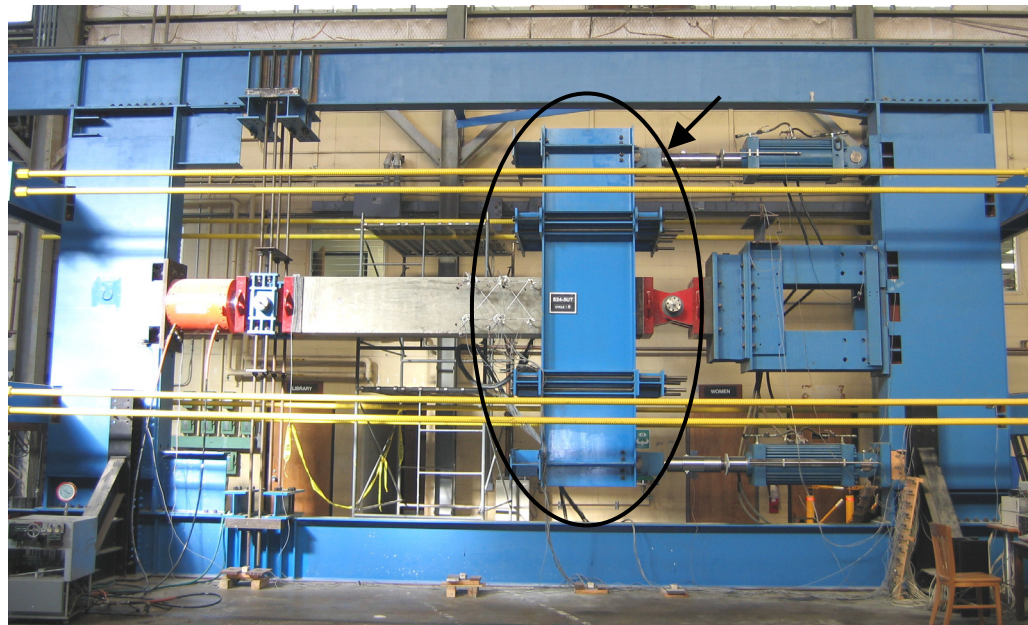


Figure 3.12 Test Setup



(a) Installation of a Column Specimen



(b) Installation of Transfer Beams

*Figure 3.13 Specimen Installation*

### **3.7 TESTING**

At the beginning of each test, axial load was applied to the column specimen. Through the use of a load maintainer, the axial load was kept constant during the test. After the application of the axial load, the specimen was subjected to progressively increasing lateral displacement cycles following the displacement protocol, shown in Figure 3.14. As such, three fully reversed cycles were applied for each displacement step as required by FEMA 356 (2000) and ACI ITG/T1.1 (2001).

At the first displacement cycle, approximately 75% of the predicted maximum column shear strength was applied in both the positive and negative directions. From the resulting load-displacement response, an experimental value for the yield displacement ( $\Delta_y$ ) was calculated by extrapolating a straight line from the origin through the peak load-displacement coordinate at  $0.75V_{max}$  to the predicted maximum load ( $V_{max}$ ). This procedure is illustrated in Figure 3.15. The yield displacement ( $\Delta_y$ ) used in the tests was the average of the values found in both directions.

### **3.8 SUMMARY**

In this chapter, specimen preparation and construction were discussed in detail. Mechanical properties of the materials used, geometric properties of test specimens and reinforcing bar details were described. In addition, the loading protocol used in the experimental program was also given.

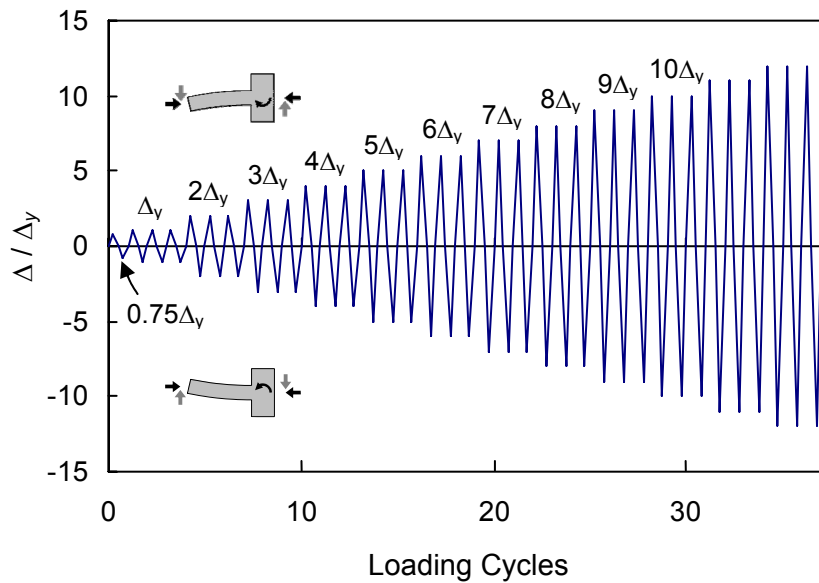


**Figure 3.14 Typical Lateral Displacement History**

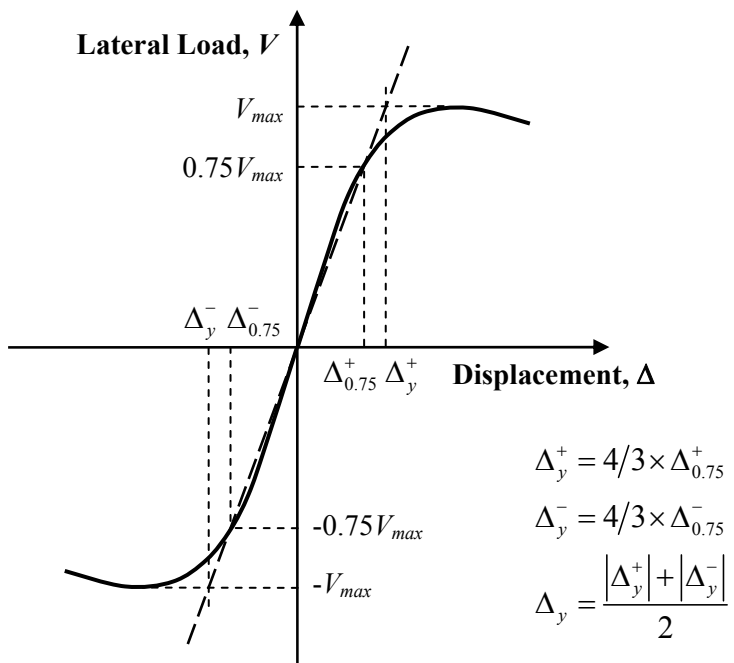


**Figure 3.15 Definition of Yield Displacement**

# CHAPTER 4

## TEST RESULTS

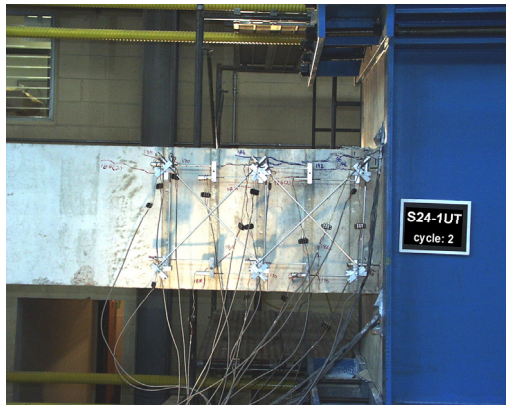
### 4.1 INTRODUCTION

Results from five column tests are reported in this chapter. The column specimens were tested under constant axial loads and reversed cyclic lateral displacement excursions. In Section 4.2, the observations made during the tests are reported. The response of specimens is presented in Section 4.3, followed by discussions on the backbone curves and ductility parameters.

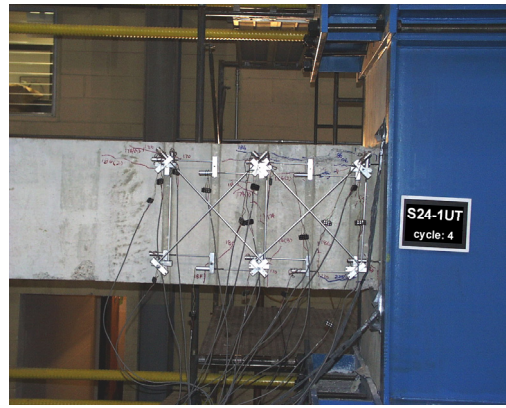
### 4.2 TEST OBSERVATIONS

Figures 4.1 through 4.5 show the progression of damage and failure for each column. Figure 4.6 shows test specimens at the end of tests. For all of the tested specimens, flexural cracks in the columns were observed adjacent to the stub. The location of the first flexural crack was about 6 in. away from the stub.

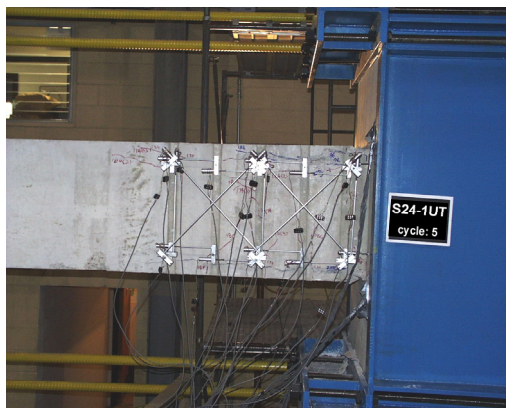
At  $\mu_{\Delta} = 2$ , longitudinal cracks along flexural reinforcement in the compression region occurred suddenly. This was accompanied by a slight reduction in flexural capacity. The loss of flexural strength was regained due to confining pressure applied by the transverse reinforcement and strain hardening of longitudinal reinforcement. The top and bottom cover concrete spalled off along the splitting cracks in the following cycles. During the eighth cycle ( $\mu_{\Delta} = 3$ ), cracking propagated to the sides of column specimens. Subsequently, cover spalling at the sides of column specimens was observed.



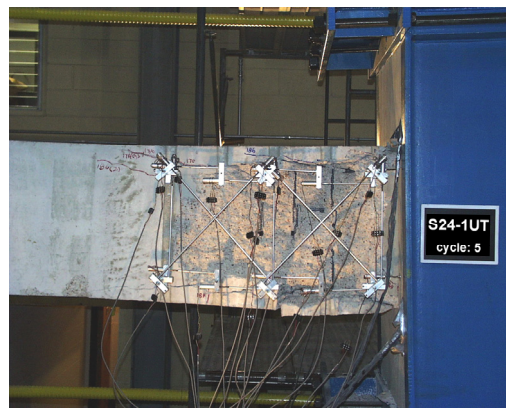
(a)  $\mu_{\Delta} = 1$



(b)  $\mu_{\Delta} = 1$



(c)  $\mu_{\Delta} = 3$



(d)  $\mu_{\Delta} = 4$

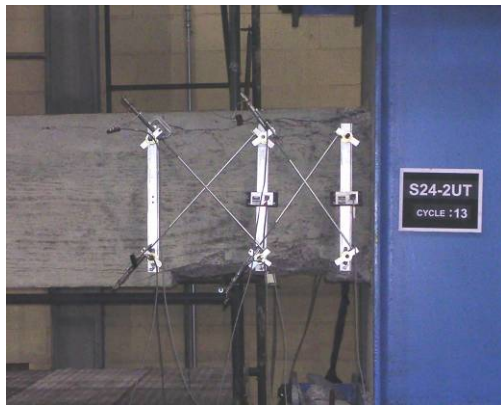


(e)  $\mu_{\Delta} = 5$

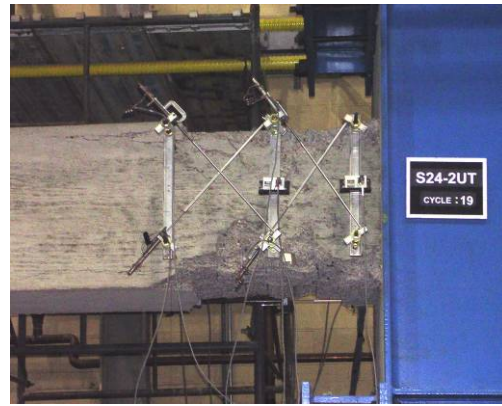


(f)  $\mu_{\Delta} = 5$

*Figure 4.1 Specimen S24-1UT*



(a)  $\mu_{\Delta} = 3$



(b)  $\mu_{\Delta} = 4$



(c)  $\mu_{\Delta} = 5$



(d)  $\mu_{\Delta} = 7$



(e)  $\mu_{\Delta} = 7$



(f)  $\mu_{\Delta} = 7$

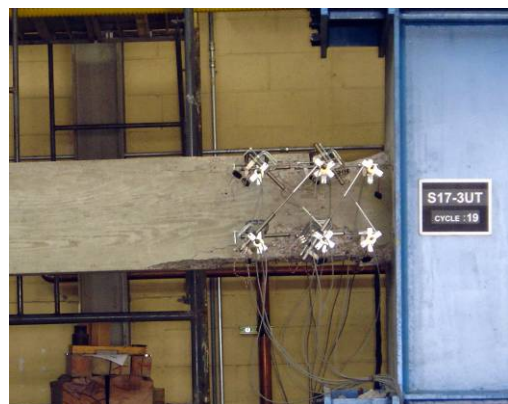
*Figure 4.2 Specimen S24-2UT*



(a)  $\mu_{\Delta} = 2$



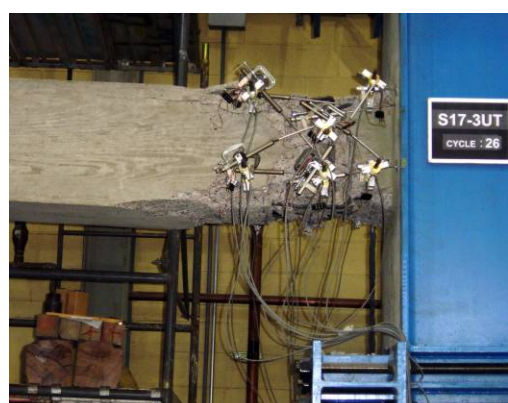
(b)  $\mu_{\Delta} = 3$



(c)  $\mu_{\Delta} = 4$



(d)  $\mu_{\Delta} = 6$



(e)  $\mu_{\Delta} = 7$

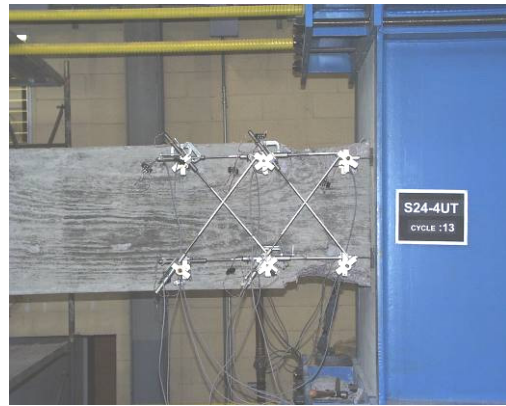


(f)  $\mu_{\Delta} = 7$

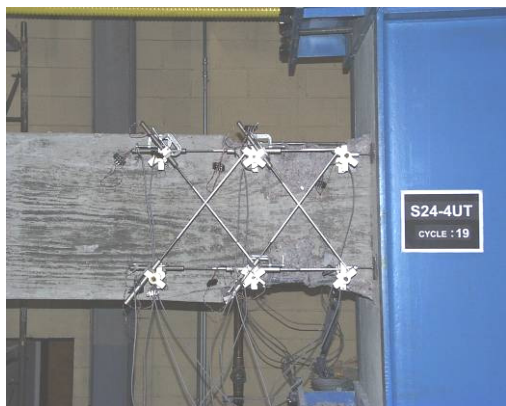
*Figure 4.3 Specimen S17-3UT*



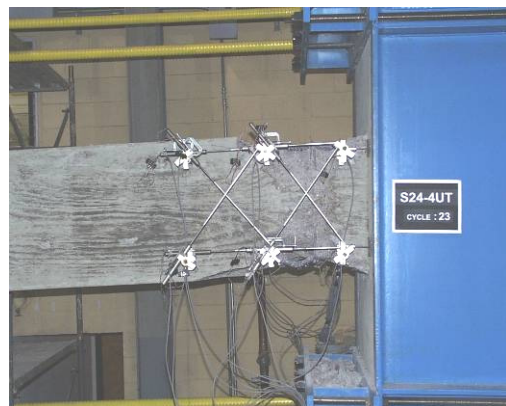
(a)  $\mu_{\Delta} = 2$



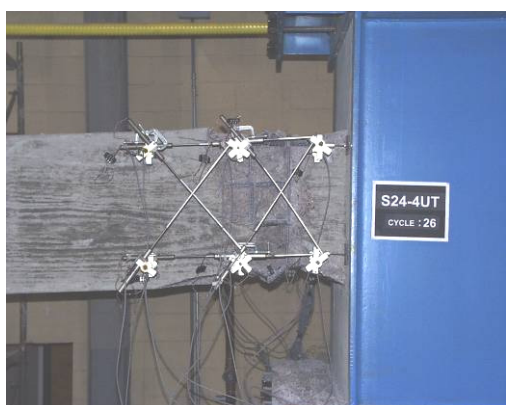
(b)  $\mu_{\Delta} = 3$



(c)  $\mu_{\Delta} = 5$



(d)  $\mu_{\Delta} = 6$



(e)  $\mu_{\Delta} = 7$

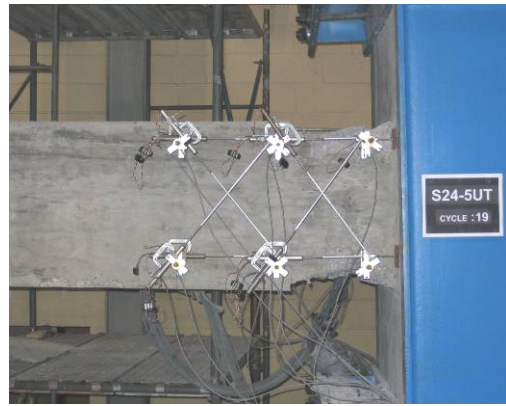


(f)  $\mu_{\Delta} = 8$

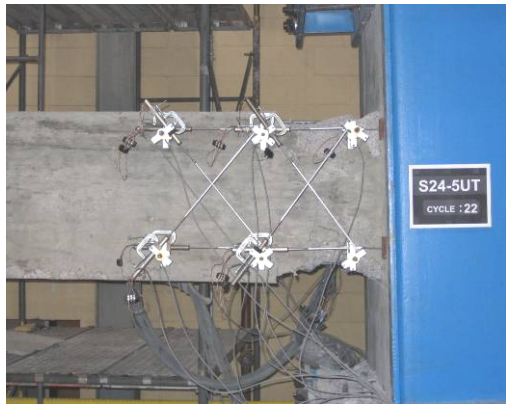
*Figure 4.4 Specimen S24-4UT*



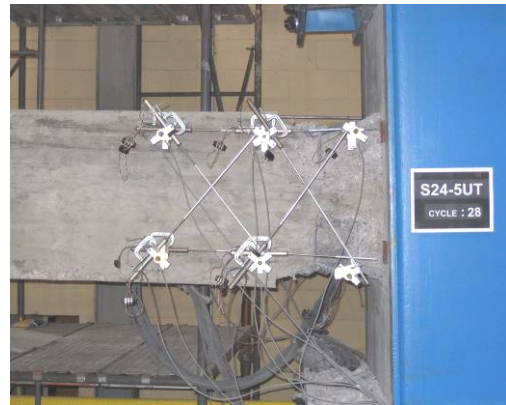
(a)  $\mu_{\Delta} = 4$



(b)  $\mu_{\Delta} = 5$



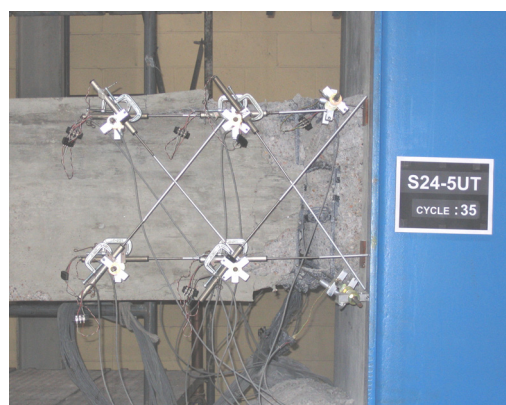
(c)  $\mu_{\Delta} = 6$



(d)  $\mu_{\Delta} = 8$

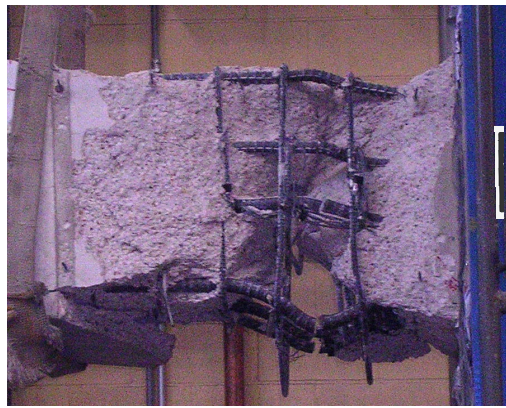


(e)  $\mu_{\Delta} = 9$



(f)  $\mu_{\Delta} = 10$

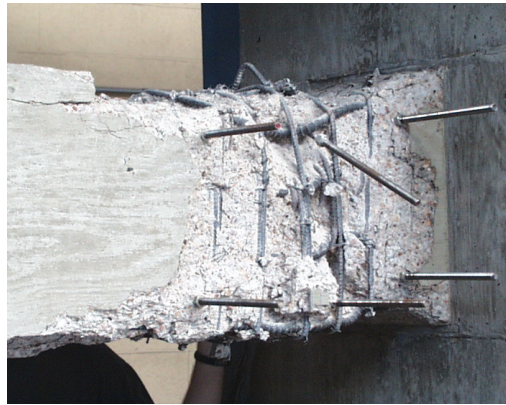
*Figure 4.5 Specimen S24-5UT*



(a) S24-1UT



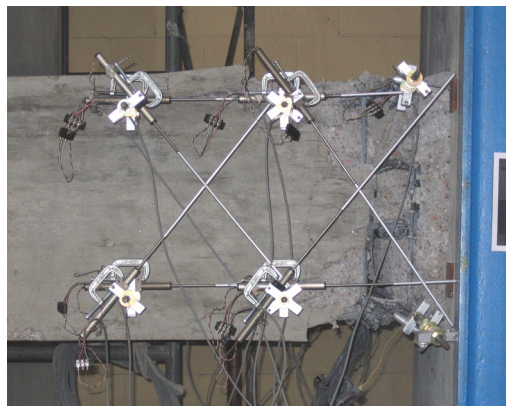
(b) S24-2UT



(c) S17-3UT



(d) S24-4UT



(e) S24-5UT

*Figure 4.6 Comparison of Failure of All Test Specimens*

Spalling of the top and bottom cover concrete extended from the face of the stub to the column for a distance of about 30 in. (760 mm) to 48 in. (1200 mm). The top and bottom cover concrete was completely spalled off at around  $\mu_\Delta = 4$ .

The initiation of longitudinal bar buckling was observed around at  $\mu_\Delta = 4$  to 6. Specimens of S24-1UT, S24-2UT and S17-3UT, tested under high axial loads ( $P = 0.5P_o$ ), experienced a sudden failure. At  $\mu_\Delta = 6$  to 8, these specimens could not sustain the applied axial loads due to the excessive damage of core concrete and failed in an axial load collapse mode. Before the axial load collapse, low-cycle fatigue fracture was observed in some of the longitudinal bars.

For specimens of S24-4UT and S24-5UT, tested under low axial loads ( $P = 0.2P_o$ ), all top and bottom longitudinal bars buckled and ruptured at  $\mu_\Delta = 6$  to 8. The residual flexural capacities were significantly reduced after these displacement levels. These specimens, however, could continue to support the applied axial loads, and failure was not observed until the specimens were subjected to slightly larger lateral displacements ( $\mu_\Delta = 8$  to 10). As the lateral displacements became larger, crushing of concrete within the core progressed and the remaining flexural capacity was further reduced. Finally, these specimens failed immediately after the buckling of the intermediate layers of longitudinal bars and extensive crushing of core concrete.

To avoid premature failure due to longitudinal bar buckling, Chapter 21 provisions of the ACI 318 code require the tie spacing-to-longitudinal bar diameter ratio of less than 6 in potential plastic hinge regions. Similar tie spacing limits were recommended by Mander et al. (1988) and Mau and El-Mabsout (1989). For the specimens tested under high axial loads ( $0.5P_o$ ), the tie spacing-to-longitudinal bar diameter ratio ranged between 4.3 and 5.4, satisfying the ACI code requirements. For specimens S24-4UT and S24-5UT, tested under low axial

loads ( $P = 0.2P_o$ ), the tie spacing-to-longitudinal bar diameter ratio was relaxed to 6.9. Premature bar buckling was not observed in the tests. At very large inelastic curvatures, many longitudinal bars buckled due to severe damage of core concrete. As the core concrete experienced severe damage, the restraint from core concrete reduced; in order to maintain equilibrium, longitudinal bars were forced to carry additional compressive forces. Scribner (1986) reported that even large, closely spaced ties ( $3d_b$ ) could not prevent buckling of reinforcing bars subjected to very large inelastic strains.

As can be seen in Figure 4.7, Chapter 21 of the ACI 318-05 code requires the use of hook lengths greater than  $6d_b$  or 3 in. for  $135^\circ$  hooked anchorages to avoid opening of hoops. The hook length used in specimen S24-1UT was 4 in. ( $8d_b$ ). However, two sets of hoops in the plastic hinge region completely opened during the final stages of testing, as shown in Figure 4.8. Following this observation, the hook length was increased to 7.5 in. ( $15d_b$ ) for the remaining specimens to prevent the opening of the hoops. Such a large hook length proved to be very effective, and opening of  $135^\circ$  hooked anchorages of the ties was not observed in the other tests.

The longitudinal bars are generally assumed to buckle outward from core concrete. However, the longitudinal bars in specimens of S24-2UT and S17-3UT buckled in various directions. Some buckling modes involved inward buckling toward the damaged core concrete. Under high axial loads and large inelastic curvatures, the severe damage of core concrete extended to several tie spacings. As a result, crushing of core concrete was observed. Consequently, the restraint provided by core concrete became ineffective and the contact between core concrete and ties was completely lost. At this stage, the longitudinal bars could buckle inward over several tie spacings or outward between two sets of ties.

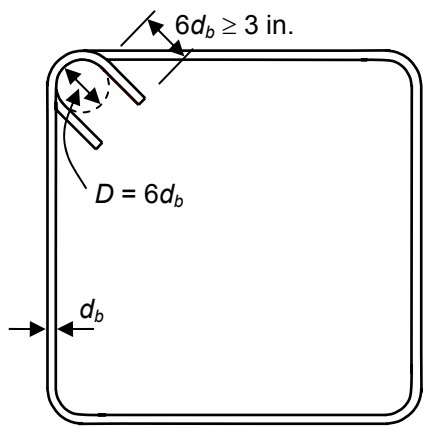


*Figure 4.7 Hook Length of Transverse Reinforcement  
Required by Chapter 21 of ACI 318-05*



*Figure 4.8 Opening of Hoops in Specimen S24-IUT*

### 4.3 ANALYSIS OF TEST DATA

Test specimens were prepared to investigate the seismic performance of concrete columns in multistory building frames between the point of contraflexure and the point of maximum moment. In the subsequent sections, comparative evaluations of the behavior of test specimens are provided. The lateral load-tip displacement and moment-curvature responses of column specimens are used in these comparisons. In this section, definitions of various load and displacement components are provided. These definitions are provided to clarify and define the process used to construct the lateral load-tip displacement and moment-curvature responses.

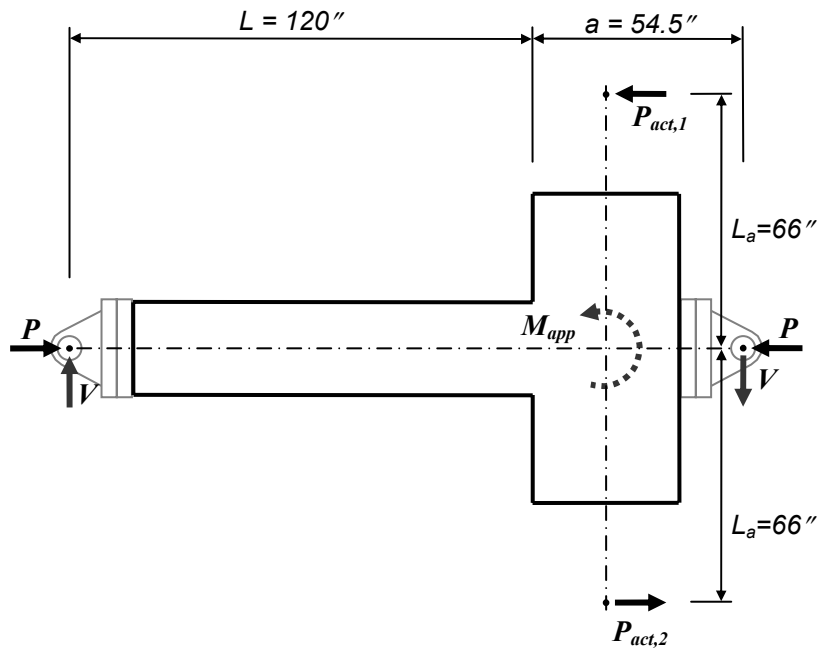
Figure 4.9 illustrates the loading scheme and the deflected shape of test specimens. The moment applied to the base of a test specimen can be calculated using Equation (4.1). The lateral load ( $V$ ) applied to the column can be calculated using Equation (4.2). The displacement component ( $\Delta_1$ ) is the relative vertical displacement of two hinge supports, which is estimated from the displacement readings obtained from the string potentiometers located at centers of hinges (SP-1 and SP-4 in Figure 3.9). “ $\Delta_t$ ” represents the tip displacement of the column considering the length “ $L$ ” as a cantilever. The moment at the column-stub connection can be calculated using Equation (4.4).

$$M_{app} = (P_{act,1} + P_{act,2}) \cdot L_a \quad (4.1)$$

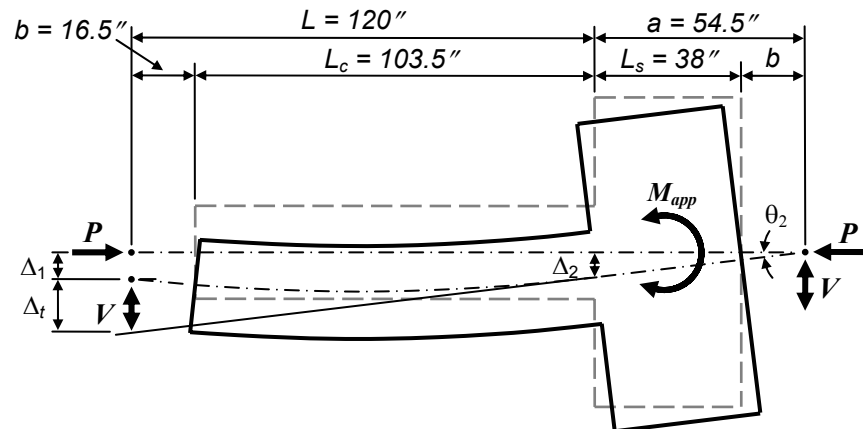
$$V = \frac{M_{app}}{(L + a)} \quad (4.2)$$

$$\Delta_t = (L + a) \cdot \theta_2 - \Delta_1 \quad (4.3)$$

$$M_{col} = V \cdot L + P \cdot \Delta_2 \quad (4.4)$$



(a) Forces acting on a Specimen



(b) Deflected Shape of a Specimen

*Figure 4.9 Applied Loads and Deflected Shape of Test Specimen*

### 4.3.1 Response of Specimens

Responses of the specimens are presented in the form of lateral load-drift relationship (Figures 4.10 to 4.14) and moment-curvature relationship (Figures 4.15 to 4.18). Equations (4.1) to (4.4) were used in preparing Figures 4.10 to 4.18. Displacements and curvatures are normalized with respect to yield displacement ( $\Delta_y$ ) and yield curvature ( $\phi_y$ ) and are also shown in these figures. The definition of yield displacement ( $\Delta_y$ ) is shown in Figure 3.15, except in constructing Figures 4.10 to 4.14 the maximum lateral load from test results was used instead of the predicted maximum lateral load. The yield curvature ( $\phi_y$ ) is also estimated in a similar way. The definitions of displacement ductility and curvature ductility are given in Section 4.3.3. In addition, the nominal lateral load capacity ( $V_{ACI}$ ) is estimated by using ACI 318-05 and also shown in these figures. This nominal lateral load capacity is calculated as follows:

$$V_{ACI} = \frac{M_{ACI}}{L} - P \cdot \delta \quad (4.5)$$

where

$M_{ACI}$  = nominal moment capacity as per ACI 318

$L$  = height of a cantilever column

$P$  = applied axial force

$\delta = \Delta_y/L$  = drift

Curvatures were calculated from the displacement readings measured by the upper and lower linear potentiometers located at the most damaged region (Figure 3.9). Gauge lengths were kept constant in all specimens, except the specimen S17-3UT, where the lengths were reduced by 17.25/24 in proportion to the relative section size. Spalling of top and bottom cover concrete, yielding of ties, and buckling and rupture of longitudinal bars are marked on the graphs. The

tests were terminated when the specimens were unable to carry the applied axial load. All the graphs are plotted until the end of the test, except the moment-curvature relationship of the specimen S24-5UT. For this case, the threaded rods supporting the linear potentiometers were separated at the 26<sup>th</sup> loading cycle from the core concrete due to severe damage at large inelastic displacements. As such, displacement readings used in curvature calculations could not be taken after that event.

In testing specimen S24-1UT, pressure transducers were used to estimate the applied loads instead of load cells. As unacceptably large fluctuations (+/- 5%) in hydraulic pressures were recorded by these pressure transducers, it was decided to use load cells in the subsequent tests. The moment-curvature relationship could not be obtained because of the movements of thin threaded rods used to support the linear potentiometers. All of these problems were resolved and the test conducted in the subsequent specimens provided high-quality data. In short, the first test is referred to as the pilot test where all setup, instrumentation and testing related problems were identified and resolved.

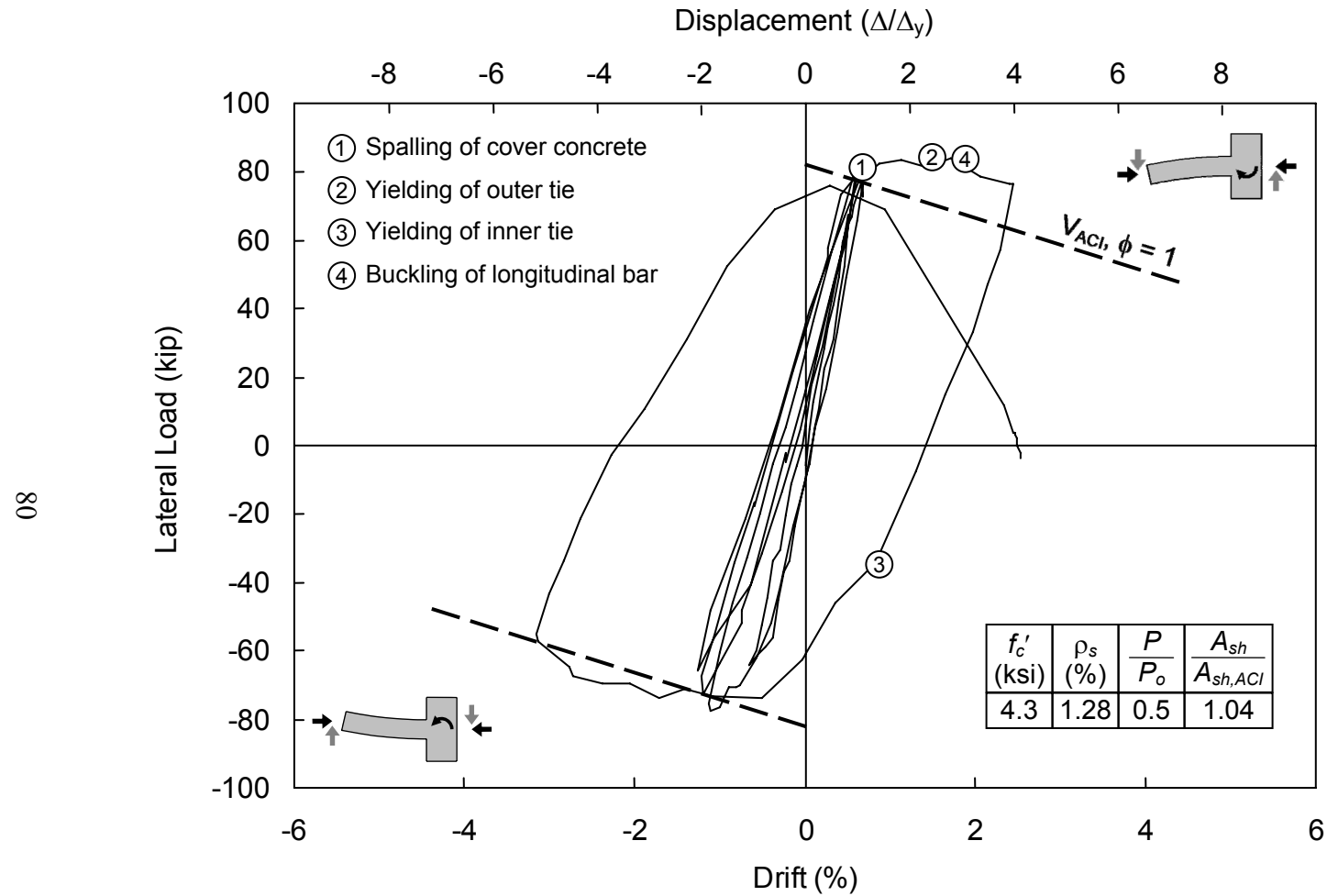


*Figure 4.10 Lateral Load versus Drift Behavior of Specimen S24-1UT*

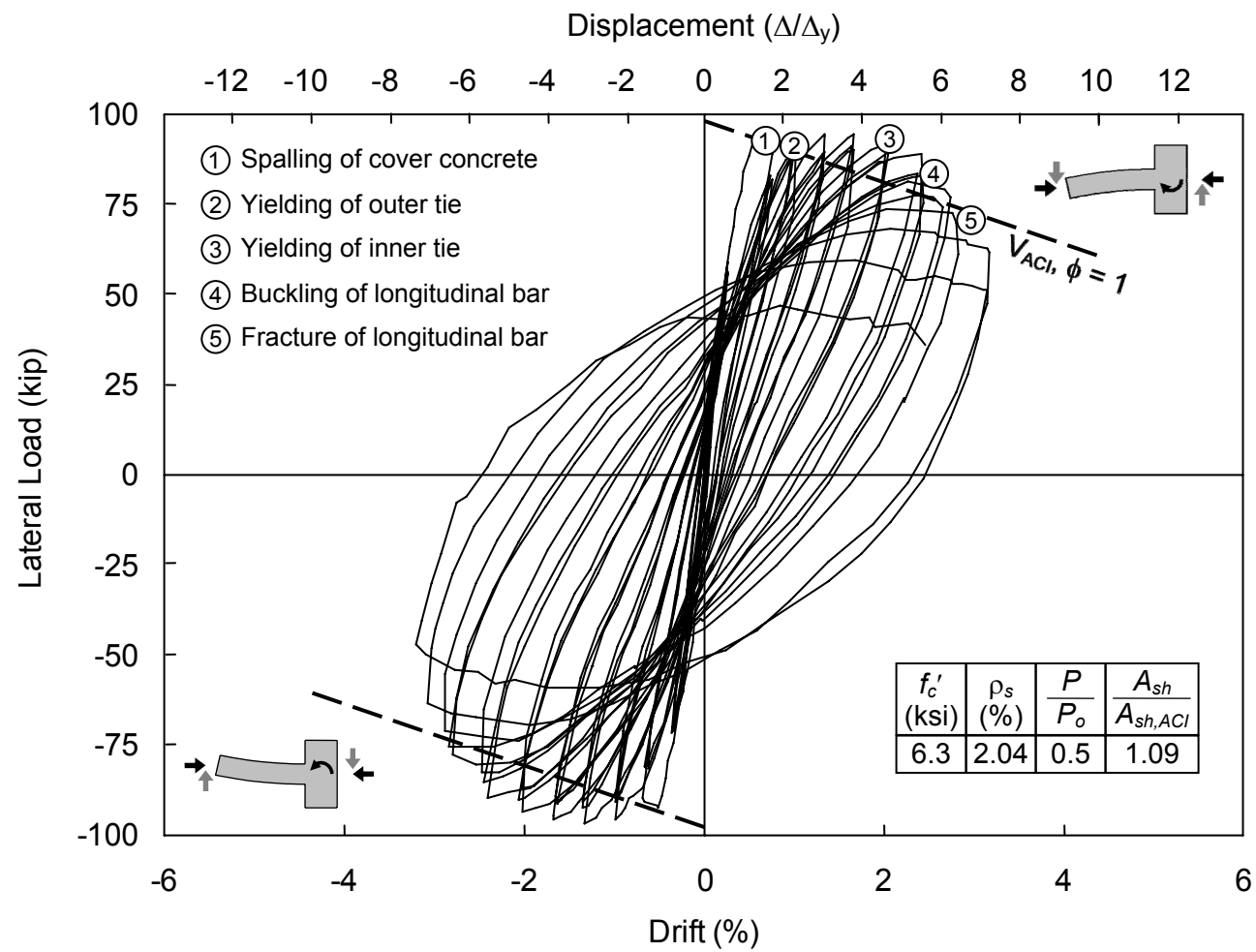


Figure 4.11 Lateral Load versus Drift Behavior of Specimen S24-2UT

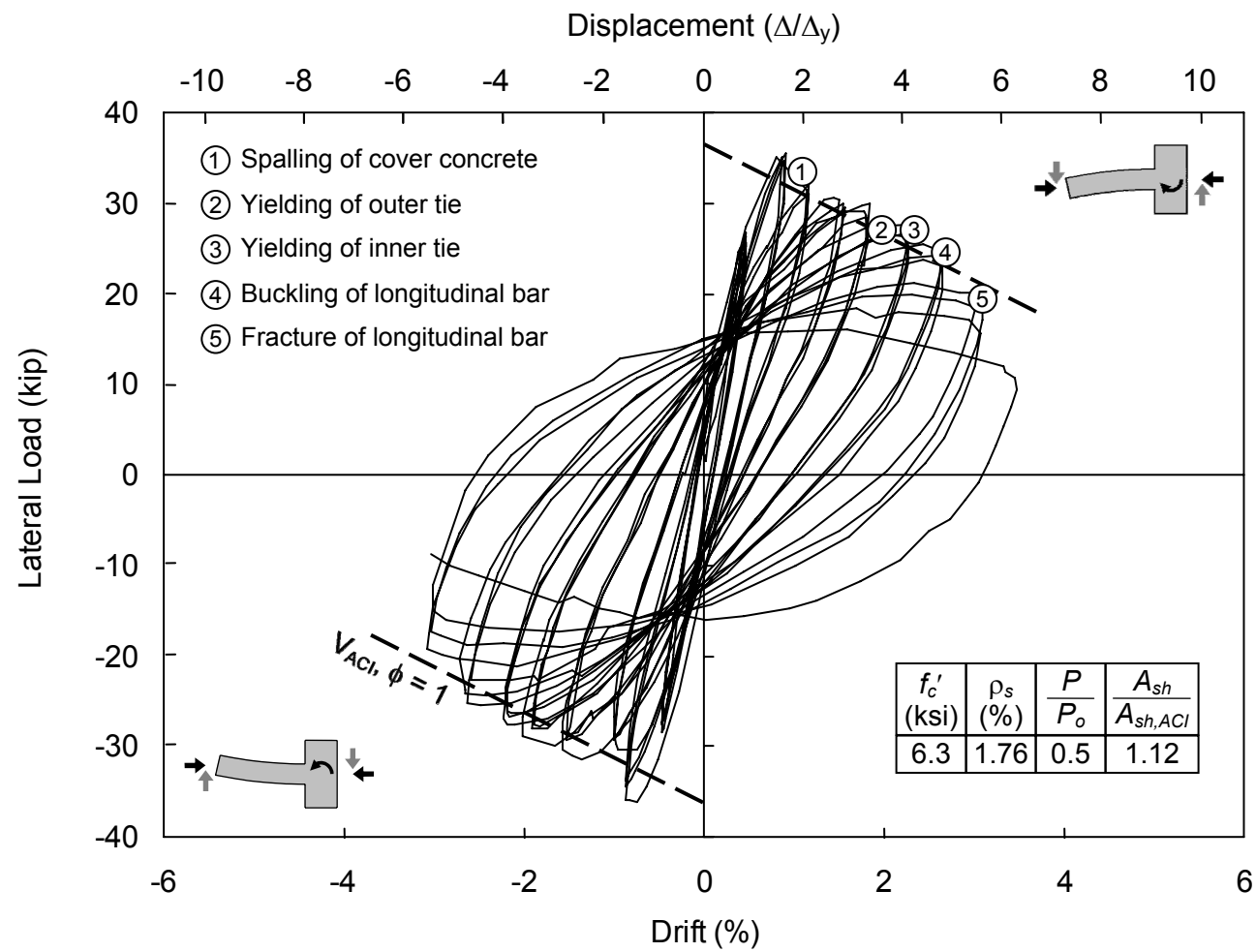


Figure 4.12 Lateral Load versus Drift Behavior of Specimen S17-3UT

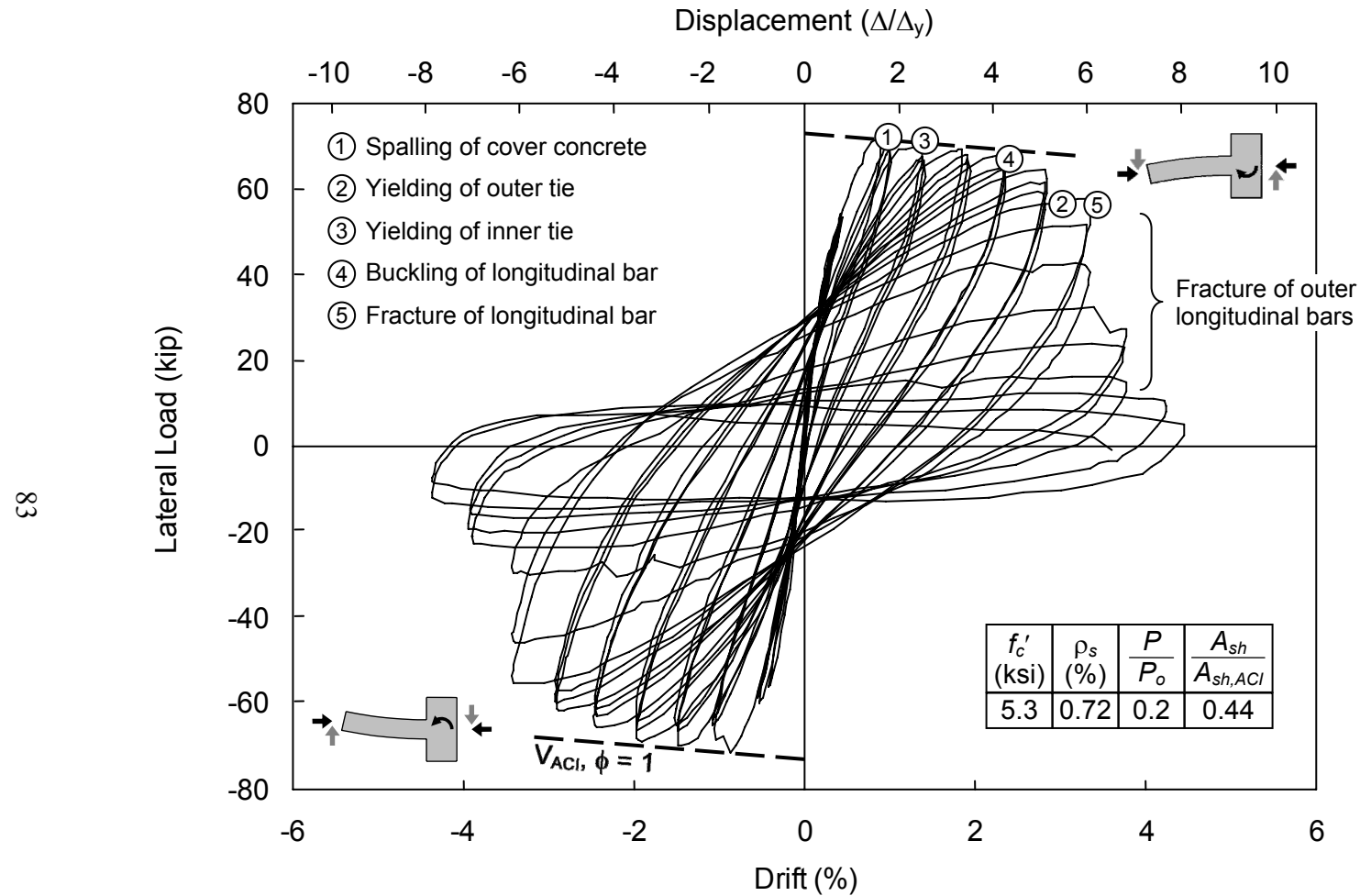


Figure 4.13 Lateral Load versus Drift Behavior of Specimen S24-4UT

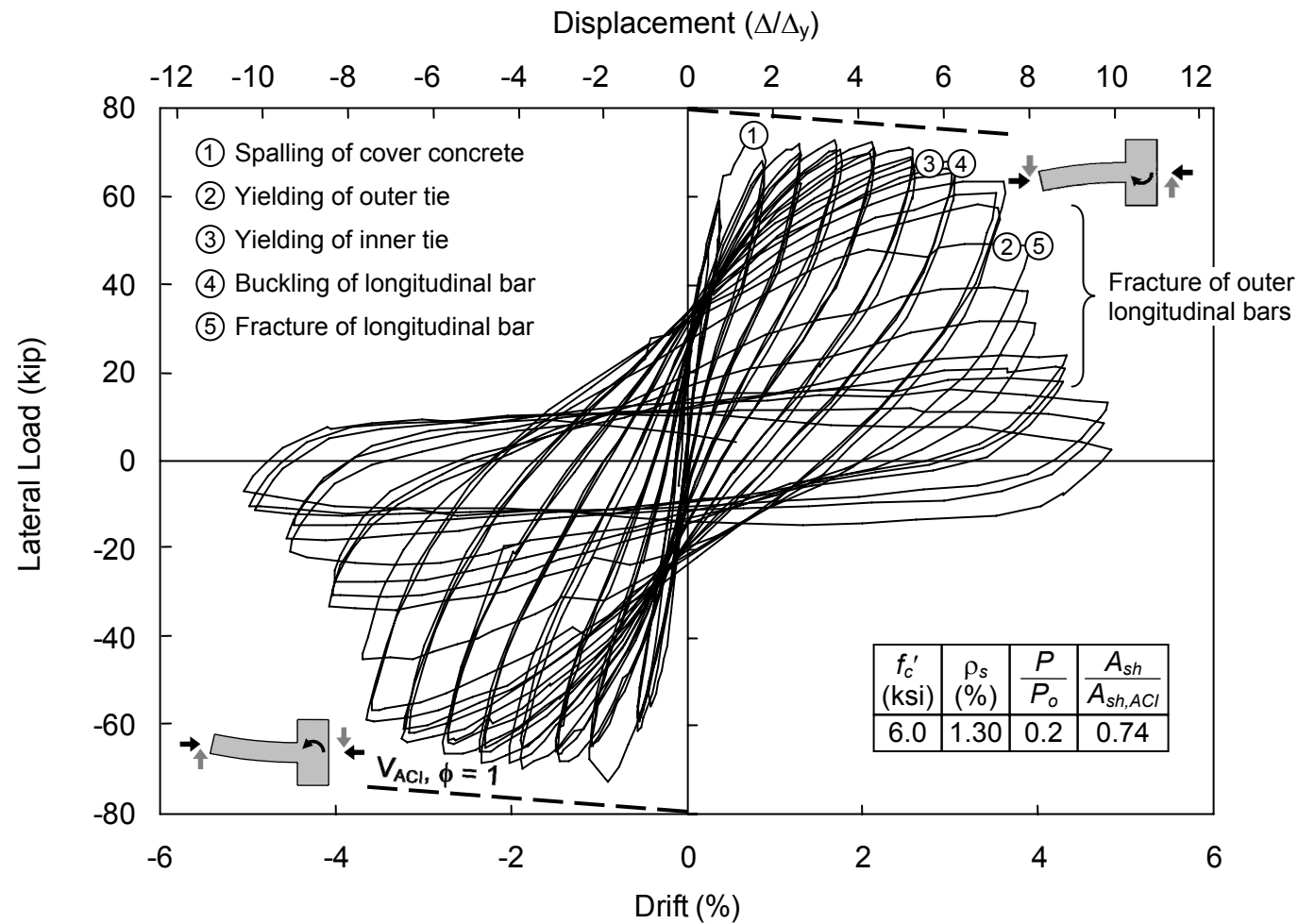
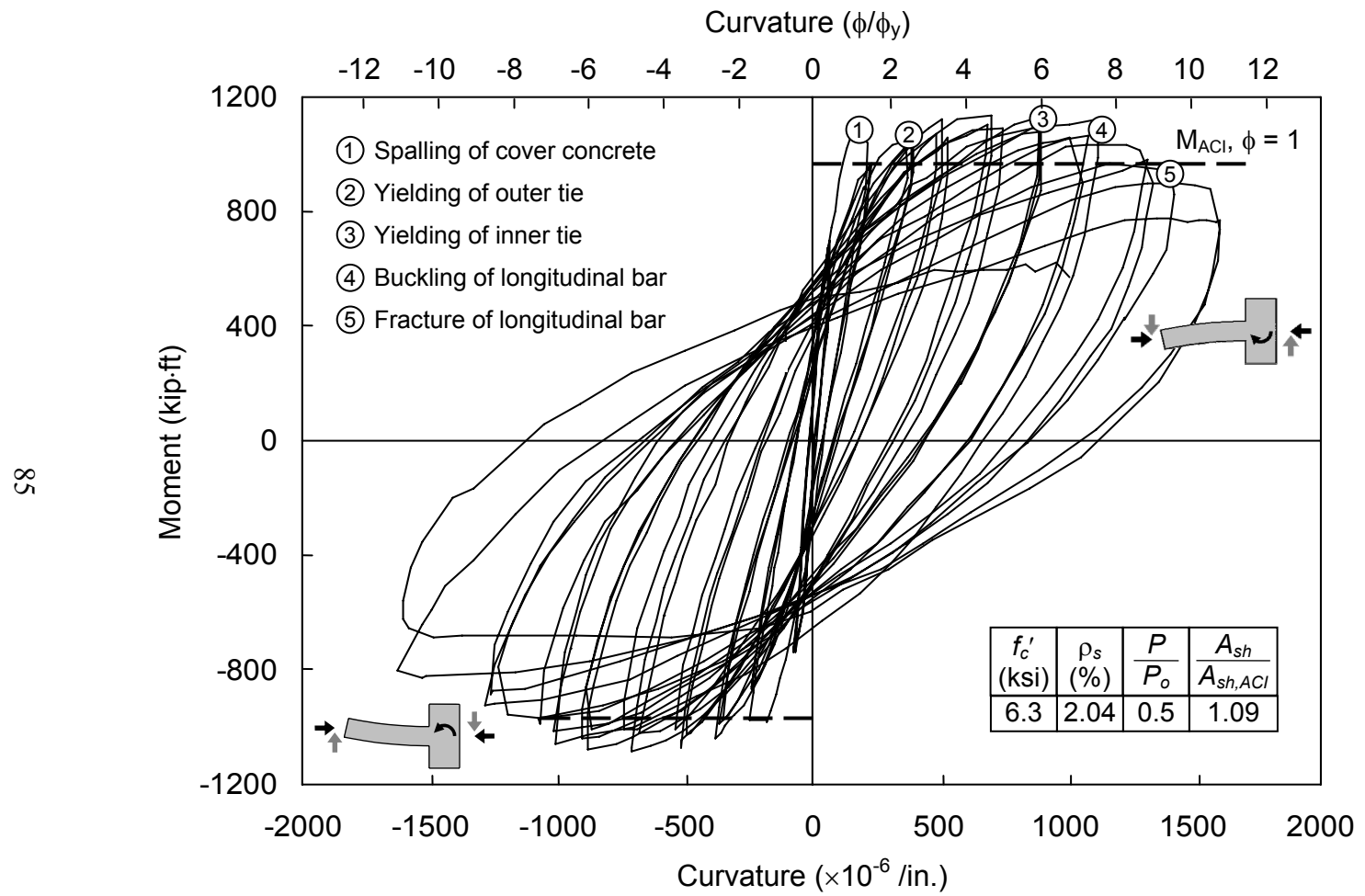


Figure 4.14 Lateral Load versus Drift Behavior of Specimen S24-5UT



**Figure 4.15 Moment versus Curvature Behavior of Specimen S24-2UT**

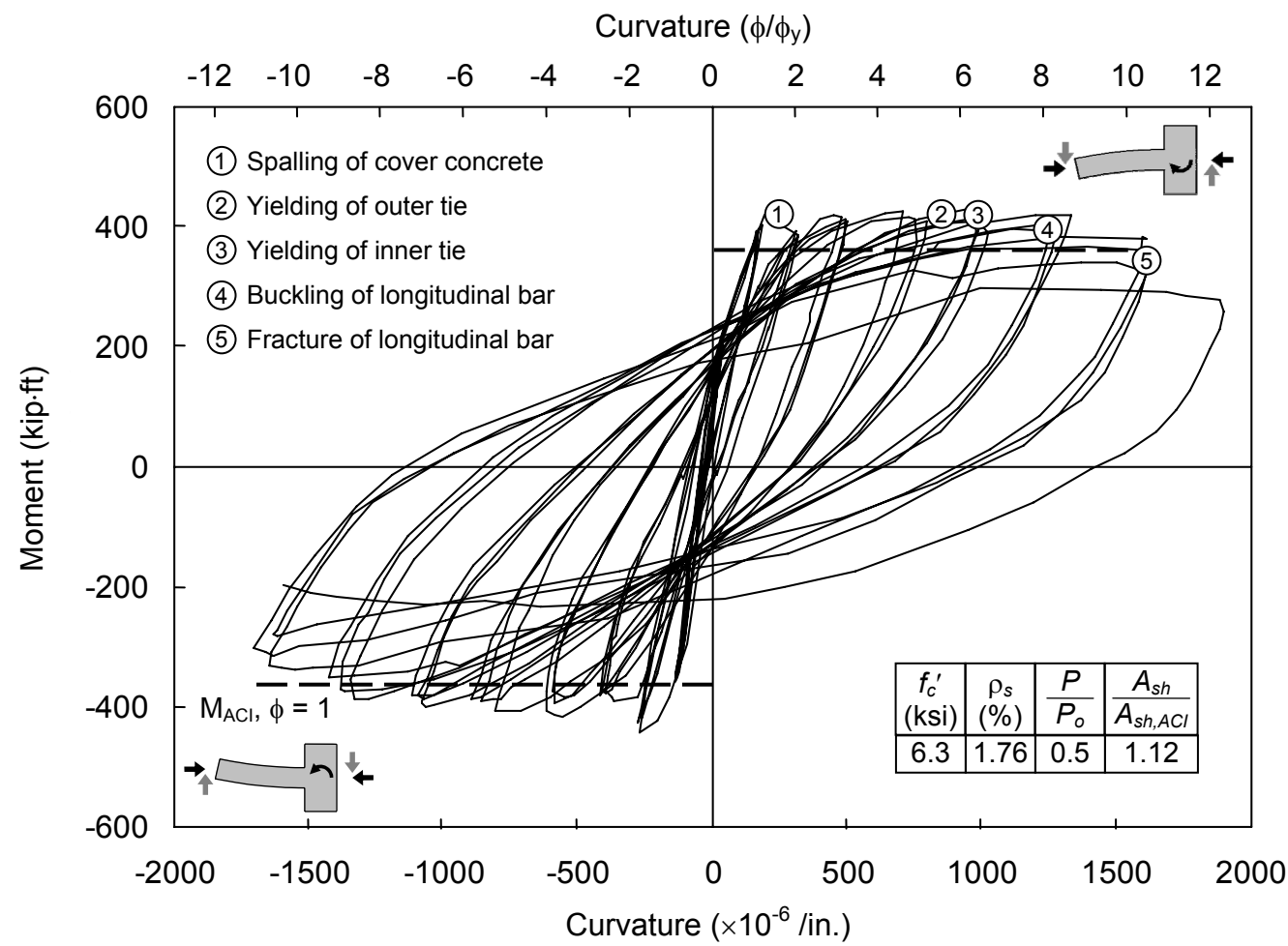


Figure 4.16 Moment versus Curvature Behavior of Specimen S17-3UT

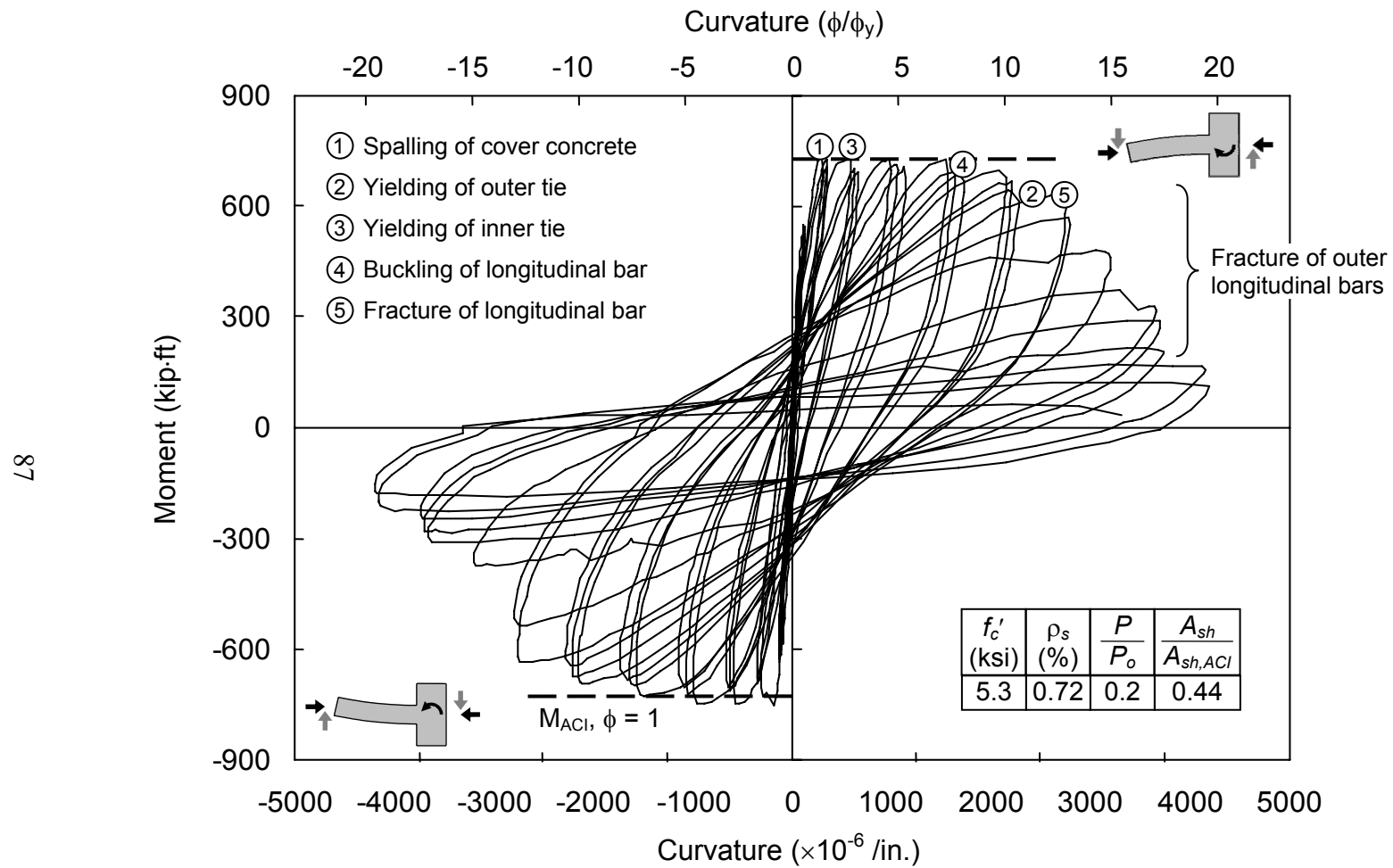


Figure 4.17 Moment versus Curvature Behavior of Specimen S24-4UT

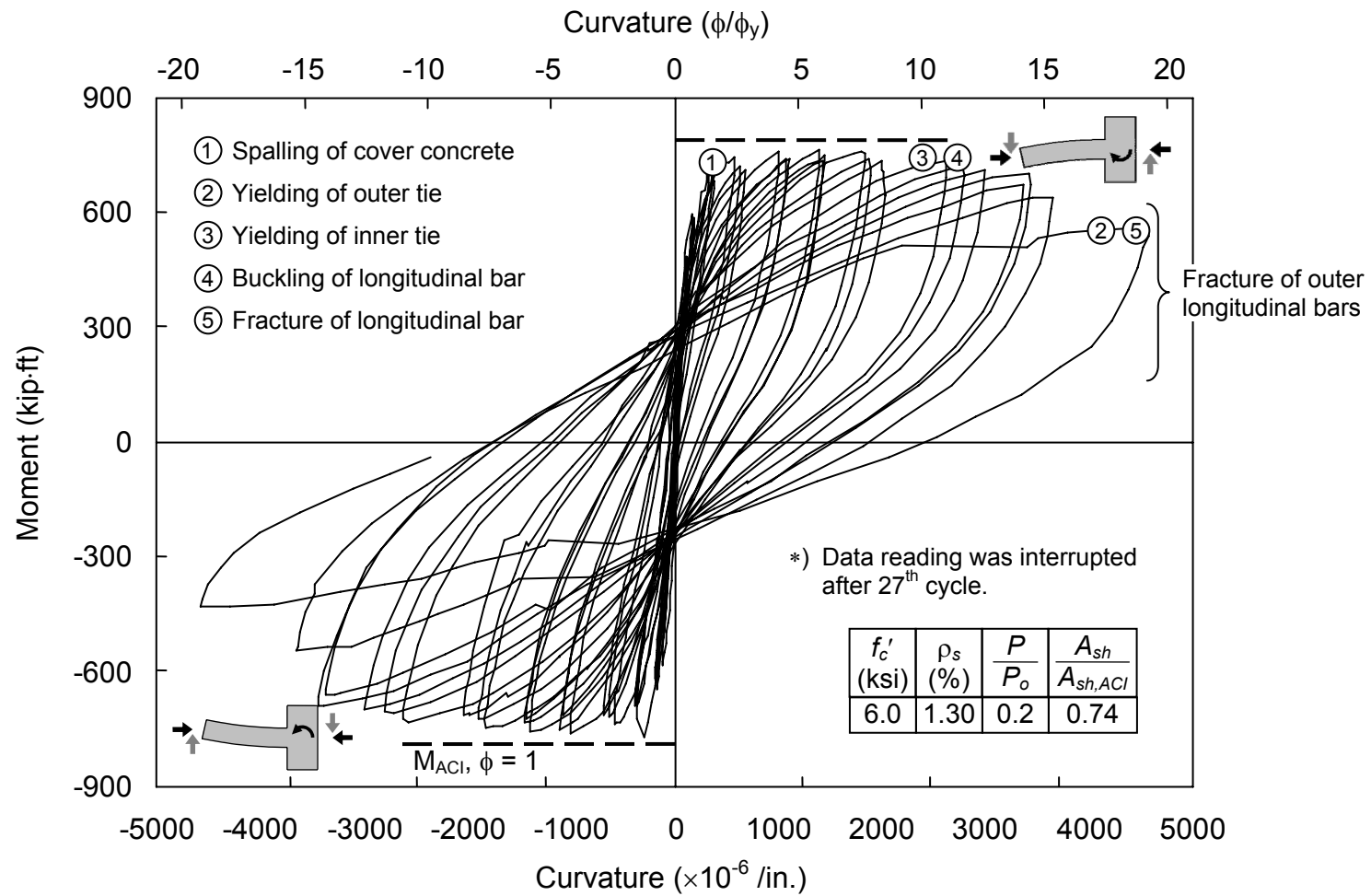


Figure 4.18 Moment versus Curvature Behavior of Specimen S24-5UT

### 4.3.2 Backbone Curves

In order to facilitate the comparison of the behavior of the test specimens, backbone curves were plotted. The backbone curves were generated for the moment-curvature and lateral load-drift backbone relationships. The procedure to develop backbone curves was adopted from FEMA 356 (Sec. 2.8.3):

*“The backbone curve shall be constructed as follows:*

- (1) *The appropriate quadrant of data from the lateral-force-deformation plot from the experimental report shall be taken.*
- (2) *A smooth “backbone” curve shall be drawn through the intersection of the first cycle curve for the (i)th deformation step with the second cycle curve of the (i-1)th deformation step.*
- (3) *The backbone curve so derived shall be approximated by a series of linear segments, drawn to form a multi-segmented curve.”*

The backbone curves for moment-curvature and lateral load-drift relationships are shown in Figures 4.19 and 4.20. These backbone curves were converted to the normalized moment-curvature, normalized lateral load-displacement, and normalized lateral load-drift relationships for comparison purposes, as presented in Figures 4.21 to 4.23. The ductility parameters were calculated in both the positive and negative directions from the backbone curves and averaged. The calculated ductility parameter in each direction was close to each other, resulting in less than 3% difference with the average for all cases. The calculated average ductility parameters are summarized in Table 4.1.

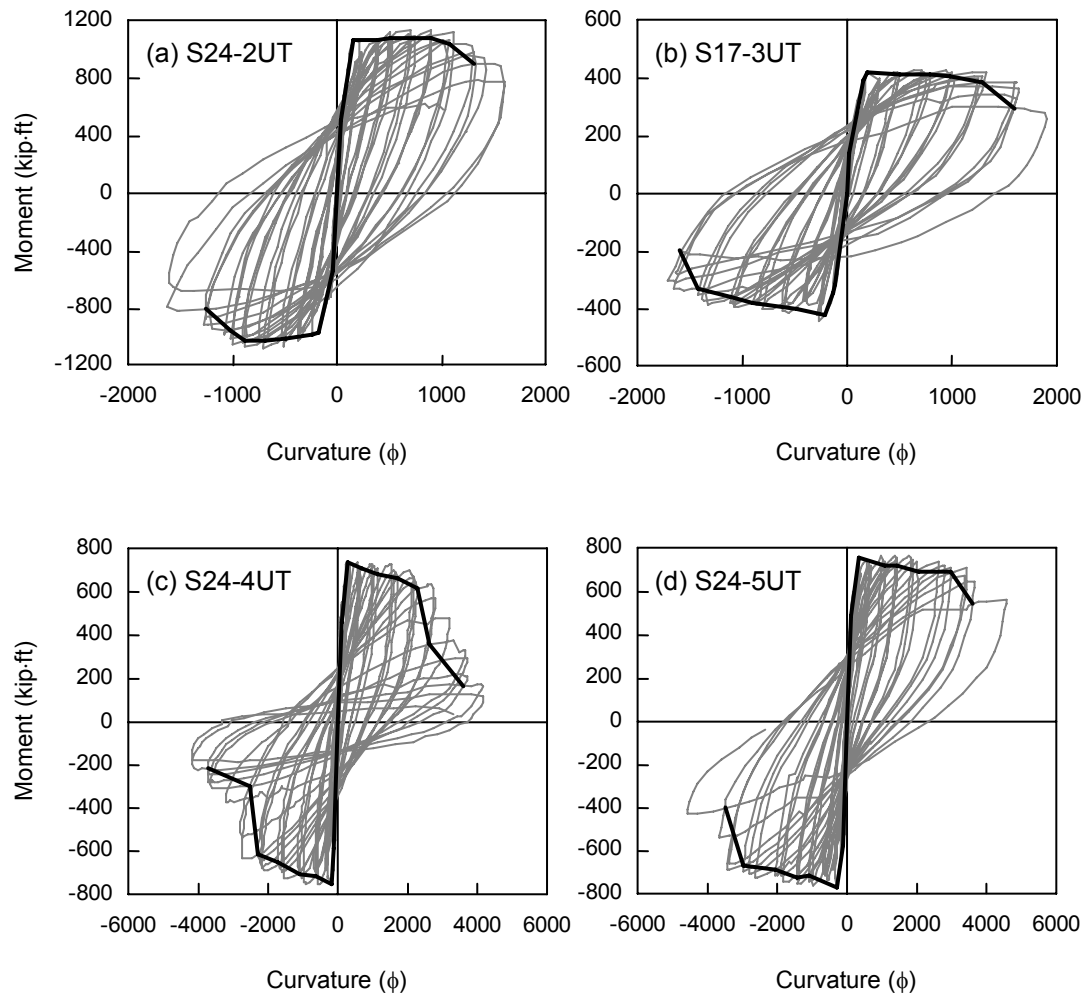


**Figure 4.19 Backbone Curves for Moment-Curvature Relationship**

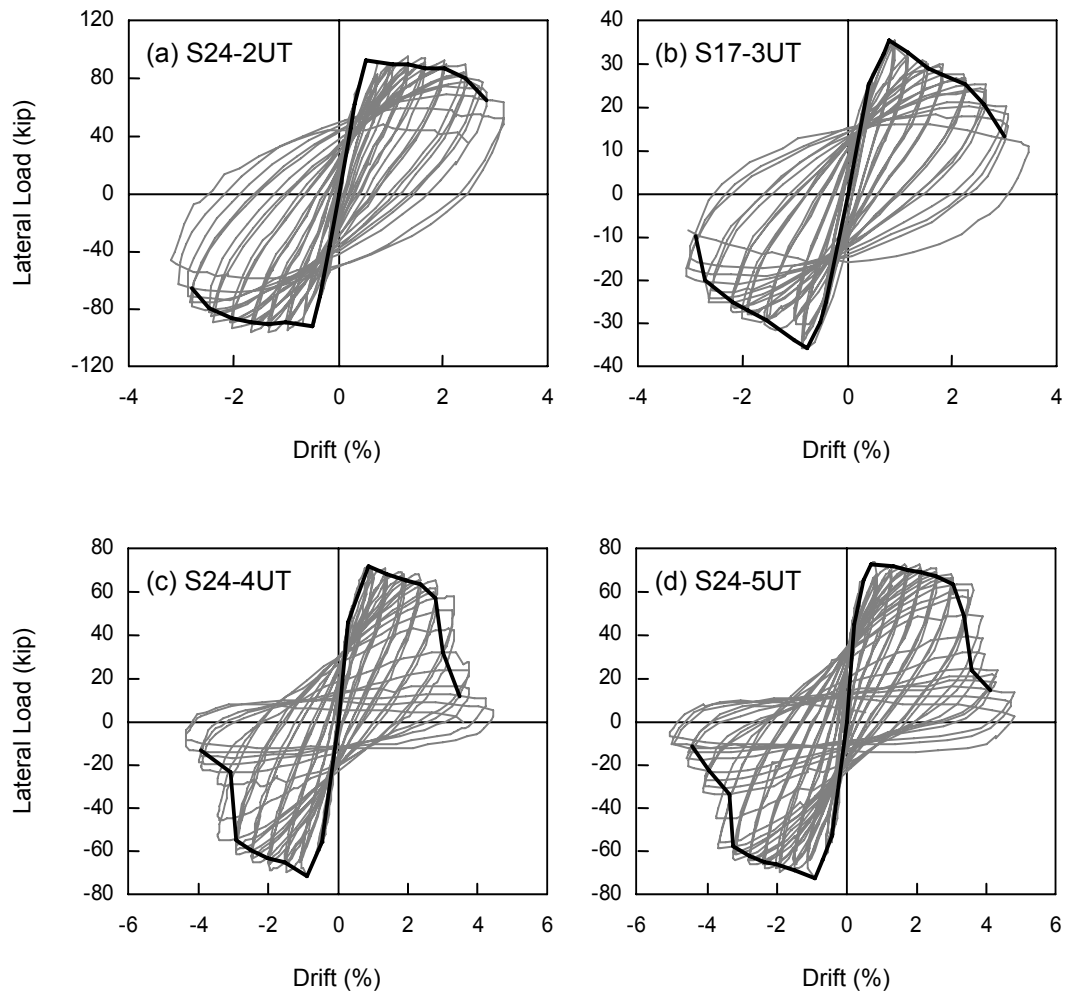


**Figure 4.20 Backbone Curves for Lateral Load-Drift Relationship**

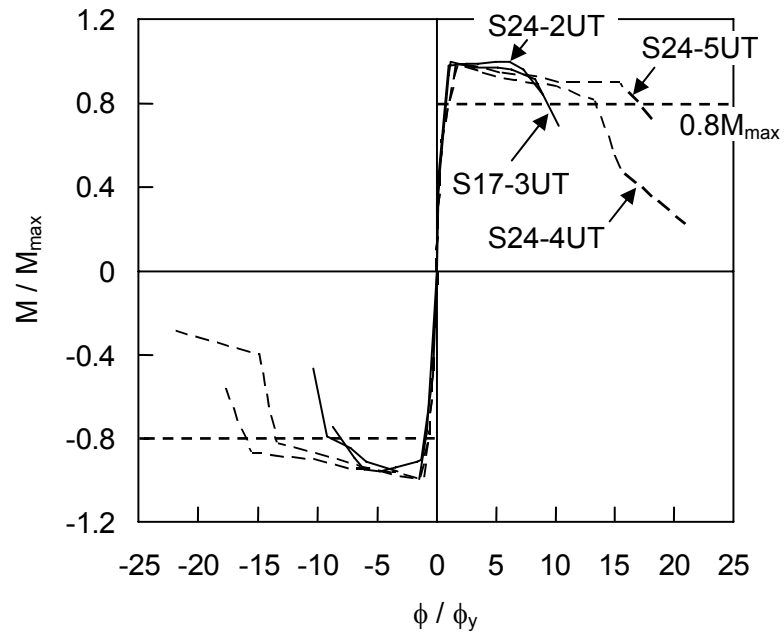


*Figure 4.21 Normalized Moment-Curvature Backbone Curves*

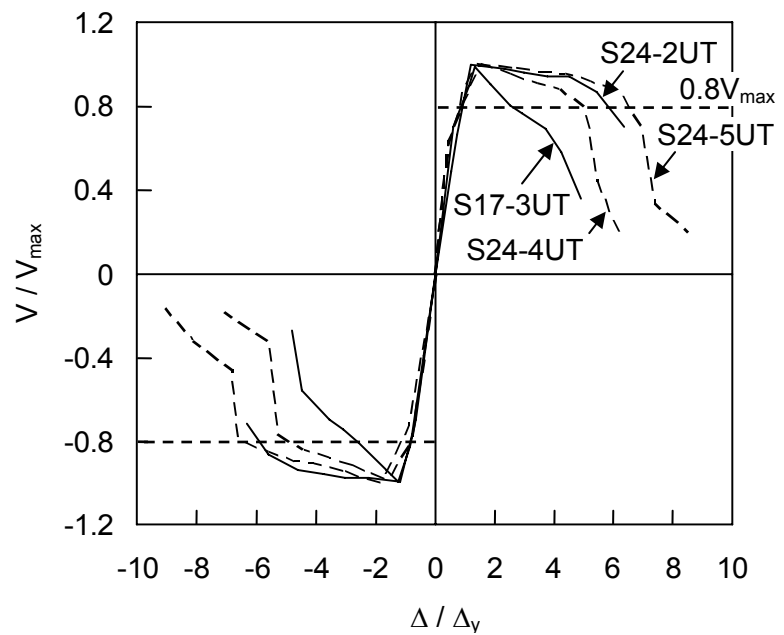


*Figure 4.22 Normalized Lateral Load-Displacement Backbone Curves*

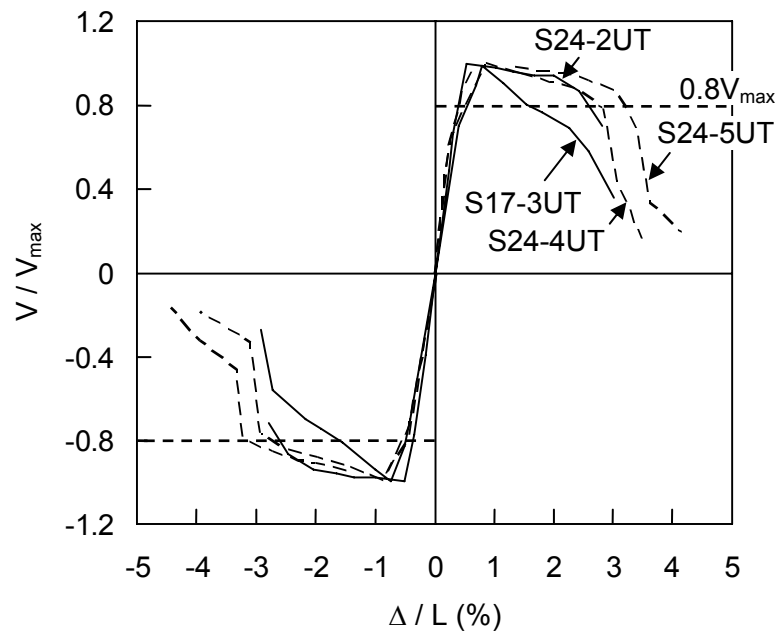


*Figure 4.23 Normalized Lateral Load-Drift Backbone Curves*

*Table 4.1 Ductility Parameters of Specimens*

Specimen	$f'_c$ (ksi)	$\Delta_y$ (in)	$\phi_y$ ( $\times 10^{-6}$ /in)	$\delta$ (%)	$\mu_\Delta$	$\mu_\phi$
S24-2UT	6.3	0.44	146.7	2.6	5.9	8.8
S17-3UT	6.3	0.61	154.9	1.6	2.7	9.1
S24-4UT	5.3	0.56	171.0	2.8	4.9	13.4
S24-5UT	6.0	0.49	194.4	3.2	6.5	16.3

### 4.3.3 Definitions of Ductility Parameters

The section-level and member-level ductility parameters are discussed in the following sections. Figures 4.24 and 4.25 show the definitions of ductility parameters used in this study. These parameters are curvature and displacement ductility factors ( $\mu_\phi$ ,  $\mu_\Delta$ ), cumulative curvature and displacement ductility ratios ( $N_\phi$ ,  $N_\Delta$ ) and energy and work damage indicators ( $E$ ,  $W$ ). The energy and work damage indicators used in this study were originally defined by Ehsani and Wight (1990).

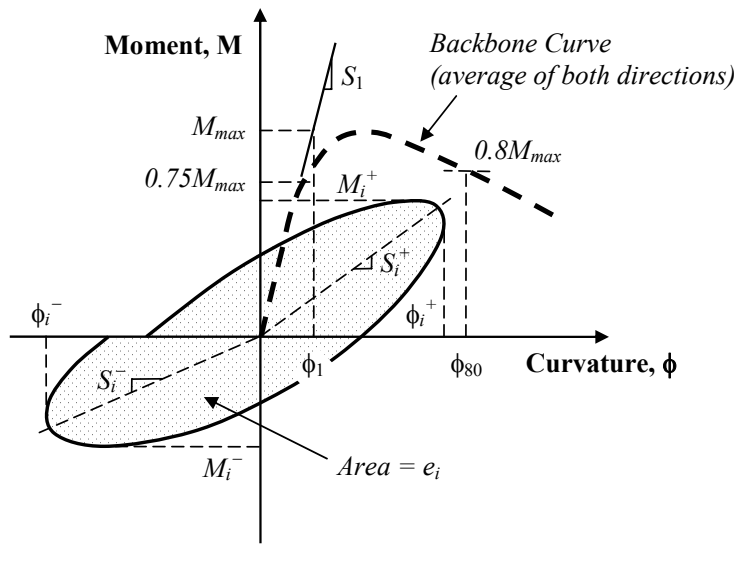
#### 4.3.3.1 Curvature and Displacement Ductility Factors

Curvature and displacement ductility factors ( $\mu_\phi$ ,  $\mu_\Delta$ ) are calculated from the backbone curves, described in Section 4.3.2. The yield curvature ( $\phi_1$ ) and yield displacement ( $\Delta_1$ ) are previously defined in Section 4.3.1 and they are graphically illustrated in Figures 4.24 and 4.25. The maximum useful curvature and displacement capacities ( $\phi_{80}$ ,  $\Delta_{80}$ ) are defined as the curvature and displacement corresponding to a 20% reduction in moment and lateral load capacity on the descending branch of the response backbone curves, respectively.

#### 4.3.3.2 Cumulative Curvature and Displacement Ductility Ratios

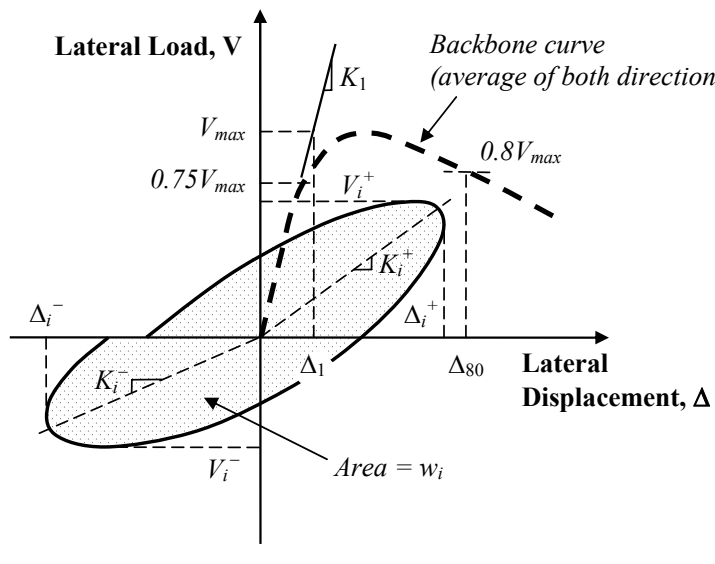
The cumulative curvature and displacement ductility ratios ( $N_\phi$ ,  $N_\Delta$ ) are defined as the cumulative ratios of the peak curvature or displacement at the  $i^{\text{th}}$  loading cycle ( $\phi_i$  and  $\Delta_i$ ) normalized with respect to the yield curvature or displacement ( $\phi_1$  and  $\Delta_1$ ), as shown in Figures 4.24 and 4.25.  $N_\phi$  is defined as follows:

$$N_\phi = \sum_{i=1}^n \frac{\phi_i}{\phi_1} \quad (4.6)$$



$$\begin{aligned}
 \mu_\phi &= \frac{\phi_{80}}{\phi_1} \\
 \phi_i &= \frac{(\phi_i^+ + \phi_i^-)}{2} \\
 M_i &= \frac{(M_i^+ + M_i^-)}{2} \\
 S_i &= \frac{(S_i^+ + S_i^-)}{2} \\
 N_\phi &= \sum_{i=1}^n \frac{\phi_i}{\phi_1} \\
 E &= \frac{1}{M_{\max} \phi_1} \sum_{i=1}^n (e_i) \left( \frac{L_f}{h} \right) \left( \frac{S_i}{S_1} \right) \left( \frac{\phi_i}{\phi_1} \right)^2
 \end{aligned}$$

**Figure 4.24 Definitions of Section Ductility Parameters**



$$\begin{aligned}
 \mu_\Delta &= \frac{\Delta_{80}}{\Delta_1} \\
 \Delta_i &= \frac{(\Delta_i^+ + \Delta_i^-)}{2} \\
 V_i &= \frac{(V_i^+ + V_i^-)}{2} \\
 K_i &= \frac{(K_i^+ + K_i^-)}{2} \\
 N_\Delta &= \sum_{i=1}^n \frac{\Delta_i}{\Delta_1} \\
 W &= \frac{1}{V_{\max} \Delta_1} \sum_{i=1}^n (w_i) \left( \frac{K_i}{K_1} \right) \left( \frac{\Delta_i}{\Delta_1} \right)^2
 \end{aligned}$$

**Figure 4.25 Definitions of Member Ductility Parameters**

$\phi_i$  = maximum curvature reached in the  $i^{\text{th}}$  cycle as an average of both loading directions

$\phi_1$  = yield curvature as defined in Figure 4.24

$n$  = number of cycles up to a certain stage

Similarly,  $N_\Delta$  is defined as follows:

$$N_\Delta = \sum_{i=1}^n \frac{\Delta_i}{\Delta_1} \quad (4.7)$$

where

$\Delta_i$  = maximum displacement reached in the  $i^{\text{th}}$  cycle as an average of both loading directions

$\Delta_1$  = yield displacement as defined in Figure 4.25

$n$  = number of cycles up to a certain stage

The parameters,  $N_{\phi 80}$  and  $N_{\Delta 80}$ , can be defined as the cumulative curvature or displacement ductility ratio up to the cycle in which approximately 20% loss in the moment or lateral load capacity occurs and that is followed by a cycle in which this loss is greater than 20%. In the same way, the parameters,  $N_{\phi t}$  and  $N_{\Delta t}$ , can be defined as the cumulative curvature or displacement ductility ratio up to the end of the test. Figures 4.26(a) and 4.26(b) illustrate the cumulative curvature and displacement ductility ratios of the test specimens at each loading cycle.

#### 4.3.3.3 Damage Indicators

Energy absorption and dissipation characteristics of specimens are measured using the two damage indicators, namely, energy-damage indicator and work-damage indicator. Energy dissipated in the plastic hinge region is represented by the energy-damage indicator ( $E$ ), defined in Equation (4.8).

$$E = \frac{1}{M_{\max} \phi_1} \sum_{i=1}^n (e_i) \left( \frac{L_f}{h} \right) \left( \frac{S_i}{S_1} \right) \left( \frac{\phi_i}{\phi_1} \right)^2 \quad (4.8)$$

where

$M_{\max}$  = maximum moment reached throughout the test as an average of both loading directions

$\phi_1$  = yield curvature as defined in Figure 4.24

$e_i$  = energy dissipated in the  $i^{\text{th}}$  cycle within the unit length of hinging zone, and measured as the area enclosed in the  $i^{\text{th}}$  cycle of the  $M$ - $\phi$  loop

$L_f$  = length of the most damaged region measured from the actual test  
 $=$  plastic hinge length ( $l_p$ ) in Table 4.4

$h$  = depth of the column section

$S_i$  = backbone flexural stiffness in the  $i^{\text{th}}$  cycle which is defined as the slope of a line connecting the origin and the point of maximum curvature,  $\phi_i$ , as an average of both loading directions

$S_1$  = flexural stiffness corresponding to the yield curvature,  $\phi_1$

The work-damage indicator ( $W$ ) represents the work done on the column by lateral load (Figure 4.25) and is expressed as,

$$W = \frac{1}{V_{\max} \Delta_1} \sum_{i=1}^n (w_i) \left( \frac{K_i}{K_1} \right) \left( \frac{\Delta_i}{\Delta_1} \right)^2 \quad (4.9)$$

where

$V_{\max}$  = maximum lateral load reached throughout the test as an average of both loading directions

$\Delta_1$  = yield displacement as defined in Figure 4.25

- $w_i$  = total energy dissipated in the  $i^{\text{th}}$  cycle, and measured as the area enclosed in the  $i^{\text{th}}$  cycle of the  $V-\Delta$  loop  
 $K_i$  = backbone stiffness in the  $i^{\text{th}}$  cycle which is defined as the slope of a line  
 $K_1$  = stiffness corresponding to the yield displacement,  $\Delta_1$

Based on Equations (4.8) and (4.9), the energy or work damage indicators ( $E_{80}$  or  $W_{80}$ ) can be calculated up to the cycle in which the loss in the moment or lateral load capacity is approximately 20%. The total energy or work damage indicator ( $E_t$  or  $W_t$ ) can be obtained if the summation is considered up to the end of the test. The energy damage indicator and work damage indicator are computed for each specimen and the results are included in Figures 4.27(a) and 4.27(b). The section and member ductility parameters are summarized in Tables 4.2 and 4.3.

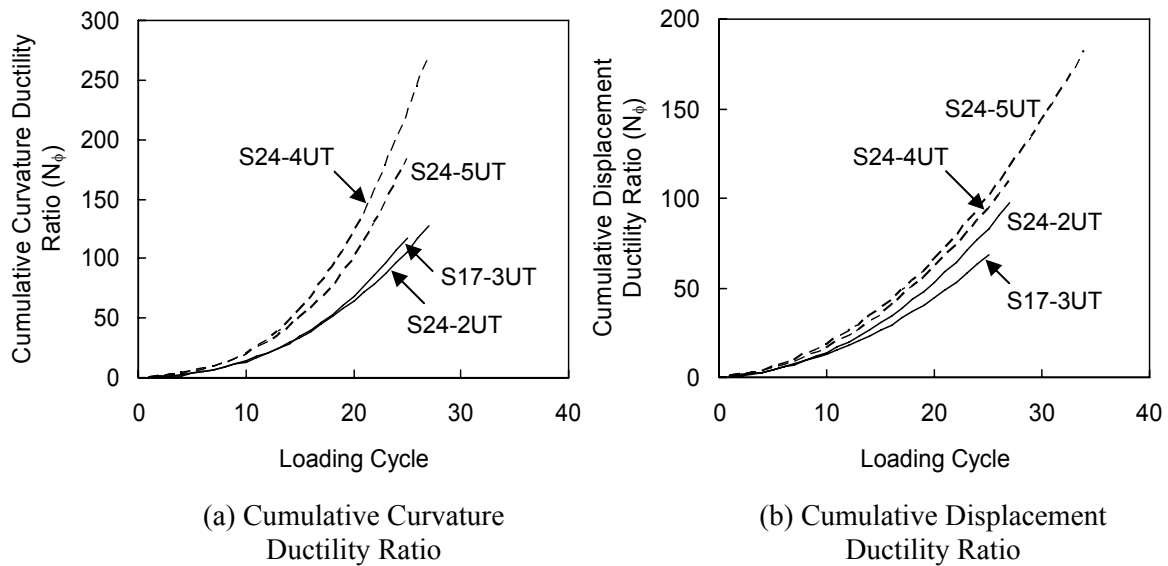


**Figure 4.26 Cumulative Ductility Ratios**

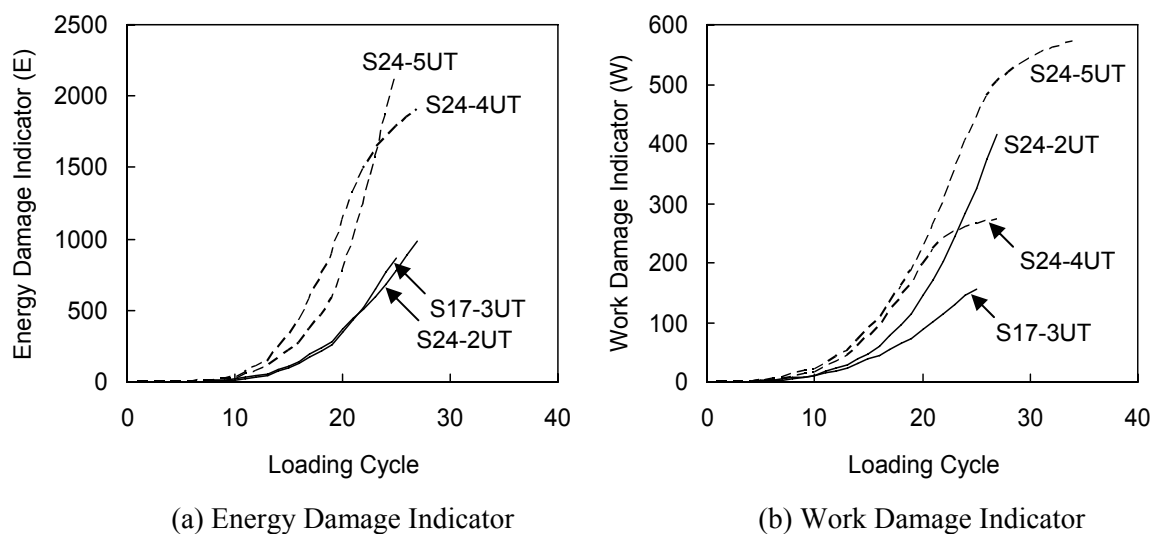


**Figure 4.27 Damage Indicators**

**Table 4.2 Section Ductility Parameters**

Specimen	$f'_c$ (ksi)	Lateral Steel		Axial Load	Ductility Factor	Cumulative Ductility Ratio		Energy Damage Indicators	
		$\rho_s$ (%)	$\frac{A_{sh}}{A_{sh,ACI}}$	$\frac{P}{P_o}$	$\mu_\phi$	$N_{\phi 80}$	$N_{\phi t}$	$E_{80}$	$E_t$
S24-2UT	6.3	2.04	1.09	0.5	8.8	106	128	777	988
S17-3UT	6.3	1.76	1.12	0.5	9.1	107	118	768	866
S24-4UT	5.3	0.72	0.44	0.2	13.4	122	271	1138	1909
S24-5UT	6.0	1.30	0.74	0.2	16.3	165	184*	1875	2169*

\*: Curvature reading was terminated due to the movement of supporting rods before the specimen failed.

**Table 4.3 Member Ductility Parameters**

Specimen	$f'_c$ (ksi)	Lateral Steel		Axial Load	Ductility Factor	Cumulative Ductility Ratio		Work Damage Indicators	
		$\rho_s$ (%)	$\frac{A_{sh}}{A_{sh,ACI}}$	$\frac{P}{P_o}$	$\mu_\Delta$	$N_{\Delta 80}$	$N_{\Delta t}$	$W_{80}$	$W_t$
S24-2UT	6.3	2.04	1.09	0.5	5.9	77	97	283	415
S17-3UT	6.3	1.76	1.12	0.5	2.7	29	68	44	157
S24-4UT	5.3	0.72	0.44	0.2	4.9	61	105	197	273
S24-5UT	6.0	1.30	0.74	0.2	6.5	93	182	405	570

## 4.4 DISCUSSION OF TEST RESULTS

### 4.4.1 Shear Span-to-Depth Ratio ( $L/h$ )

The effect of shear span-to-depth ratio ( $L/h$ ) on the behavior of concrete columns is studied by comparing the behaviors of specimens S24-2UT and S17-3UT. Specimens S24-2UT and S17-3UT had 24-in. and 17.25-in. square sections, respectively, with the same column height of 103.5 in. These two specimens had similar sectional properties with respect to concrete strength, amount and detail of longitudinal and transverse reinforcement. The only difference between these two specimens was the shear span-to-depth ratio, resulting from different section sizes. The shear span-to-depth ratios ( $L/h$ ) of S24-2UT and S17-3UT were 5 and 7, respectively. The shear span ( $L$ ) of a column specimen is calculated as the sum of the height of a column specimen (103.5 in.) and the distance between the center of a hinge to the tip of column specimen (16.5 in.). Figure 4.9 illustrates the shear span ( $L$ ) of a column specimen.

The normalized moment-curvature backbone curves in Figure 4.21 show that specimens S24-2UT and S17-3UT had similar sectional performance. The curvature ductility factors of specimens S24-2UT and S17-3UT were 8.8 and 9.1, respectively (Table 4.2). Other section ductility parameters of S24-2UT and S17-3UT also support the similarity in sectional performances (Figure 4.26(a), Figure 4.27(a), and Table 4.2).

Figures 4.22 and 4.23 show the normalized lateral load-displacement and the normalized lateral load-drift backbone curves for specimens S24-2UT and S17-3UT, respectively. These figures illustrate the member-level deformation capacities of these two specimens are considerably different. An increase in the shear span-to-depth ratio from 5 to 7 resulted in a significant decrease in displacement ductility from 5.9 to 2.7 (Table 4.3). Similarly, the drift capacity

decreased from 2.6% to 1.6%. Other member ductility parameters of specimen S24-2UT are also considerably better than those of specimen S17-3UT (Figure 4.26(b), Figure 4.27(b) and Table 4.3).

Based on the above comparisons, it can be concluded that the overall member performance of the test columns were significantly affected by the shear span-to-depth ratio. In other words, similar sectional performances did not produce similar member performances when shear span-to-depth ratios of concrete columns were different.

#### 4.4.2 Axial Load Level

The detrimental effect of axial load on deformation capacity of concrete columns has been widely recognized. As a result, larger amounts of confining reinforcement are required at higher axial loads in some design codes and performance-based design procedures. However, the axial load is not considered as part of the relationship between curvature ductility and displacement ductility (Equation (2.19)). In order to study the effect of axial load on the relationship among different ductility parameters, specimens S24-4UT and S24-5UT were tested under low axial loads ( $P = 0.2P_o$ ) and their behaviors are compared to that of specimen S24-2UT, which was tested under a high axial load level ( $P = 0.5P_o$ ).

Specimens S24-4UT and S24-5UT did not meet the ACI code requirements for confining reinforcement. The amount of confining reinforcement provided in specimen S24-4UT was 44% of that required by Chapter 21 provisions of ACI 318-05. Specimen S24-5HT contained 77% of the code required amount of transverse reinforcement. On the other hand, specimen S24-2UT met the code requirements for confinement ( $A_{sh}/A_{sh,ACI} = 1.09$ , where  $A_{sh,ACI}$  is the amount of confining reinforcement required by Chapter 21 provisions of

ACI 318-05). These specimens (S24-2UT, S24-4UT and S24-5UT) had the same shear span-to-depth ratio ( $L/h = 5$ ).

The sectional performance of specimen S24-2UT is inferior to the sectional performance displayed by specimens S24-4UT and S24-5UT with respect to its deformation capacity (Figure 4.21). However, the trend observed at the section level can not be observed at the member level. The normalized lateral load-displacement response of S24-4UT appears to be less ductile than the response of specimen S24-2UT (Figure 4.22). The normalized lateral load-drift response of the specimens is similar to that observed in the normalized lateral load-displacement curves (Figure 4.23).

Parallel to the aforementioned observations, the section-level ductility parameters calculated for specimens S24-4UT and S24-5UT also indicate that their sectional performance is superior to that of specimen S24-2UT (Table 4.2). On the other hand, the member-level ductility parameters for specimen S24-2UT are better than those of specimen S24-4UT, but worse than those of specimen S24-5UT (Table 4.3).

Therefore, the performance of test specimens can be evaluated differently depending on the ductility parameter used. If the sectional performance is used as a basis of comparison, it can be concluded that the large amount of confining reinforcement provided in S24-2UT is not enough to compensate for the detrimental effects of high axial loads. However, if the member performance is used, the opposite conclusion can be reached.

It was discussed that in the performance-based design procedures, larger amounts of confining reinforcement are required at high axial loads when the sectional performance criterion is used rather than the member performance criterion (Figure 2.1 in Section 2.4). This trend is consistent with the conclusion

made in this section, which is the effect of axial load on sectional performance is different than its effect on member performance.

#### 4.4.3 Plastic Hinge Length

It was previously discussed that the shear span-to-depth ratio and the axial load level could affect the member behavior. In this section, the length of the plastic hinges that developed in the tested specimens is further studied. In order to estimate the plastic hinge length of cantilever column specimens, the expression proposed by Park and Paulay (1975) is used. Using a simple curvature distribution along the length of a column (Figure 4.28) and the second moment area theorem, Park and Paulay (1975) proposed that the tip displacement of a column can be expressed as:

$$\Delta_{tip} = \frac{\phi_y L^2}{3} + (\phi - \phi_y) l_p (L - 0.5l_p) \quad (4.10)$$

Plastic hinge lengths are estimated at the first cycle of each displacement demand level where  $\mu_\Delta$  is greater than 2. The results are shown in Table 4.4. The plastic hinge lengths listed in this table indicate that they are influenced by axial load level and shear span-to-depth ratio. The plastic hinge length increased as the shear span-to-depth ratio or the level of axial load increased.

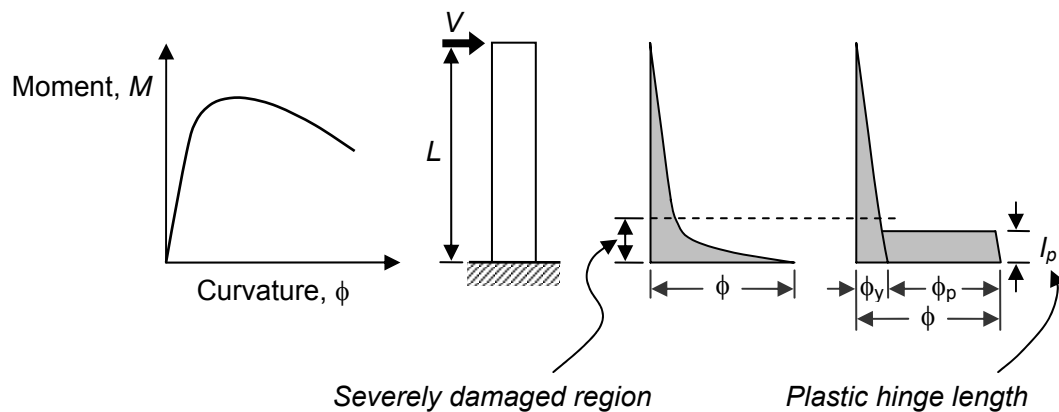


**Figure 4.28 Definition of Plastic Hinge Length (Park and Paulay 1975)**

**Table 4.4 Plastic Hinge Length: Experiments and Estimations**

Specimen	Cycle #	Equivalent Plastic Hinge Length		$P/P_o$	$L/h$	Photograph
		$l_p/h$	Average			
S24-2UT	14	0.64	0.66	0.5	5	
	17	0.66				
	20	0.70				
	23	0.68				
	26	0.61				
S17-3UT	14	1.02	0.91	0.5	7	
	17	0.89				
	20	0.82				
	23	0.80				
S24-4UT	14	0.57	0.49	0.2	5	
	17	0.52				
	20	0.50				
	23	0.43				
	26	0.44				
S24-5UT	14	0.50	0.47	0.2	5	
	17	0.50				
	20	0.44				
	23	0.41				

#### **4.5 SUMMARY**

The comparative evaluation presented above indicates that the sectional and member performances of concrete columns were influenced by the shear span-to-depth ratio, the level of axial load, the amount of confining reinforcement, and the plastic hinge length. It is also shown that the sectional and member-level performance of a concrete column can be affected by shear span-to-depth ratio, axial load and plastic hinge length.

The role of axial load on concrete column performance is complicated. As the axial load increases, the sectional performance of concrete columns deteriorates, resulting in poor member performance. At the same time, increasing axial load induces a longer plastic hinge length, which improves the member performance for a given sectional performance. In order to shed light on this interaction, the behavior of concrete columns is further studied in the subsequent chapters as follows:

- (1) Plastic hinge length: The effect of axial load on plastic hinge lengths is further examined with test results. An analytical method for use in estimating the plastic hinge lengths is developed. Using this analytical method, various parameters that affect the plastic hinge length are studied (Chapter 5).
- (2) Buckling of reinforcing bars: Experimental observations indicate that buckling of longitudinal bars occur at the commencement of failure. Since in conventional sectional analysis buckling behavior of the longitudinal bars is ignored, the accuracy of the results obtained from sectional analyses can be improved by developing a reinforcing bar buckling model. Based on extensive experimental research, conducted by Bayrak and

Sheikh (2001) and Mieses (2002), a simple bar buckling model is developed (Chapter 6).

- (3) Estimation of deformation capacity: Analytical methods are commonly used to predict column behavior. A state-of-the art analytical method which employs the proposed plastic hinge length expression (Chapter 5) and the reinforcing bar buckling model (Chapter 6) is developed. A simple closed-form expression that can be used to estimate the drift capacity of concrete columns is also derived. Results from a large number of concrete column tests are collected through the UW/PEER column database (<http://maximus.ce.washington.edu/~peera1/>). This database is used to examine the accuracy and conservativeness of the proposed methods in predicting the drift capacity of columns (Chapter 7).

# **CHAPTER 5**

## **PLASTIC HINGE LENGTH**

### **5.1 INTRODUCTION**

Predicting the lateral load-displacement response of reinforced concrete columns is of value in performance-based earthquake engineering. In its simplest form, the tip deflection of a reinforced concrete column can be estimated by integrating curvatures along its length. Typically, in estimating the overall load-displacement response of a reinforced concrete column, integration of curvatures and application of the second moment-area theorem is straightforward for the ascending part of the response. However, the post-peak part of the response is somewhat more difficult to predict, especially for columns where considerable strength degradation takes place after the peak load (or peak moment). In the analysis, this numerical difficulty is commonly handled through the use of plastic hinges. Plastic hinges are assumed to form close to the sections experiencing maximum bending moments. Curvatures are typically assumed to be constant within the plastic hinge region, and as such the rotation of plastic hinges can be calculated with relative ease. Consequently, an accurate estimation of a plastic hinge length is necessary to predict the displacement capacity of a column.

The length of a plastic hinge depends on many factors. The following is a list of several important factors that influence the length of a plastic hinge:

- Level of axial load
- Moment gradient
- Level of shear stress in the plastic hinge region
- Mechanical properties of longitudinal and transverse reinforcement

- Concrete strength
- Level of confinement and its effectiveness in the potential hinge region

Numerous researchers (Baker 1956; Baker and Amarakone 1964; Mattock 1964, 1967; Corley 1966; Park, Priestley and Gill 1982; Priestley and Park 1987; Paulay and Priestley 1992; Sheikh and Khouri 1993; Mendis 2001) have experimentally investigated the plastic hinge length of concrete members and suggested various expressions that can be used to estimate the plastic hinge length. In this chapter, the previous research on plastic hinge length is reviewed and the test results reported in Chapter 4 are analyzed. Finally, a new expression to estimate the plastic hinge length is proposed.

## 5.2 PLASTIC HINGE LENGTH

Plastic hinges form at the maximum moment regions of reinforced concrete columns. As a column experiences lateral displacement, severe damage is observed in the maximum moment regions. Large inelastic curvatures form in the plastic hinges. The plastic curvatures in plastic hinges are typically assumed to be constant. If the plastic hinge length is known, the tip displacement of columns can be easily obtained by integrating curvatures and vice versa. Therefore, accurate assessment of the plastic hinge length is important in relating section-level response to member-level response of concrete columns.

In the 1950's and 1960's, researchers (Baker 1956; Baker and Amarakone 1964; Mattock 1964 and 1967; Corley 1966) studied plastic hinge length to estimate the flexural deformation capacity of reinforced concrete beams. The rotation capacity of plastic hinges is calculated using Equation (5.1).

$$\theta_p = \frac{\epsilon_{cu} - \epsilon_{ce}}{d} \times l_p \quad (5.1)$$

where

$\theta_p$  = plastic rotation

$\varepsilon_{cu}$  = maximum concrete compressive strain

$\varepsilon_{ce}$  = elastic concrete compressive strain

$d$  = effective depth of a beam

$l_p$  = plastic hinge length

Park and Paulay (1975) expanded this concept to a cantilever column. They simplified the curvature distribution along the length of a column using a plastic hinge (Figure 4.28). Using the second moment area theorem, they calculated the tip displacement of a column (Equation (5.2)).

$$\Delta_{tip} = \Delta_y + \Delta_p = \frac{\phi_y L^2}{3} + (\phi - \phi_y) l_p (L - 0.5 l_p) \quad (5.2)$$

By further simplifying Equation (5.2), they obtained the relationship between curvature and displacement ductilities (Equation (5.3)).

$$\mu_\Delta = 1 + 3(\mu_\phi - 1) \frac{l_p}{L} \left( 1 - 0.5 \frac{l_p}{L} \right) \quad (5.3)$$

An examination of Equations (5.2) and (5.3) indicates that the effect of axial loads is not considered in deriving these equations. Equations (5.2) and (5.3) have been commonly used to estimate the plastic hinge lengths of concrete columns (Park et al. 1982; Priestley and Park 1987; Paulay and Priestley 1992; Sheikh and Khoury 1993; Sheikh et al. 1994; Bayrak and Sheikh 1998). The experimentally measured curvatures and tip displacements were used for this purpose. It is important to note that the tip displacement of a concrete column in Equation (5.2) is the summation of all displacement components which include

not only flexural displacement, but also displacements due to bar slip and shear effects.

### 5.3 PREVIOUS RESEARCH

#### 5.3.1 Baker (1956)

In order to investigate moment-curvature relationship of beams and columns, ninety-four beam/column tests were conducted by six laboratories under the auspices of the European Concrete Committee in the 1960s. The main test variables included the concrete strength, yield strength or amount of tension reinforcement, amount of compression reinforcement, single or double concentrated loads, and axial load. Typical test specimens and loading schemes are shown in Figure 5.1. The concrete strength varied from 2,500 psi to 5,800 psi and the yield strength of reinforcement was in the range of 40 ksi to 85 ksi. The amount of tension reinforcement was in the range of 0.25% to 4%. The ratio of “binding steel” ranged between 0.05% and 1.51%. According to Baker (1956), this ratio of binding steel is defined as the volumetric ratio of binding steel (one stirrup plus compression steel between stirrups) to confined concrete (stirrup spacing  $\times$  area enclosed by stirrup). Axial loads of  $0.15f'_c A_g$  to  $1.0f'_c A_g$  were applied to the test specimens, as illustrated in Figures 5.1(b) and 5.1(d). Based on the test results, Baker (1956) proposed the following equation to calculate the plastic hinge length ( $l_p$ ):

$$l_p = k_1 k_2 k_3 \left( \frac{z}{d} \right)^{0.25} d \quad (5.4)$$

where

$$\begin{aligned} k_1 &= 0.7 \text{ for mild steel} \\ &= 0.9 \text{ for cold worked steel} \end{aligned}$$

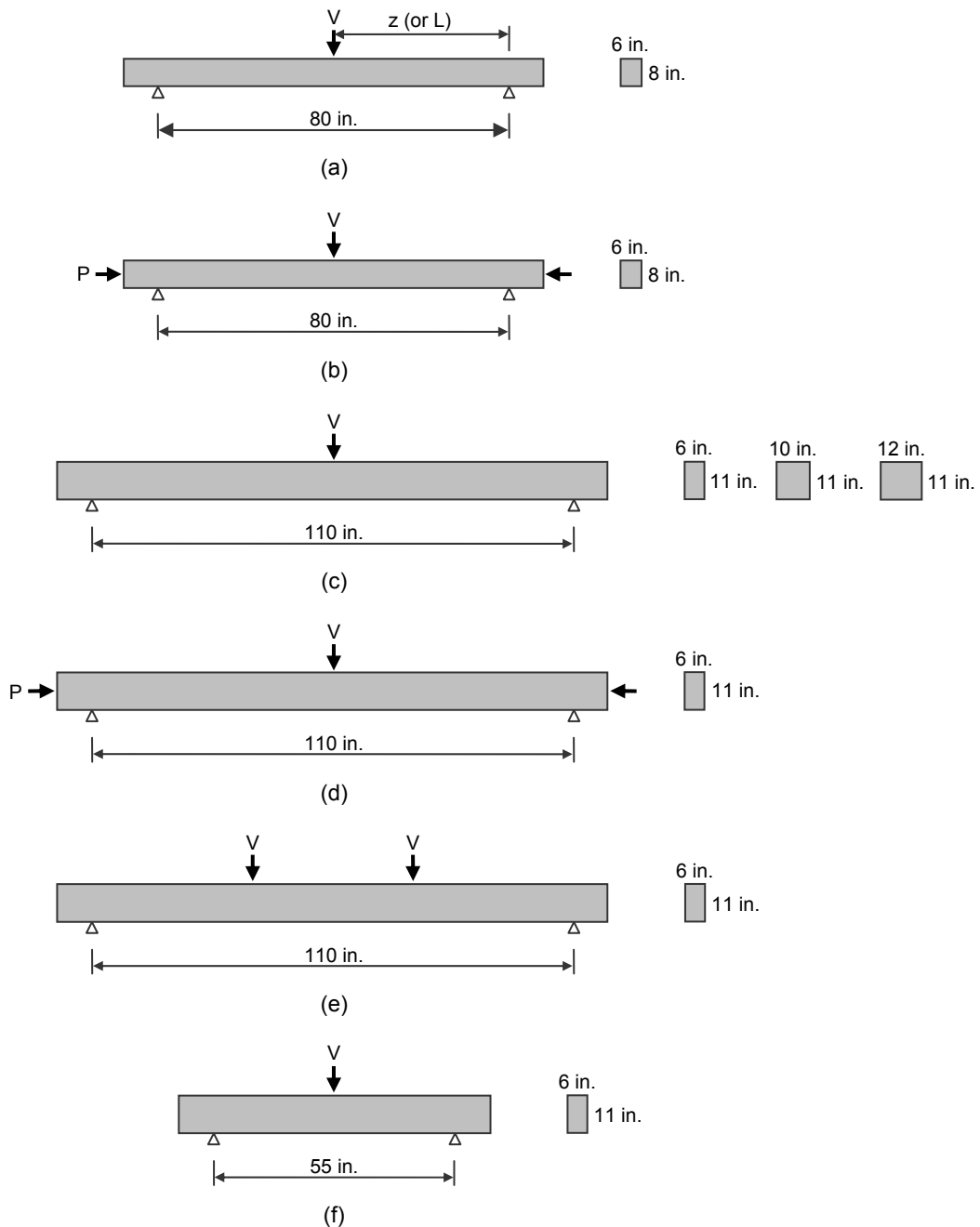


*Figure 5.1 Typical Test Specimens (Baker 1956)*

$$k_2 = 1 + 0.5 \frac{P}{P_o}$$

$$k_3 = 0.9 - \frac{0.3}{23.5} (f'_c - 11.7) \quad (f'_c \text{ in MPa})$$

$z$  = distance from critical section to point of contraflexure  
(Figure 5.1(a))

$d$  = effective depth of a beam

Baker reported that the plastic hinge lengths ranged from  $0.4d$  to  $2.4d$  for practical values of  $z/d$ . The  $z/d$  ratio was used to represent the effect of moment gradient, which is a similar parameter to the shear span-to-depth ratio ( $L/h$ ). Baker and Amarakone (1964) simplified Equation (5.4) to the following:

$$l_p = 0.8k_1 k_3 \left( \frac{z}{d} \right) c \quad (5.5)$$

where  $c$  is the neutral axis depth at collapse.

### 5.3.2 Mattock (1964)

Mattock (1964) conducted thirty-seven beam tests and investigated the effect of various parameters on the behavior of reinforced concrete beams (Figure 5.2). The parameters studied by Mattock were concrete strength ( $f'_c = 4,000$  to  $6,000$  psi), effective depth of beam ( $d = 10$  and  $20$  in.), moment gradient ( $z/d = 2.75$  to  $11$ ), and amount ( $\rho_l = 1\%$  to  $3\%$ ) and yield strength ( $f_y = 47$  to  $60$  ksi) of tension reinforcement.

Based on the test results, Mattock (1964) concluded that the spread of plasticity along a beam length increased as the  $z/d$  ratio increased, and as the net tension reinforcement  $((q - q') / q_b)$  decreased. Mattock (1964) proposed the following empirical relationship to calculate the plastic hinge length ( $l_p$ ).

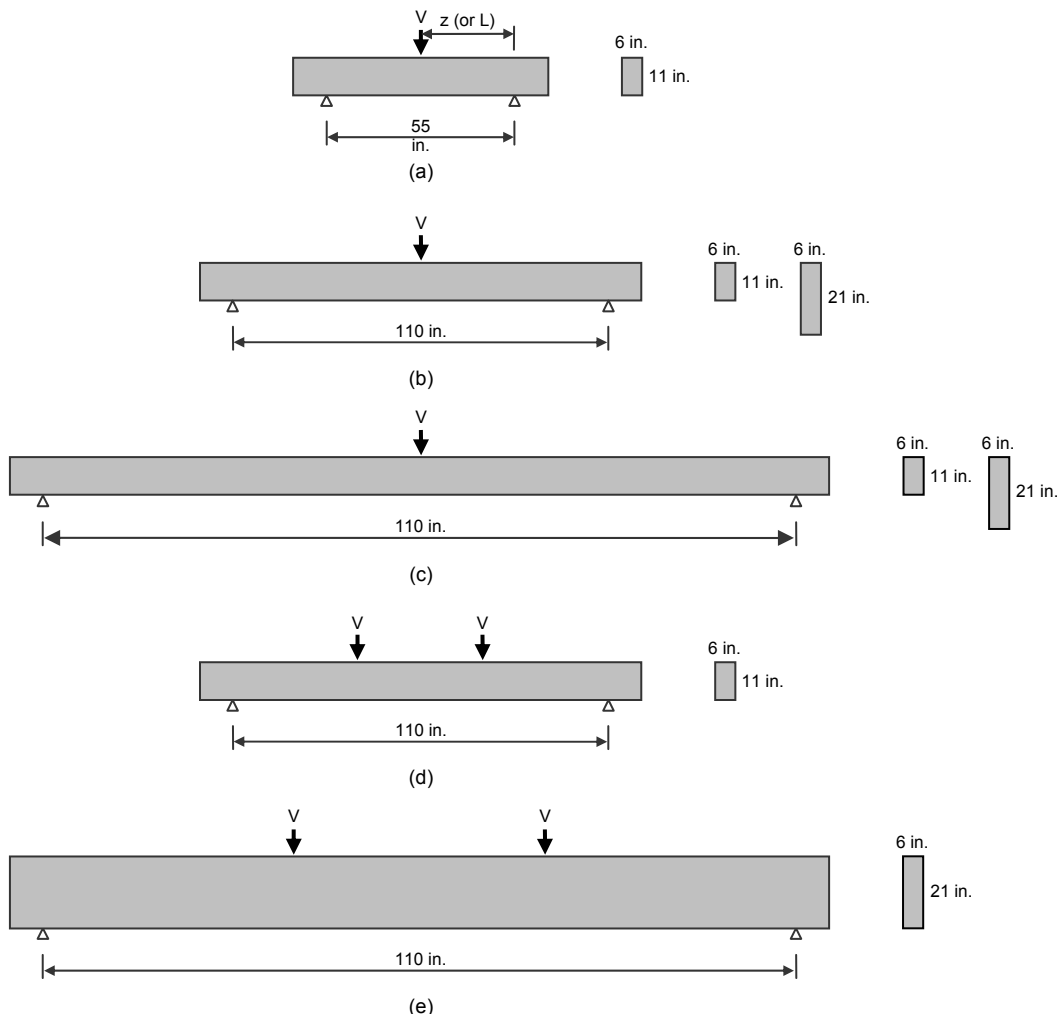


**Figure 5.2 Test Beam Specimens (Mattock 1964)**

$$l_p = \frac{d}{2} \left[ 1 + \left( 1.14 \sqrt{\frac{z}{d}} - 1 \right) \left\{ 1 - \left( \frac{q - q'}{q_b} \right) \sqrt{\frac{d}{16.2}} \right\} \right] \quad (5.6)$$

where

$d$  = effective depth of a beam (in inches)

$z$  = distance of critical section to point of contraflexure (in inches)

$q$  = tension reinforcement index [ $= (A_s / bd) \times (f_y / f'_c)$ ]

$q'$  = compressive reinforcement index [ $= (A_s' / bd) \times (f_y / f'_c)$ ]

$q_b$  = balanced tension reinforcement index [ $= (A_b / bd) \times (f_y / f'_c)$ ]

### 5.3.3 Corley (1966)

To expand Mattock's work (1964), Corley (1966) tested forty simply supported concrete beams subjected to single point loads. The confinement and size effects were the primary variables investigated. In addition, the effects of moment gradient and amount of tension reinforcement were studied. The ranges of major variables in the test program were as follows: (1) width of test beams: 3, 9, and 12 in.; (2) effective depth of test beams: 5, 10, 24, 30 in.; (3) span of test beams: 36, 72, 144, 165, 240, and 330 in.; (4) amount of tension reinforcement: between 1% and 3%; (5) ratio of "binding steel", defined in Section 5.3.1, between 0.3% and 9%. He reported that the spread of the plastic hinge region was primarily a function of the geometry of a concrete beam and that the size of a beam did not have a significant influence on the rotational capacity. Based on the scatter in the measured values of the plastic hinges, he concluded that the effect of  $(q - q')/q_b$  could be ignored. Corley suggested the use of a simple expression for calculating the plastic hinge length ( $l_p$ ).

$$l_p = \frac{d}{2} + 0.2 \frac{z}{\sqrt{d}} \quad (5.7)$$

where both  $d$  and  $z$  are in inches.

### 5.3.4 Mattock (1967)

Mattock simplified Equation (5.6) in 1967. He stated that even though there was considerable scatter, the trend in the observed plastic hinge lengths could be represented reasonably well by the following simple expression:

$$l_p = \frac{d}{2} + 0.05z \quad (5.8)$$

### 5.3.5 Park, Priestley and Gill (1982)

Park et al. (1982) tested four full-scale concrete columns with square sections of  $22 \times 22$  in.<sup>2</sup> ( $550 \times 550$  mm<sup>2</sup>) and shear span-to-depth ratios of 2. The axial loads applied to the column specimens were in the range of  $0.2f'_c A_g$  to  $0.6f'_c A_g$ . Park, Priestley and Gill estimated the plastic hinge lengths of the test specimens using Equation (5.2). They concluded that the experimentally obtained plastic hinge lengths were comparatively insensitive to axial load level and had an average value of  $0.42h$ , where  $h$  is the overall depth of a column. They suggested using a simple plastic hinge length of  $0.4h$  for concrete columns.

Using a similar approach, Priestley and Park (1987) proposed the following equation for the calculation of plastic hinge length in reinforced concrete columns.

$$l_p = 0.08L + 6d_b \quad (5.9)$$

where

$L$  = distance from the critical section to the point of contraflexure

$d_b$  = diameter of longitudinal reinforcement

The suggested plastic hinge length (Equation (5.9)) has two components. Priestley and Park (1987) stated that the first term mainly accounted for column bending, while the second accounted for bar slip due to the elongation of longitudinal bars beyond the theoretical base (tensile strain penetration into the joint or foundation).

Paulay and Priestley (1992) revised Equation (5.9) to account for different grades of flexural reinforcement. The revised expression is given in Equation (5.10).

$$l_p = 0.08L + 0.15d_b f_y \text{ (} f_y \text{ in ksi)} \quad (5.10)$$

$$l_p = 0.08L + 0.022d_b f_y \text{ (} f_y \text{ in MPa)}$$

Paulay and Priestley (1992) reported that Equation (5.10) resulted in values of  $l_p \approx 0.5h$  for typical concrete columns.

### 5.3.6 Sakai and Sheikh (1989)

Based on an extensive review of the literature, Sakai and Sheikh (1989) reported that the plastic hinge length increased as the aspect ratio ( $L/h$  or  $L/D$ ), which is equivalent to the shear span-to-depth ratio, increased, as shown in Figure 5.3. Bilinear curves illustrating the relationship between the plastic hinge length and the aspect ratio were reported as trend lines by the authors, as shown in Figure 5.3. They concluded that the plastic hinge length was affected by the amount of transverse reinforcement, axial load level, and aspect ratio.

### 5.3.7 Sheikh (1993, 1994 and 1998)

Sheikh and Khory (1993), Sheikh et al. (1994) and Bayrak and Sheikh (1998) reported that the measured plastic hinge lengths were approximately equal to  $1.0h$  in their column tests. It is important to note that most of their column tests were conducted under high axial loads.

### 5.3.8 Mendis (2001)

Mendis conducted tests on thirteen simply supported concrete beams subjected to single point loads and examined their plastic hinge lengths. He reported that the plastic hinge length increased as the shear span-to-depth ratio or the longitudinal reinforcement ratio increased, but decreased as the amount of lateral reinforcement increased.

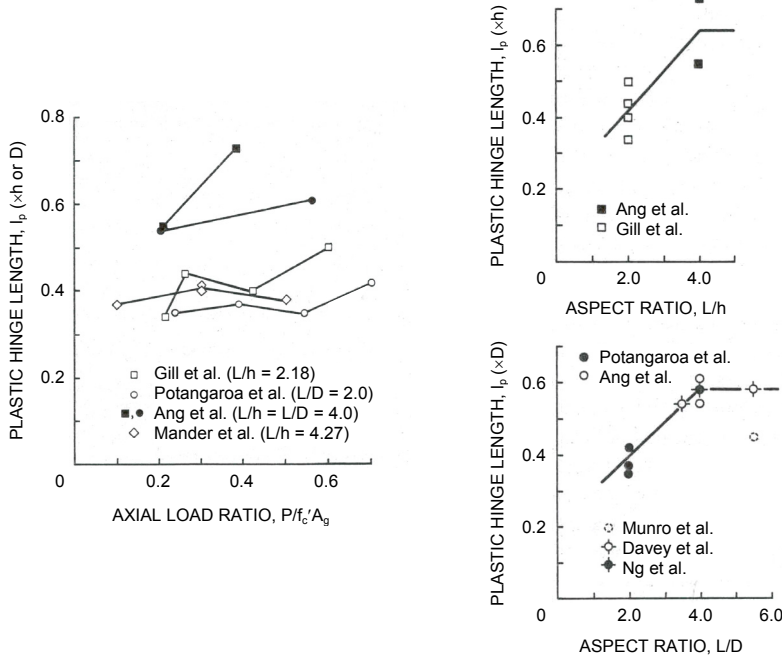


**Figure 5.3 Effects of Various Parameters on Plastic Hinge Lengths  
(Sakai and Sheikh 1989)**

Based on four column tests where the axial load levels were low ( $P/f'_c A_g = 0.06$  to 0.20), Mendis concluded that the plastic hinge length was not sensitive to the level of axial load.

#### 5.4 DISCUSSION ON PREVIOUS RESEARCH

Various expressions, recommended for use in plastic hinge length estimations, were briefly discussed in the previous sections. A comparison of the previously reported plastic hinge length expressions is provided in Figure 5.4. This figure clearly illustrates that large variations exist among the suggested plastic hinge lengths.

It is interesting to note that most of these expressions do not consider axial loads as a parameter, except for the expressions proposed by Baker (1956) and

Baker and Amarakone (1964). In early research (Baker 1956; Baker and Amarakone 1964; Mattock 1964, 1967; Corley 1966), the behavior of concrete beams was the major focus in investigating the plastic hinge length. In the more recent research (Park et al. 1982; Priestley and Park 1987; Paulay and Priestley 1992; Sheikh and Khoury 1993), the behavior of concrete columns has been the focus of plastic hinge length investigations.

Although the effect of axial load on the plastic hinge length of concrete columns has been reported by several researchers, the reported results are contradictory. As discussed in the previous sections, Park et al. (1982) and Mendis (2001) concluded that the plastic hinge lengths were insensitive to axial load level based on their test results. In contrast, Atalay and Penzien (1975) reported that the spread of damaged region increased as the axial load level increased. Tanaka and Park (1990) reported that the plastic hinge length increased from  $0.46h$  to  $0.75h$ , as the applied axial load level increased from  $0.1f'_c A_g$  to  $0.3f'_c A_g$ . The test results by Thomsen and Wallace (1994) and Légeron and Paultre (2000) indicated that the increase of plastic hinge lengths with the axial loads could also be observed for high strength concrete columns. Therefore, an investigation into the plastic hinge length of reinforced concrete columns is needed in order to estimate more accurate plastic hinge lengths for various axial load levels.

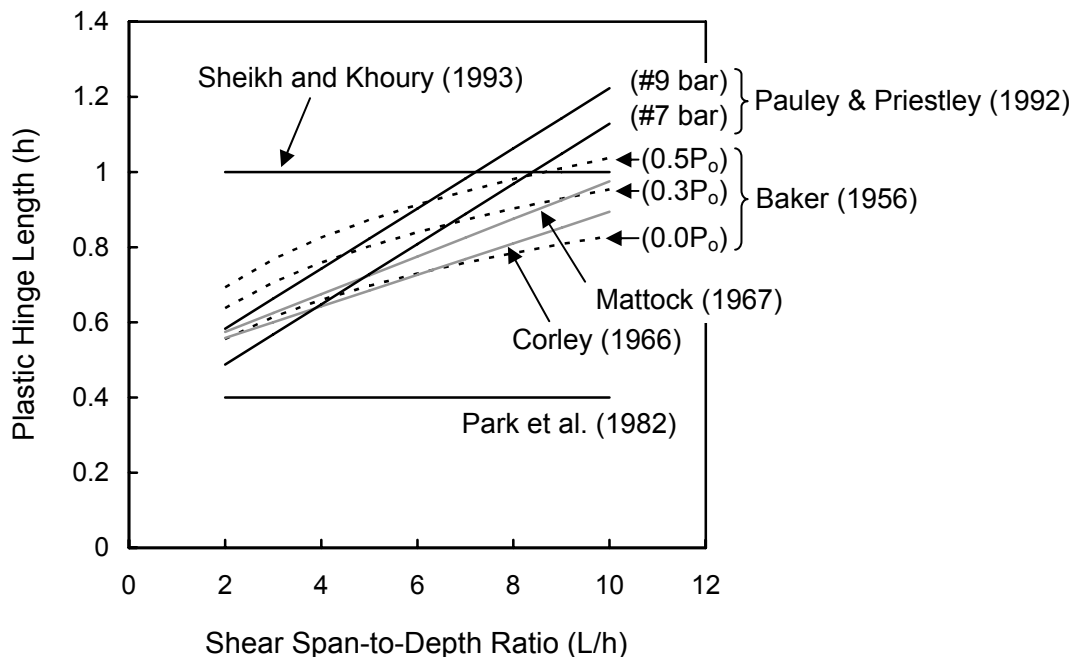


**Figure 5.4 Comparison of Various Plastic Hinge Length Estimates**

#### 5.4.1 Discussion of Current Test Results

The damage observed within the plastic hinge region of each test specimen and the corresponding tie strains along the columns are shown in Figures 5.5 and 5.6. Specimens S24-2UT and S24-3UT were tested under an axial load level of  $0.5P_o$ , while specimens S24-4UT and S24-5UT were tested under a lower axial load level of  $0.2P_o$ . The photographs in Figures 5.5 and 5.6 show that the severely damaged regions of specimens S24-2UT and S17-3UT were longer than those of specimens S24-4UT and S24-5UT. The tie strains along the column specimens at the 20<sup>th</sup> loading cycle in Figures 5.5 and 5.6 illustrate that specimens S24-2UT and S17-3UT experienced inelastic tie strains over a longer length than specimens S24-4UT and S24-5UT. Many ties in specimens S24-2UT and S17-

3UT experienced larger inelastic strains after the 20<sup>th</sup> loading cycle than the measurement limits of strain gauges. Therefore, it can be concluded that for the specimens tested in this study, plastic hinge lengths increased as levels of axial load increased.

Figures 5.7 and 5.8 illustrate the sectional and member performances of specimens S24-2UT and S24-4UT. Specimen S24-2UT and S24-4UT have the same section size (24 in.) and shear span-to-depth ratio ( $L/h = 5$ ). These specimens were tested under different axial load levels ( $P/P_o = 0.5$  for S24-2UT and  $P/P_o = 0.2$  for S24-4UT). Figure 5.7 illustrates that the sectional performance of S24-4UT is somewhat better than that of S24-2UT with respect to the deformation capacity. However, the opposite trend can be seen in Figure 5.8. The reversal in the trends is attributed to the difference observed in the plastic hinge lengths of specimens S24-2UT and S24-4UT. In addition, the plastic hinge lengths listed in Table 4.4 support the influence of axial load on the plastic hinge lengths.

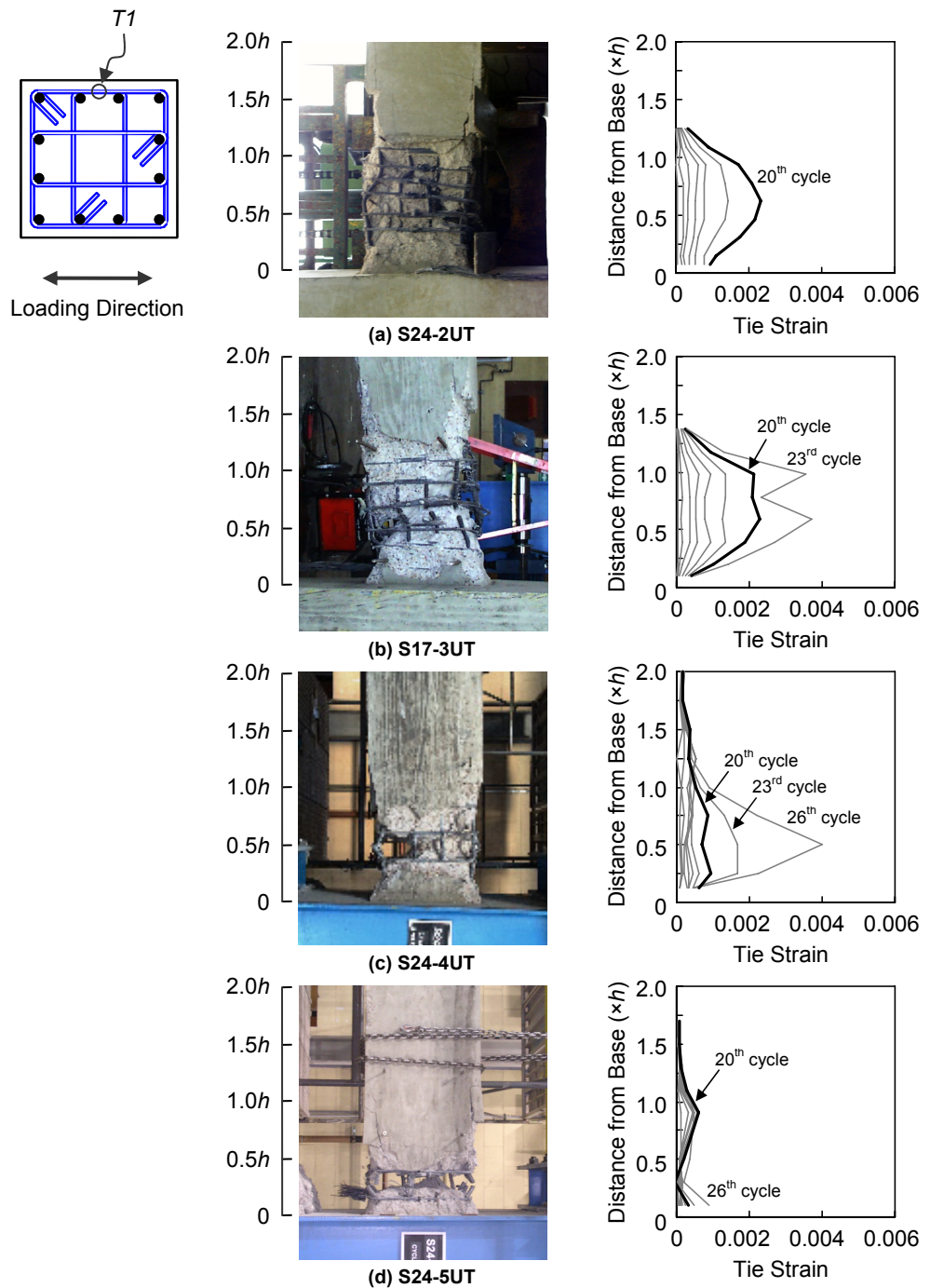


**Figure 5.5 Strain Distribution in Outer Hoops**

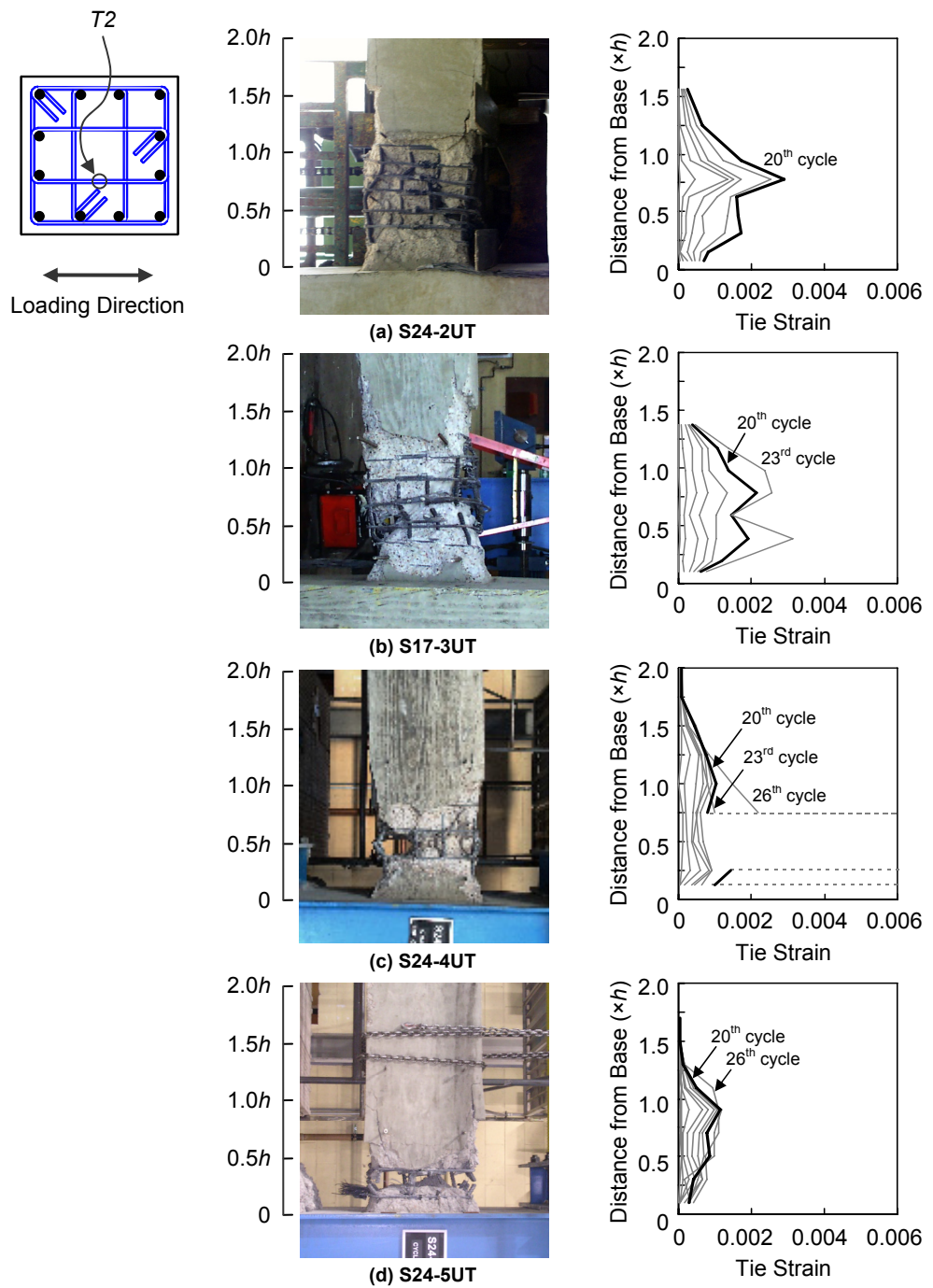


**Figure 5.6 Strain Distribution in Inner Hoops**

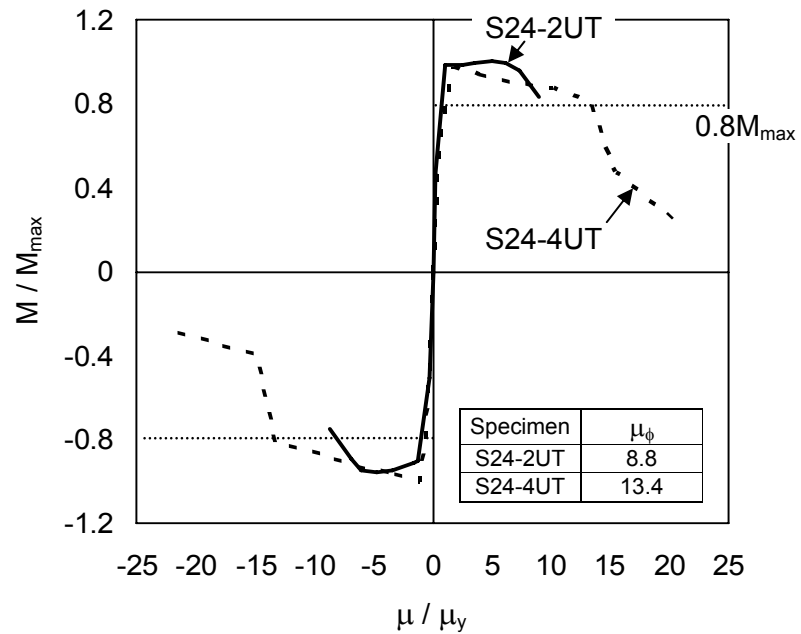


Figure 5.7 Normalized Moment-Curvature Backbone Curves

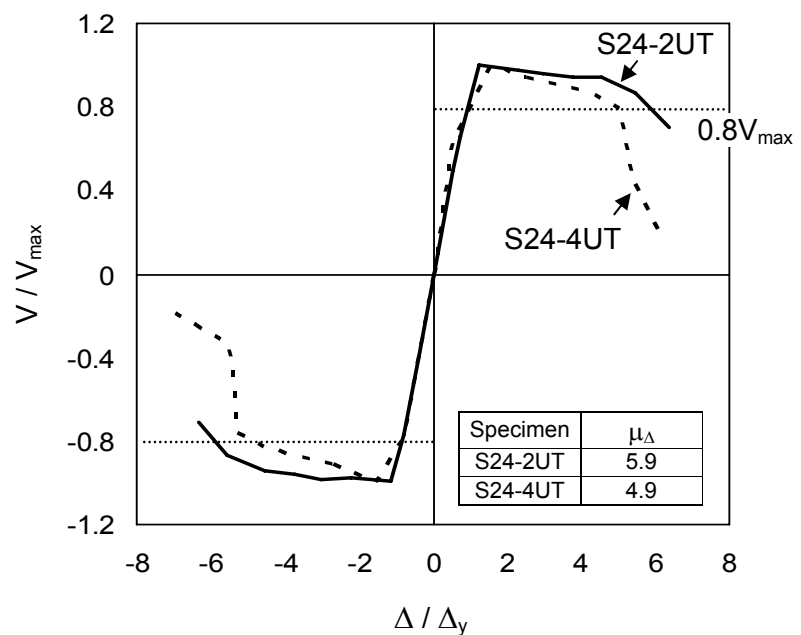


Figure 5.8 Normalized Lateral Load-Displacement Backbone Curves

## **5.5 PLASTIC HINGE LENGTH: ANALYTICAL APPROACH**

Estimating with analytical programs the length of plastic hinges that may form in reinforced concrete columns is difficult. Because of this difficulty, plastic hinge lengths have typically been based on experimental results. A plastic hinge is defined as the zone where severe damage of a concrete section occurs. By observing that large cracks typically occur at curvatures greater than the yield curvature, some researchers (Chan 1955; ACI-ASCE Committee 428 1968) attempted to relate the yield moment to the plastic hinge length. This approach is practical when the curvature increases with moment (i.e., in the ascending branch of the response), but its application to members that experience post-peak strength degradation is questionable.

In this section, an analytical approach that can be used to estimate the plastic hinge lengths of concrete columns is introduced. Following the description of this analytical approach, the important factors are studied by conducting sensitivity analyses. Based on the results of the sensitivity analyses, a simple expression that can be used in estimating the length of the plastic hinges is proposed. Finally, the influence of the plastic hinge length estimations on the lateral load-displacement response predictions is discussed.

### **5.5.1 Compressive Strain Profile of Core Concrete**

As reinforced concrete columns are subjected to earthquake induced lateral displacements while supporting gravity loads, plastic hinges form within the core concrete. The magnitude of damage in concrete members is closely related to the intensity of concrete compressive strains measured at critical sections. Under increasing curvatures, concrete strains on the compression side of the member increase. As the concrete compressive strains increase and reach a critical value, the cover concrete spalls off. Subsequently, yielding of longitudinal

bars on the compression side occurs. This is followed by crushing of core concrete. With accumulation of damage under increasing compressive strains, plastic hinges form. Therefore, the magnitude of concrete compressive strains experienced by the core concrete should give a good indication on the formation of a plastic hinge. In order to estimate the length of a plastic hinge that may form at the base of a reinforced concrete column (Figure 5.9(a)), the following procedure can be used:

- (1) The moment-curvature response of a typical column section within the potential plastic hinge region is obtained from a sectional analysis.
- (2) Neglecting the second order effects, the bending moment diagram is drawn (Figure 5.9(c)). The moment value at the center of the potential plastic hinge ( $\sim 0.5h$  away from the base) is assumed to be equal to the maximum moment capacity of the section obtained from the sectional analysis in step (1). In other words, failure is assumed to take place at the center of the assumed plastic hinge. This assumption would imply that the sections between the center of the plastic hinge and the base of the column have a larger flexural capacity than predicted using the sectional analysis. The shift in the location of critical section (Figure 5.9(d)) is due to the confinement provided by the concrete stub to the neighboring sections. This effect, commonly referred to as stub confinement effect, has been observed in previous experimental research (Soesianawati et al. 1986; Sheikh and Khoury 1993; Bayrak and Sheikh 1998; Légeron and Paultre 2000).
- (3) Using the bending moment diagram from step (2) and the moment-curvature analysis' results from step (1), the compressive strain experienced by the outer fiber of core concrete can be determined for a

sufficient number of sections along the length of a column. If these compressive strains are plotted along the length of a column, the compressive concrete strain profile at the maximum moment along the length of a column can be obtained (Figure 5.9(d)).

- (4) The compressive strains at the outer fiber of the core concrete are equal to the reinforcing bar strains. In effect, the compressive strain profile obtained in step (3) represents the variation of compressive longitudinal bar strain along the length of a column. By examining the compressive strain profile, such as the one shown in Figure 5.9(d), the length of the region in which longitudinal bars are yielding in compression can be estimated. The identification of this length establishes a key step in estimating the plastic hinge of a column.
- (5) As indicated in step (2), the critical section shifts away from the face of the stub due to additional confinement effects provided by the stub. Because of the additional confinement provided by the stub to adjacent sections, sections within a distance of about  $0.25h$  from the stub remain nearly undamaged. In order to estimate the length of the plastic hinge region, where columns are expected to dissipate large amount of inelastic energy by undergoing large inelastic deformations,  $0.25h$  is subtracted from the overall length in which compressive rebar strains greater than the yield strain are calculated.

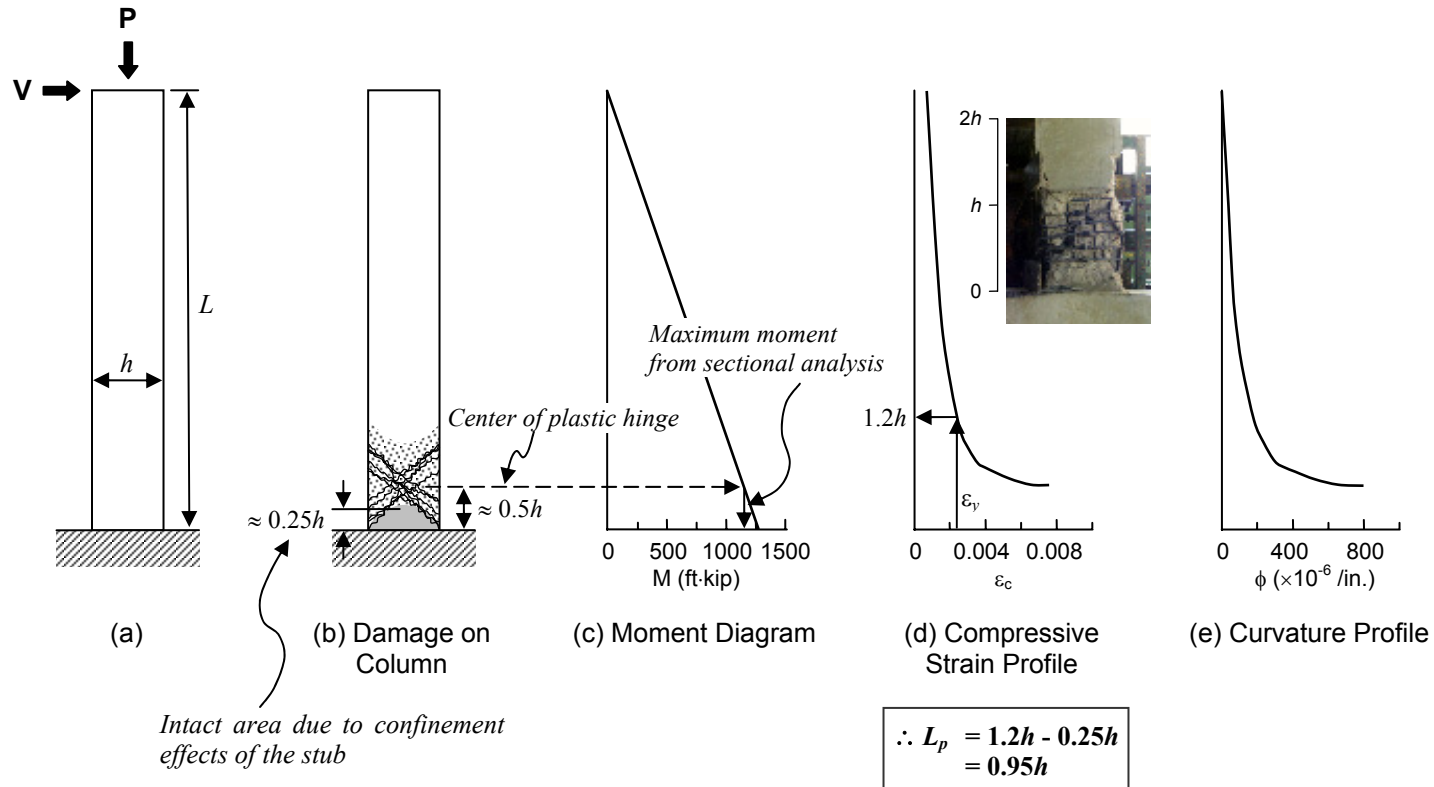
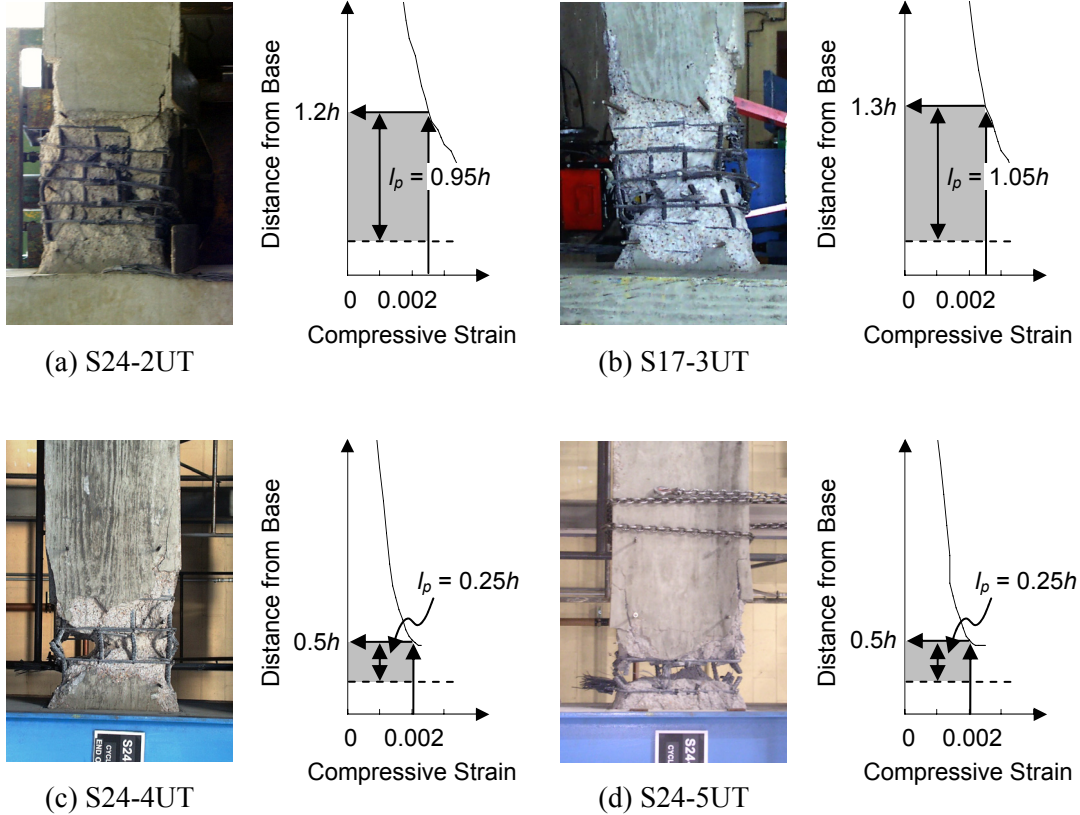


Figure 5.9 Estimation of Plastic Hinge Length (S24-2UT)

A detailed discussion on constitutive models used for sectional analysis and the step-by-step procedure discussed above is provided in Appendix B. Similar trends are observed in the curvature profile depicted in Figure 5.9(e) and the compressive strain profile shown in Figure 5.9(d). Hence, the use of curvature distribution along the length of a column can be considered as an alternative for identifying the zone in which inelastic curvatures are localized. While this curvature profile has been used by early researchers (Chan 1955; ACI-ASCE Committee 428 1968), the use of the compressive strain profile facilitates a clearer observation of the strains imposed by the axial compressive loads. In addition, since the damage in concrete is more closely related to the magnitude of the concrete strains than the curvatures, compressive strains were used in the method described above.

In this approach, it is assumed that the plastic hinges start to form when the maximum moment capacity is reached and therefore, important information on the plastic hinge formation can be obtained by analyzing the compressive strain profile when the maximum moment is reached. It is important to note that the plastic hinge lengths estimated in this manner can be used to estimate flexural deformations, since sectional analysis is used as the basis of calculations. To calculate the tip deformation of columns, deformations due to bar slip and shear deformations need to be calculated separately and added to the flexural deformations.

The lengths of the potential plastic hinge regions of specimens S24-2UT through S24-5UT are estimated by using the analysis procedure described above. By using the compressive strain profiles along the length of the test specimens, the plastic hinge lengths were estimated and the results of these analyses are shown in Figure 5.10. This figure illustrates that the proposed method provides



**Figure 5.10 Estimated Plastic Hinge Lengths of Tested Column Specimens**

good estimations for the plastic hinge lengths of the column specimens tested in this study.

## 5.6 PARAMETRIC STUDY ON PLASTIC HINGE LENGTH

It was shown that the proposed analytical approach provided good estimations for the plastic hinge lengths of the columns tested in this study. Using the method proposed in Section 5.5, the influence of various parameters on the plastic hinge lengths is studied. The effect of axial load level ( $P/P_o$ ), shear span-to-depth ratio ( $L/h$ ), and amount of longitudinal reinforcement ( $\rho_l = A_s/A_g$ ) are investigated.

### 5.6.1 Axial Load Level ( $P/P_o$ )

In order to study the effect of axial load on the plastic hinge length, a square column ( $24 \times 24 \times 120$  in.<sup>3</sup>) is studied. The percentage of longitudinal reinforcement is kept constant at 1% ( $\rho_l = 0.01$ ) and a ratio of the center-to-center distance of extreme reinforcement layers to the overall column depth ( $\gamma$ ) is assumed to be 0.8. Concrete strength of 6,000 psi is used. The yield and ultimate strength of reinforcing bars are assumed to be 60 ksi and 90 ksi, respectively. The curvature and compressive concrete strain profiles along the length of columns are investigated for various axial load levels. Figure 5.11 illustrates a summary of the results of the analyses. As can be observed in this figure, the curvature profiles do not effectively show the difference among various axial load levels. However, the compressive strain profiles clearly illustrate the influence of axial load.

For each of the cases studied in Figure 5.11, the length of the plastic hinge is estimated using the procedure described in Section 5.5. In other words, spread of reinforcing bars yielding in compression is examined to establish the length of the plastic hinges. Figure 5.12 summarizes the results of this analysis. As can be seen in this figure, the length of the plastic hinge is nearly constant for low axial loads ( $P \leq 0.2P_o$ ). For low axial loads, the plastic hinge length is approximately equal to  $h/4$ . Starting at an axial load of about  $0.2P_o$ , the plastic hinge length increases with increasing axial loads. It is interesting to note that Mendis (2001) reported that the plastic hinge lengths measured in the columns tested in his research were not sensitive to the axial load level. Considering the fact that all of the columns tested by Mendis (2001) had low axial load levels ( $P \leq 0.2P_o$ ), and bearing in mind the findings of this parametric study summarized in Figure 5.11, the conclusion reported by Mendis (2001) can be better appreciated.

The plastic hinge length estimate of  $0.25h$  (Figure 5.10) can be compared with  $0.4h$  recommended by Park et al. (1982) and  $0.5h$  recommended by Paulay

and Priestley (1992). The differences observed in the plastic hinge length estimates can be attributed to the displacement components used to estimate the plastic hinge. The flexural displacements are used in the proposed analysis, as the strains experienced by compression bars are obtained from the moment-curvature relationship. On the other hand, the tip displacements are used in estimating the plastic hinge length by Park et al. (1982) and Paulay and Priestley (1992).

Chapter 21 of the ACI code assumes that the length of the potential plastic hinge region to be the largest of the overall depth of a column, one-sixth of the clear height of a column, or 18 in. (457 mm). Figure 5.12 shows that the estimated plastic hinge length approaches  $0.8h$  at an axial load of  $0.52P_o$  ( $= \phi P_{n,max} = \phi \times 0.8P_o = 0.65 \times 0.8P_o$  for tie reinforcement), which is the maximum axial load permitted by ACI 318-05. It is also important to note that an additional length of  $0.25h$  has to be considered due to stub confinement effect (Figure 5.9 and Figure 5.10). Summing the largest estimated plastic hinge length and a distance of  $0.25h$  due to the stub confinement effect, the required confined length ( $1.05h$ ) needs to be slightly larger than the overall depth of a column ( $h$ ) at high axial loads. In short, the potential plastic hinge length specified by ACI 318-05 is likely to be satisfactory in most cases except for columns supporting high axial loads.

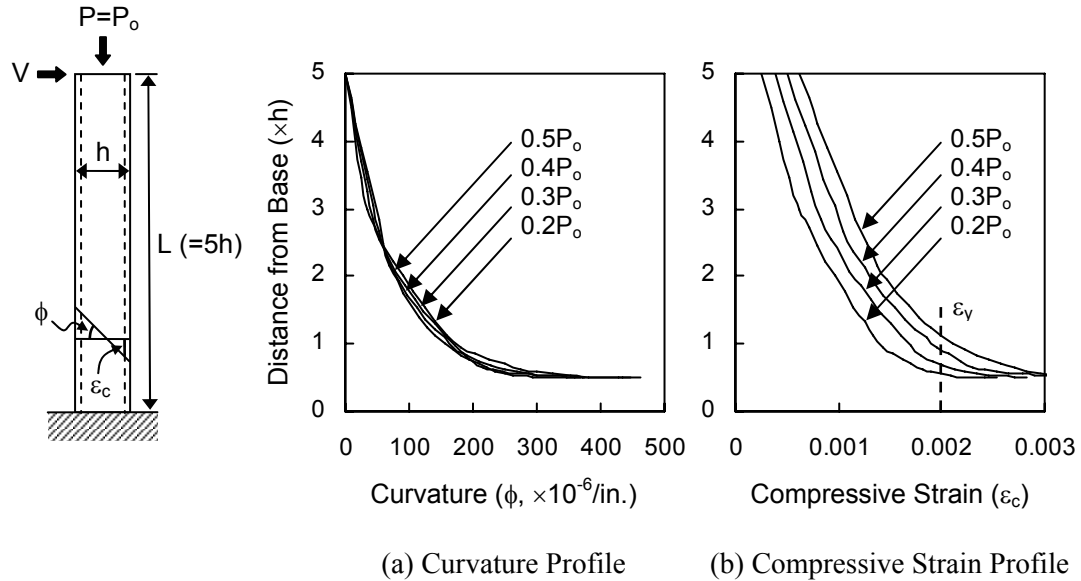


**Figure 5.11 Effect of Axial Load on Curvature and Compressive Strain Profiles**

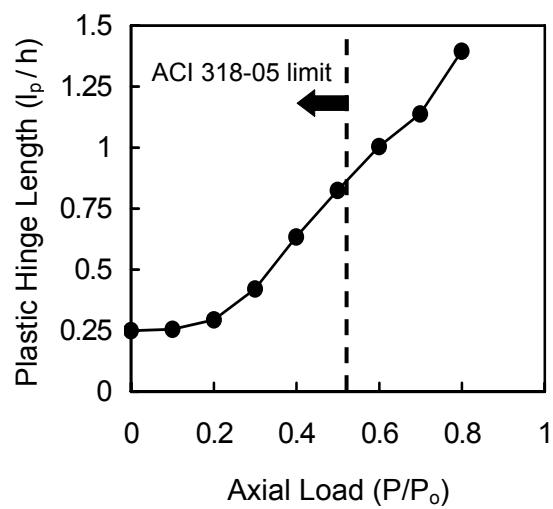


**Figure 5.12 Relationship between Plastic Hinge Length and Axial Load**

### 5.6.2 Shear Span-to-Depth Ratio ( $L/h$ )

Researchers (Baker 1956; Baker and Amarakone 1964; Mattock 1964, 1967; Corley 1966; Priestley and Park 1987; Paulay and Priestley 1992; Mendis 2001) recognized that the length of a plastic hinge is influenced by the shear span-to-depth ratio ( $L/h$ ). In order to investigate the influence of the shear span-to-depth ratio on the plastic hinge length, a series of analyses were conducted. At this stage of the parametric study, a  $24 \times 24$  in.<sup>2</sup> square column with varying shear span-to-depth ratios is considered. The longitudinal reinforcement is kept constant ( $\rho_l = 0.01$ ) and a  $\gamma$  value of 0.8 is used. The results of the analyses are summarized in Figure 5.13.

As can be observed in the figure, the plastic hinge length increases with increasing shear span-to-depth ratios for a given axial load level. However, for low axial loads ( $\approx 0.2P_o$ ), the increases observed in plastic hinge lengths with increasing shear span-to-depth ratios are insignificant.

For a given shear span-to-depth ratio, the plastic hinge length increases with increasing axial loads. The increases in plastic hinge lengths observed at small shear span-to-depth ratios ( $2 < L/h < 3$ ) are less pronounced than those observed at high shear span-to-depth ratios. It is interesting to note that Park et al. (1982) tested a series of columns with a shear span-to-depth ratio of 2.2. Based on the test results, they recommended a plastic hinge length of  $0.4h$ . Figure 5.11 clearly illustrates that for a shear span-to-depth ratio of 2.2, the effect of axial loads on the plastic hinge length are relatively small in comparison to the effects seen at high shear span-to-depth ratios.

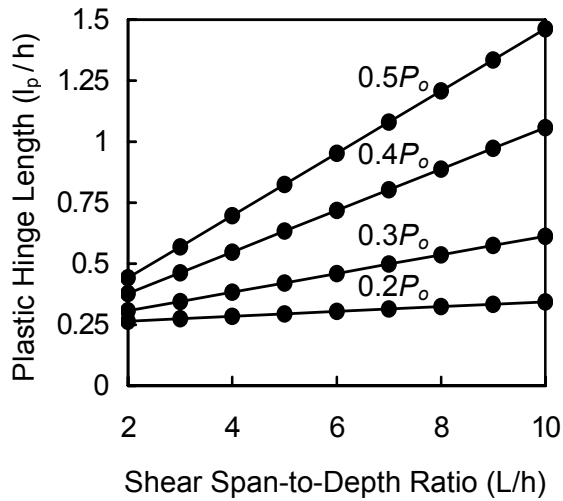


**Figure 5.13 Relationship between Plastic Hinge Length and Shear Span-to-Depth Ratio**

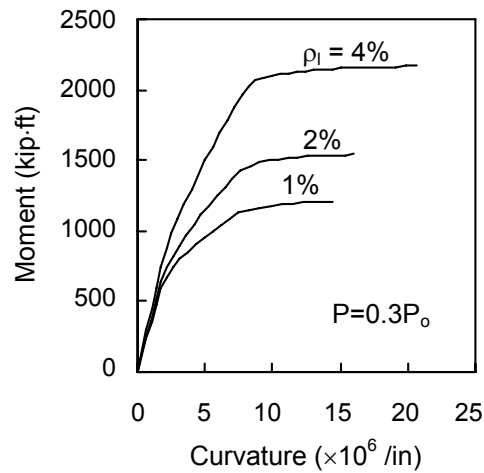
### 5.6.3 Amount of Longitudinal Reinforcement ( $\rho_l = A_s/A_g$ )

Mattock (1964) reported that the plastic hinge length increased with a decrease in the net tension reinforcement ( $(A_s - A'_s)/A_b$ , where  $A_s$  is the area of tension reinforcement,  $A'_s$  is the area of compression reinforcement, and  $A_b$  is the area of balanced reinforcement). The effect of net tension reinforcement was questioned by Corley (1966). Recently, Mendis (2001) reported that the plastic hinge length increased with increasing amount of tension reinforcement. These conclusions (Mattock 1964; Corley 1966; Mendis 2001) were primarily based on the results from tests conducted on reinforced concrete beams.

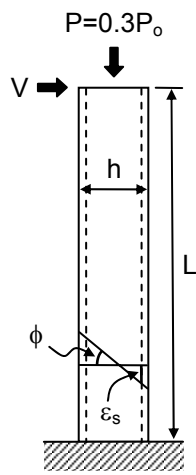
Due to the lack of consensus among various researchers, the amount of longitudinal reinforcement has been ignored by most previous proposals for estimating the plastic hinge length. To study the effect of longitudinal reinforcement on plastic hinge lengths, a  $24 \times 24$  in.<sup>2</sup> square column with a column height of 120 in., a shear span-to-depth ratio of 5 and a  $\gamma$  value of 0.8 is studied.

The results of the parametric study conducted on a  $24 \times 24$  in.<sup>2</sup> square column are summarized in Figures 5.14 and 5.15. As can be observed in Figure 5.14, the post-cracking stiffness and strength of the column sections increase with increasing reinforcement ratios.

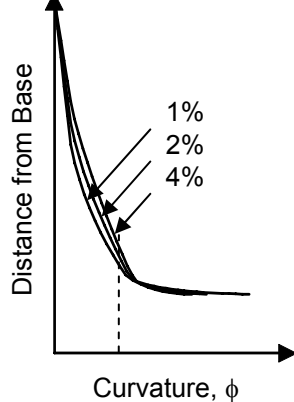
The curvatures and reinforcing bar strains on the compression side are evaluated at maximum lateral load capacity and plotted along the length of the column (Figure 5.14). An examination on the curvature and compressive strain profiles along the length of the column indicates that with increasing longitudinal reinforcement ratio ( $\rho_l$ ), the length of the plastic hinge increases. Figure 5.15 indicates this trend very clearly for various axial load levels. For all of the axial load levels, plastic hinge length increases with increasing  $\rho_l$  values.



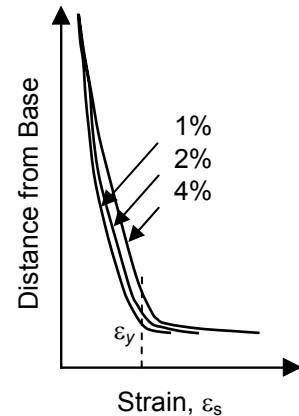
(a) Moment-Curvature Relationship



(b) Column



(c) Curvature Profile



(d) Compressive Strain Profile

**Figure 5.14 Effects of Longitudinal Reinforcement Ratio on Curvature and Compressive Strain Profiles**

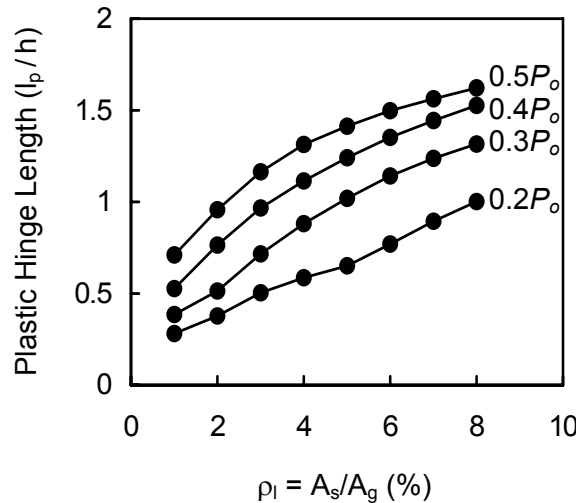
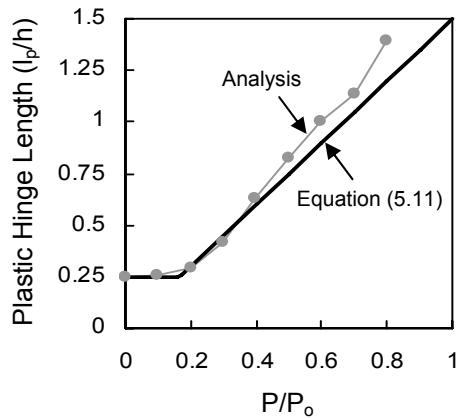


**Figure 5.15 Effect of Amount of Longitudinal Reinforcement**

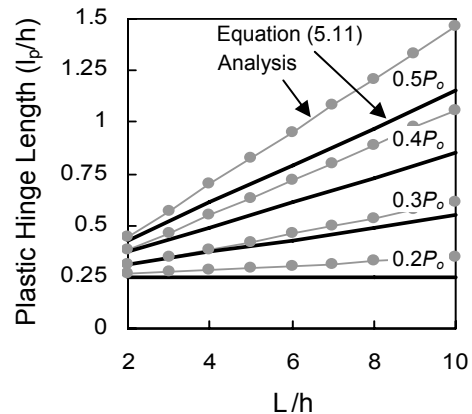
### 5.7 PLASTIC HINGE LENGTH: A NEW EXPRESSION

A series of sensitivity analyses were conducted to identify the primary variables influencing the length of plastic hinges. The sensitivity analyses showed that axial load, shear span-to-depth ratio and amount of longitudinal reinforcement had significant influences on the length of plastic hinges. Based on the analysis results, linear relationships between these parameters ( $P/P_o$ ,  $L/h$  and  $A_s/A_g$ ) and the plastic hinge length are used in calibrating the plastic hinge length expression for simplicity. Equation (5.11) is the result of a series of least squares analyses conducted on the UW/PEER column database (<http://maximus.ce.washington.edu/~peera1/>).

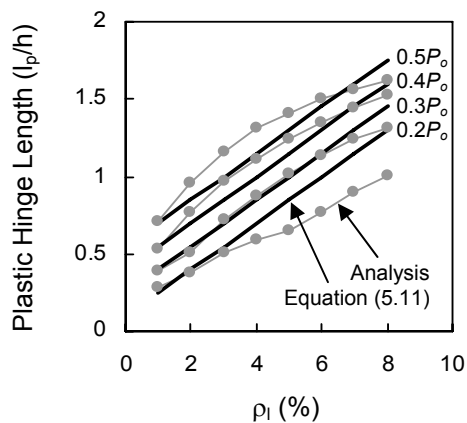
$$\frac{l_p}{h} = \left[ 0.3\left(\frac{P}{P_o}\right) + 3\left(\frac{A_s}{A_g}\right) - 0.1 \right] \left(\frac{L}{h}\right) + 0.25 \geq 0.25 \quad (5.11)$$



(a) Axial Load



(b) Shear Span-to-Depth Ratio



(c) Amount of Longitudinal Reinforcement

**Figure 5.16 Plastic Hinge Length: Equation (5.11) versus Analysis**

Figure 5.16 shows comparisons of the predicted plastic hinge lengths obtained from the analysis of compressive strains and those from Equation (5.11). There are some discrepancies in the plastic hinge lengths estimated by the analytical approach and Equation (5.11) especially at high axial loads and large shear span-to-depth ratios. It is important to note that the estimated plastic hinge lengths obtained from the analysis of compressive strains are approximate values. Considering that, Equation (5.11) is intended to be a simple expression that underestimates plastic hinge lengths such that conservative estimations for the deformation capacity of concrete columns can be obtained. Figure 5.16 shows that Equation (5.11) provides conservative plastic hinge length estimates for practical ranges of axial load, shear span-to-depth ratio, and amount of longitudinal reinforcement.

## 5.8 PLASTIC HINGE LENGTH: ESTIMATIONS AND EXPERIMENTS

Accurate estimation of the length of a plastic hinge formation in a reinforced concrete column plays an important role in estimating the displacement capacity of the column. Given the moment-curvature response of a column section, the lateral load-tip deflection response of the column can be obtained with relative ease if the plastic hinge length is known.

In order to investigate the sensitivity of calculated lateral load-tip deflection response to the accuracy of plastic hinge length estimations, a series of analyses are conducted. The sectional and member responses of four full-scale concrete column specimens which were tested in this study are used as benchmarks in the analyses. In order to establish a basis of comparison, the plastic hinge lengths of specimens S24-2UT, S17-3UT, S24-4UT, and S24-5UT are estimated using the expressions proposed by Baker (1956), Corley (1966), Mattock (1967), Park et al. (1982), Paulay and Priestley (1992), Sheikh et al.

(1993), and the expression proposed in Section 5.7 (Equation (5.11)). In addition, the lengths of the extensively damage regions of the test specimens were measured after each test, as shown in Table 4.4. These lengths are referred as the measured plastic hinge lengths (Table 5.1). In order to evaluate lateral load-tip deflection response of concrete columns, a computer program, developed during the course of this research study, is used. The details of the computer program are discussed in Chapter 7 and Appendix B.

The moment-curvature and lateral load-tip deflection plots of the specimens tested under high axial loads are illustrated in Figures 5.17 and 5.18. As can be seen in Figure 5.17, the use of the plastic hinge length expression proposed by Park et al. ( $l_p = 0.4h$ ) results in considerable underestimation of the drift capacity. The expressions proposed by Paulay and Priestley ( $l_p = 0.8h$ ) and Sheikh et al. ( $l_p = 1.0h$ ) result in satisfactory predictions. The same trends can be observed for specimen S17-3UT, as shown in Figure 5.18.

Results of the analyses conducted on specimens S24-4UT and S24-5UT are included in Figures 5.19 and 5.20. These specimens were tested under low axial load levels. Figures 5.19 and 5.20 show that the use of the plastic hinge length expression proposed by Park et al. ( $l_p = 0.4h$ ) results in a reasonably good estimation for the drift capacity. However, the expressions proposed by

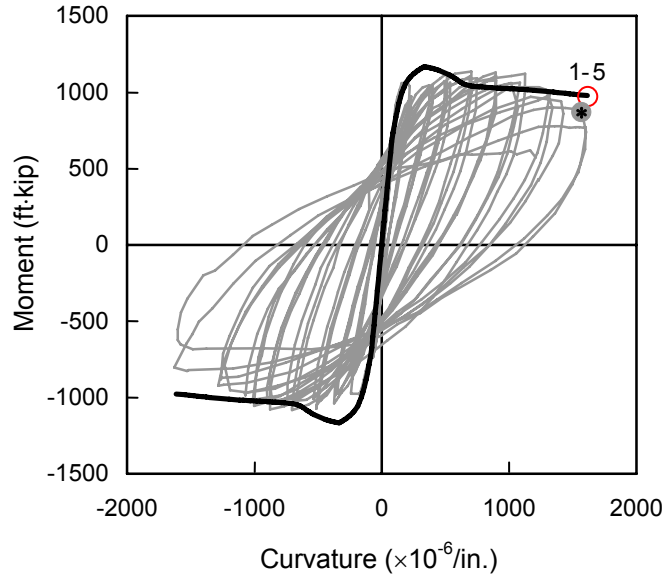
**Table 5.1 Predicted Plastic Hinge Lengths**

Specimen	Baker (1956)	Corley (1966)	Mattock (1967)	Park et al. (1982)	Paulay & Priestley (1992)	Sheikh et al. (1993)	Measured	Proposed
S24-2UT	0.60h	0.49h	0.70h	0.40h	0.80h	1.00h	0.66h	0.69h
S17-3UT	0.65h	0.52h	0.80h	0.40h	0.96h	1.00h	0.91h	0.86h
S24-4UT	0.62h	0.49h	0.70h	0.40h	0.72h	1.00h	0.49h	0.25h
S24-5UT	0.56h	0.49h	0.70h	0.40h	0.72h	1.00h	0.47h	0.25h

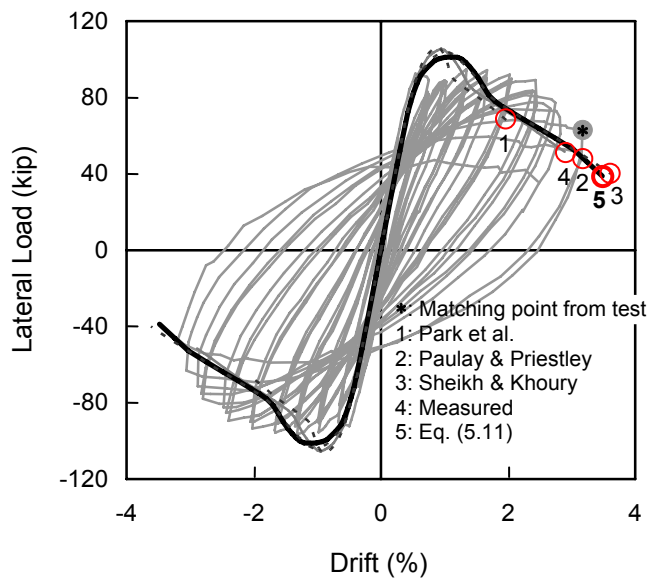
Paulay and Priestley ( $l_p = 0.72h$ ) and Sheikh et al. ( $l_p = 1.0h$ ) result in overestimated predictions of the drift capacity.

Therefore, it can be concluded that the use of some plastic hinge length expressions work for high axial loads, whereas they fail to provide satisfactory estimates for low axial loads and vice versa. However, the use of Equation (5.11) results in satisfactory predictions both for high and low axial load levels.

In performance-based design, prediction of the deformation capacity of reinforced concrete columns is important. An analysis of Figures 5.17 through 5.20 clearly shows the influence of the plastic hinge length estimations on the drift capacity predictions. This analysis indicates the importance of an expression that can provide reasonable estimations for plastic hinge lengths forming in columns supporting high or low axial loads.

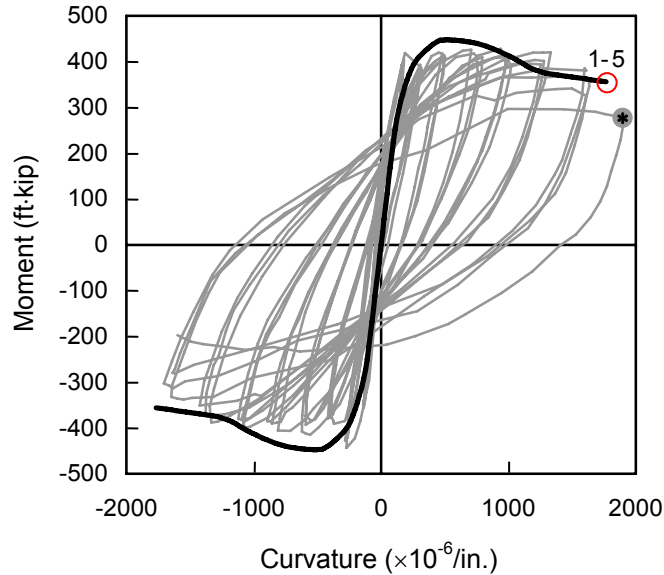


(a) Moment-Curvature Response

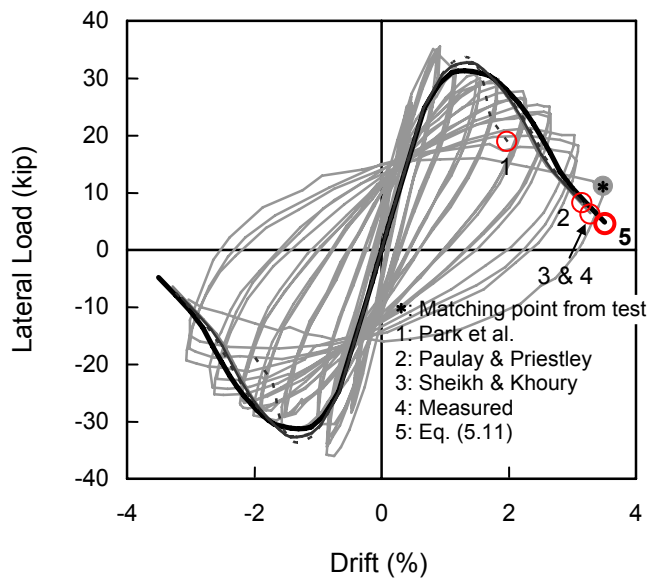


(b) Lateral Load-Drift Response

**Figure 5.17 Comparison of Predicted Responses from Various Plastic Hinge Estimations (S24-2UT)**

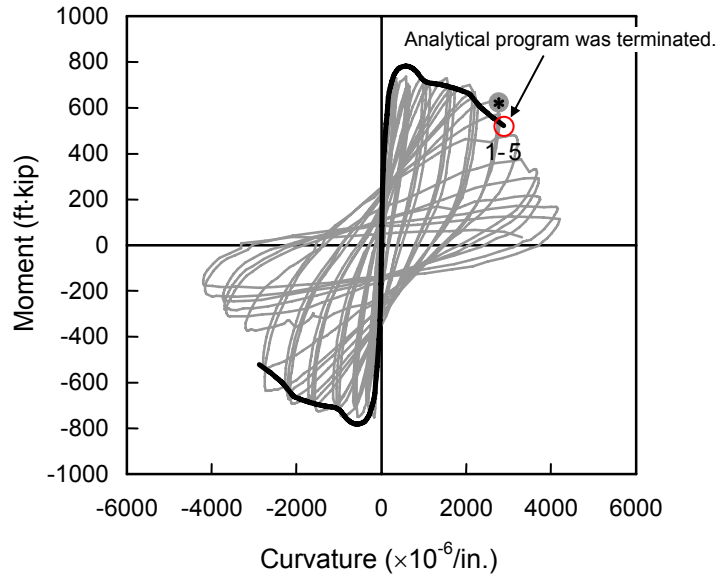


(a) Moment-Curvature Response

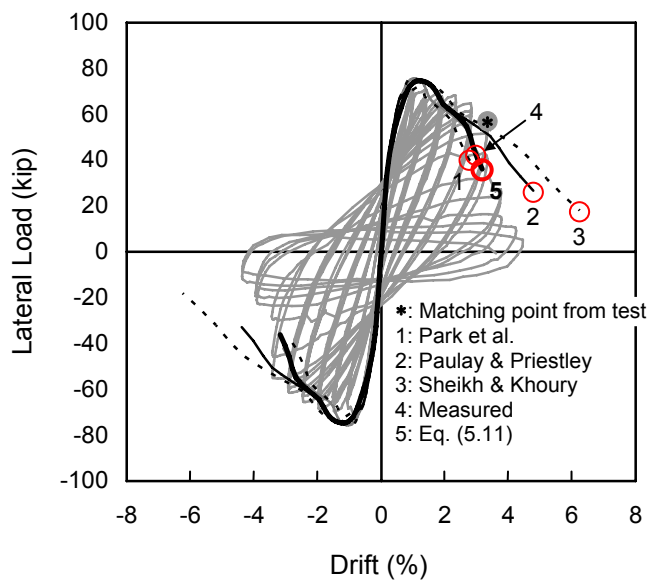


(b) Lateral Load-Drift Response

**Figure 5.18 Comparison of Predicted Responses from Various Plastic Hinge Estimations (S17-3UT)**

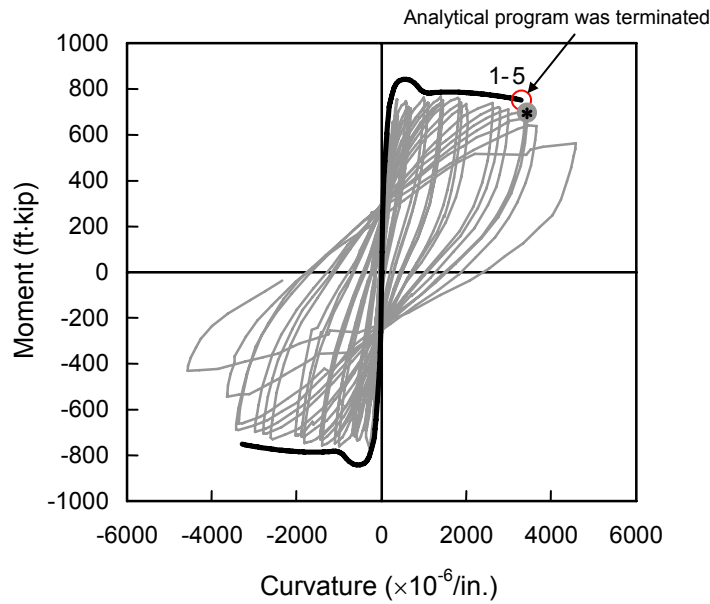


(a) Moment-Curvature Response

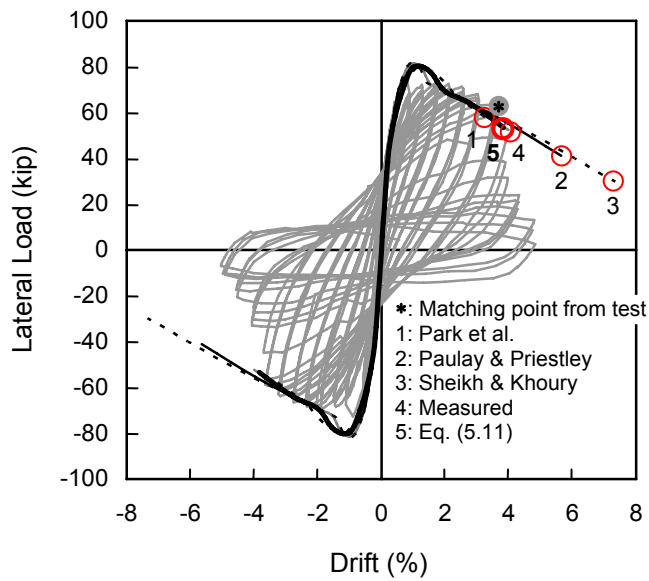


(b) Lateral Load-Drift Response

**Figure 5.19 Comparison of Predicted Responses from Various Plastic Hinge Estimations (S24-4UT)**



(a) Moment-Curvature Response



(b) Lateral Load-Drift Response

**Figure 5.20 Comparison of Predicted Responses from Various Plastic Hinge Estimations (S24-5UT)**

## 5.9 SUMMARY

Based on the experimental and analytical research into the seismic behavior of concrete columns reported in this study, the following conclusions can be drawn:

- (1) The level of axial load influenced the length of the plastic hinges that formed in the full-scale column specimens tested in this research. Specimens tested under high axial loads developed longer plastic hinges than those tested under low axial loads.
- (2) Accurate estimation of the length of a plastic hinge formation in a reinforced concrete column plays an important role in predicting the lateral drift capacity of a column. Given the moment-curvature response of a column section, the lateral load-tip deflection response of the column can be obtained with relative ease if the plastic hinge length is known.
- (3) The following equation, developed in this research, can be used to estimate the length of the plastic hinges forming in columns supporting a wide range of axial loads.

$$\frac{l_p}{h} = \left[ 0.3\left(\frac{P}{P_o}\right) + 3\left(\frac{A_s}{A_g}\right) - 0.1 \right] \left(\frac{L}{h}\right) + 0.25 \geq 0.25$$

# CHAPTER 6

## BUCKLING BEHAVIOR OF REINFORCING BARS

### 6.1 INTRODUCTION

In all the column specimens tested in this study, buckling of longitudinal bars was observed after yielding of perimeter ties and inner ties, which was an indication of the commencement of failure. Figure 6.1 illustrates the typical plastic hinge region of a specimen.

Longitudinal bar buckling is not typically considered in conventional sectional analysis. In general, the behavior of reinforcing bars in compression is assumed to be similar to that in tension. In reality, the behavior of reinforcing bars in compression is different from that in tension. As a result, conventional sectional analysis cannot capture the post-peak response of concrete columns accurately and often over-estimates the post-peak response with respect to strength and ductility.

Although considerable research has been conducted to study the buckling behavior of reinforcing bars (Bresler and Gilbert 1961; Mander et al. 1984; Scribner 1986; Papia et al. 1988; Papia and Russo 1989; Mau and El-Mabsout 1989; Mau 1990; Monti and Nuti 1992; Bayrak and Sheikh 2001), a simple bar buckling model has not been proposed yet due to the complexity of inelastic buckling behavior of reinforcing bars and the lack of sufficient data. Therefore, it is important to develop a simple bar buckling model, which can be easily incorporated into sectional analysis programs, in order to get more reliable estimates of the post-peak response of concrete columns.

In this chapter, the experimental research conducted by Mieses (2002) is briefly summarized. Based on the test results of Bayrak and Sheikh (2001) and Mieses (2002), a simple bar buckling model is developed. The proposed bar buckling model is combined with an energy-based method, proposed by Dhakal and Maekawa (2002), which predicts the buckling length of the longitudinal bars. This proposed model is then incorporated into an analytical program that can be used to calculate the lateral load-displacement behavior of reinforced concrete columns. Finally, the impact of inclusion of the proposed bar buckling model on the accuracy of the calculations is discussed by comparing experimental results with calculated lateral load-displacement response of concrete columns.



**Figure 6.1 Longitudinal Bar Buckling in Specimen S24-4UT**

## 6.2 BUCKLING BEHAVIOR OF LONGITUDINAL REINFORCEMENT

The behavior of reinforcing bars in compression is different from that in tension. The difference is mainly attributed to the geometric nonlinearity associated with large lateral deformations of buckled reinforcing bars. In other words, the buckling behavior of reinforcing bars is influenced by the geometric properties of longitudinal reinforcement and reinforced concrete column dimensions in addition to the basic material properties (Figure 6.2). This figure shows that the longitudinal bar diameter ( $d_b$ ) and tie spacing ( $s$ ) are important geometric parameters defining the buckling behavior of reinforcing bars. This figure also illustrates the influence of longitudinal bar buckling behavior on a typical moment-curvature response of a column section.

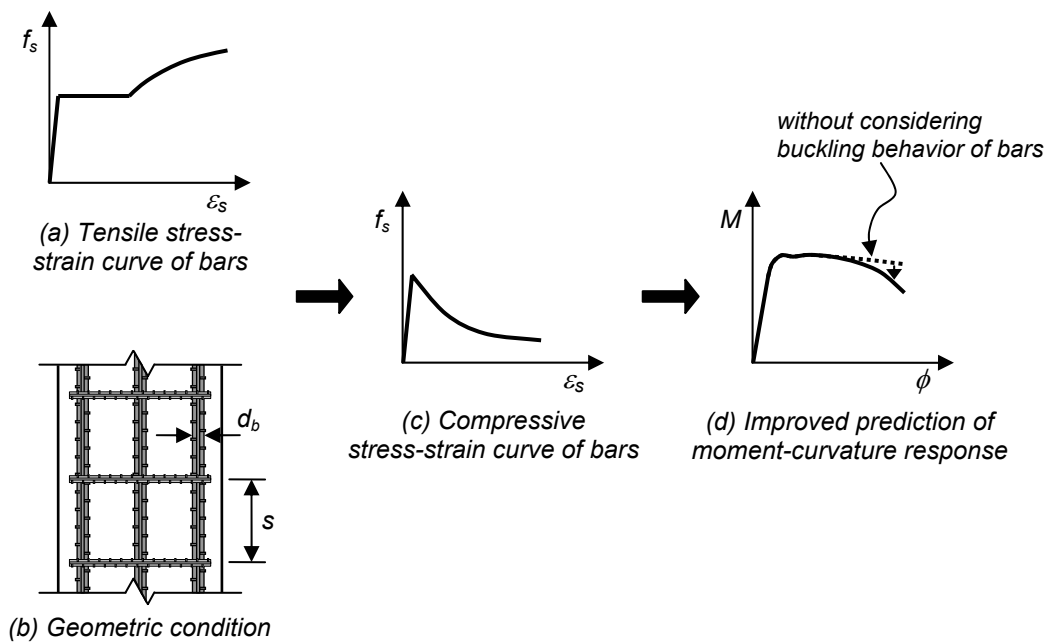


**Figure 6.2 Buckling Behavior of Bars**

### 6.3 EXPERIMENTAL PROGRAM (MIESES 2002)

Mieses (2002) tested one hundred sixty-two bars to study their inelastic buckling behavior. The main objective of her research was to investigate the sensitivity of buckling length to bar diameter ratio ( $s/d_b$ ), initial imperfections measured as mid-span eccentricity to bar diameter ratio ( $e/d_b$ ), and material properties ( $f_u/f_y$ ) on the behavior of reinforcing bars subjected to compressive loads (Figure 6.3).

Grade 60 No. 8 ( $d_b = 1.00$  in.,  $A_s = 0.79$  in $^2$ ) and No. 10 ( $d_b = 1.27$  in.,  $A_s = 1.27$  in $^2$ ) domestic reinforcing bars were tested in this study. The material properties of bars obtained from standard tensile coupon tests are summarized in Table 6.1. The ultimate strain ( $\varepsilon_u$ ) defined in Table 6.1 is the strain corresponding to the ultimate strength ( $f_u$ ), which is equivalent to the tensile strength as defined by ASTM A370.

Monotonic compression tests of the bars were performed. A range of nine buckling length-to-bar diameter ratios ( $s/d_b = 4, 5, 6, 7, 8, 9, 10, 11$ , and  $12$ ) and six initial eccentricity-to-bar diameter ratios ( $e/d_b = 0.0, 0.1, 0.2, 0.3, 0.4$ , and  $0.5$ ) were used for each bar size. For the No. 8 bar tests, two specimens of each  $e/d_b$  and  $s/d_b$  combination were tested, and for the No. 10 bar tests, only one specimen was tested per combination, resulting in 108 specimens of No. 8 bars and 54 specimens of No. 10 bars.

**Table 6.1 Tensile Properties of Reinforcing Bar Specimens (Mieses 2002)**

Bar Size	Elastic Region			$\varepsilon_{sh}$	Strain Hardening Region	
	$f_y$ (ksi)	$\varepsilon_y$	$E_s$ (ksi)		$f_u$ (ksi)	$\varepsilon_u$
No. 8	63.4	0.0022	28,804	0.0092	105.6	0.147
No. 10	64.4	0.0022	29,298	0.0091	92.5	0.158

A universal testing machine was used to test all the specimens. Two linear potentiometers were used to measure axial displacements (and axial strains) and one linear potentiometer was used to monitor transverse displacements (Figure 6.4). The buckling length ( $s$ ) was measured as the distance between the innermost restraining bolts, as shown in Figure 6.3.

Direct contact between a reinforcing bar and cylindrical end restraints was assured for an accurate measurement of axial displacement. The bolts shown in Figure 6.4 provided lateral restraint while the end of the reinforcing bar specimens reacted against the restraining cylinders. The deformation of the restraining cylinders was negligible since the cross-sectional area of the cylinders was significantly greater than that of the reinforcing bars. The initial slope of the stress-strain curve obtained from compression tests was in good agreement with the corresponding slope obtained from tension tests, validating the accuracy of deformation measurements. Strain gauges were not employed for the following reasons:

- Installation of strain gauges would disturb the geometry of reinforcing bars and cause a decrease in the cross-sectional area.
- Strain gauges would give the local strains measured over a gauge length of 0.2-0.4 in. (5-10 mm). These strains have no actual physical meaning after the initiation of longitudinal bar buckling in a column test. Once buckling initiates in a column, the reinforcing bar strain would be different from the concrete core strain at that section. Therefore, from a theoretical perspective, this strain would not correspond to the longitudinal strains calculated from a sectional analysis. What is more important is the average strain or total deformation calculated between the two supports, simulating the two tie sets that anchor the longitudinal bar to the concrete core.

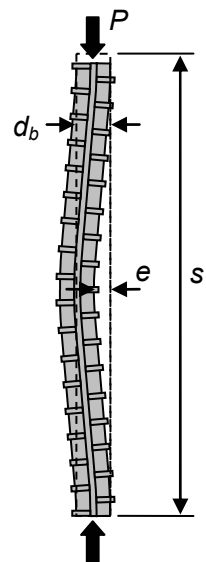


Figure 6.3 Reinforcing Bar Specimen



Figure 6.4 Test Setup

Because of the existence of ribs in reinforcing bars, they had strong and weak axes. The buckling of the bars occurred consistently along the weak axis. The test results are summarized in Figures 6.5 through 6.8.

Effect of unsupported bar length to longitudinal bar diameter ratio ( $s/d_b$ ) is shown in Figures 6.5 and 6.6. These figures illustrate that the inelastic buckling behavior of a reinforcing bar is very sensitive to the  $s/d_b$  ratio, such that the load-carrying capacity and ductility decrease as the  $s/d_b$  ratio increase.

The  $e/d_b$  ratio was used as a measure of initial eccentricity of a reinforcing bar. A zero  $e/d_b$  means an initially straight bar. Initial eccentricity can occur during the construction stage or by lateral volumetric increase of concrete core in reinforcing cage at large inelastic deformation levels. Six different  $e/d$  ratios from 0.0 to 0.6 were studied in the test (Figures 6.5 and 6.6). For initially straight bars ( $e/d_b = 0.0$ ), the yield strength obtained from the tensile curve was achieved for most  $s/d_b$  ratios. As the  $e/d_b$  ratio increased, the maximum stress attained in compression tests reduced.

Figures 6.7 and 6.8 show the axial stress-transverse displacement response of bars with  $s/d_b = 4, 6, 8$  and  $10$ . Reinforcing bars with  $s/d_b = 4$ , transverse displacement response becomes flat once they reach their maximum capacity, showing a very stable post buckling behavior. For other  $s/d_b$  ratios, the response curves converge as transverse displacements increase for all  $e/d_b$  ratios.

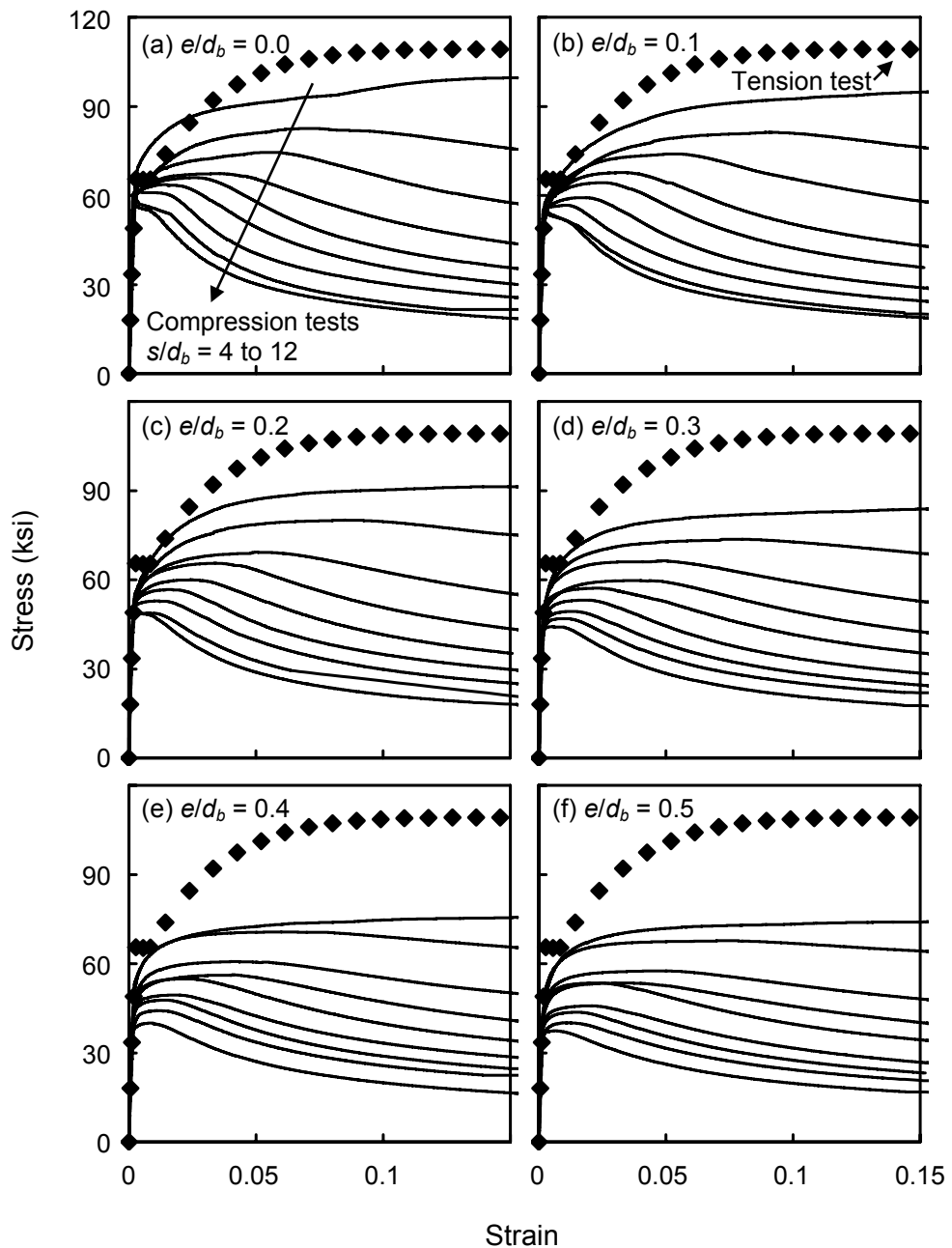


**Figure 6.5 Stress-Strain Curves of No. 8 Bars (Mieses 2002)**

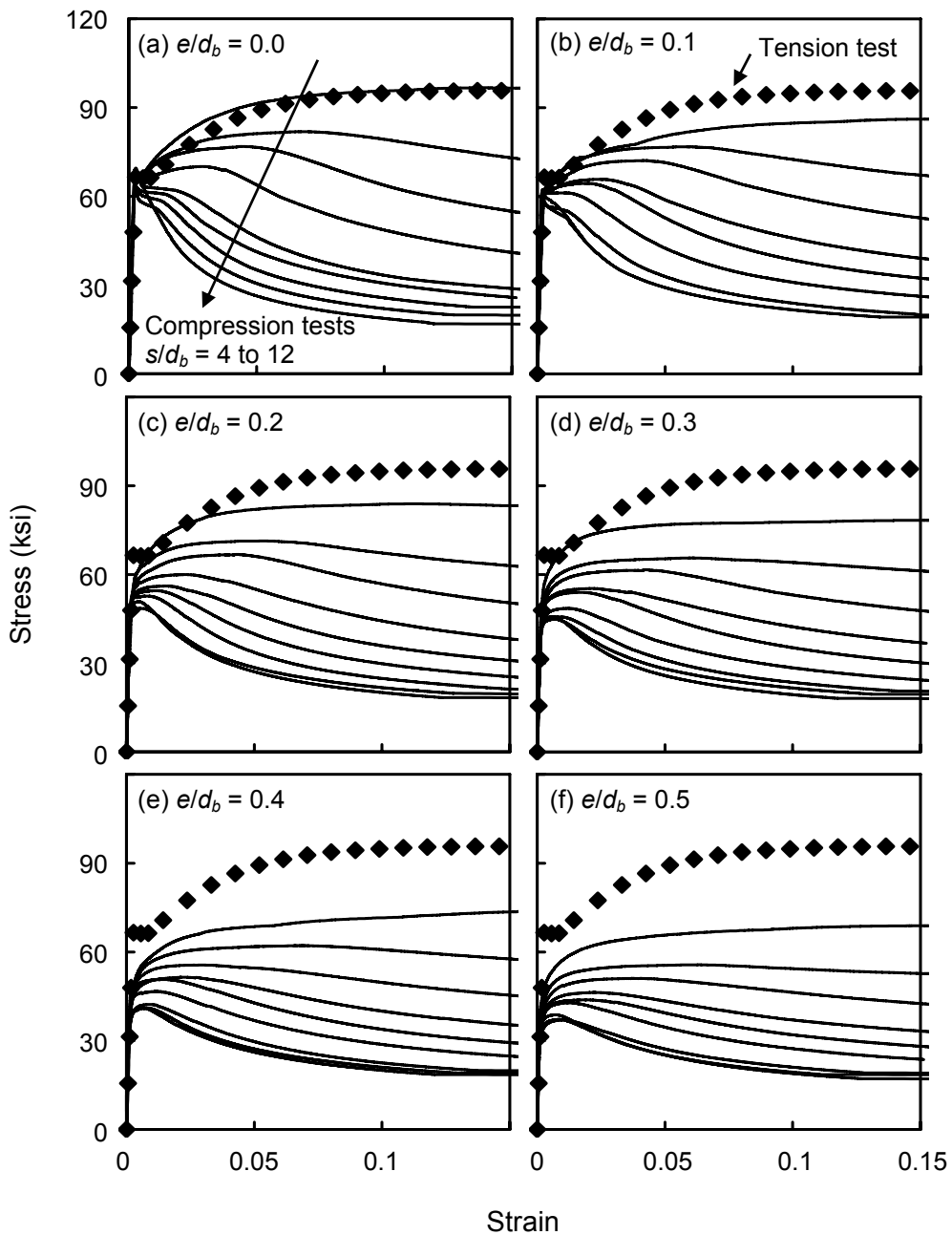


**Figure 6.6 Stress-Strain Curves of No. 10 Bars (Mieses 2002)**

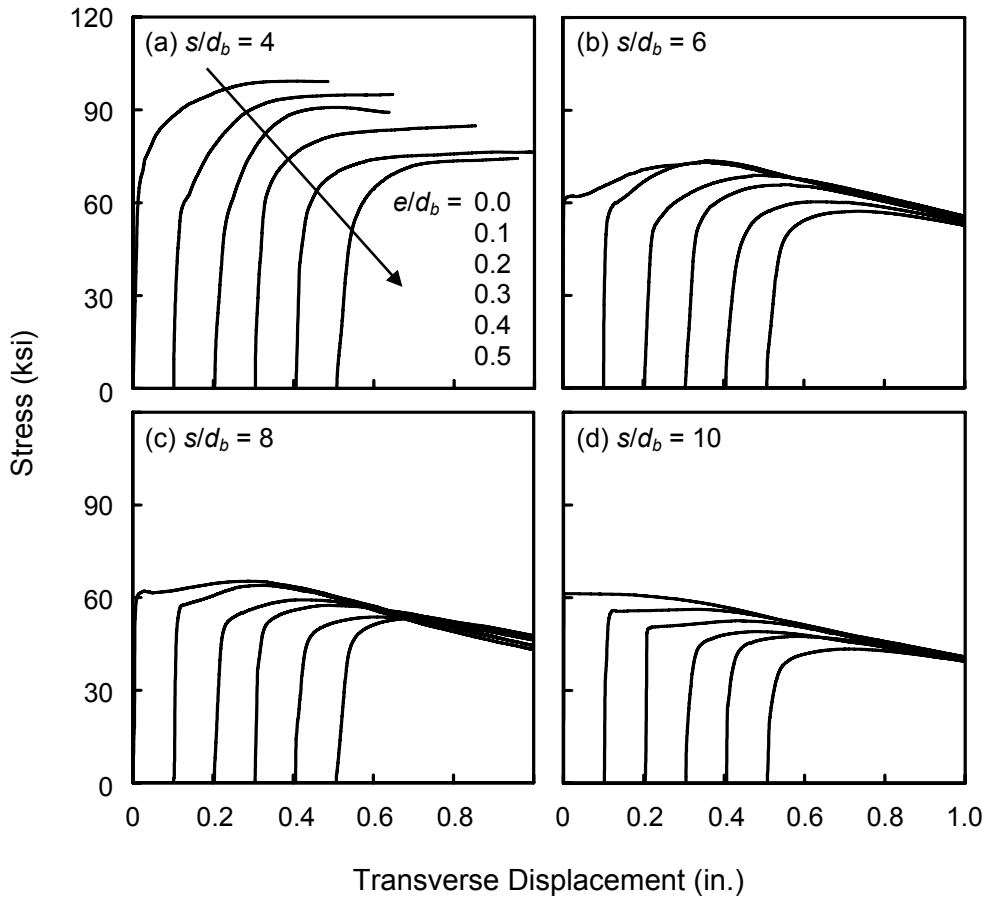


*Figure 6.7 Stress-Transverse Displacement Curves of No. 8 Bars (Mieses 2002)*

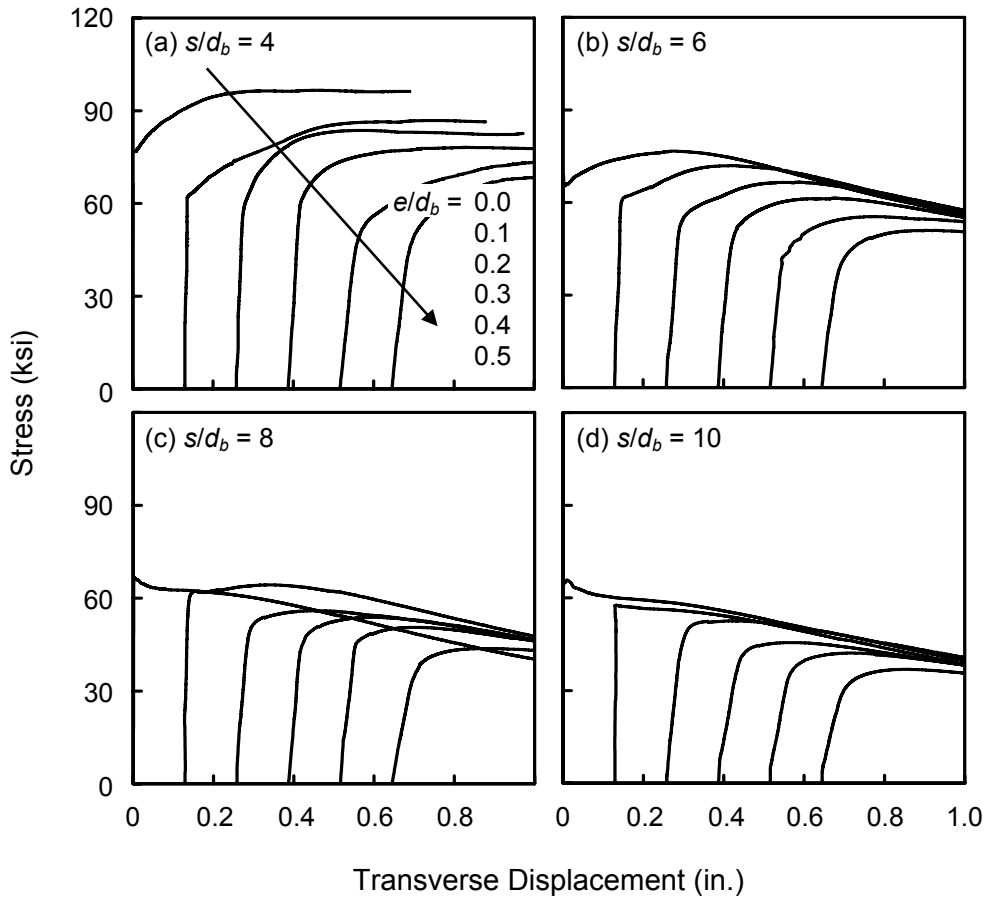


**Figure 6.8 Stress-Transverse Displacement Curves of No. 10 Bars  
(Miseses 2002)**

## 6.4 PROPOSED INELASTIC BUCKLING MODEL

The buckling behavior of a reinforcing bar is a second-order inelastic problem. The difference between the behavior of reinforcing bars that are buckling under compressive loads and the behavior of reinforcing bars that are subjected to tensile loads can be attributed to the geometric nonlinearity associated with large lateral deformations experienced by buckling reinforcing bars. Otherwise, the local stress-strain relationship of reinforcing bars in compression is similar to the stress-strain relationship in tension. Mau and El-Mabsout (1989) suggested that the total axial displacement and average axial strain of reinforcing bars could be represented as follows:

$$u = u_a + u_b \quad (6.1)$$

$$\varepsilon_{avg} = \frac{du_a}{dx} - z \frac{d^2 w}{dx^2} \quad (6.2)$$

where

- $u$  = total axial displacement
- $u_a$  = axial displacement due to axial deformation
- $u_b$  = axial displacement induced by the transverse displacement
- $\varepsilon_{avg}$  = average axial strain
- $x$  = distance measured in longitudinal direction from the end of a bar  
(Figure 6.9)
- $z$  = distance measured in transverse direction (Figure 6.9)
- $w$  = transverse displacement of a bar

Equations (6.1) and (6.2) show that the total axial displacement (or average axial strain) can be separated into two components: (1) the axial displacement (or axial strain) due to axial deformation and (2) the axial displacement (or axial strain) induced by transverse deformation.

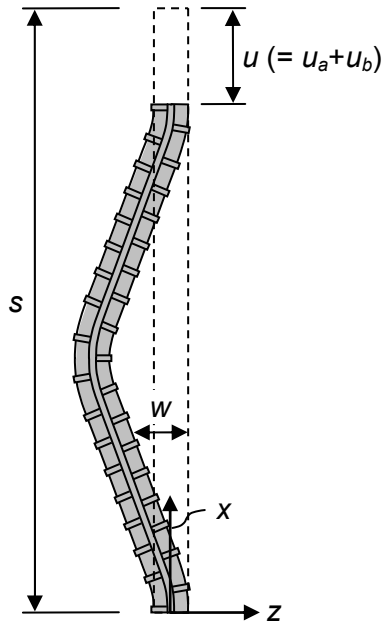


**Figure 6.9 Deflected Shape of a Reinforcing Bar**

The axial displacement due to axial deformation can be estimated directly from the stress-strain curve of bars subjected to tensile loads. The axial displacement induced by transverse deformations is related to the geometric properties of a bar. Figures 6.5 and 6.6 show that the behavior of buckling bars appear to be reasonably close to the stress-strain curve of the bars in tension as the  $s/d_b$  ratio decreases. This implies that the axial displacement due to axial deformation governs the buckling behavior at small  $s/d_b$  ratios, but the axial displacement induced by transverse deformations becomes more pronounced at large  $s/d_b$  ratios.

Equation (6.2), originally proposed by Mau and El-Mabsout (1989), is used in modeling the inelastic buckling behavior of reinforcing bars. The average axial strain is assumed as the summation of the axial strain due to axial stress and

the axial strain resulting from the transverse deformation of a bar experiencing inelastic buckling, as shown in Equation (6.3).

$$\epsilon_{avg} = \epsilon_s + \epsilon_{tra} \quad (6.3)$$

where

$\epsilon_{avg}$  = average axial strain

$\epsilon_s$  = axial strain due to axial stress

$\epsilon_{tra}$  = axial strain resulting from transverse displacement

Bayrak and Sheikh (2001) reported a plastic hinge analysis technique which included the effect of initial eccentricity on the buckling behavior of longitudinal bars. The eccentricity of longitudinal bars can occur from the reinforcing cage-concrete core interaction. To estimate this eccentricity, they used the ratio of transverse strain to axial strain, which was experimentally obtained from well-instrumented tied columns tested under monotonic concentric axial compression. While this approach may be considered acceptable for their purposes, the inclusion of initial eccentricity and modeling of reinforcing cage-concrete core interaction render modeling the behavior of reinforcing bars in compression practically impossible. As such, the presence of initial imperfections is not considered in the modeling work reported herein and is considered beyond the scope of the current analytical work. The analytical work presented here can be considered as a simplification to the plastic hinge analysis procedure reported by Bayrak and Sheikh (2001).

#### 6.4.1 Axial Strain due to Axial Stress

The axial strain due to axial stress can be easily obtained from a given axial load (or stress) using the tensile stress-strain curve. The expression proposed by Mander et al. (1984) is used to model the material behavior in the strain

hardening region. According to Mander et al. (1984), the relationship between the stress ( $f_s$ ) and the strain ( $\varepsilon_s$ ) in the strain hardening region of a reinforcing bar can be expressed by:

$$f_s = f_u + (f_y - f_u) \left( \frac{\varepsilon_u - \varepsilon_s}{\varepsilon_u - \varepsilon_{sh}} \right)^p \quad (6.4)$$

where

- $f_y$  = yield strength from tensile stress-strain curve
- $f_u$  = ultimate strength from tensile stress-strain curve
- $\varepsilon_{sh}$  = strain at which strain hardening commences
- $\varepsilon_u$  = strain corresponding to the ultimate strength  $f_u$

In this model, a typical bilinear relationship of reinforcing bar is used up to the point at which strain hardening begins. The parameter  $p$  is defined as:

$$p = E_{sh} \left( \frac{\varepsilon_u - \varepsilon_{sh}}{f_u - f_y} \right) \quad (6.5)$$

where

- $E_{sh}$  = modulus of elasticity at the initiation of strain hardening

The accuracy of estimated tensile behavior of the reinforcing steel using the strain hardening model proposed by Mander et al. (1984) is illustrated in Figure 6.10. The tensile behavior of the reinforcing bars shown in Figure 6.10 was experimentally evaluated and was previously discussed in Chapter 3. Figure 6.10 shows that Mander's strain hardening model provides accurate estimations.

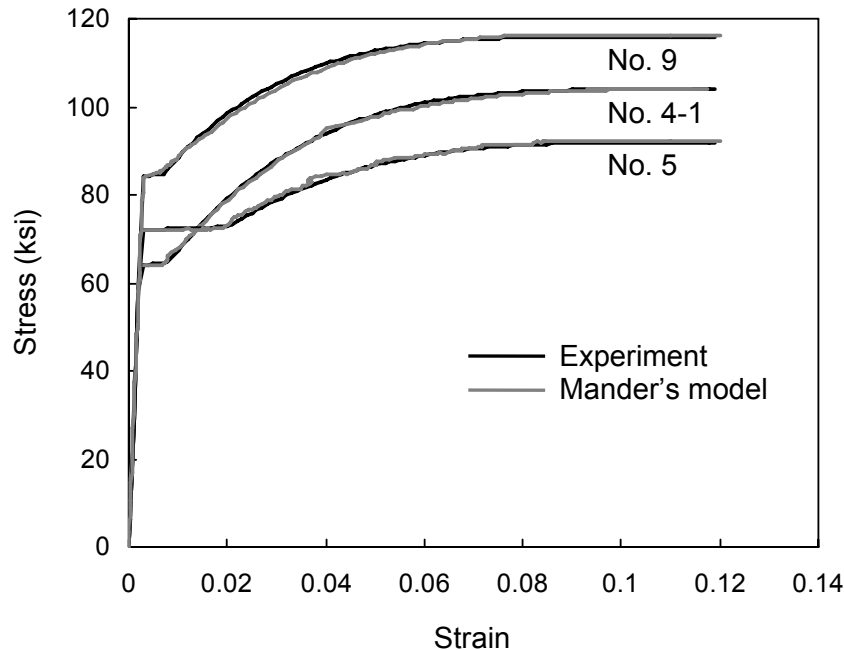


**Figure 6.10 Comparison of Stress-Strain Curves for Reinforcing Steel**

#### 6.4.2 Axial Strain due to Transverse Deformation

The axial strain induced by transverse deformations is calculated by the following two steps:

- (1) The transverse displacement ( $w$ ) in Figure 6.9 during buckling is obtained from the relationship between axial stress and transverse displacement.
- (2) The axial strain ( $\epsilon_{tra}$ ) is obtained from the relationship between axial strain and transverse displacement.

#### **6.4.2.1 The relationship between axial stress and transverse displacement**

In calculating the axial strain due to transverse displacement, the data from the reinforcing bar buckling tests conducted by Mieses (2002) are used (Figures 6.7 and 6.8). The axial stress and transverse displacement responses in those figures are reorganized for  $e/d_b = 0$ , as shown in Figures 6.11(a) and 6.11(c). Based on the test results, several assumptions are made to simplify the modeling of the relationship:

- (1) Reinforcing bars begin to buckle when the yield strength is reached.
- (2) Strength of bars starts to degrade after the lateral displacement exceeds 4% of the unsupported length.
- (3) Average post-buckling stress can be assumed to be a constant after it drops to 20% of the yield strength.

It is important to note that these assumptions are purely based on the experimental results in order to simplify the modeling. Based on these assumptions, the relationship between axial stress ( $f_s$ ) and transverse displacement ( $\Delta_{tra}$ ) during buckling is expressed in the following expressions (Figure 6.12):

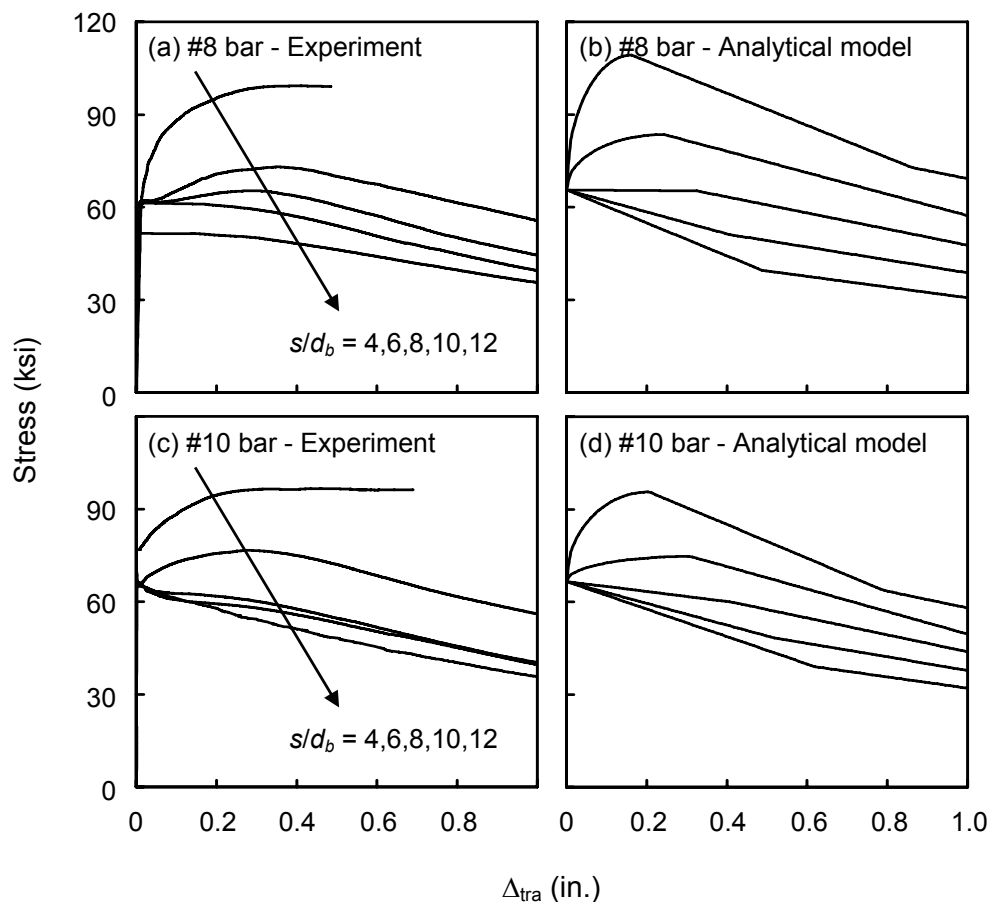


**Figure 6.11 Axial Stress-Transverse Displacement Estimations**

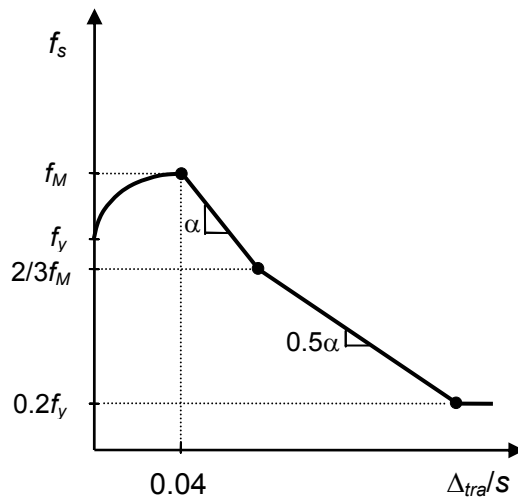


**Figure 6.12 Proposed Model for Axial Stress-Transverse Displacement Response**

$$\frac{\Delta_{tra}}{s} \leq 0.04 ; f_s = f_y + (f_M - f_y) \times \sqrt{1 - \left( \frac{1}{0.04} \cdot \frac{\Delta_{tra}}{s} - 1 \right)^2} \quad \text{for } f_M > f_y \quad (6.6)$$

$$f_s = \frac{(f_M - f_y)}{0.04} \cdot \frac{\Delta_{tra}}{s} + f_y \quad \text{for } f_M \leq f_y \quad (6.7)$$

$$\frac{\Delta_{tra}}{s} > 0.04 ; f_s = f_y \cdot \alpha \left( \frac{\Delta_{tra}}{s} - 0.04 \right) + f_M \quad \text{for } f_s \geq \frac{2}{3} f_M \quad (6.8)$$

$$f_s = f_y \cdot \frac{\alpha}{2} \left( \frac{\Delta_{tra}}{s} - \beta \right) + \frac{2}{3} f_M > 0.2 f_y \quad \text{for } f_s < \frac{2}{3} f_M \quad (6.9)$$

where

$$\frac{f_M}{f_y} = -0.45 \xi^{1.5} \left[ \ln \left( \frac{s/d_b}{4} \right) \right] + \xi \leq \xi$$

$$\xi = f_u / f_y$$

$\Delta_{tra}$  = transverse displacement of a bar at the mid-span

$$\begin{aligned}
s &= \text{buckling length of bar} \\
d_b &= \text{nominal bar diameter} \\
\alpha &= 4(\xi - 1)^2 - 5 \\
&= \text{initial slope of the descending branch (Figure 6.12)} \\
\beta &= 0.04 - \frac{1}{3\alpha} \cdot \frac{f_M}{f_y}
\end{aligned}$$

Comparisons between the experimental and analytically-derived transverse displacements are shown in Figure 6.11. As can be observed in this figure, the correlation between the estimated and experimental axial stress-transverse displacement response is acceptable for most  $s/d_b$  ratios. However, there are some discrepancies, especially for  $s/d_b = 4$ . Unlike the estimates, the experimental results for  $s/d_b = 4$  show a stable behavior after the peak load. The axial strain of a bar with small  $s/d_b$  ratio is influenced significantly by the axial strain due to axial stress. Hence, the discrepancy between the data and estimated response for such short unsupported lengths ( $s/d_b = 4$ ) can be considered unimportant. However, for large unsupported rebar lengths, the proposed closed-form expression does a good job of tracing the experimental data. This may be considered as one of the strengths of the proposed approach.

#### **6.4.2.2 The relationship between transverse displacement and axial strain**

The experimental results indicate that the relationship between transverse displacement and axial strain of a buckling bar can be assumed to be bi-linear and the slope of lines as a function of the  $s/d_b$  ratio. The following equation is proposed for this purpose (Figure 6.13).

$$\begin{aligned}
\varepsilon_{tra} &= \left( \frac{0.035 \cos \theta + \theta}{\cos \theta - 0.035 \theta} \right) \frac{\Delta_{tra}}{d_b} \\
&\geq \frac{1}{\cos \theta - 0.07 \theta} \times (0.07 \cos \theta + \theta) \left( \frac{\Delta_{tra}}{d_b} - 0.035 \right)
\end{aligned} \tag{6.10}$$

where

$$\theta = \frac{6.9}{(s/d_b)^2} - 0.05$$

Analytically-derived values are compared with experimental results in Figure 6.14. As can be seen in Figure 6.14, the analytical results or predictions are in good agreement with the experimental results for all  $s/d_b$  ratios.

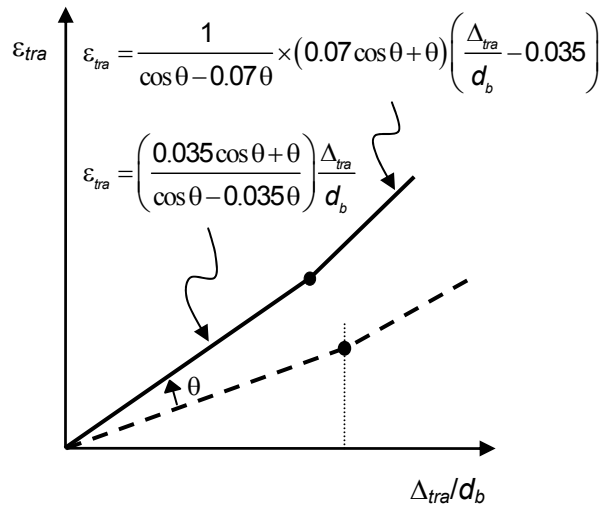


**Figure 6.13 Proposed Model for Axial Strain-Transverse Displacement Response**

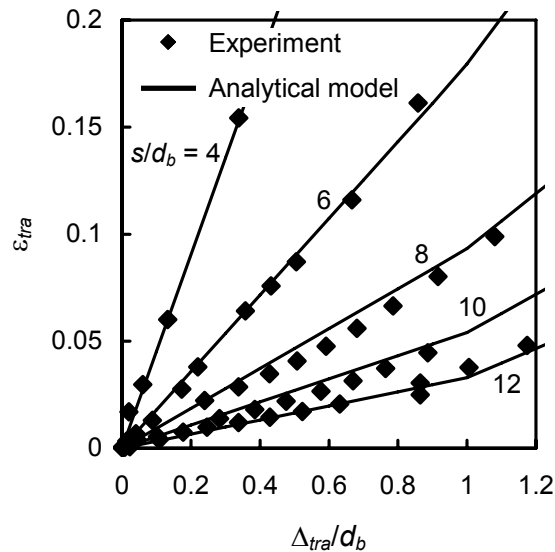


**Figure 6.14 Axial Strain-Transverse Displacement Estimations**

#### 6.4.3 Reinforcing Bar Buckling Model: Summary

The development of the reinforcing bar buckling model is presented in the previous sections. In this section, an overview of this procedure is provided. The following is a step-by-step summary of the analytical procedure that can be used to predict the buckling behavior of reinforcing bars in compression:

- (1) Linear elastic response is used until the axial stress ( $f_s$ ) reaches the yield stress ( $f_y$ ).
- (2) After the yield stress, the bar begins to buckle and transverse displacements start contributing to axial deformations. Since the analysis is conducted in a displacement-controlled manner, for a given value of the transverse displacement, the axial stress corresponding to that value of transverse displacement can be estimated by using Equations (6.6) through

(6.9). Consequently, axial stress-transverse displacement behavior can be established.

- (3) Axial strain ( $\varepsilon_s$ ) due to axial stress can be calculated using a tensile stress-strain curve represented by a bilinear relationship until the commencement of strain hardening and Equations (6.4) and (6.5) can be used to model the strain hardening response.
- (4) Axial strain induced by transverse displacement ( $\varepsilon_{tra}$ ) can be estimated by using the relationship between transverse displacement and axial strain (Equation (6.10)).
- (5) Axial strain due to axial stress ( $\varepsilon_s$ ) and the axial strain resulting from the transverse deformations ( $\varepsilon_{tra}$ ) can be added to calculate the total average axial strain  $\varepsilon_{avg}$  (Equation (6.3)). Alternatively, this average strain can be multiplied by the unsupported bar length to estimate the movement of a reinforcing bar between the supports (or ties anchoring this bar into the concrete core).
- (6) Assumed transverse displacement in step (2) is gradually increased and steps (3) to (5) can be repeated until the overall stress-strain curve of a particular rebar under consideration is evaluated for a given set of geometric and material properties.

This procedure is also summarized in a flowchart shown in Figure 6.15. The axial stress and axial strain relationships for No. 8, No. 10 (reinforcing bars tested by Mieses 2002), and 20M (reinforcing bars tested by Bayrak and Sheikh 2001) are estimated using the procedure summarized in Figure 6.15. The results of the analyses are compared with the experimental data in Figure 6.16. As can be seen in Figure 6.16, the stress-strain curves estimated by using the analytical procedure developed in this study are in good agreement with the experimental

results for all of the cases. It is interesting to note that a wide range of unsupported bar length-to-bar diameter ratios and ultimate-to-yield strength ratios are covered in these plots.

Although the use of the analytical procedure presented in this section provides good estimates for the stress-strain response of buckling bars, this estimation can be carried out for cases where the unsupported length of the reinforcing bars is known. In the plastic hinge region of a reinforced concrete column, buckling of reinforcing bars may take place over one tie spacing, two tie spacings or more. Estimation of the “buckling length” of reinforcing bars remains a key step before the reinforcing bar buckling model developed here can be implemented into a sectional analysis program.

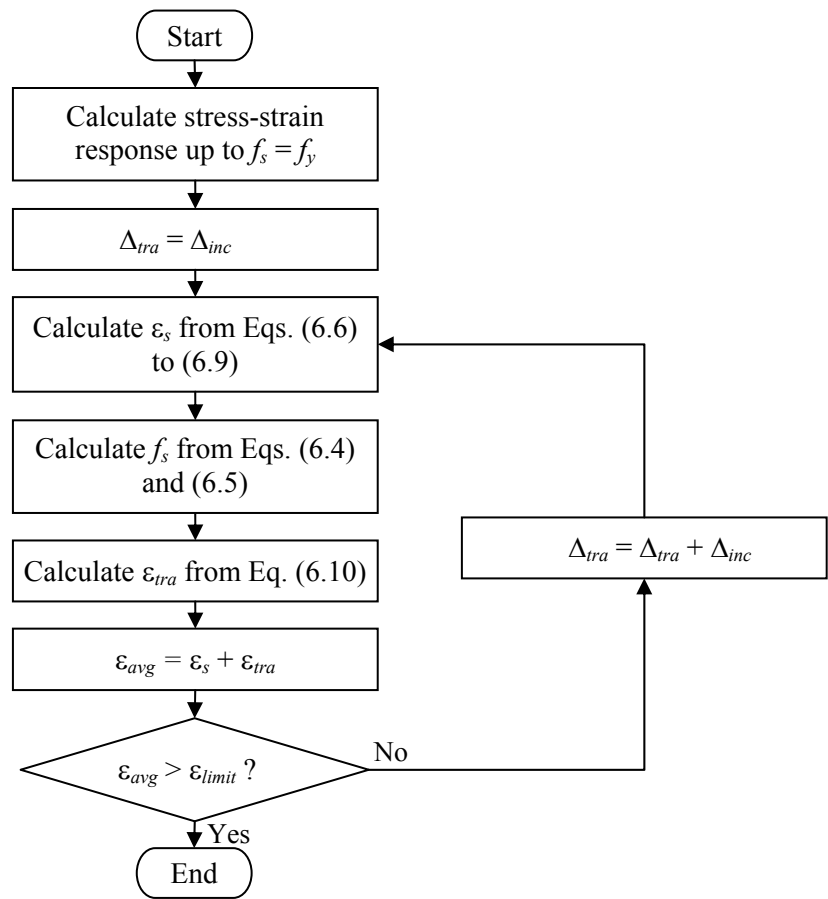


**Figure 6.15 Analysis of Buckling Response of Bar**

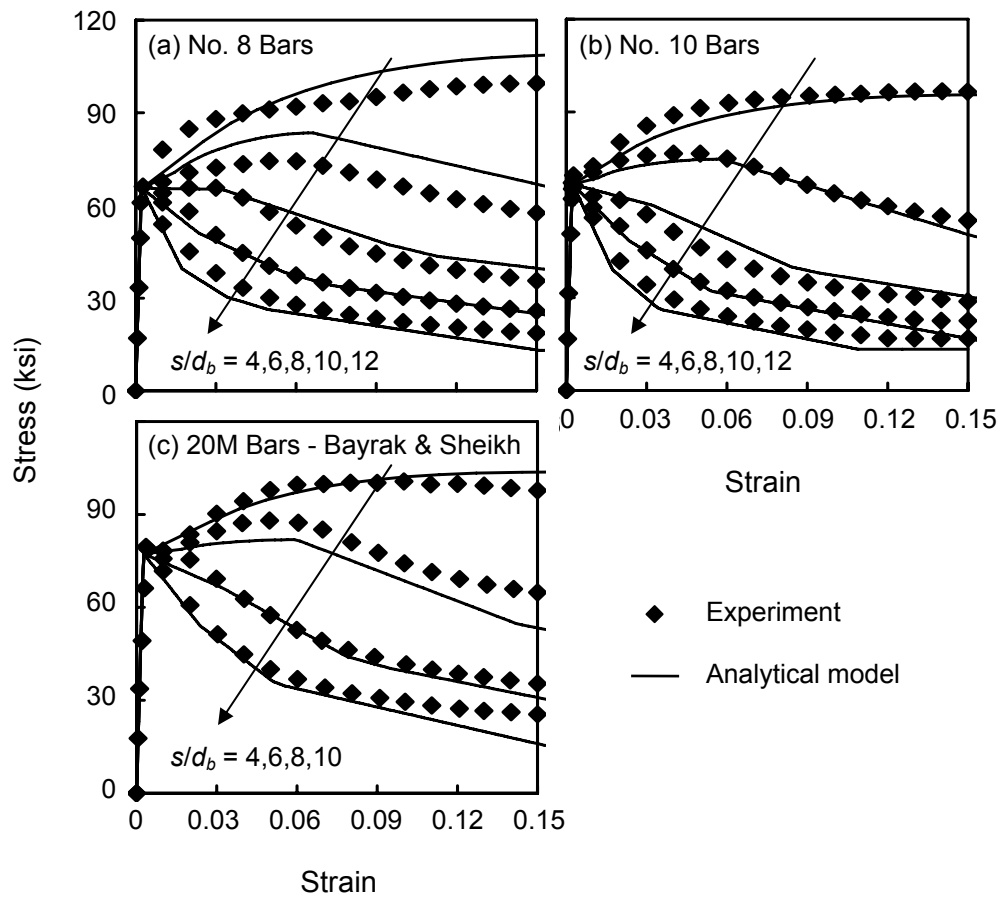


*Figure 6.16 Axial Stress-Axial Strain Estimations*

## 6.5 BUCKLING LENGTH OF LONGITUDINAL REINFORCING BARS

As mentioned earlier, one of the important parameters that governs the buckling behavior of reinforcing bars is the unsupported length of the buckling bars, i.e., buckling length. The assumption that the buckling length of longitudinal reinforcing bars ( $s$ ) is equal to the spacing of lateral ties ( $s_t$ ) does not hold true for all plastic hinges forming in reinforced concrete columns. An analysis of the data on the seismic performance of reinforced concrete columns indicates that in some special cases buckling length of the reinforcing bars may be equal to the tie spacing. These special cases include columns with very stiff lateral ties and columns with ties that are spaced widely (i.e., cases where the  $s_t/d_b$  ratio is large). Dhakal and Maekawa (2002) proposed an energy-based method to predict the buckling length of longitudinal reinforcing bars. This procedure (Dhakal and Maekawa 2002) is illustrated in Figure 6.17.

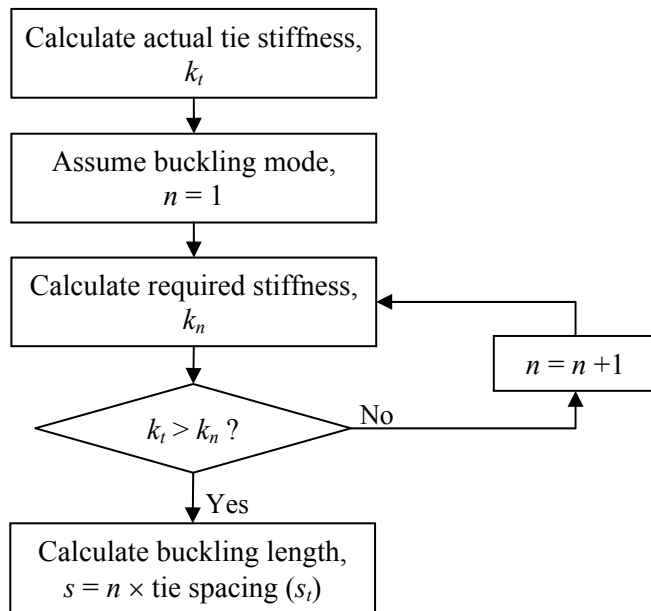


**Figure 6.17 Buckling Length of Reinforcing Bars (Dhakal and Maekawa 2002)**

In the energy-based approach reported by (Dhakal and Maekawa 2002), first, the effective stiffness ( $k_t$ ) of lateral reinforcement providing restraint to longitudinal reinforcing bars is computed. Next, the minimum tie stiffness required to provide sufficient restraint to a longitudinal reinforcing bar in different buckling modes is determined using energy principles. Here, buckling mode relates to the number of tie spacings ( $s_t$ ) included in the buckling length. If the actual tie stiffness is less than the required stiffness for mode  $n-1$ , but exceeds that for mode  $n$ , the ties are assumed to provide sufficient lateral restraint to the longitudinal reinforcing bars buckling in the  $n^{\text{th}}$  mode. It is important to note that although an energy-based approach may not be appropriate or exact in estimating the buckling length of the longitudinal bars, a series of assumptions made by Dhakal and Maekawa (2002) made it possible to estimate the buckling length of the reinforcing bars.

### 6.5.1 Tie Stiffness ( $k_t$ )

The tendency of longitudinal bars to buckle induces tensile forces in the lateral reinforcement providing restraint to longitudinal bars. Hence, axial stiffness of the transverse reinforcement is directly associated with the lateral restraint provided to the longitudinal reinforcement. The axial stiffness of each tie leg can be expressed as  $E_t A_t / l_e$ , where  $E_t$ ,  $A_t$ , and  $l_e$  are the modulus of elasticity, cross-sectional area, and the length of a tie leg, respectively. Assuming that the total stiffness of  $n_t$  tie legs along the buckling direction equally contribute to  $n_b$  longitudinal bars that are prone to simultaneous buckling, the effective stiffness of the tie system providing restraint against buckling of each longitudinal bar can be calculated using the following equation.

$$k_t = \frac{E_t A_t}{l_e} \times \frac{n_l}{n_b} \quad (6.11)$$

where

- $E_t$  = elastic modulus of transverse reinforcement
- $A_t$  = cross-sectional area of transverse reinforcement
- $l_e$  = effective leg-length of transverse reinforcement
- $n_l$  = number of tie legs providing restraint to a longitudinal bar
- $n_b$  = number of longitudinal bars prone to simultaneous buckling

The values of  $n_b$  and  $n_l$  for common arrangements of longitudinal and transverse reinforcement are illustrated in Figure 6.18. It is important to note that the values shown in this figure are for flexural loading, where only the reinforcing bars on the compression side are prone to simultaneous buckling.

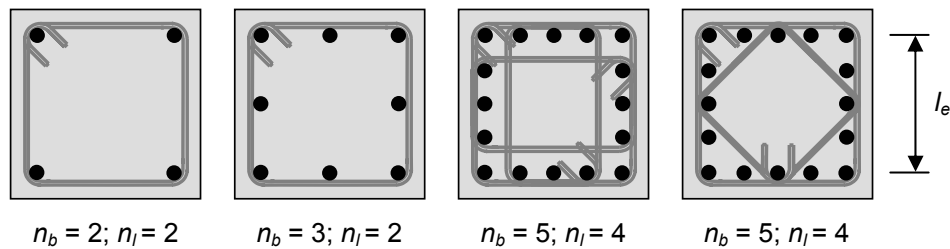
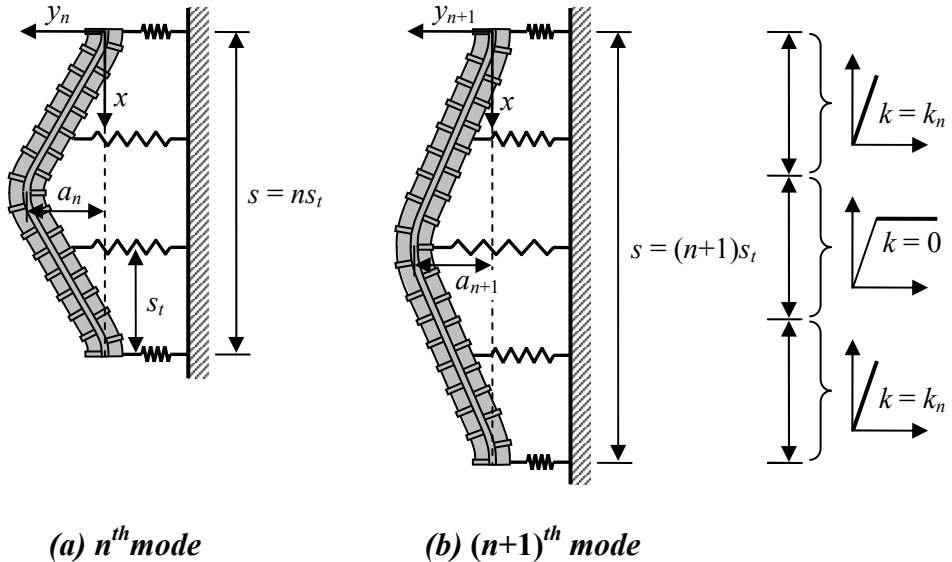


**Figure 6.18 Values of  $n_b$  and  $n_l$  for Typical Reinforcement Arrangements**  
(Dhakal and Maekawa 2002)

### 6.5.2 Required Tie Stiffness ( $k_n$ )

As shown in Figure 6.19, deriving the required spring stiffness ( $k_n$ ) corresponding to an arbitrary mode  $n$  should address two consecutive buckling modes  $n$  and  $n+1$ . Here, it is assumed that the longitudinal bars tend to buckle at the  $n^{\text{th}}$  mode and avoid buckling at the  $(n+1)^{\text{th}}$  mode. The lower modes need not



(a)  $n^{\text{th}}$  mode

(b)  $(n+1)^{\text{th}}$  mode

$$y_n = \frac{a_n}{2} \left( 1 - \cos \frac{2\pi x}{ns_t} \right)$$

$$y_{n+1} = \frac{a_{n+1}}{2} \left( 1 - \cos \frac{2\pi x}{(n+1)s_t} \right)$$

**Figure 6.19 Estimation of Buckling Length (Dhakal and Maekawa 2002)**

be considered because they are already checked in the previous steps and proved not to exist. Then, the cumulative potential energy,  $U$ , can be defined as the sum of the energies  $U_n$  and  $U_{n+1}$ , which are associated with the two buckling modes  $n$  and  $n+1$  (Equation (6.12)). As shown in Equations (6.13) and (6.14), energy corresponding to each buckling mode includes the strain energy of the reinforcing bar, energy stored in the springs, and energy due to shortening of the bar.

$$U = U_n + U_{n+1} \quad (6.12)$$

$$U_n = \int_0^{ns} \frac{EI}{2} \left( \frac{d^2 y_n}{dx^2} \right)^2 dx + c_i \sum_{i=1}^n \frac{k_n}{2} y_n^{is2} - \int_0^{ns} \frac{P_n}{2} \left( \frac{dy_n}{dx} \right)^2 dx \quad (6.13)$$

$$U_{n+1} = \int_0^{(n+1)s} \frac{EI}{2} \left( \frac{d^2y_{n+1}}{dx^2} \right)^2 dx + c_i \sum_{i=1}^{n+1} \frac{k_n}{2} y_{n+1}^{is^2} - \int_0^{(n+1)s} \frac{P_n}{2} \left( \frac{dy_{n+1}}{dx} \right)^2 dx \quad (6.14)$$

where

$c_i$  = coefficient to incorporate the plasticity of lateral ties

= 0 for the eliminated springs

= 1 for the rest.

$k_n$  = critical spring stiffness

$P_n$  = axial load corresponding to the  $n$ th mode

By using the prescribed deformed shapes shown in Figure 6.19 and minimizing  $U$  with respect to each of the maximum amplitudes  $a_n$  and  $a_{n+1}$ , Dhakal and Maekawa (2002) derived the following expressions (Equations (6.15) and (6.16)).

$$\frac{\partial U}{\partial a_n} = 0 : \frac{2\pi^4 EI}{n^3 s_t^3} + \frac{c_i k_n}{4} \sum_{i=1}^n \left( 1 - \cos \frac{2i\pi}{n} \right)^2 - \frac{P_n \pi^2}{2ns_t} = 0 \quad (6.15)$$

$$\frac{\partial U}{\partial a_{n+1}} = 0 : \frac{2\pi^4 EI}{(n+1)^3 s_t^3} + \frac{c_i k_n}{4} \sum_{i=1}^{n+1} \left( 1 - \cos \frac{2i\pi}{n+1} \right)^2 - \frac{P_n \pi^2}{2(n+1)s_t} = 0 \quad (6.16)$$

Dhakal and Maekawa (2002) also assumed that the sets of springs located around the middle of a buckled bar will yield during buckling of a bar and, therefore, provide zero stiffness, as illustrated in Figure 6.19(b). Implementing this assumption (yielding ties have no axial stiffness and hence they do not provide effective lateral restraint against buckling) to Equations (6.15) and (6.16) result in the required spring stiffness ( $k_n$ ) and the corresponding load ( $P_n$ ). The results of the required tie stiffness are shown in Table 6.2. The average flexural rigidity of the longitudinal bars in Table 6.2 is expressed as  $EI = 0.5E_s I \sqrt{f_y/58}$ ,

**Table 6.2 Required Spring Stiffness for Different Buckling Modes**

Buckling mode, $n$	Required spring stiffness, $k_n (\times \pi^4 EI / S_t^3)$
1	0.750
2	0.165
3	0.098
4	0.045
5	0.008

where  $f_y$  is the yield strength expressed in ksi (or,  $0.5E_s I \sqrt{f_y/400}$  where  $f_y$  is expressed in MPa).

## 6.6 APPLICATION OF REINFORCING BAR BUCKLING MODEL

As mentioned earlier, development a realistic constitutive relationship for reinforcing bars subjected to compression and incorporation of this model into the sectional analysis are important steps toward improving the accuracy of the response predictions. It is believed that with the inclusion of reinforcing bar buckling in the sectional analyses, more realistic estimations for the post-peak response, and hence the deformation capacity, can be obtained. In fact, this was the main premise behind the study reported in this chapter. The validity of this hypothesis is checked in this section.

To demonstrate the effect of the inclusion of reinforcing bar buckling in predicting the behavior of concrete columns, four columns tested by Soesianawati et al. (1986) and Muguruma et al. (1989) are used. In order to establish a basis of comparison, two sets of analyses are conducted. In the first set of analyses, the buckling of longitudinal bars is not modeled. The unconfined concrete model of Collins et al. (1993) is used for cover concrete and the confined concrete model proposed by Razvi and Saaticoglu (1988) is used for core concrete. In the second

set of analyses, the buckling lengths of the longitudinal bars were estimated by using the energy-based model proposed by Dhakal and Maekawa (2002) (Figure 6.17). Subsequently, constitutive relationships for reinforcing bars subjected to compressive stresses are obtained by following the procedures described in Figure 6.15. Hence, buckling of the longitudinal bars was considered in the analyses.

Since most experimental results on concrete columns are only reported in the form of lateral load-drift response plots, the lateral load-displacement responses are generated for these four columns. A detailed description of the analytical method used to generate the lateral load-tip deflection response is given in Chapter 7. Figure 6.20(a) shows that the inclusion of the buckling behavior of longitudinal reinforcement does not significantly affect the predicted response. This column specimen was tested under low axial loads ( $P/P_o = 0.1$ ). Under low axial loads, the compressive strain demands are relatively small even at large curvatures. As a result, the buckling of longitudinal reinforcement will occur at impractically large curvatures and consequently longitudinal bar buckling will not significantly affect the overall column behavior within the practical range of response.

In contrast, when the axial loads are high ( $P > 0.3P_o$ ), the buckling of longitudinal reinforcement initiates at relatively small curvatures and, therefore, the bar buckling plays an important role in determining the column behavior. The improvement in the accuracy of predicted responses can be observed in Figures 6.20(b) through 6.20(d). These columns were tested under high axial loads and had reasonable amounts of longitudinal reinforcement, as shown in Figure 6.20.

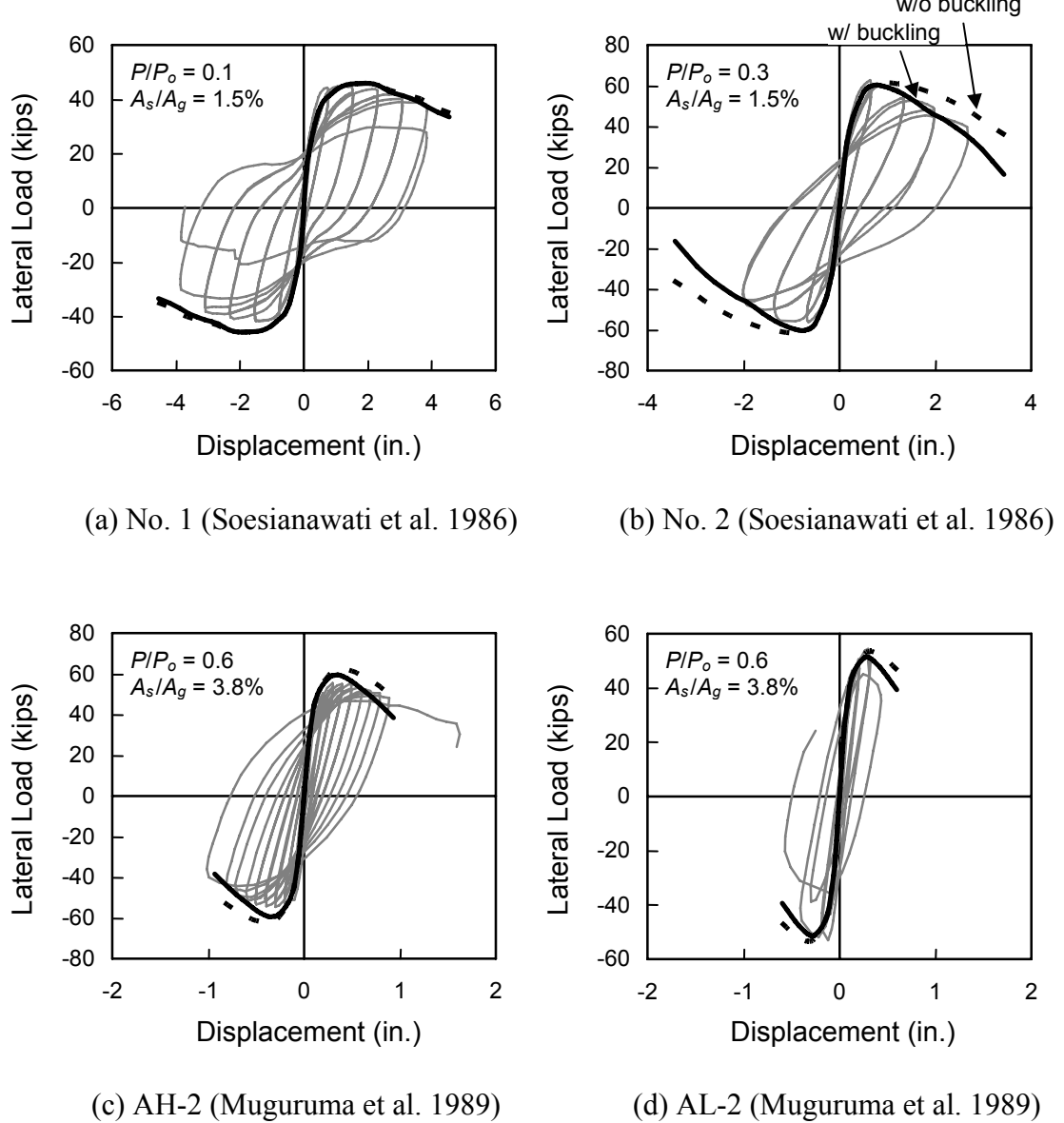


**Figure 6.20 Effect of Inclusion of Buckling Behavior on the Column Response**

It is important to note that if the amount of longitudinal reinforcement is too small, the difference in the behavior of longitudinal reinforcement will not be important because the contribution of longitudinal reinforcement on the behavior is small. Therefore, it can be concluded that the accuracy of response predictions obtained for the post-peak part of predicted responses can be improved by including the reinforcing bar buckling and the improvement will be significant in the presence of high axial loads.

## 6.7 SUMMARY

In this chapter, closed-form equations that can be used to model the behavior of longitudinal bars subjected to compressive stresses is developed. The proposed reinforcing bar buckling model is calibrated using the experimental data reported by Bayrak and Sheikh (2001) and Miseses (2003). An energy-based method to predict the buckling length of longitudinal bars, proposed by Dhakal and Maekawa (2002), is also described and adopted in an analytical study to accurately estimate the behavior of reinforcing bars buckling in the plastic hinge region of a column. The importance of the inclusion of rebar buckling in predicting concrete column responses is illustrated by predicting the behavior of concrete columns tested by other researchers.

# **CHAPTER 7**

## **DRIFT CAPACITY**

### **7.1 INTRODUCTION**

Performance-based earthquake engineering, as it applies to the seismic design of reinforced concrete columns, is dependent on the ability of a design engineer to estimate the deformation capacity of a reinforced concrete column. If such capacities can be estimated, it may also be possible to design columns for an anticipated deformation capacity. In order to estimate the deformation capacity of reinforced concrete columns, extensive experimental and analytical research has been conducted during the last three decades. Analytical procedures that can be used to estimate the behavior of confined concrete (Kent and Park 1971; Scott et al. 1982; Sheikh and Uzumeri 1982; Sheikh and Yeh 1992; Mander et al. 1988; Saatcioglu and Razvi 1992; Saatcioglu et al. 1995; Razvi and Saatcioglu 1999; Cusson and Paultre 1995; Légeron and Paultre 2003), reinforcing bar slip displacement (Alsiwat and Saatcioglu 1992) and shear displacement (Park and Paulay 1975; Lehman and Moehle 2000) have been developed. Based on these models, several analytical methods (Watson and Park 1989; Wehbe et al. 1997; Yalcin and Saatcioglu 2000) have been developed to estimate the behavior of a reinforced concrete column. These analytical methods and associated research have also been used to develop design equations that can be used to calculate the amount of confining reinforcement necessary to achieve sufficient ductility (ATC-32; Watson and Park 1989; Saatcioglu and Razvi 2002). However, the complexity of these analytical methods renders them impractical for use in common seismic design and evaluation practice. In most cases, the accuracy of the analytical methods described above has been evaluated using a limited

number of column test data. This necessitates an evaluation of the accuracy and conservativeness of the analytical models reported in the literature. Preferably, this evaluation should be performed by using data from all relevant tests reported in the literature and those conducted during this research.

Two different approaches that can be used to estimate the deformation capacity of a reinforced concrete column are presented in this chapter. One approach may be considered as a state-of-the-art analytical method, which includes the new plastic hinge length expression (Chapter 5) and the new bar buckling model (Chapter 6) developed in this research. The other approach involves the derivation of simple, closed-form equations that can be used to quantify the influence of secondary moments by the  $P$ - $\Delta$  effect on the lateral load response of reinforced concrete columns. To investigate the validity and conservativeness of these methods in estimating the deformation capacity of reinforced concrete columns, data from a large number of column tests are used. The necessary data were drawn from the UW/PEER column database (<http://maximus.ce.washington.edu/~peera1/>). The lateral drift capacities of the columns tested by numerous researchers (Table 7.1) are estimated using the two approaches described above. The estimated drift capacities are compared with the experimental values. In this way, the accuracy and conservativeness of (1) a rigorous analytical procedure and (2) a simple closed-form expression are evaluated.

**Table 7.1 Summary of Test Specimens**

Researchers	Section size (in.×in.)	Concrete strength (ksi)	Yield strength of longitudinal bars (ksi)	Shear span-to- depth ratio*
Azizinamini et al. (1992)	18×18	5 - 6	64	3.0
Bayrak and Sheikh (1997)	12×12	10 - 15	66	6.0
Galeota et al. (1996)	10×10	12	77 - 84	4.6
Kanda et al. (1988)	10×10	4	54	3.0
Matamoros et al. (2003)	8×8	6 - 7	83 - 85	3.0
Mo and Wang (2000)	15.7×15.7	4	72	3.5
Muguruma et al. (1989)	8×8	12 - 17	58	2.5
Ohno and Nishioka (1984)	16×16	4	52	4.0
Paultre and Légeron (1992)	12×12	14 - 15	62 - 65	6.6
Paultre et al. (2001)	12×12	11 - 16	65	6.6
Saatcioglu and Grira (1999)	14×14	5	66	4.7
Saatcioglu and Ozcebe (1989)	14×14	5 - 6	63	2.9
Sakai et al. (1990)	10×10	14	50 - 55	2.0
Soesianawati et al. (1986)	16×16	6 - 7	65	4.0
Sugano (1996)	9×9	17	57	2.0
Tanaka and Park (1990)	22×22	5	74	3.0
	16×16	4	69	4.0
Thomsen and Wallace (1994)	6×6	10 - 15	66 - 69	3.9
Watson and Park (1989)	16×16	6	69	4.0
Wehbe et al. (1997)	24×15	4	65	3.8
Xiao and Martirosyan (1998)	10×10	11 - 12	74	2.0
Zahn et al. (1986)	16×16	4 - 6	64	4.0
Bae (2005)	24×24	4 - 6	58 - 84	5.0
	17.25×17.25	6	72	7.0
Average	-	9.5	68	-

\*: Shear span-to-depth ratio is defined as the ratio of the distance between the sections experiencing zero-moment and maximum moment ( $L$ ) to the overall depth of a column specimen ( $h$ ).

## 7.2 ANALYTICAL METHOD

The following deformation components contribute to the tip displacement of a cantilever reinforced concrete column: (1) flexural deformations, (2) fixed end rotations resulting from the slip of longitudinal bars out of joints, and (3) shear deformations. Therefore, total lateral displacement at the tip of a reinforced concrete column can be expressed as follows:

$$\Delta = \Delta_{flexure} + \Delta_{slip} + \Delta_{shear} \quad (7.1)$$

In evaluating these displacement components, the  $P\Delta$  effect should be taken into account. The secondary moments generated by the  $P\Delta$  effect increase the lateral displacement measured at the tip of a cantilever column. In some cases, such as slender columns supporting large gravity-induced axial loads, a significant portion of the flexural resistance of a column may be consumed by the  $P\Delta$  effect.

### 7.2.1 Flexural Deformations

The contribution of flexural deformations to the tip displacement of a cantilever column ( $\Delta_{flexure}$ ) can be computed by integrating curvatures ( $\phi$ ) over the height of a column ( $L$ ) as follows:

$$\Delta_{flexure} = \int_0^L \phi(x) x dx \quad (7.2)$$

where

$L$  = height of a cantilever column

$x$  = distance from the tip of a column

$\phi(x)$  = curvature of section at distance  $x$  from the tip of a column

Equation (7.2) can be successfully used to model the ascending branch of the lateral load-deformation response. However, theoretical difficulties arise while

using this equation in an analysis to estimate the descending branch of the response. In order to overcome this difficulty, the plastic hinge concept is commonly used and inelastic curvatures are assumed to be concentrated within the plastic hinge zones. In the analytical approach presented in this chapter, the plastic hinge concept is used to approximate the descending part of the lateral load response of reinforced concrete columns. More specifically, the proposed plastic hinge length expression (Chapter 5), developed in this research, is used to estimate the plastic hinge length of concrete columns.

### 7.2.2 Deformations due to Reinforcing Bar Slip

The formation of flexural cracks at the interface of a column and a typical beam-column joint (or foundation) strain the longitudinal bars crossing the crack. Widening of such cracks produces inelastic strains in the bar. This results in the penetration of yielding into the anchorage zone, causing extension of the bar. Hence, reinforced concrete columns experience additional rigid body rotations at their base due to bar slip. Alsiwat and Saatcioglu (1992) stated that the omission of bar slip in computing the displacement capacity of a column might lead to erroneous results.

In this study, displacement due to bar slip is computed using the analytical model proposed by Alsiwat and Saatcioglu (1992). This model incorporates yield penetration and associated inelasticity in an anchored bar, as well as the possibility of slip. Once the bar slip at the end of a column is computed, the end rotation and lateral displacement of a cantilever column due to bar slip can be determined as follows:

$$\theta_{slip} = \frac{u_{st}}{d - c} \quad (7.3)$$

$$\Delta_{slip} = \theta_{slip} \times L \quad (7.4)$$

where

- $u_{st}$  = slip of the column bars closest to the tension face
- $d$  = distance from extreme compression fiber of concrete to center of extreme tensile bar
- $c$  = depth of neutral axis
- $L$  = height of cantilever column

### 7.2.3 Shear Deformations

The shear deformations within the linear elastic range can be calculated using the principles of elasticity. Although small, the shear deformations are included in all stages of the column response. As such, the following equation is used within the linear elastic range.

$$\Delta_{shear} = \frac{V \cdot L}{A \cdot G}; G = \frac{E_c}{2(1+\nu)} \quad (7.5)$$

where

- $V$  = lateral load acting on column
- $L$  = height of cantilever column
- $A$  = cross sectional area of column
- $G$  = shear modulus
- $E_c$  = modulus of elasticity of the concrete
- $\nu$  = Poisson's ratio

Lehman and Moehle (2000) used an effective shear modulus and effective area terms in order to estimate the contribution of the shear deformations after cracking to the tip displacement of a column. Following the suggestion of Lehman and Moehle (2000), the contribution of shear deformations to the lateral tip displacement is calculated as follows.

$$\Delta_{shear} = \int_0^L \frac{V(x)}{A_{eff}(x) \cdot G_{eff}(x)} dx = V \cdot \int_0^L \frac{dx}{A_{eff}(x) \cdot G_{eff}(x)} \quad (7.6)$$

where  $G_{eff}(x) = \frac{E_{c,sec}(x)}{2(1+\nu)}$

$A_{eff}$  = effective shear area of column

$\approx$  area of concrete subjected to compressive strains

$E_{c,sec}(x)$  = secant modulus of elasticity of core concrete assessed from the corresponding compressive stress and strain at the extreme fiber of the concrete core

$\nu$  = Poisson's ratio ( $\approx 0.3$ )

#### 7.2.4 Additional Deformations due to $P-\Delta$ Effect

When columns supporting substantial axial loads experience lateral displacements, the gravity-induced axial loads produce pronounced secondary moments (Figure 7.1). The distribution of secondary moments is related to the deflected shape of a column along the height of a column. Therefore, combining the moment diagram by lateral loads and the  $P-\Delta$  effect, curvatures along the column height can be obtained and the associated tip deflection can be estimated. Since the secondary moment distribution along the column depends on the deflected shape of a column, an iterative procedure is required.

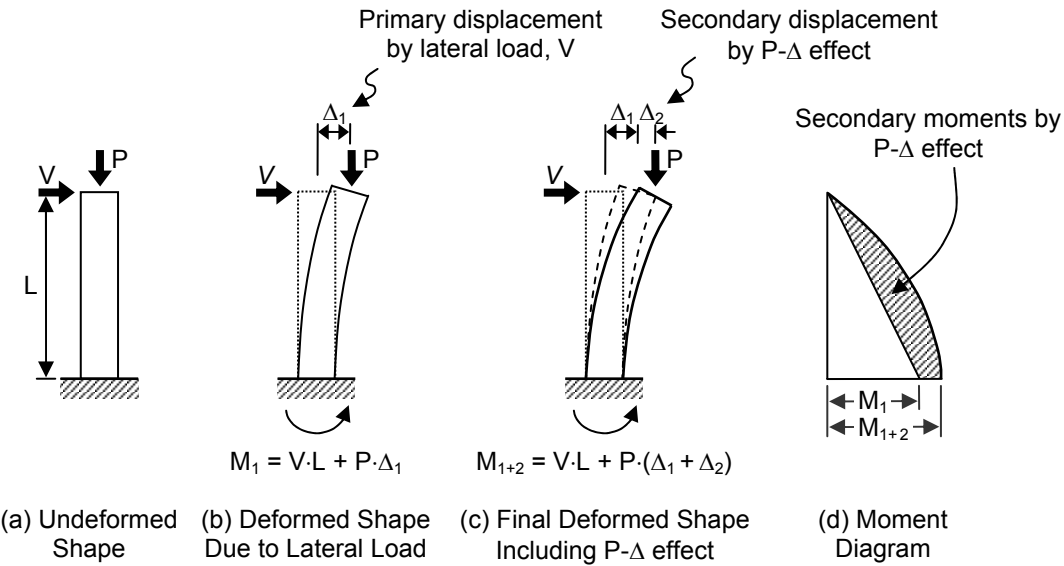


**Figure 7.1 Effect of  $P\Delta$  Effect on Column Behavior**

### 7.2.5 Confined Concrete

Various analytical models have been proposed to quantify the effects of confinement on the strength and ductility of concrete. Kent and Park (1971) proposed a confined concrete model. This model takes into account the ductility enhancement due to confining reinforcement. Scott et al. (1982) modified the confinement model proposed by Kent and Park to include the strength enhancement due to confinement and also to include the effects of strain rate on the analytical model.

Sheikh and Uzumeri (1982) introduced the concept of effectively confined concrete and proposed a confined concrete model. They concluded that uniform distribution of longitudinal reinforcement around the perimeter ties and smaller tie spacings would result in higher strength and ductility increase. Sheikh and Yeh (1992) modified the concrete model of Sheikh and Uzumeri (1982) to include the effect of strain gradient.

Mander et al. (1988) proposed a concrete model using the effectively confined concrete concept. The effects of cyclic loading and strain rate are considered in this model.

Saatcioglu and Razvi (1992) developed the equivalent uniform pressure concept and proposed a concrete confinement model based on this concept. Three years after the original proposal, this model was modified to include the effect of eccentric loading by Saatcioglu et al. (1995). Subsequently, this constitutive model was further calibrated for both normal and high-strength concrete by Razvi and Saatcioglu (1999).

Cusson and Paultre (1995) proposed a concrete model for high-strength concrete. This constitutive model was later modified to increase its range of applicability to both normal and high-strength concrete (Légeron and Paultre 2003).

Although it is possible to use all of the aforementioned constitutive models in the analysis, the confined concrete model proposed by Razvi and Saatcioglu (1999) is used in the proposed analytical method. This confinement model was chosen because of the following considerations: (1) its incorporation into the analysis yielded somewhat better estimations than the other confinement models and (2) it is applicable to normal-strength and high-strength concrete columns (4 - 19 ksi).

The concrete model proposed by Razvi and Saatcioglu (1999) is based on the computation of confinement pressures from material and geometric properties of columns. Different distributions of pressure, resulting from different arrangements of reinforcement are expressed in terms of equivalent uniform pressures ( $f_{le}$ ). The equivalent uniform pressure is derived from the average pressure ( $f_l$ ). The average pressure is computed from tensile forces in transverse reinforcement by considering the transverse steel area and stress at peak concrete

stress. The model incorporates the effects of unequal confinement pressures in two orthogonal directions and the superposition of pressures resulting from different types of confinement reinforcement.

Accordingly, Razvi and Saatcioglu (1999) proposed that the strength of confined concrete can be calculated as:

$$f'_{cc} = f'_{co} + k_1 f_{le} \quad (7.7)$$

$$k_1 = 6.7(f_{le})^{-0.17} \quad (7.8)$$

$$f_{le} = k_2 f_l \quad (7.9)$$

$$f_l = \frac{\sum A_s f_s \sin \alpha}{b_c s} \quad (7.10)$$

where

$$k_2 = 0.15 \sqrt{\frac{b_c^2}{s \cdot s_l}} \leq 1.0$$

$A_s$  = area of one leg of transverse reinforcement

$$f_s = E_s \left[ 0.0025 + 0.04 \left( \frac{k_2 \rho_c}{f'_{co}} \right)^{1/3} \right] \leq f_{yt}$$

$\alpha$  = angle between leg of transverse reinforcement and  $b_c$

$b_c$  = core dimension measured center-to-center of perimeter hoop

$s$  = spacing of transverse reinforcement

$s_l$  = spacing of laterally supported longitudinal reinforcement

$$\rho_c = \frac{\sum A_{sx} + \sum A_{sy}}{s(b_{cx} + b_{cy})}$$

$f'_{co}$  = unconfined concrete compressive strength

$b_{cx}, b_{cy}$  = core dimensions measured center-to-center of perimeter hoop in  $x$ - and  $y$ - directions

Ductility of confined concrete was modeled by using the strain at peak concrete stress ( $\varepsilon_1$ ) and the strain corresponding to 85% of peak stress ( $\varepsilon_{0.85}$ ).

$$\varepsilon_1 = \varepsilon_{01}(1 + 5k_3K) \quad (7.11)$$

$$\varepsilon_{0.85} = 260k_3\rho_c\varepsilon_1[1 + 0.5k_2(k_4 - 1)] + \varepsilon_{0.85} \quad (7.12)$$

where

$$k_3 = \frac{40}{f'_{co}} \leq 1.0$$

$$k_4 = \frac{f_{yt}}{500} \geq 1.0$$

$$K = \frac{k_1 f_{le}}{f'_{co}}$$

$$\varepsilon_{01} = 0.0028 - 0.0008k_3$$

= strain at peak stress of unconfined concrete

$$\varepsilon_{0.85} = \varepsilon_{01} + 0.0018k_3^2$$

= strain corresponding to 85% of peak stress of unconfined concrete

The stress-strain relationship of confined concrete proposed by Razvi and Saatcioglu (1999) consists of a nonlinear ascending branch up to peak stress ( $f_{cc}'$ ) and a linear descending branch beyond the peak stress, as shown in Figure 7.2. Razvi and Saatcioglu (1999) adopted the ascending branch of the stress-strain relationship proposed by Popovics (1973).

$$f_c = \frac{f'_{cc} \left( \frac{\varepsilon_c}{\varepsilon_1} \right)^r}{r - 1 + \left( \frac{\varepsilon_c}{\varepsilon_1} \right)^r} \quad (7.13)$$

$$r = \frac{E_c}{E_c - E_{sec}} \quad (7.14)$$

where

$$E_{sec} = \frac{f'_{cc}}{\varepsilon_1}$$

$$E_c = 3,320\sqrt{f'_c} + 6,900 > E_{sec} \quad (f'_c \text{ in MPa})$$

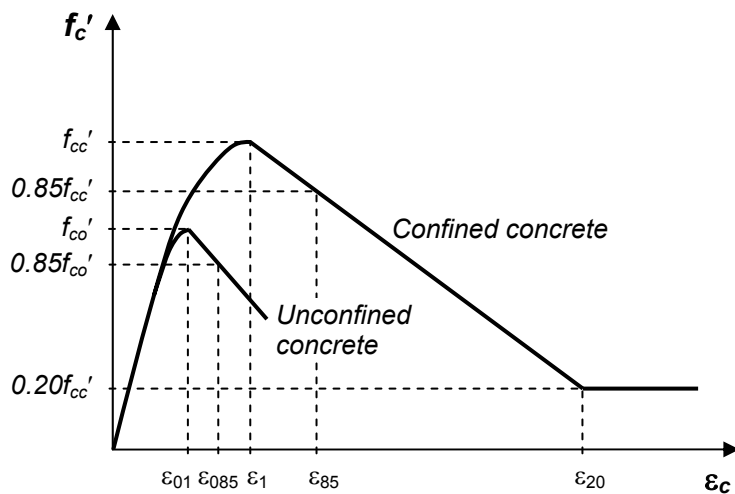


**Figure 7.2 Stress-Strain Relationship of Confined Concrete  
(Razvi and Saatcioglu 1999)**

### 7.2.6 Reinforcing Bars

The stress-strain response of reinforcing bars in tension is simply modeled using a bi-linear relationship until the initiation of strain hardening. The stress-strain model proposed by Mander et al. (1984) is used to model the behavior of reinforcing bars in the strain hardening region. According to Mander et al. (1984), the relationship between the stress ( $f_s$ ) and the strain ( $\varepsilon_s$ ) in the strain hardening region can be expressed by:

$$f_s = f_u + (f_y - f_u) \left( \frac{\varepsilon_u - \varepsilon_s}{\varepsilon_u - \varepsilon_{sh}} \right)^p \quad (7.15)$$

where

$f_y$  and  $f_u$  = yield and ultimate strengths of reinforcing bar

$\varepsilon_{sh}$  = strain at which strain hardening commences

$\varepsilon_u$  = strain corresponding to the ultimate strength ( $f_u$ )

The parameter  $p$  is defined as:

$$p = E_{sh} \left( \frac{\varepsilon_u - \varepsilon_{sh}}{f_u - f_y} \right) \quad (7.16)$$

where

$E_{sh}$  = tangent modulus of elasticity at the initiation of strain hardening

The reinforcing bar buckling model, presented in Chapter 6, is used in the analyses to simulate the behavior of longitudinal bars subjected to compressive stresses. The importance of the inclusion of rebar buckling in sectional analyses was previously illustrated in Chapter 6.

### **7.2.7 Verification of Proposed Analytical Method**

The constitutive models described in the preceding sections are implemented into the analysis program developed during the course of this research. This computer program is included in Appendix B. A flowchart illustrating the important steps of the analysis is given in Figure 7.3. In order to estimate the lateral load response of a reinforced concrete column, first the behavior of a typical section located in the plastic hinge zone is estimated. Using this sectional behavior and other phenomenological models described above, the lateral load-displacement behavior of a column is estimated.

The analytical method presented in Figure 7.3 is intended for use in estimating the lateral load behavior of concrete columns which are vulnerable to flexural failure. In other words, this analytical procedure should not be used for short columns ( $L/h < 2$ ). An example problem that illustrates the details of the analytical method is included in Appendix D.

In order to verify the accuracy of estimated drift capacities of reinforced concrete columns, a large number of reinforced concrete columns tested under simulated seismic loads are obtained from the UW/PEER column database. More specifically, data from one-hundred-twenty-one tests are used for model verification purposes. Data from very small tests specimens ( $h < 6$  in.) were excluded. For all the data used in model verification, the original references were carefully examined to ensure that the columns included in this study were tested to failure or at least a 20% drop in the lateral load resistance was reported in all cases. The ultimate strength of reinforcing bars used in some of the columns is not reported (both in the UW/PEER column database and the original research papers). For those columns, the ultimate strength ( $f_{su}$ ) of reinforcing bars is assumed to be 50% larger than the yield strength, strain hardening is assumed to commence at a strain ( $\epsilon_{sh}$ ) of 0.007, and an ultimate strain ( $\epsilon_{su}$ ) value of 0.13 is

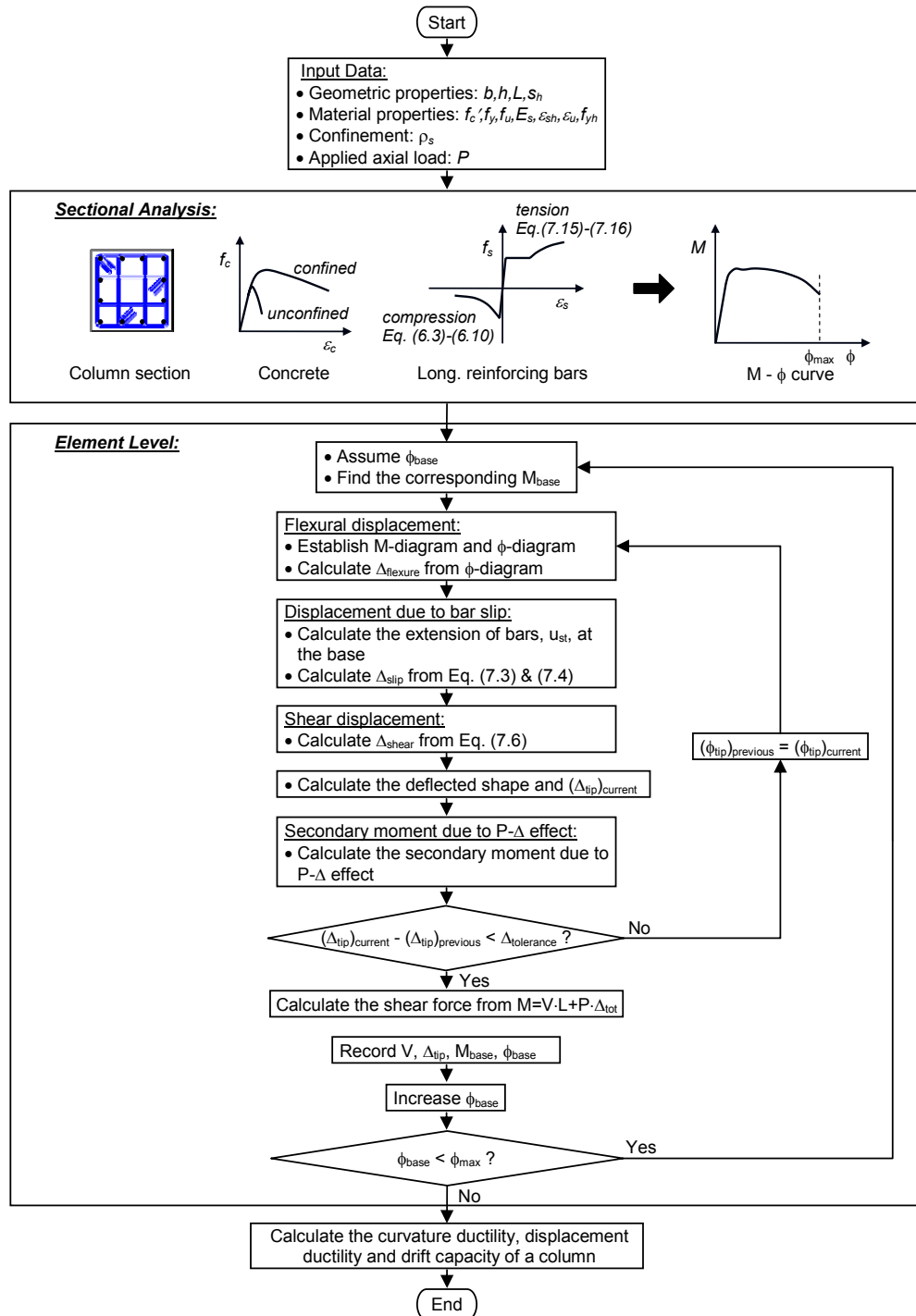


**Figure 7.3 Analytical Procedure**

used. The drift capacity of columns is defined as  $\Delta_{80}/L$ , where  $\Delta_{80}$  is illustrated in Figure 4.25.

Figure 7.4(a) illustrates a comparison of the estimated drift capacities with the measured drift capacities. This figure indicates that the proposed procedure provides reasonably good drift capacity estimations for most cases. The error in the drift estimations is measured by using the ratio of the estimated drift capacity to the experimental drift capacity. The mean, standard deviation and coefficient of variation of the error are 0.97, 0.24 and 0.25, respectively. In an effort to examine the magnitude of over- and under-estimations of the drift capacities, data are presented in a different manner in Figure 7.4(b). Once again, for most cases the drift capacities of the columns are estimated reasonably accurately ( $\pm 25\%$ ). However, in other cases, the magnitude of the over- and under-estimations approaches 50%. The problems associated with the drift capacity estimations are examined in the next section.

### 7.2.8 Accuracy of Drift Capacity Estimations

As discussed in the previous section, the accuracy of the drift capacity estimations obtained through the use of a sophisticated analytical method may not be acceptable in some cases. To identify the sources of error, the estimated and experimental response of all of the specimens considered in the model verification were examined and common sources of errors were identified. Figure 7.5 shows typical examples of estimated responses, compared with the test results. The errors seen in the estimated drift capacities are also shown in the figure. Figure 7.5 shows that even though the estimated responses are in good agreement with the test results, large errors in the estimated drift capacities can occur. The primary sources of these errors are: (1) inaccurate estimation of the maximum lateral load and (2) the stiffness of post-peak responses. The effects of these two

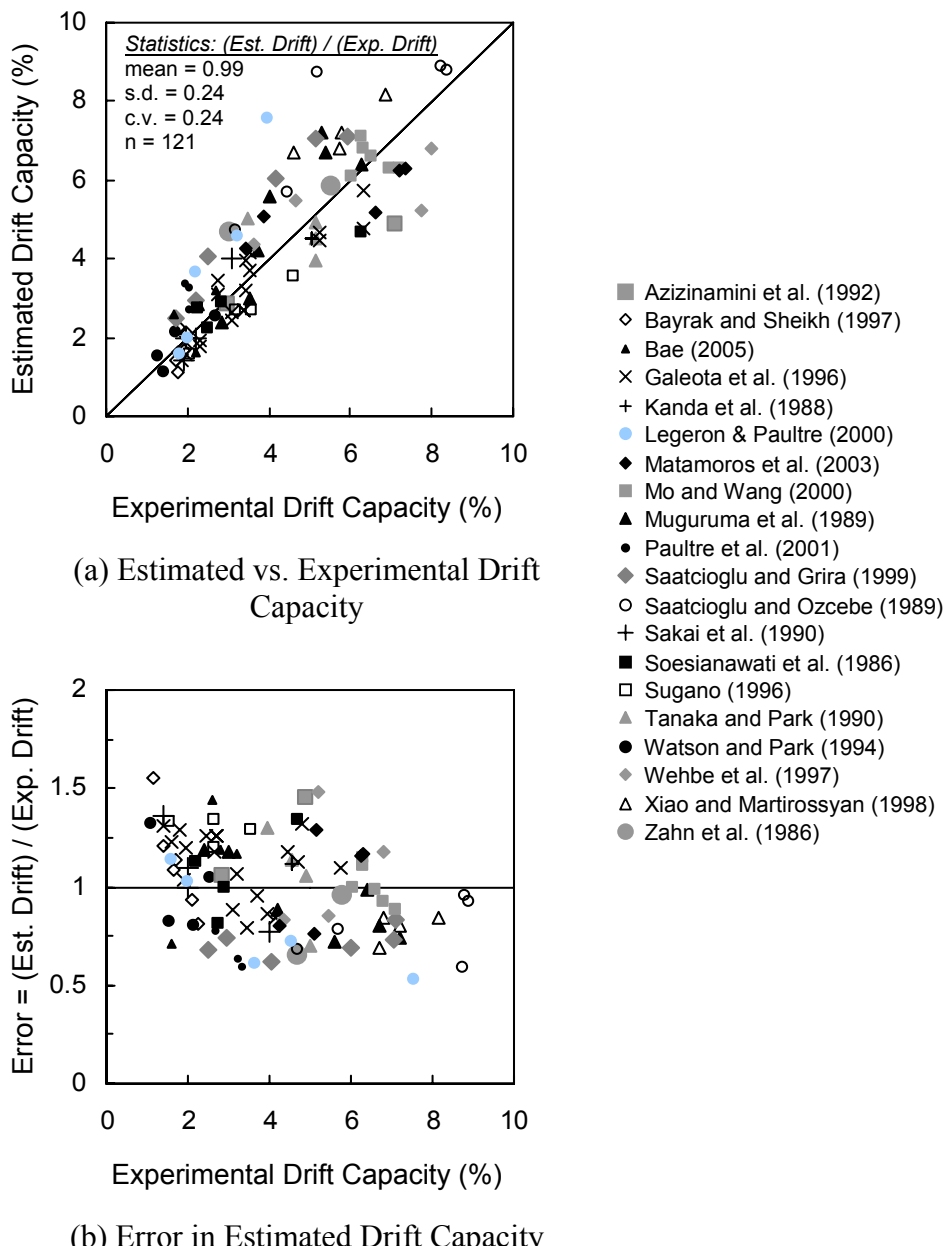


**Figure 7.4 Model Verification**

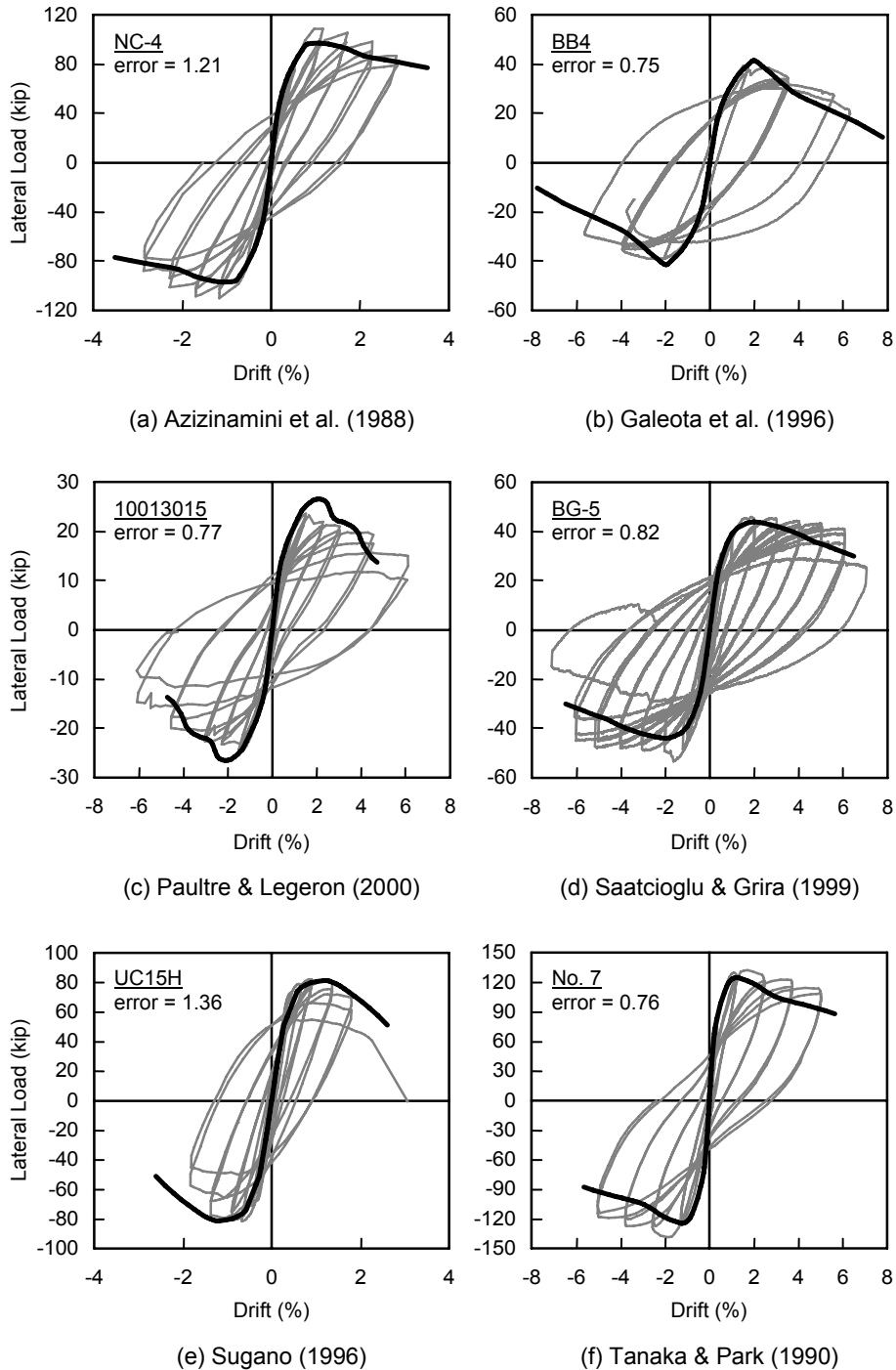


**Figure 7.5 Lateral Load Response: Estimations and Experiments**

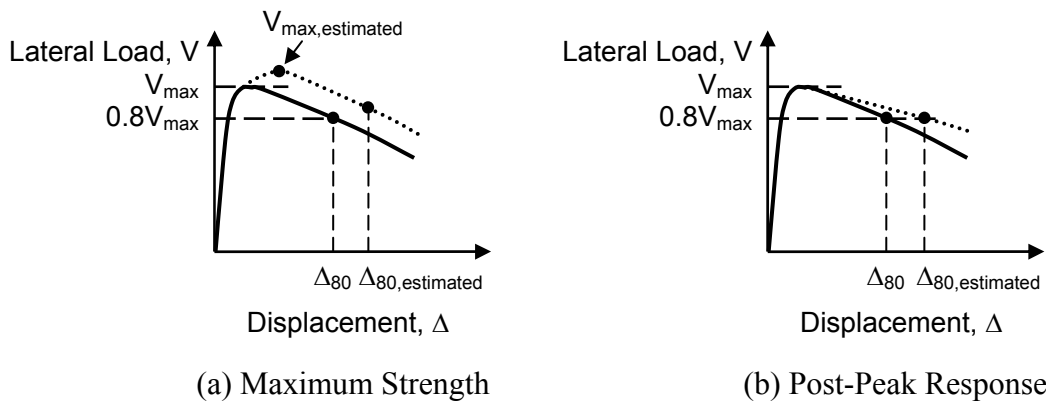


**Figure 7.6 Sources of Errors in Estimating Deformation Capacity**

major sources of error are shown in Figure 7.6. This figure illustrates that a small error in either the maximum lateral load or the post-peak response estimations can yield large errors in the estimated drift capacities.

The error in estimating the maximum lateral load can be caused by the stub confinement effect or the cover concrete behavior. Large stubs are commonly used by researchers to simulate footings or beam-column joints. The presence of a large volume of concrete adjacent to the maximum moment section in a test specimen results in additional lateral restraint applied to this section. This lateral restraint typically shifts the critical section away from the stub. This effect was studied by Sheikh and Khoury (1993), Sheikh et al. (1994), Bayrak and Sheikh (1997), and Légeron and Paultre (2000). The confining effects of a stub can be influenced by many factors, such as the size of the stub relative to the size of the column section, the level of axial load, amount and spacing of transverse reinforcement within the stub. Since the details of stubs are not sufficiently described in research papers, accurate modeling of these effects is not possible.

The behavior of cover concrete can also be a source of error in estimating the maximum lateral loads. Cover concrete is typically treated as unconfined

concrete. Even though this is a reasonable assumption, the compressive strain at which cover spalling takes place may vary greatly based on the compressive strength of the concrete. Research (Bayrak 1999; Bae and Bayrak 2003) has shown that the cover spalling strain decreases with increasing amounts of confinement reinforcement. More importantly, for high-strength concrete columns the cover spalling strain may be well below 0.003. Bayrak (1999) reported cover spalling strains as low as 0.0022 for high-strength concrete columns. With different thicknesses of cover concrete used in the specimens tested by various researchers, the magnitude of the error stemming from incorrect estimations of cover spalling strain varies.

The error in estimating the slope of the post-peak response can be related to many factors. These factors include the errors stemming from the inaccuracies associated with analytical models for confinement, reinforcing bar buckling, plastic hinge length, reinforcing bar slip and shear deformations. In addition, the constitutive models used in the analyses are meant to model the monotonic response and hysteretic modeling is considered beyond the scope of this research due to the many complexities associated with hysteretic models. In short, the errors associated with the factors discussed above cannot be avoided. Therefore, it can be concluded that the analysis program developed during the course of this research can provide reasonably accurate estimations for the lateral load behavior of reinforced concrete columns in most cases. However, in some cases the analytical method cannot provide accurate estimations for the deformation capacity. Although it may be possible to increase the accuracy of estimations through the use of cyclic material models, it is believed that the levels of scatter seen in the estimated drift capacity of the columns cannot be completely eliminated.

### **7.3 ESTIMATION OF DRIFT CAPACITY: A SIMPLE METHOD**

Even though sophisticated analytical methods can be used in estimating the drift capacity of reinforced concrete columns, it is not possible to recommend the use of such methods in seismic design practice considering the complexity of the analytical methods. The source code of the computer program used for these analyses is included in Appendix B. An examination of this source code clearly demonstrates the level of complication associated with this analytical technique. Although, it can be argued that the accuracy of estimations can be improved through the implementation of hysteretic material models into this software, it is believed that these improvements will come at the expense of complicating the analysis further. Performance-based design of reinforced concrete columns can only be performed in the presence of a simple transparent analysis technique. In order to pursue this goal, a simple closed-form expression is developed in this section.

The loss of lateral load resistance of a reinforced concrete column can be caused by (1) the degradation of moment capacity and (2) the  $P\Delta$  effect, as shown in Figure 7.7. The lateral displacement capacity of a column is usually expressed as the lateral displacement at which a 20% loss in lateral load capacity occurs (Figure 7.7). The deformation capacity of a reinforced concrete column can be improved by reducing or eliminating the degradation of moment resistance beyond the peak moment. In order to minimize or eliminate the post-peak degradation, the amount of confining reinforcement used within the potential plastic hinge regions can be increased. This approach has been used in all of the performance-based confining reinforcement design procedures proposed previously (Watson and Park 1994; Sheikh and Khoury 1997; Wehbe et al. 1997; Saatcioglu and Razvi 2002). Alternatively, the slenderness of a column can be controlled and hence the secondary moments generated by the  $P\Delta$  effect can be

minimized. In short, improving the displacement capacity of a column requires either reducing the degradation of moment capacity by providing large amounts of confining reinforcement or controlling the secondary moments generated by the  $P\Delta$  effect.

Since the  $P\Delta$  effect is a function of the axial load and the tip displacement of a column, the loss of lateral load resistance due to the  $P\Delta$  effect is unavoidable. In other words, the loss of lateral load resistance due to the secondary moments generated by the  $P\Delta$  effect is not directly related to the sectional performance of concrete columns. Based on this fact, and using a lower-bound approach, simple closed-form equations that can be used to estimate the deformation capacity of concrete columns can be derived.

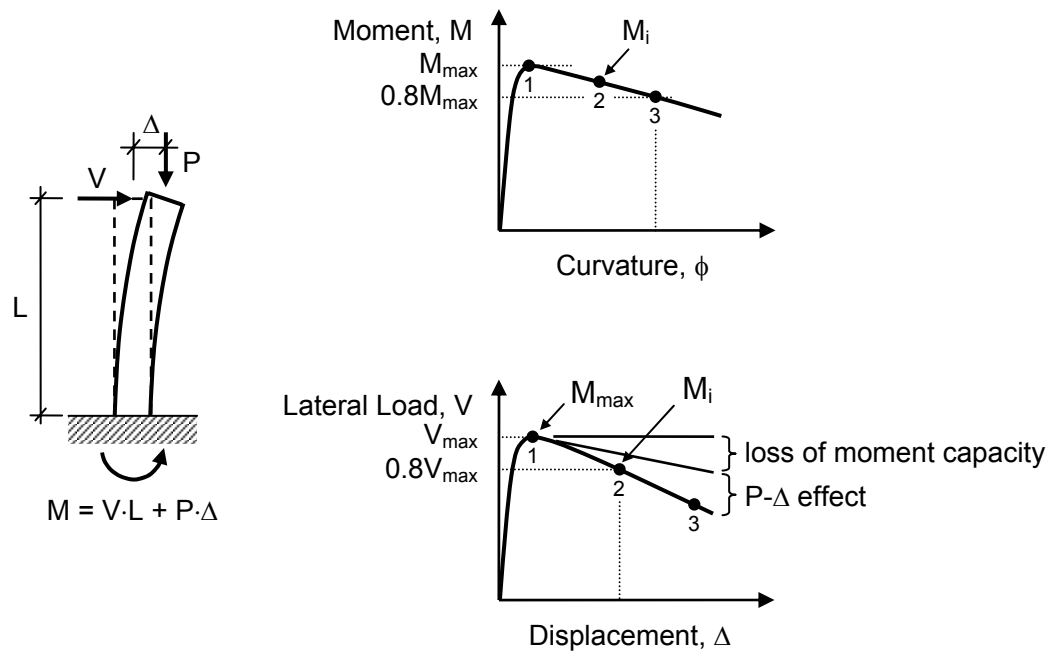


**Figure 7.7 Lateral Load Response of Reinforced Concrete Columns**

### 7.3.1 Displacement Capacity

In order to investigate the influence of the  $P\Delta$  effect on lateral deformation capacity of a column in its simplest form, the moment-curvature relationship of a reinforced concrete column is assumed to be elastic-perfectly-plastic. With this assumption, the loss of lateral load resistance due to the degradation of moment capacity can be ignored and the resulting displacement capacity of a column can be attributed to the  $P\Delta$  effect directly.

As can be seen in Figure 7.7, the moment at the base of a cantilever column can be calculated as follows:

$$M_{base} = V \cdot L + P \cdot \Delta \quad (7.17)$$

Figure 7.8 illustrates the assumed moment-curvature response and the corresponding lateral load-displacement response. It is important to recognize that the post-peak part of the lateral load response is solely controlled by the  $P\Delta$  effect. Assumed bi-linear moment-curvature and lateral load-deformation relationships shown in Figure 7.8 form the basis of the derivation included in this section. To simplify the derivation, the  $y$ -intercept of the straight line extrapolated from the descending branch of the load-deformation response is labeled as  $V_{max}$  (Figure 7.8). Alternatively,  $V_{max}$  can be envisioned as the lateral load capacity of a very stiff column with a very small yield displacement ( $\Delta_y \approx 0$ ). In this case, the relationship between the maximum moment and shear force can be established as follows:

$$\begin{aligned} M_{max} &= V \cdot L + P \cdot 0 \\ \therefore V &= \frac{M_{max}}{L} = V_{max} \end{aligned} \quad (7.18)$$

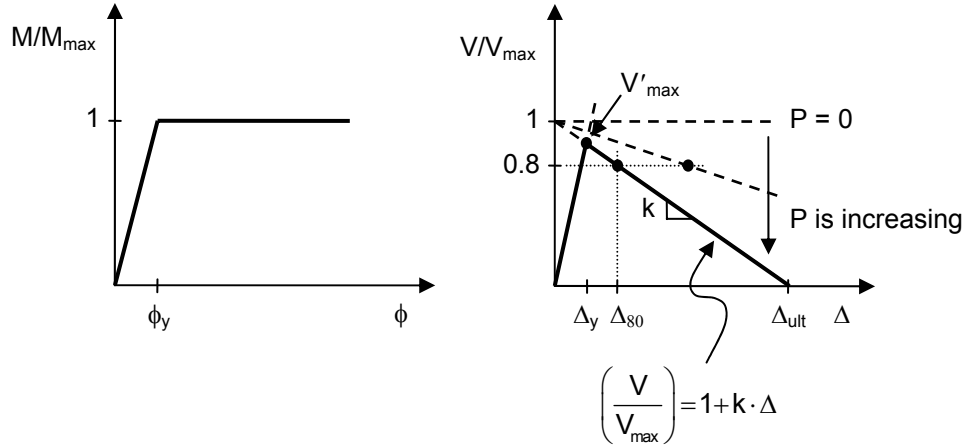


**Figure 7.8 Influence of  $P$ - $\Delta$  Effect on Lateral Load Response**

In a similar manner, the ultimate displacement ( $\Delta_{ult}$ ) can be defined as the displacement where lateral load capacity drops to zero due to the  $P$ - $\Delta$  effect.

$$M_{max} = 0 \cdot L + P \cdot \Delta$$

$$\therefore \Delta = \frac{M_{max}}{P} = \Delta_{ult} \quad (7.19)$$

Studying the lateral load-displacement response, the  $P$ - $\Delta$  effect can be quantified. The influence of the secondary moments can be computed by using the maximum lateral load and the ultimate displacement, as shown in Figure 7.8. As such, the slope of the descending branch of the assumed lateral load response shown in Figure 7.8 can be expressed as:

$$\therefore k = -\frac{1}{\Delta_{ult}} = -\frac{P}{M_{max}} \quad (7.20)$$

Based on the slope given in Equation (7.20), the following expression representing the post-peak part of the response can be obtained.

$$\left( \frac{V}{V_{max}} \right) = 1 + k \cdot \Delta = 1 - \frac{P}{M_{max}} \cdot \Delta \quad (7.21)$$

The displacement capacity ( $\Delta_{80}$ ) is generally defined as the displacement at which a 20% drop in the lateral load capacity is observed. As the lateral load capacity ( $V'_{max}$  in Figure 7.6) is also influenced by the  $P$ - $\Delta$  effect, the expression for the lateral load capacity will be somewhat complicated to include in a closed-form derivation. Typically, the magnitude of the secondary moments at the lateral load capacity ( $V'_{max}$ ) is not very significant because the magnitude of yield displacements is small. In order to simplify the subsequent parts of the derivation, 20% drop in the lateral load capacity is calculated using the maximum lateral load ( $V_{max}$ ) rather than the actual lateral load capacity ( $V'_{max}$ ). As can be seen in Figure 7.8, this simplifying assumption yields a slightly under-estimated displacement capacity ( $\Delta_{80}$ ). As such, the displacement capacity ( $\Delta_{80}$ ) can be expressed as:

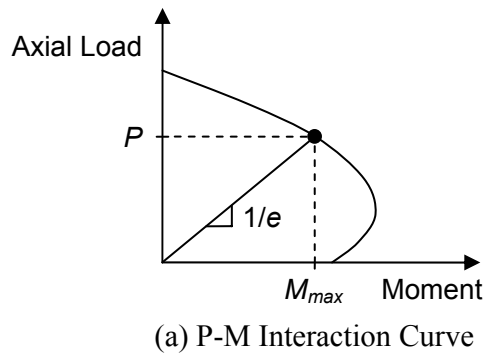
$$0.8 = 1 - \frac{P}{M_{max}} \cdot \Delta_{80}$$

$$\frac{P}{M_{max}} \cdot \Delta_{80} = 0.2$$

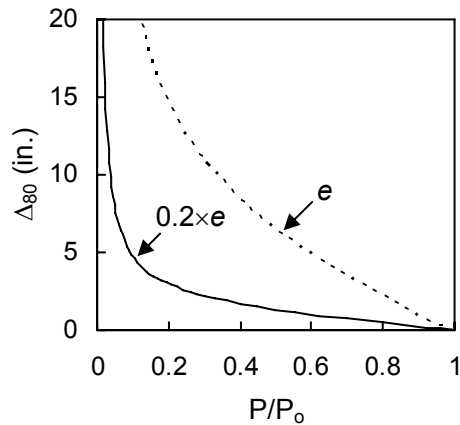
$$\Delta_{80} = 0.2 \times e \quad (7.22)$$

where  $e = \frac{M_{max}}{P}$ .

Equation (7.22) indicates that the displacement capacity ( $\Delta_{80}$ ) due to the  $P$ - $\Delta$  effect is equal to 20% of the eccentricity ( $e$ ) of a column. The eccentricity of an applied load acting on a column can be easily calculated from the  $P$ - $M$  interaction curve, as shown in Figure 7.9(a).



(a) P-M Interaction Curve



(b) Maximum Displacement ( $\Delta_{80}$ )

**Figure 7.9 Effect of Axial Load on Displacement Capacity**

Figure 7.9(b) shows that the displacement capacity of specimen S24-2UT tested in this research. The nominal moment capacity ( $M_n$ ) is used in estimating the maximum moment capacity ( $M_{max}$ ) for sake of simplicity. The displacement capacity is greatly reduced with an increase in the axial load level. This observation implies that a large displacement capacity can be obtained easily when the axial load level is not high ( $P/P_o \leq 0.2$ ). However, obtaining a large drift capacity is more difficult for columns supporting high axial loads.

Figure 7.9(b) also illustrates that the displacement capacity becomes asymptotic to the vertical axis as the axial load approaches zero. As the loss of lateral load resistance due to the  $P\Delta$  effect will be negligible at low axial loads, and considering the simplifying assumptions made in the derivation of Equation (7.22), this phenomenon can be explained. It is important to note that a perfectly elasto-plastic moment-curvature relationship was used in the derivation of Equation (7.22). Since the actual moment-curvature relationship of a reinforced concrete column will not be an elastic-perfectly-plastic and since there will be finite curvature capacity at the sectional level, the displacement capacities calculated for very low axial loads through the use of Equation (7.22) are expected to be unrealistically large. This phenomenon is inherently tied to the assumptions made in the derivation of Equation (7.22). This issue will be handled by placing limits on Equation (7.22) in Section 7.3.3 where expressions are recommended for use in performance-based design.

### 7.3.2 Drift Capacity

Based on the maximum displacement capacity presented in Equation (7.22), the maximum drift capacity ( $\delta$ ) can be calculated.

$$\delta(\%) = \frac{\Delta_{80}}{L} \times 100 = 20 \times \frac{e}{L} \quad (7.23)$$

where  $L$  is the height of cantilever column.

Figure 7.10 shows the drift capacity of a typical concrete column with shear span-to-depth ratio ( $L/h$ ) of 5 supporting varying levels of axial loads. Equation (7.23) is used in estimating the drift capacities shown in this figure.

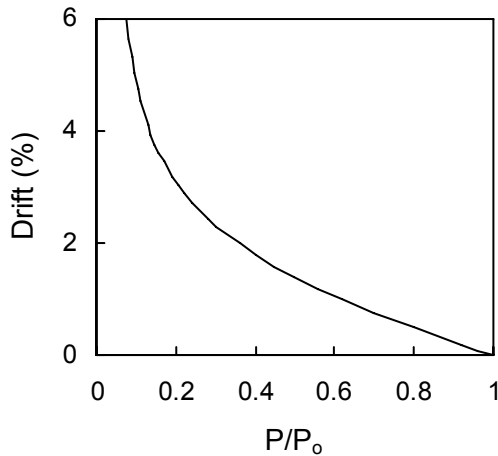


**Figure 7.10 Effect of Axial Load on Drift Capacity**

### 7.3.3 Displacement Ductility

As discussed in Chapter 5, the yield displacement can be calculated as follows.

$$\Delta_y = \frac{\phi_y L^2}{3} \quad (7.24)$$

Using Equations (7.22) and (7.24), the displacement ductility can be calculated as follows:

$$\mu_\Delta = \frac{\Delta_{80}}{\Delta_y} = \frac{0.2e}{\phi_y L^2 / 3} = \frac{0.6e}{\phi_y L^2} \quad (7.25)$$

As can be observed in Equations (7.22), (7.23) and (7.25), the height of a column ( $L$ ) influences the displacement capacity, drift capacity and the displacement ductility of a column differently. The displacement capacity ( $\Delta_{80}$ ) is not affected by the height of a column. However, the drift capacity ( $\delta$ ) and displacement ductility ( $\mu_\Delta$ ) are affected by the height of a column. The drift

capacity is inversely proportional to the height of a column ( $L$ ), while the displacement ductility inversely proportional to the square of the height of a column ( $L^2$ ). Therefore, it can be concluded that the displacement ductility is most sensitive to the height of a column among the three ductility parameters.

#### 7.3.4 Deformation Capacity of Columns

Simple closed-form equations that can be used to estimate the deformation capacity of reinforced concrete columns are presented in sections 7.3.1, 7.3.2 and 7.3.3. A series of simplifying assumptions were made in deriving Equations (7.22), (7.23) and (7.25). The sectional behavior of a column was simplified to be bi-linear as such the lateral load capacity degradation was solely related to the  $P$ - $\Delta$  effect.

Because of these simplifying assumptions the deformation capacity estimations provided by Equations (7.22), (7.23) and (7.25) tend to be unrealistically large for low axial load levels. In order to address this problem, the estimated drift capacities are capped at 4%. An analysis of Figure 7.10 indicates that, this drift capacity level corresponds to an axial load level of about  $0.15P_o$  for columns with shear span-to-depth ratio of 5. This upper limit placed on the estimated drift capacities implies that an actual drift capacity need not be calculated precisely for all practical purposes when the drift capacity is on the order of 4%. In short, a drift capacity of 4% is considered to be large enough for use in performance-based design of reinforced concrete columns. Based on this upper limit, Equations (7.26) to (7.28) are proposed for use in estimating the deformation capacity of reinforced concrete columns:

$$\delta(\%) = 20 \times \frac{e}{L} \leq 4\% \quad (7.26)$$

$$\Delta_{80} = 0.2 \times e \quad (7.27)$$

$$\mu_{\Delta} = \frac{0.6e}{\phi_y L^2} \quad (7.28)$$

where  $e = \frac{M_n}{P} \leq 0.2 \times L$

It is important to note that the eccentricity ( $e = M_n/P$ ) is calculated from axial load-bending moment interaction diagrams plotted by using the ACI 318-05 provisions for stress block factors in the proposed equations. Combining the use of the upper limit placed on eccentricity and the use of nominal moment capacity and sufficient confining reinforcement, the deformation capacity estimations obtained by using Equations (7.26) - (7.28) will be safe, lower-bound estimations of deformation capacities that can be expected for all levels of axial load. Application of Equation (7.26) to estimate the drift capacity in column design is illustrated in Appendix E.

### 7.3.5 Drift Capacity Estimation: Simplified and Sophisticated Analyses

In the preceding sections, two methods of analysis were presented. The first procedure made use of various constitutive models and numerical procedures. In the model verification stage, the first method was found to provide reasonable estimations for the deformation capacity of column in most cases. However, it was also noted that in some instances the magnitudes of the errors seen in the estimated lateral deformation capacities were approximately 50%. The second procedure involved the application of equilibrium equations on a cantilever column. In order to obtain a series of simple closed-form expressions that can be used to estimate the deformation capacity of reinforced concrete columns a series of simplifying assumptions were made. In this section the deformation capacity estimations obtained by using the sophisticated and simple methods described above are compared.

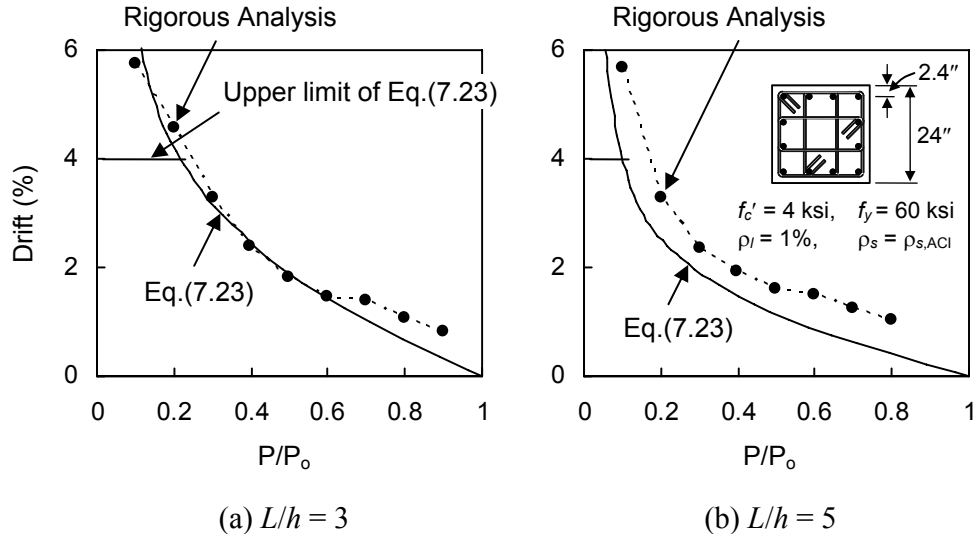


**Figure 7.11 Comparison of Estimated Drift Capacities**

For the purposes of comparison a reinforced concrete column with a 24×24-in.<sup>2</sup> square section and a longitudinal reinforcement ratio of 1.0% is used (Figure 7.11). Two different column heights (72 in. and 120 in.) resulting in shear span-to-depth ratios of 3 and 5 are used. The confining reinforcement is provided in accordance with the requirements of Chapter 21 of the ACI 318-05 code.

The results shown in Figure 7.11 illustrate that the drift capacities estimated by Equation (7.26) are close to the drift capacities obtained from a more rigorous analysis where numerous material nonlinearities are considered. It is interesting to note the use of simplified expressions yield lower drift capacities than those obtained from the rigorous analysis. The differences between the drift capacity estimations obtained through the use of these methods increase with increasing shear span-to-depth ratios.

The conservative estimations obtained by using Equation (7.26) can be attributed to the following: (1) the use of the maximum lateral load ( $V_{max}$ ) instead

of the lateral load capacity ( $V'_{max}$ ) of the lateral load-displacement relationship in the derivation of the equations (Figure 7.8) and (2) the use of ACI 318-05 provisions for stress block factors in constructing the bi-linear moment-curvature relationships.

### 7.3.6 Comparison with Column Test Database

To investigate the validity of Equation (7.26), results from 135 tests conducted on reinforced concrete columns are used. The drift capacities obtained through the use of Equation (7.26) are compared with the experimental drift capacities. These tests include the 105 tests previously used in the model verification stage. The additional data from thirty column tests include the columns tested by Ohno and Nishioka (1984) and Thomsen and Wallace (1994). Since some of the sectional properties of these additional tests were not included in the original references, these tests could not be used to verify the accuracy of the rigorous analytical procedure in Section 7.2.6.

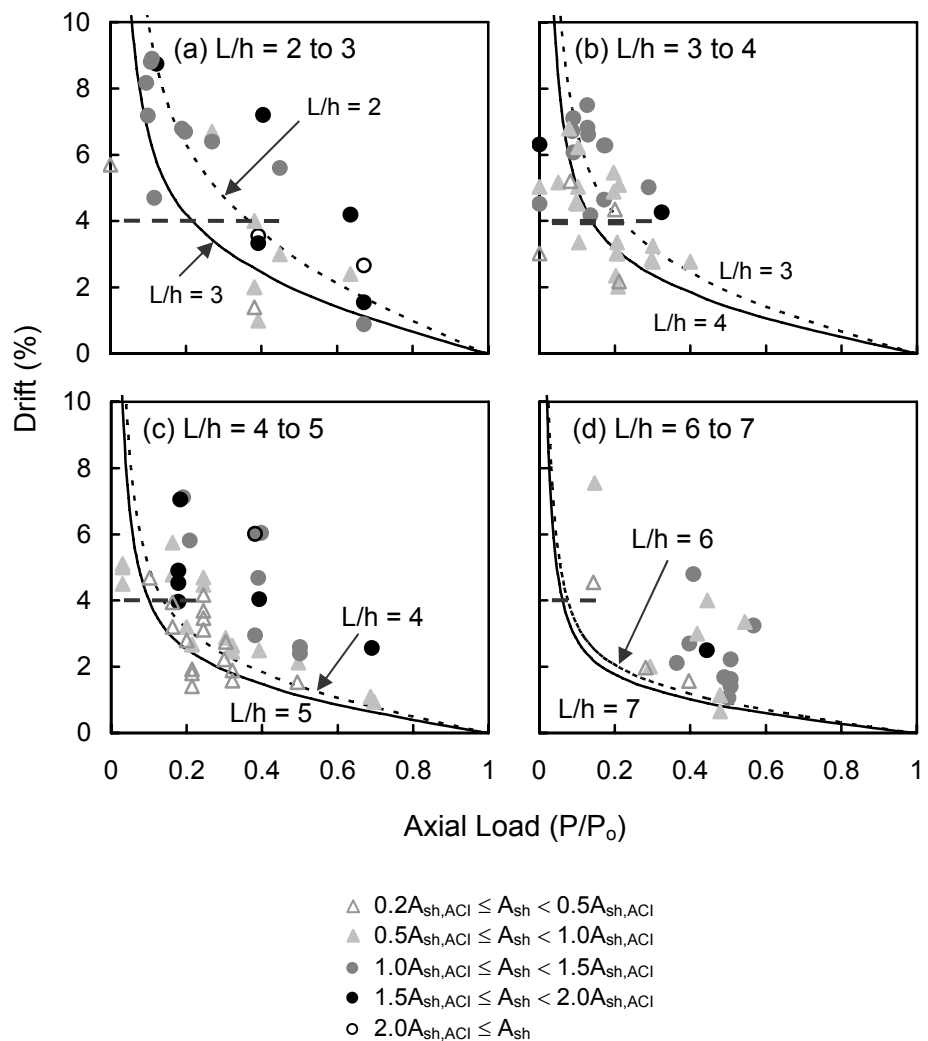
The results are shown in Figure 7.12. This figure illustrates that there is a strong correlation between the lower-bound of experimentally-obtained drift capacities and the drift capacities estimated by using the proposed method. The proposed method provides safe estimations for drift capacity in most cases. As can be seen in Figure 7.12, some test data fall short of the drift capacities estimated by using Equation (7.26). However, most of those data are from columns that do not meet the seismic design and detailing provisions (Chapter 21) of the ACI code.

In order to study the conservativeness of the drift capacity estimations and to evaluate the performance of columns that satisfy Chapter 21 provisions of ACI 318-05, test data are categorized into two groups: (1) columns that meet or exceed the confinement reinforcement provisions of Chapter 21, and (2) columns that

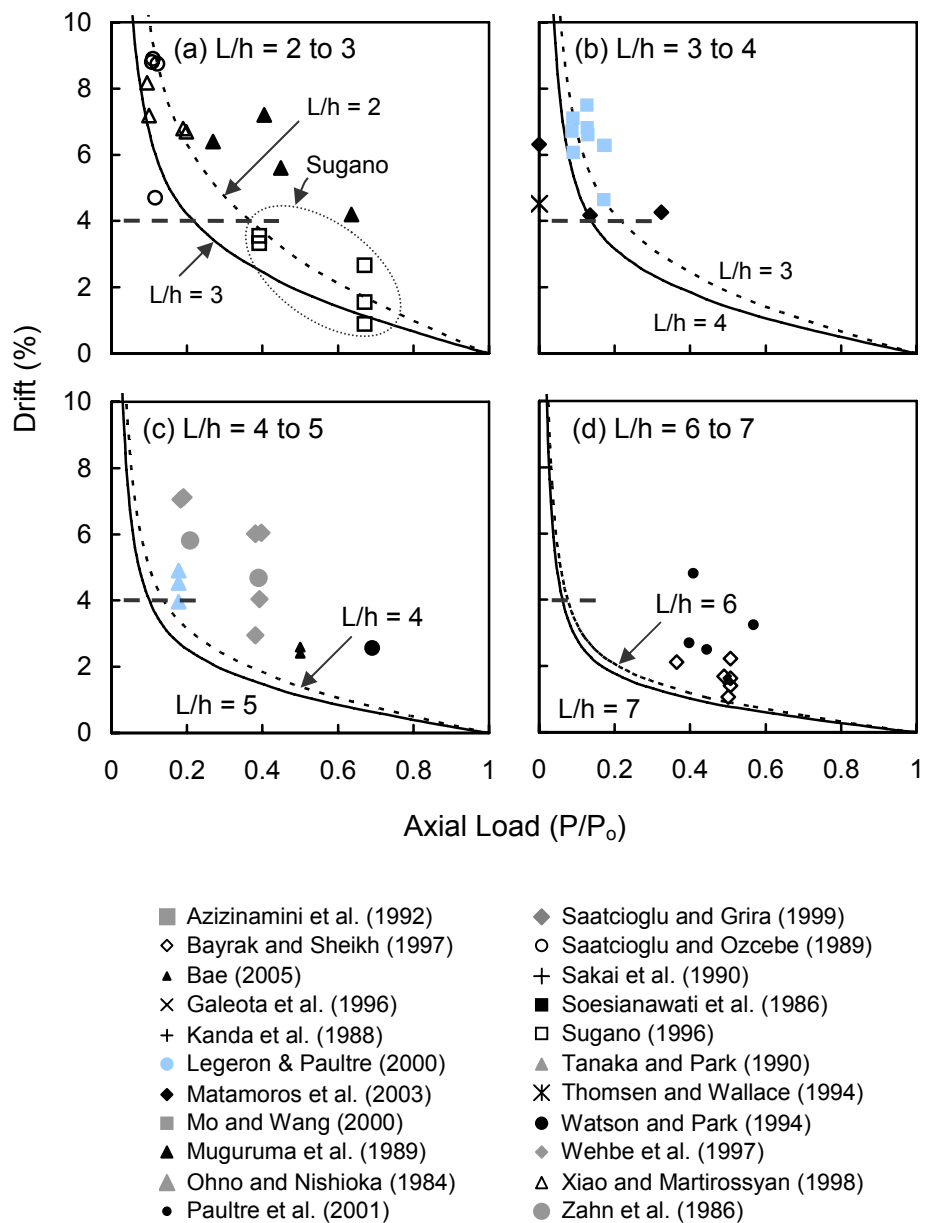
contain less confining reinforcement than that required by the seismic design provisions of ACI 318-05. The results for columns which satisfy the ACI code requirements are shown in Figure 7.13. The results presented in Figure 7.13 indicate that Equation (7.26) traces the lower bound of the data consistently for all data, except for a few columns tested by Sugano (1996). The drift capacities of some of the column specimens tested by Sugano (1996) are overestimated by the proposed method. The columns tested by Sugano (1996) were made from very high-strength concrete ( $f'_c = 17$  ksi) and had a small shear span-to-depth ratio ( $L/h = 2$ ). Columns with such small shear span-to-depth ratios can be affected by a shear failure mechanism. A shear failure can limit drift capacity of a column due to its brittle nature. In addition to the small shear span-to-depth ratio, the brittleness of very high-strength concrete used may also be a contributing factor to the limited drift capacity. In short, the proposed method (Equation (7.26)) results in safe estimations of drift capacity for all columns that satisfy Chapter 21 provisions of ACI 318-05, except some of the columns tested by Sugano (1996). It is also important to note that upper lateral drift limit of 4% provided a safe lower-bound estimation for columns tested under low axial load levels.

Figure 7.14 illustrates the drift capacity estimations for columns that contain less lateral reinforcement than that required by the Chapter 21 provisions of ACI 318-05 code. Once again, Equation (7.26) provides a reasonable lower-bound to the experimental drift capacities in most cases. However, the percentage of over-estimated drift capacities is considerably higher for this group of columns. More specifically, the proposed method could not provide conservative drift estimations for most columns tested by Sakai (1990) and Thomsen and Wallace (1994), and some of the columns tested by Galeota et al. (1996). As can be seen in Table 7.1, these specimens are all high-strength concrete columns ( $f'_c = 10$  to 15 ksi). For the specimens tested by Galeota ( $L/h = 4.6$ ), Equation (7.26) provides

safe estimations for the drift capacities for all of the columns that contain more than 30% of the lateral reinforcement required by the Chapter 21 provisions of ACI 318-05 code. The drift capacities of most of the columns tested by Sakai ( $L/h = 2$ ) and Thomsen and Wallace ( $L/h = 3.9$ ) are overestimated. Such lightly-confined concrete columns with small or moderate shear span-to-depth ( $L/h$ ) ratios are vulnerable to experience large shear deformations and hence fail prematurely.



**Figure 7.12 Comparison with Test Results**



**Figure 7.13 Comparison with Test Results ( $A_{sh} \geq A_{sh,ACI}$ )**

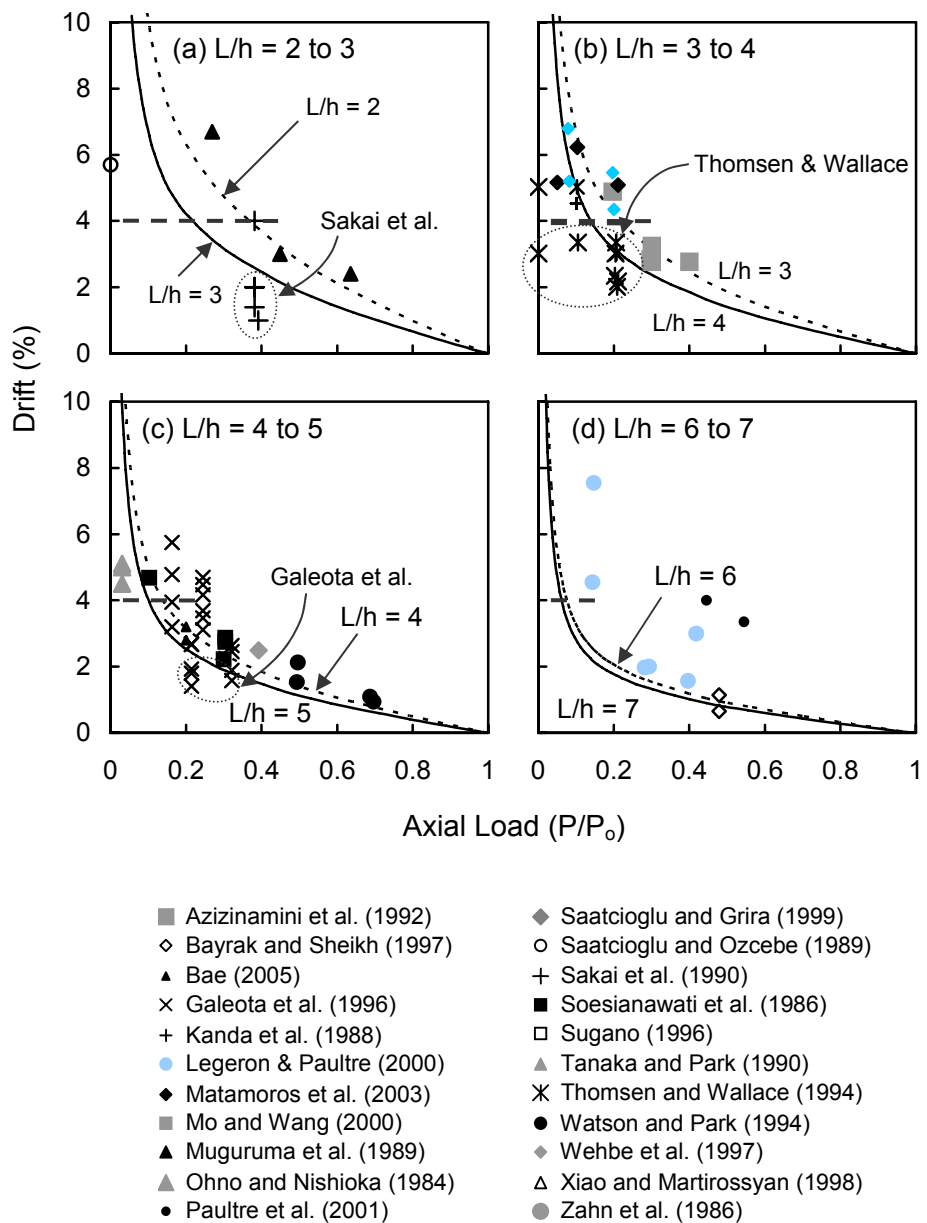


**Figure 7.14 Comparison with Test Results ( $A_{sh} < A_{sh,ACI}$ )**

### 7.3.7 Design Recommendations

It was previously discussed that the  $P\Delta$  effects influence the deformation capacity of concrete columns. The  $P\Delta$  effects are more pronounced for high axial loads and large shear span-to-depth ratios. Therefore, to ensure ductile behavior of concrete columns, it is important to control the  $P\Delta$  effect by limiting axial load levels for given shear span-to-depth ratios.

It was also discussed that a simple expression ( $\delta = 20 \times e/L \leq 4\%$ ) can provide conservative estimations of drift capacity for concrete columns that are designed in accordance with the Chapter 21 requirements of ACI 318 code. Using this simple expression, the drift capacity of columns is obtained for various shear span-to-depth ratios (Figure 7.15). A drift capacity of 2.5% is also shown in the figure. The seismic detailing and design provisions of most of the current design codes are aimed at achieving a story drift ratio of 2.0 to 2.5% for moment-resisting reinforced concrete frames (UBC 1997; IBC 2003).

Figure 7.15 illustrates that for a given target drift capacity (e.g., 2.5%), the permissible axial load limit decreases as the shear span-to-depth ratio of a column increases. The allowable axial load levels to ensure a drift capacity of 2.5% are summarized in Table 7.2. Therefore, it can be concluded that to ensure stable lateral deformation capacity of concrete columns, it is important to satisfy not only the requirements of the Chapter 21 provisions of ACI 318, but also the shear span-to-depth ratios presented in Table 7.2. It is also important to note that in order to achieve large drift capacities, the use of relatively smaller shear span-to-depth ratios and lower axial load levels are recommended. However, as large shear forces are developed at very small shear span-to-depth ratios, the column shear strength has to be checked for very small shear span-to-depth ratios.

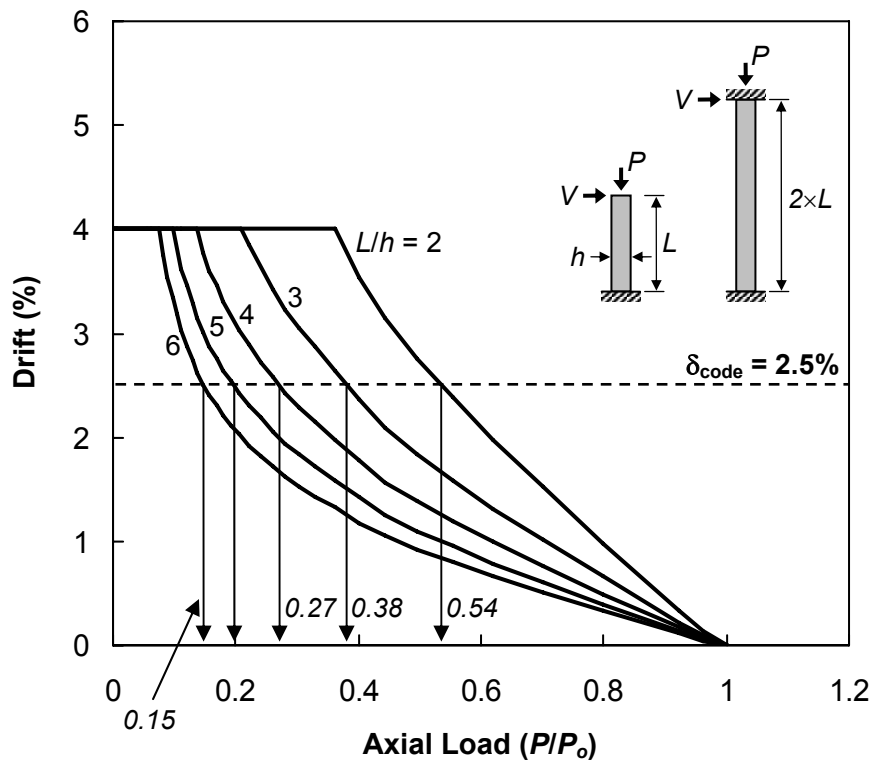


**Figure 7.15 Interaction among Drift Capacity, Axial Load and Shear Span-to-Depth Ratio**

**Table 7.2 Recommended Axial Load Levels for Various Shear Span-to-Depth Ratios**

Shear span-to-depth ratio ( $L/h$ )	Permissible axial load level ( $P/P_o$ )	Building columns	Bridge piers
2 – 3	0.4		
3 – 4	0.3		
4 – 5	0.2		
5 – 6	0.15		

Shear span-to-depth ratios of most building columns in high seismic areas range between 2 and 4 (or the story height-to-column depth ratio of 4 to 8). Table 7.2 indicates that sufficient deformation capacity (drift capacity of at least 2.5%) will be guaranteed when reinforced concrete columns are designed in accordance with the Chapter 21 provisions of ACI 318-05.

#### 7.4 SUMMARY

Two methods that can be used to estimate the lateral deformation capacity of a reinforced concrete column are presented in this chapter. One approach may be considered as a state-of-the-art analytical method, which includes the new plastic hinge length expression (Chapter 5) and the new bar buckling model (Chapter 6) developed in this research. This rigorous analysis procedure provides reasonably good drift capacity estimations for most cases. However, in some cases the magnitude of the over- and under-estimations can approach 50%. Recognizing the fact that in the analyses conducted state-of-the art phenomenological models are used, it can be concluded that the accuracy of drift capacity estimations appear to be questionable for use in design. Considering the complexity of this analytical method and the inaccuracy of estimated drift capacities seen in some cases, it is not possible to recommend the use of such methods in seismic design.

As an alternative, a simple expression ( $\delta = 20 \times e/L \leq 4\%$ ) that can be used to estimate the drift capacity of a reinforced concrete column is derived. It is shown that for columns which are designed in accordance with the ACI 318 code provisions for seismic design, a conservative estimation for the lateral drift capacity can be obtained by using the simple expression. For columns that do not comply with the ACI code, this simple expression may not provide a conservative

drift capacity estimation if high-strength concrete is used, insufficient confining reinforcement is provided in combination with small shear span-to-depth ratios.

Based on the simple expression, design recommendations are also provided to limit the levels of axial load for various shear span-to-depth ratios. It is important to recognize that this study has primarily focused on the concrete columns whose behavior is governed by flexure. Since shear failure is not considered in the analysis methods employed to estimate the deformation capacity, shear strength of columns with very small shear span-to-depth ratios has to be checked and considered explicitly in design.

# **CHAPTER 8**

## **SUMMARY, CONCLUSIONS, AND RECOMMENDATIONS**

### **8.1 SUMMARY**

The primary objective of this study was to investigate the relationship among different deformation capacity parameters and to propose a method that can be used to estimate the deformation capacity of a concrete column. For this purpose, five full-scale concrete columns were tested and their behavior was examined. The main test variables were the shear span-to-depth ratio, axial load level, and the amount of transverse confining reinforcement.

The effects of shear span-to-depth ratio and axial load on the lateral load behavior of concrete columns and on the relationship among different ductility parameters were discussed in light of the experimental results. It was also observed that the axial load affected the plastic hinge length of concrete columns.

The plastic hinge length and buckling of reinforcing bars were investigated in depth and analytical models were developed. Incorporating the proposed plastic hinge length expression and bar buckling model, a state-of-the art analytical method was presented and its accuracy was evaluated using a large number of concrete column test data. Finally, a simple closed-form equation that can be used to predict the drift capacity of reinforced concrete columns was derived.

## 8.2 CONCLUSIONS

Based on the experimental and analytical research into the behavior of reinforced concrete columns, the following conclusions can be drawn:

1. Effect of shear span-to-depth ratio:
  - a. The member performance of columns tested in this study was affected by the shear span-to-depth ratio ( $L/h$ ).
  - b. Specimens S24-2UT and S17-3UT had shear span-to-depth ratios of 5 and 7, respectively. They were tested under the same level of axial loads ( $P = 0.5P_o$ ). The sectional performances of these specimens were similar, resulting in similar curvature ductilities. However, the member performance of S24-2UT was better than that of S17-3UT.
  - c. The effect of shear span-to-depth ratio on the member behavior of columns is related to the  $P-\Delta$  effect. The  $P-\Delta$  effect becomes significant as the axial load or the shear span-to-depth ratio of columns increases. Larger  $P-\Delta$  effects will result in poor member performance even though the sectional performance may be acceptable.
2. Effect of axial load:
  - a. Concrete columns with similar levels of curvature ductility capacities can produce different levels of displacement ductility or drift capacities depending on the level of axial load.
  - b. Specimens S24-2UT, S24-4UT and S24-5UT had different amounts of confining reinforcement, but had the same shear span-to-depth ratio ( $L/h = 5$ ). Specimen S24-2UT was tested under  $P = 0.5P_o$ , while specimens S24-4UT and S24-5UT were tested under  $P = 0.2P_o$ . It was observed that the member performance of S24-2UT was similar or better than specimens S24-4UT and S24-5UT, despite the poor sectional performance of specimen S24-2UT. The estimated plastic

hinge length of specimen S24-2UT was larger than those of specimens S24-4UT and S24-5UT. This effect of axial load on plastic hinge length may be the key parameter to determine the displacement ductility or drift capacity from a given curvature ductility.

3. Amount of confining reinforcement:

- a. Most design codes and performance-based procedures take into account the axial load level to determine the required amount of confining reinforcement, except the ACI 318-05 code. However, none of design codes or procedures considers that the shear span-to-depth ratio is an important parameter. This is partly due to the fact that having a consistent sectional performance is the primary objective for many codes and procedures, and the sectional performance is not affected by the shear span-to-depth ratio.
- b. Since the shear span-to-depth ratio is an important parameter influencing member performance, it has to be considered in design in order to guarantee satisfactory behavior of columns at both sectional and member levels.
- c. The amount of confining reinforcement of specimen S24-5UT was 74% of the Chapter 21 requirements of the ACI 318-05 code. The behavior of specimen S24-5UT was satisfactory at both sectional and member levels. The behavior of specimen S24-5UT was better than that of specimen S24-2UT, which contained confining reinforcement that was 9% more than the code required amount. Therefore, it can be concluded that ACI 318-05 code requirements for confining reinforcement may be too strict for this level of axial load ( $P = 0.2P_o$ ) and shear span-to-depth ratio ( $L/h = 5$ ).

4. Plastic hinge length:
  - a. Observations on the damaged columns and the trends between sectional behavior and member behavior suggest that the plastic hinge length was affected by the level of axial load.
  - b. Examination of several existing expressions that can be used to estimate the plastic hinge length showed that the effects of axial loads were not considered in estimating the plastic hinge length. An analytical approach that can be used to estimate the plastic hinge length was developed. Experimental evidence showed that plastic hinge lengths were affected by the level of axial load, shear span-to-depth ratio and amount of longitudinal reinforcement. Based on this finding, a new expression for use in estimating the length of plastic hinges was proposed.
5. Buckling of longitudinal reinforcement:
  - a. Buckling of longitudinal reinforcement was observed in all specimens. Based on the experimental results of Bayrak and Sheikh (2001) and Mieses (2002), a simple analytical bar buckling model was proposed. The effect of the inclusion of bar buckling in sectional analysis was also discussed. It can be concluded that the buckling of reinforcing bars has to be considered in analysis in order to obtain accurate predictions of column response, especially when the axial load levels are high and large amounts of longitudinal reinforcement are provided.
6. Prediction of ductility parameters of concrete columns:
  - a. Results from over one hundred tests were used to check the accuracy and conservativeness of a rigorous analytical method in predicting the deformation capacity of reinforced concrete columns. The comparison of predicted and experimentally-obtained drift capacities showed that

the overall performance of the analytical method was satisfactory for most cases. In some cases, the magnitude of the over- and under-estimations of drift capacity reached 50%.

- b. A simple closed-form expression that can be used in estimating the drift capacity of reinforced concrete columns was presented. Through the use of this simple expression, the drift capacity of all columns satisfying Chapter 21 provisions of ACI 318-05 code, except for a few very high-strength concrete columns with very small shear span-to-depth ratios, were estimated in a conservative manner. As such, this expression is recommended for use in performance-based earthquake engineering.

### **8.3 RECOMMENDATIONS FOR FUTURE STUDY**

The following are recommended as future research areas:

1. Number of tests on full-scale concrete columns is very limited. In this research, only five column tests were conducted. More tests are needed to examine the effects of shear span-to-depth ratio, axial loads, and amount of confining reinforcement.
2. For all columns discussed here, shear failure was not considered. In other words, the columns were slender and shear failure was not critical. The behavior of shear critical columns should be investigated to better understand the column behavior.
3. After longitudinal reinforcement buckle in compression, they start to rupture at strains less than the ultimate strain when the applied moments are reversed. This is commonly called low-cycle fatigue failure of reinforcing bars. Even though this has been studied by several researchers (Corley et al. 1978, Dutta and Mander 1998, and Brown and Kunnath

2000), the low-cycle fatigue failure of reinforcing bars is not fully understood. As the strain history of reinforcing bars is one of the important factors in the low-cycle fatigue failure, tests on carefully planned strain history of reinforcing bars are needed.

## **APPENDIX A**

# **TEST FRAME**

### **A.1 DESIGN CONSIDERATIONS**

A full-scale column tester was designed and constructed at the University of Texas at Austin for this research. The test frame is capable of applying and maintaining axial loads up to 2,000 kips and the reversed cyclic moments as large as 4,000 ft-kips.

Eight high-strength dywidag bars are post-tensioned by 50 kips per rod for integrity of test frame. During testing, the test setup is loaded by the axial force in combination with the reversed cyclic loadings. Therefore, the capacity of test frame has to be checked for two different stages: (1) prior to testing phase, which internal forces are from the post-tensioning of eight high-strength dywidag bars and (2) testing phase, which internal forces are the sum of internal forces from post-stressing and internal forces from axial loads and reversed cyclic moments that are generated by the hydraulic rams.

Figure A.1 illustrates the detailed dimensions of column test frame. Figures A.2 though A.11 include the shop drawings for column test frame.

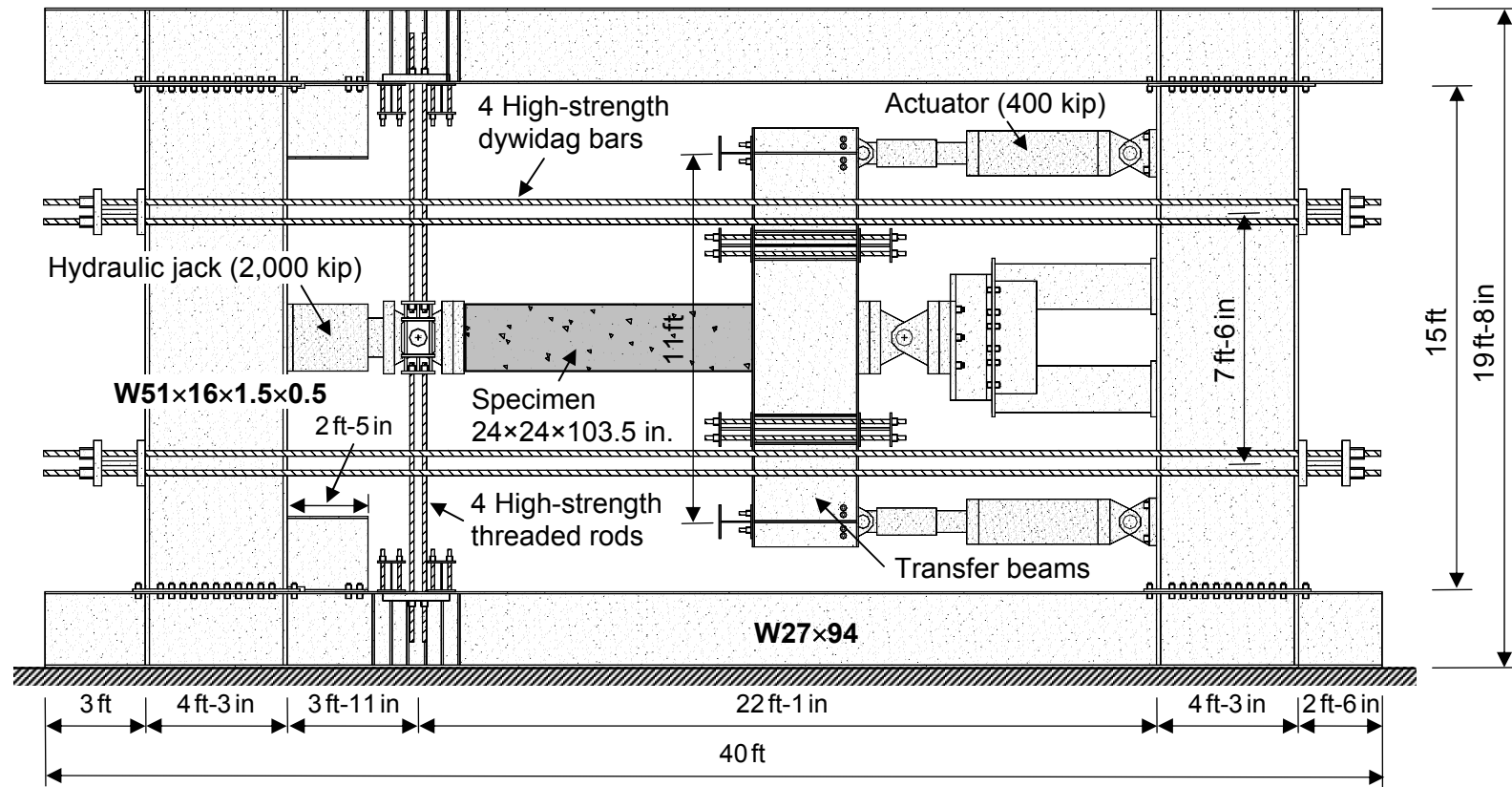
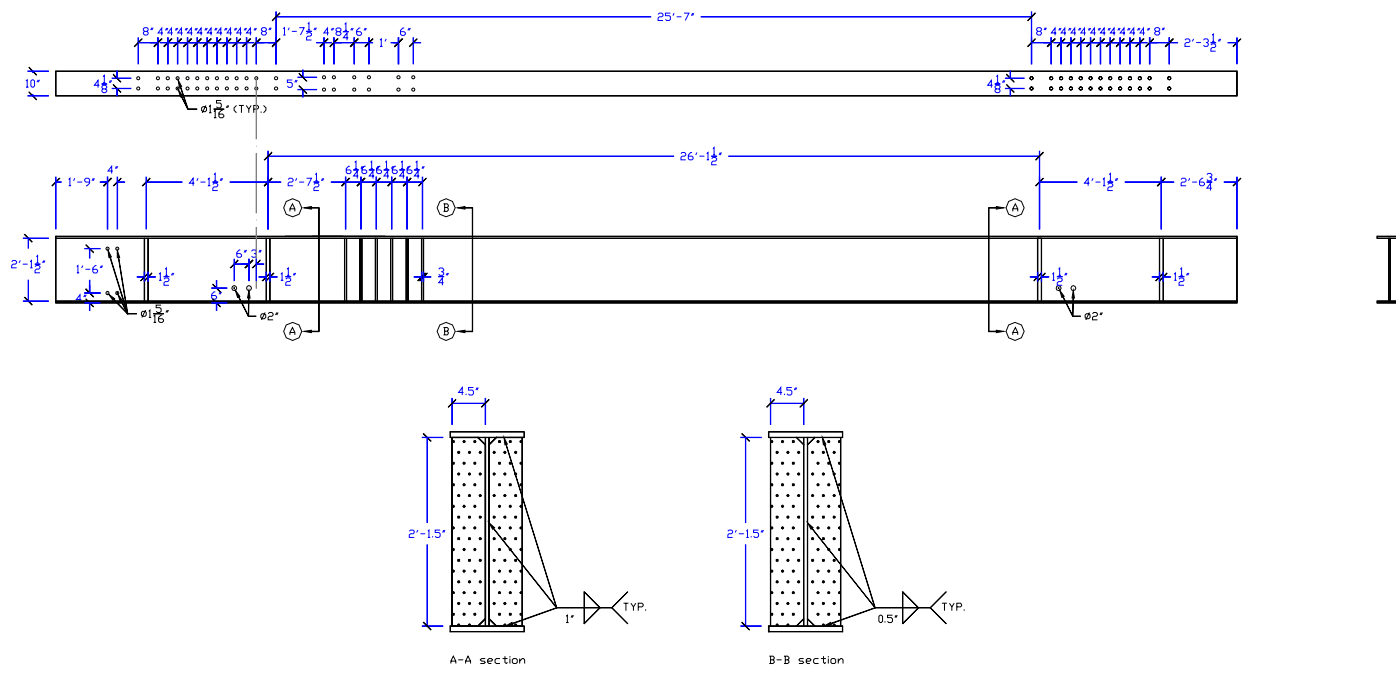


Figure A.1 Details and Dimensions of Test Setup



*Figure A.2 Detail of W27x94 Beam*

233

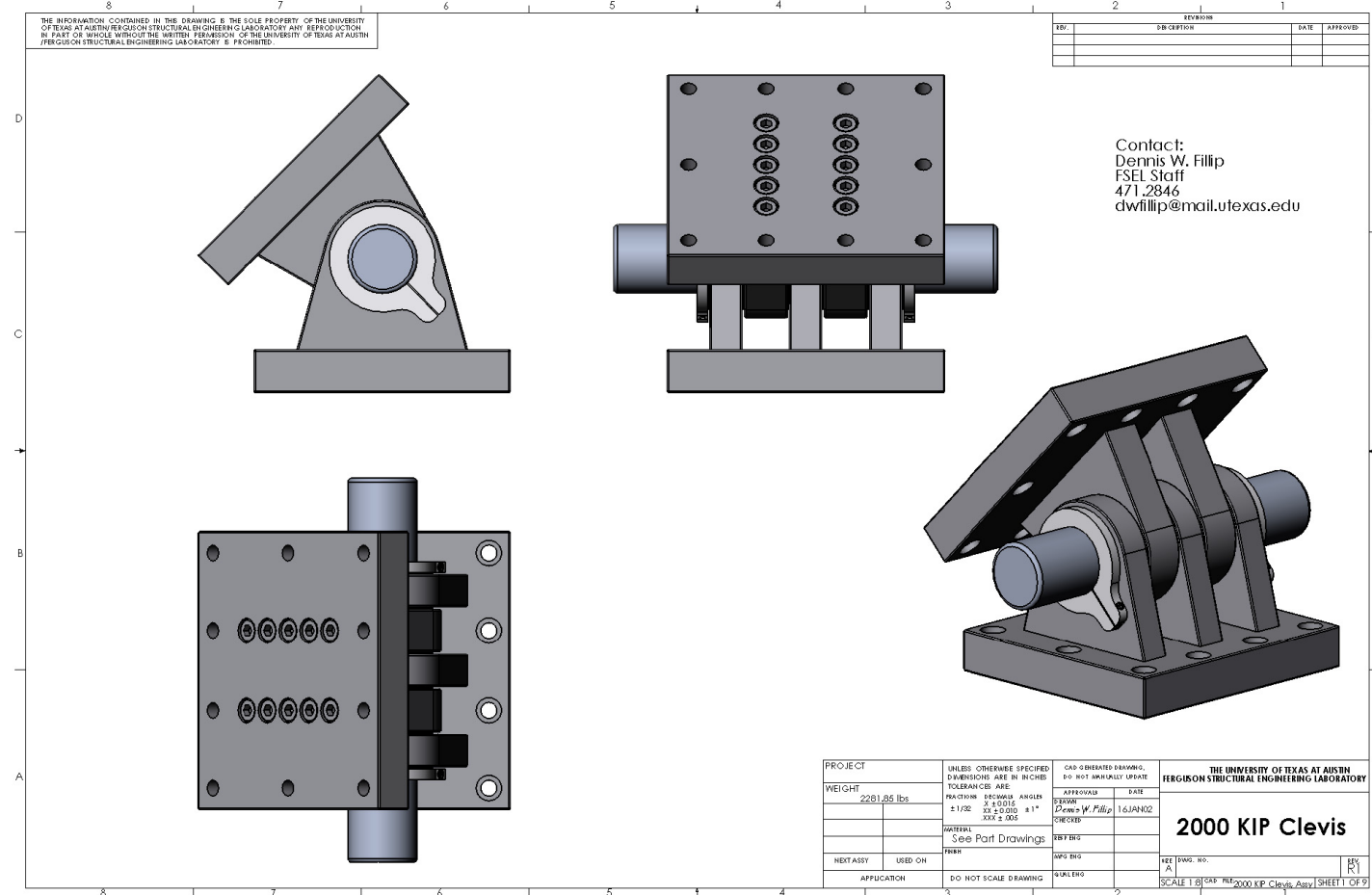
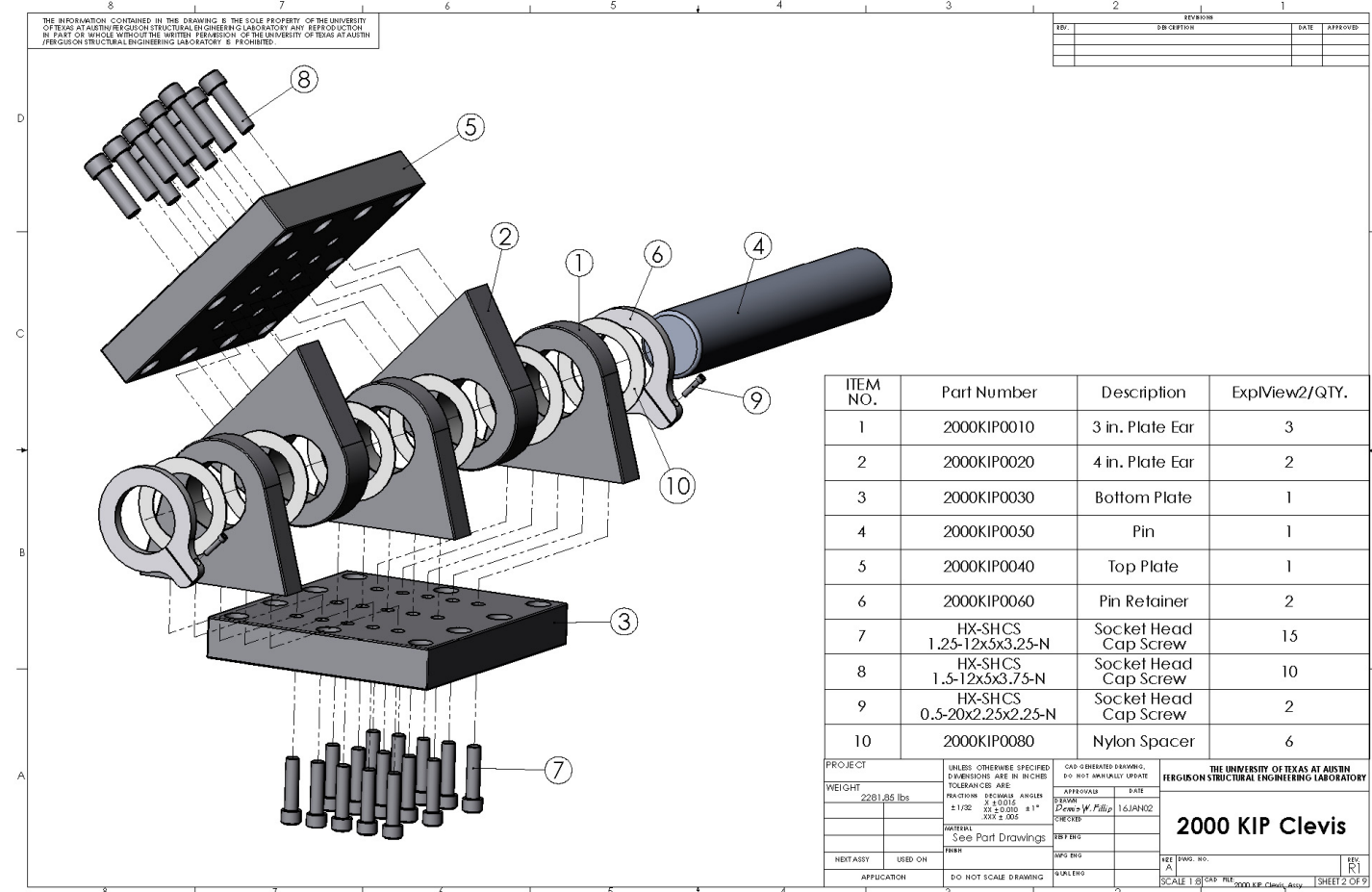
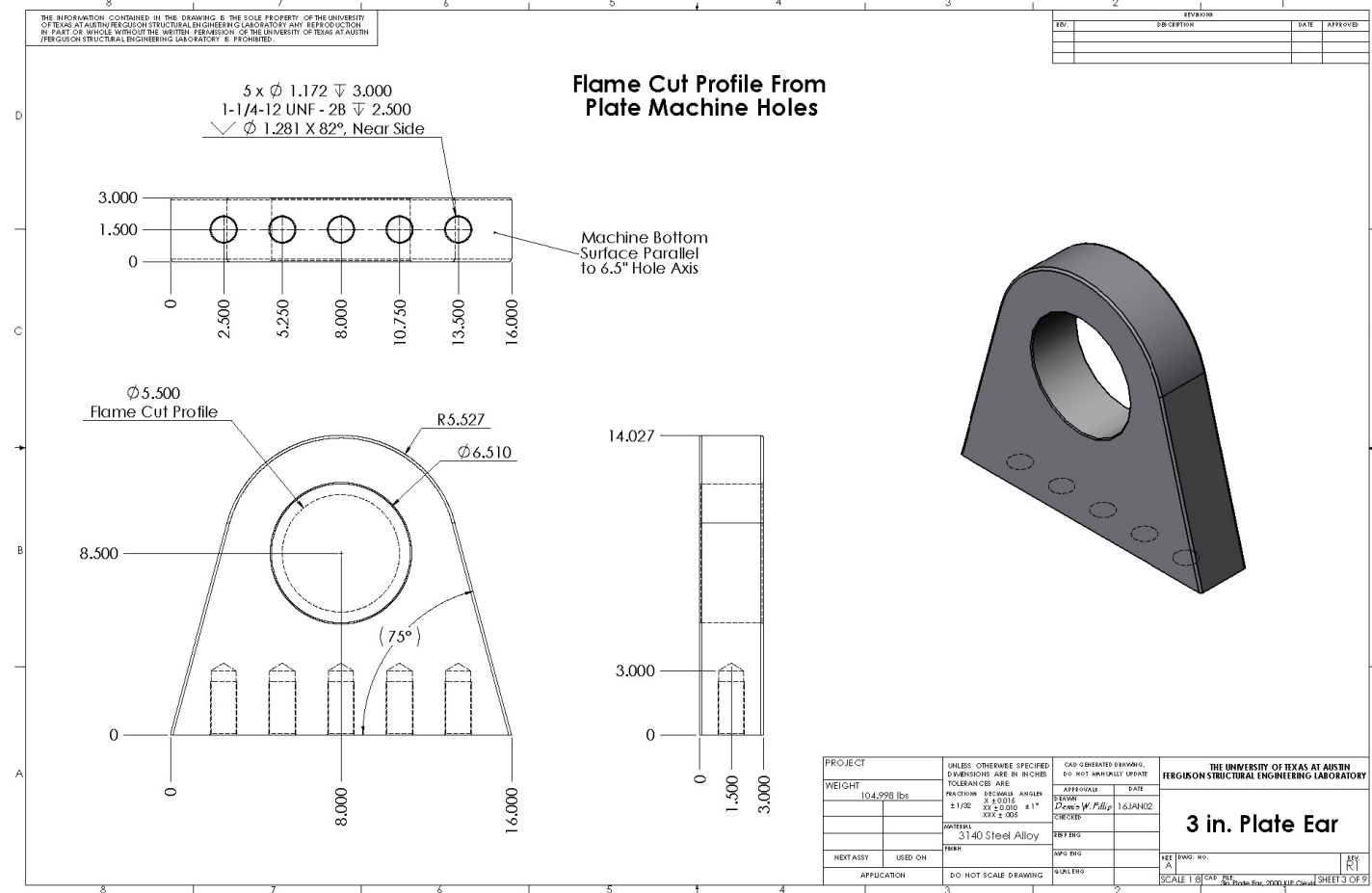


Figure A.3 Details of Clevis



*Figure A.4 Details of Clevis*

235



*Figure A.5 Details of 3 in. Plate Ear*

236

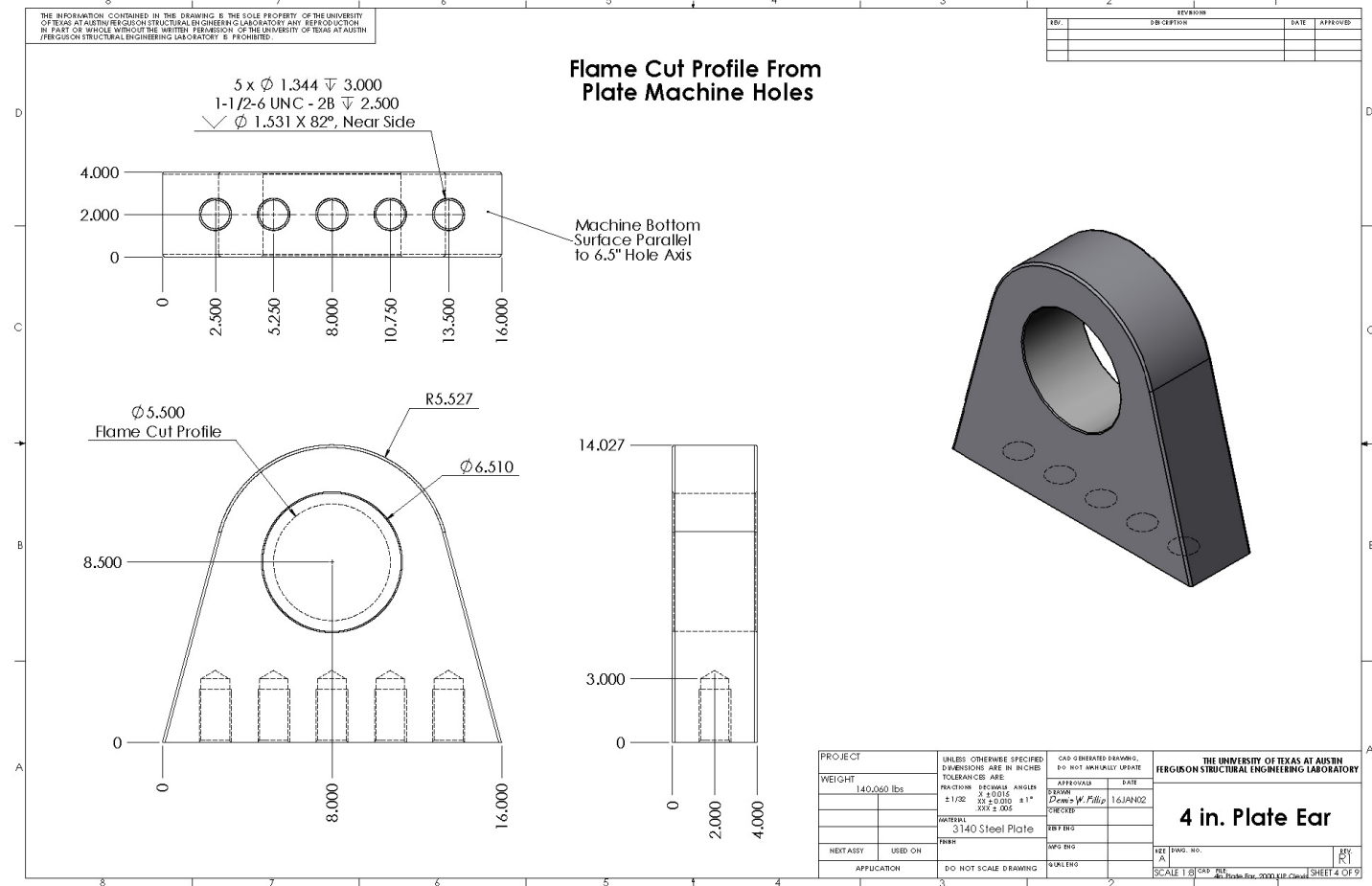
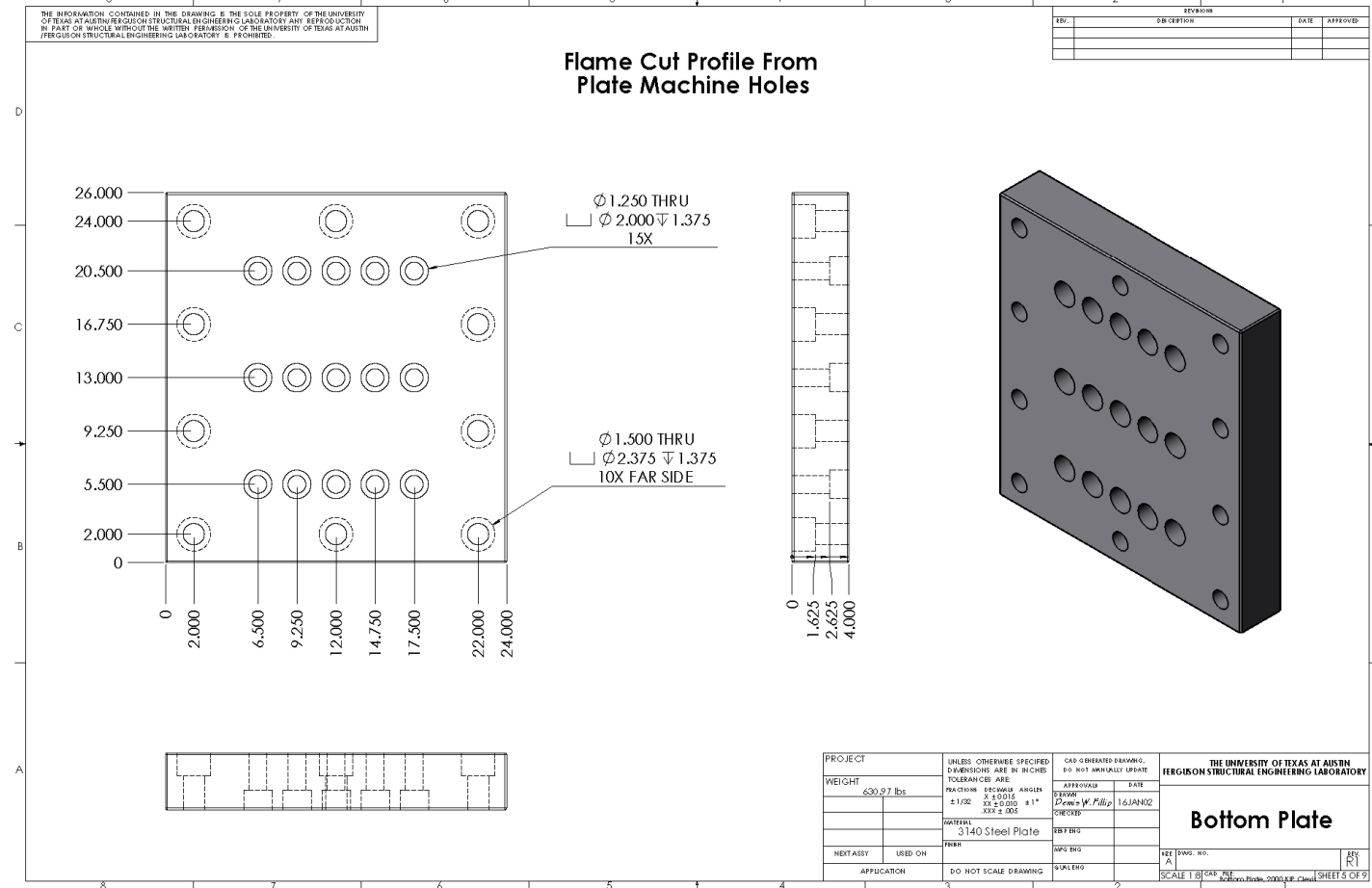


Figure A.6 Details of 4 in. Plate Ear



**Figure A.7 Details of Bottom Plate**

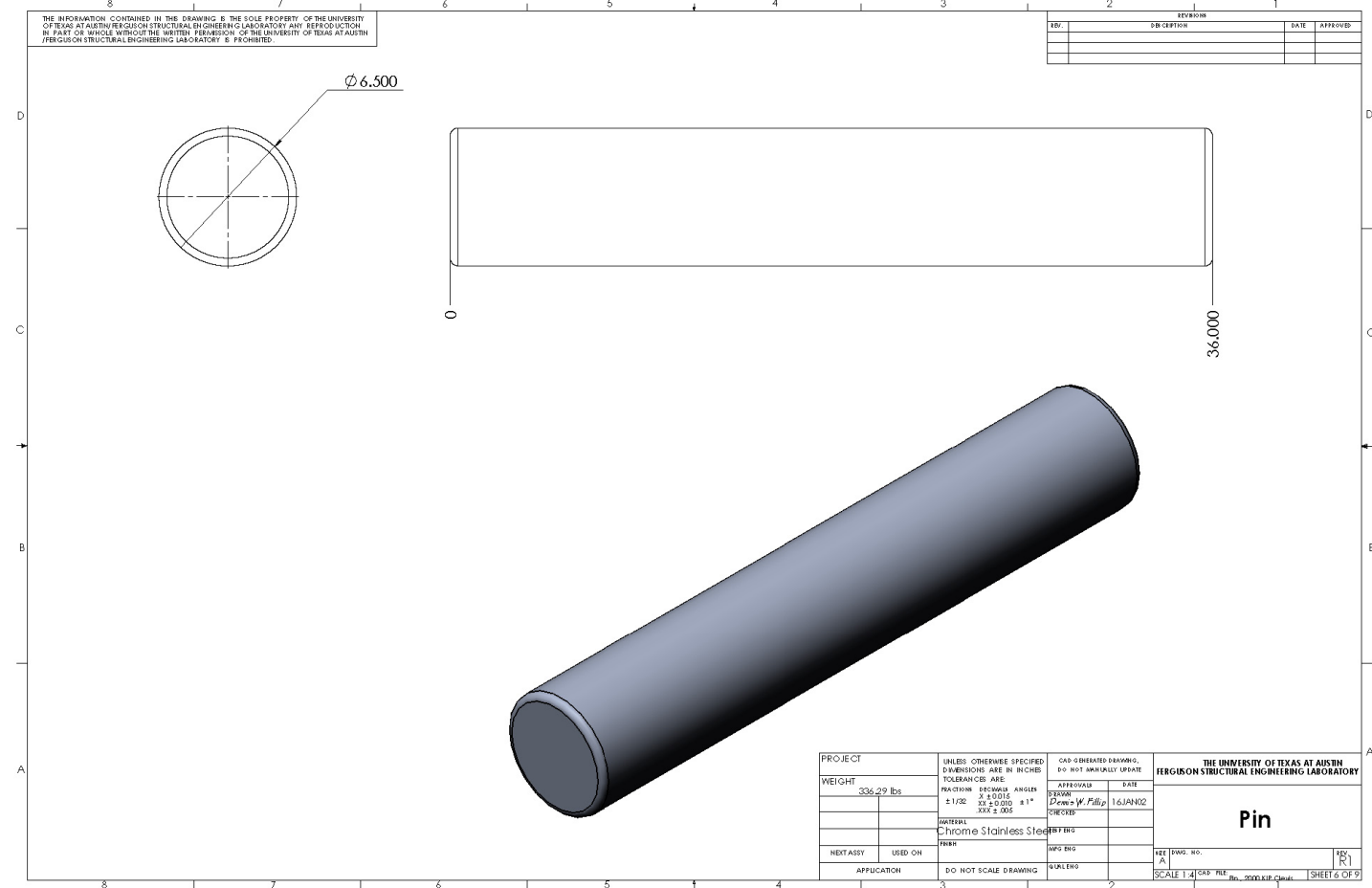


Figure A.8 Details of Pin

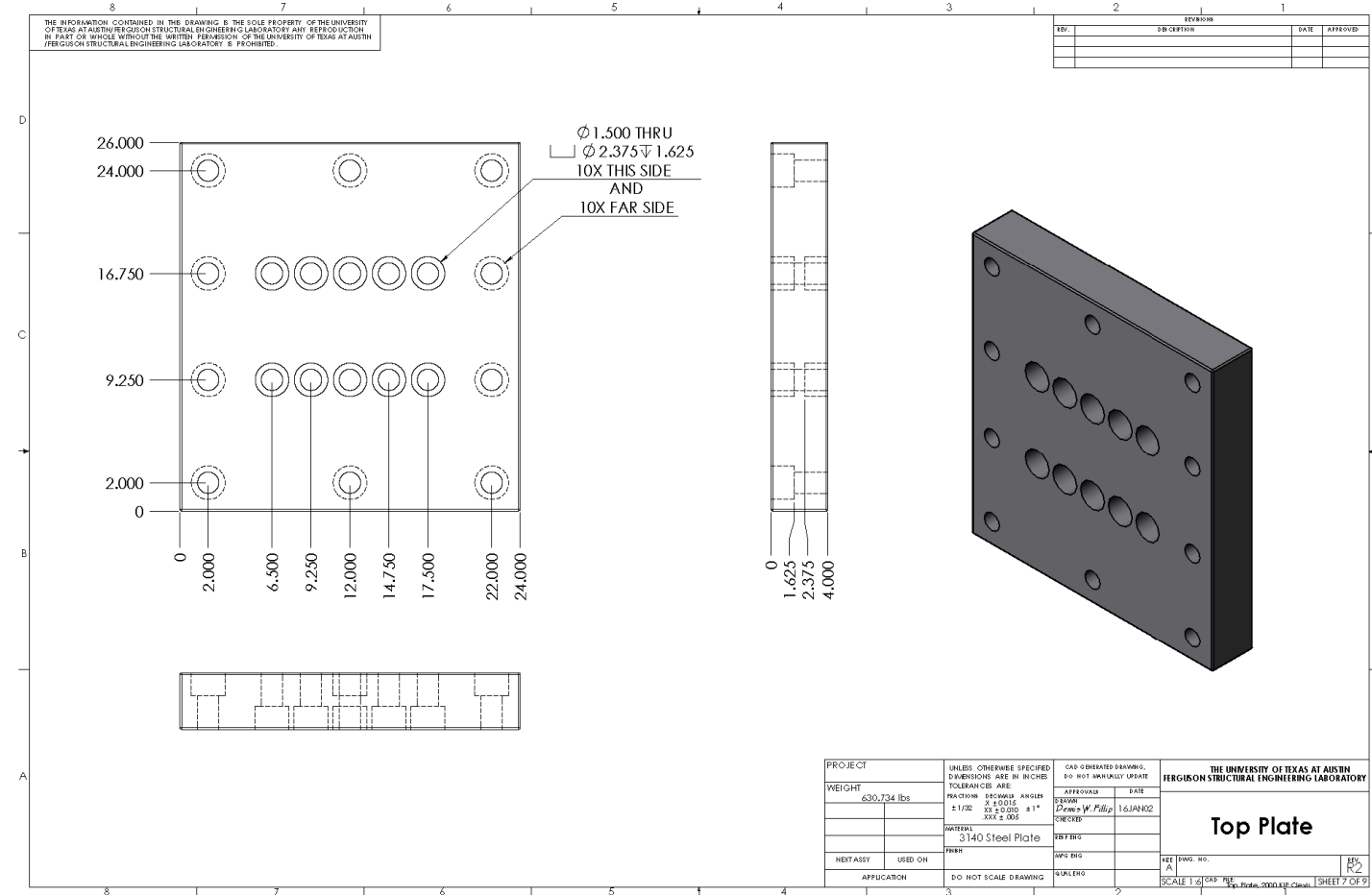


Figure A.9 Details of Top Plate

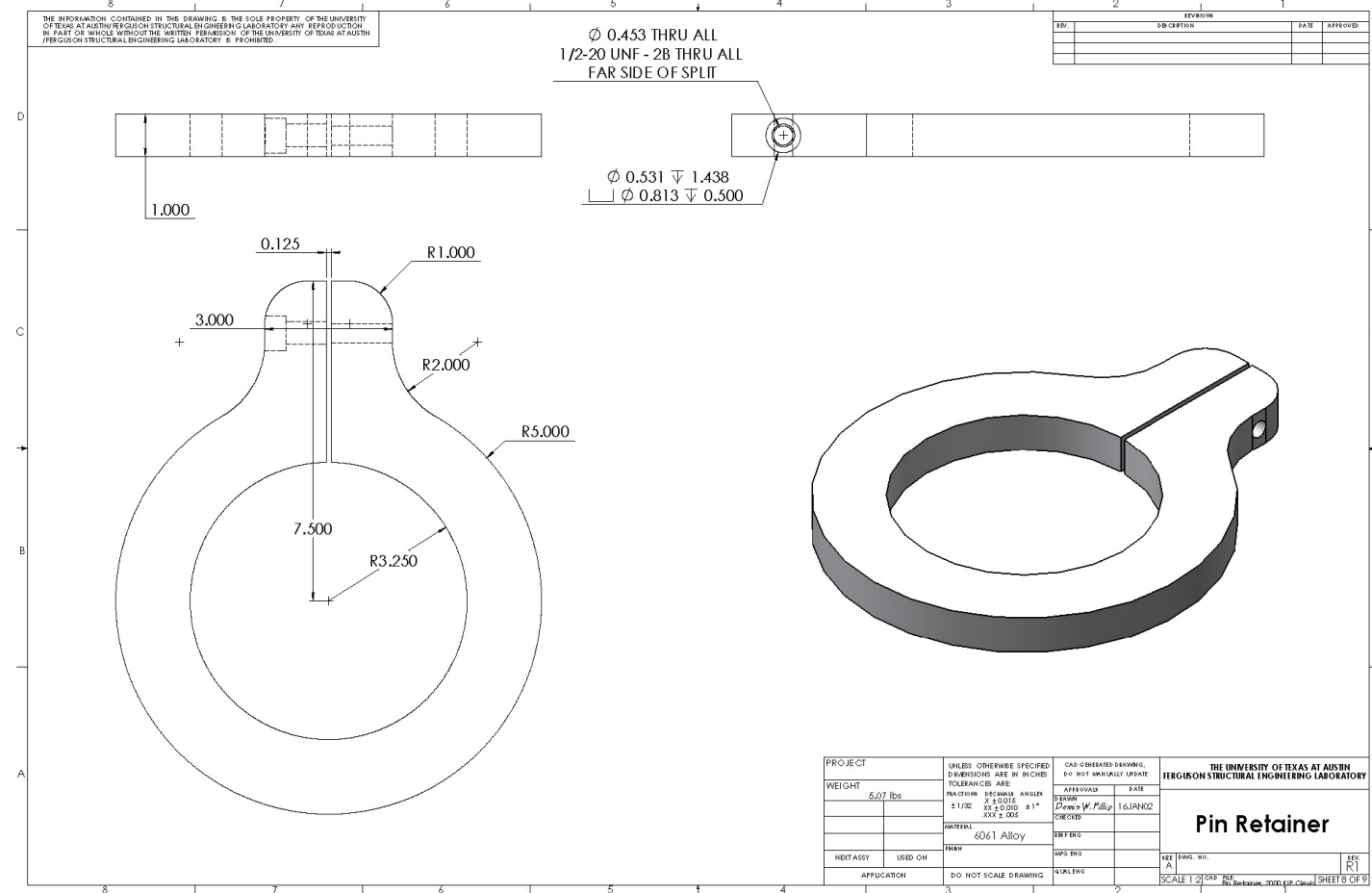


Figure A.10 Details of Pin Retainer

241

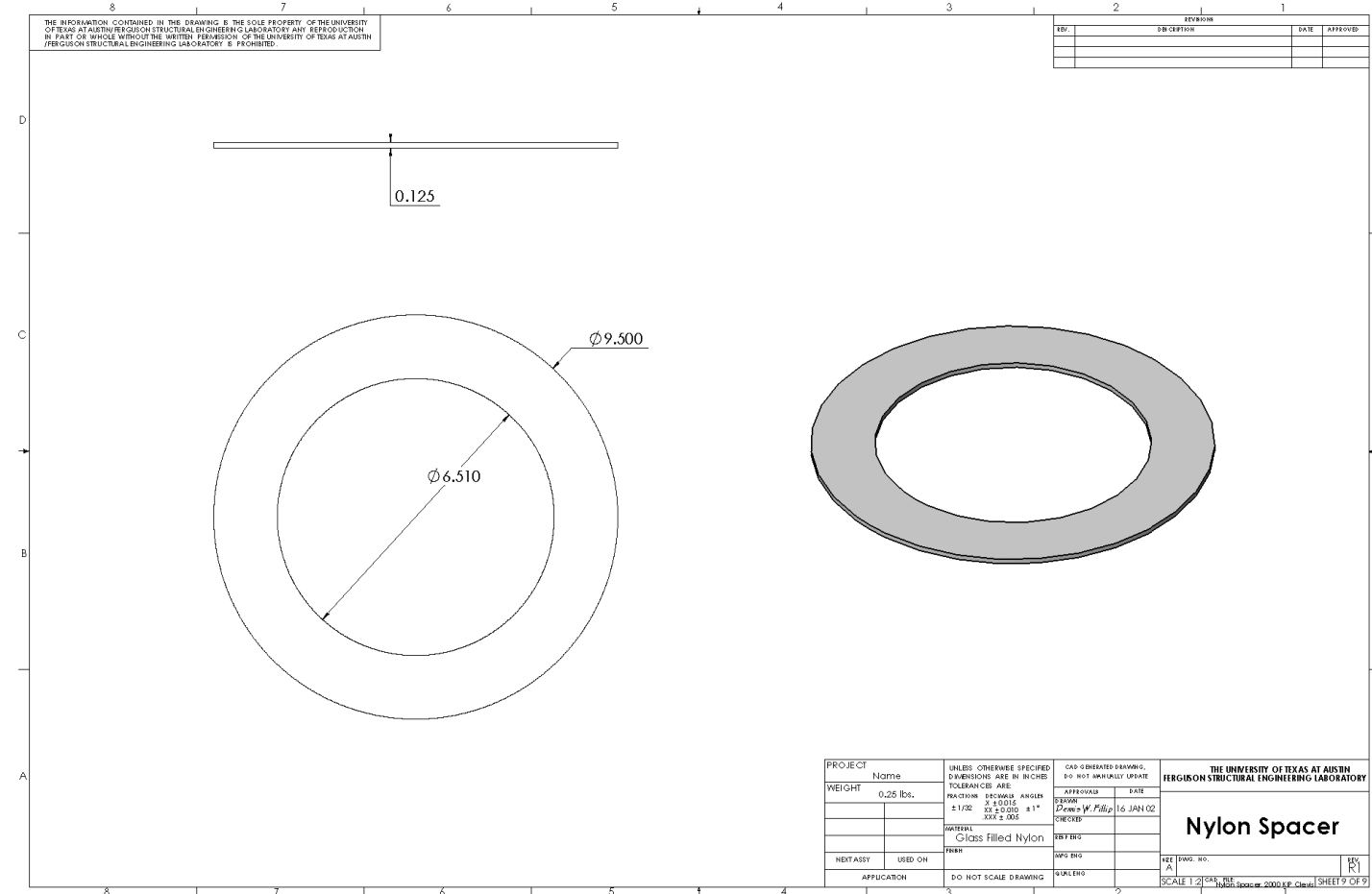


Figure A.11 Details of Nylon Spacer

## APPENDIX B

### ESTIMATION OF PLASTIC HINGE LENGTH: EXAMPLE

#### B.1 INTRODUCTION

To illustrate the analytical approach that can be used to estimate the plastic hinge length, which was presented in Chapter 5, an example problem is presented herein. For this purpose, the plastic hinge length of specimen S24-2UT is estimated and detailed calculations are presented. The following is a step-by-step procedure for estimating the plastic hinge length. Although the procedure was explicitly discussed in Chapter 5, it is repeated here for readers' convenience.

Step (1): The moment-curvature response of a typical column section within the potential plastic hinge region is obtained from a sectional analysis.

Step (2): Neglecting the second order effects, the bending moment diagram is drawn (Figure B.1(c)). The moment value at the center of the potential plastic hinge ( $\sim 0.5h$  away from the base) is assumed to be equal to the maximum moment capacity of the section obtained from the sectional analysis in step (1). In other words, failure is assumed to take place at the center of the assumed plastic hinge. This assumption would imply that the sections between the center of the plastic hinge and the base of the column have a larger flexural capacity than predicted using the sectional analysis. The shift in the location of critical section (Figure B.1(d)) is due to the confinement provided by the concrete stub to the neighboring sections. This effect, commonly referred to as stub

confinement effect, has been observed in previous experimental research (Soesinawati 1986; Sheikh and Khoury 1993; Bayrak and Sheikh 1998; Légeron and Paultre 2000).

Step (3): Using the bending moment diagram from step (2) and the moment-curvature analysis' results from step (1), the compressive strain experienced by the outer fiber of core concrete can be determined for a sufficient number of sections along the length of a column. If these compressive strains are plotted along the length of a column, the compressive concrete strain profile at the maximum moment along the length of a column can be obtained (Figure B.1(d)).

Step (4): The compressive strains at the outer fiber of the core concrete are equal to the reinforcing bar strains. In effect, the compressive strain profile obtained in step (3) represents the variation of compressive longitudinal bar strain along the length of a column. By examining the compressive strain profile, such as the one shown in Figure B.1(d), the length of the region in which longitudinal bars are yielding in compression can be estimated. The identification of this length establishes a key step in estimating the plastic hinge of a column.

Step (5): As indicated in step (2), the critical section shifts away from the face of the stub due to additional confinement effects provided by the stub. Because of the additional confinement provided by the stub to adjacent sections, sections within a distance of about  $0.25h$  from the stub remain nearly undamaged. In order to estimate the length of the plastic hinge region, where columns are expected to dissipate large amount of inelastic energy by undergoing large inelastic deformations,  $0.25h$  is subtracted from the overall length in which compressive rebar strains greater than the yield strain are calculated.

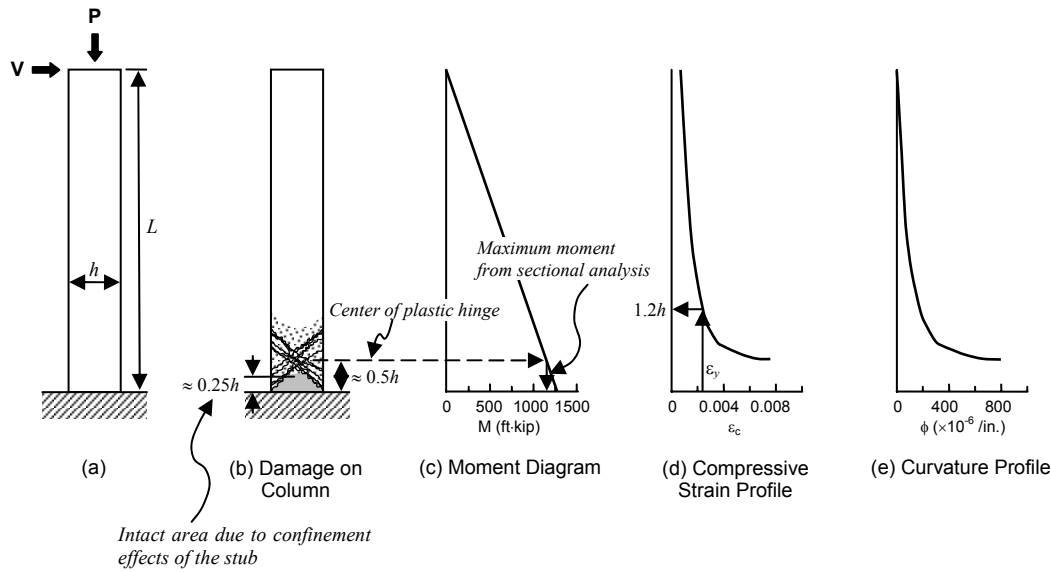


**Figure B.1 Estimation of Plastic Hinge Length: Specimen S24-2UT**

## B.2 STEP (1): CONSTRUCTION OF MOMENT-CURVATURE RELATIONSHIP

Sectional analysis is conducted to generate the moment-curvature relationship and the moment-strain at the outer layer of core relationship. The details of specimen S24-2UT are presented in Figure B.2. The confined and unconfined concrete models proposed by Razvi and Saatcioglu (1999) are used in the analysis. The behavior of the reinforcing bars is modeled to be bilinear until the initiation of strain hardening and the model proposed by Mander et al. (1984) is used in the strain hardening region. Core concrete is modeled as confined concrete, while cover concrete is modeled as unconfined concrete. Bar buckling behavior in compression reinforcement is not considered because the ascending branch of the moment-curvature relationship is of concern. Reinforcing bar buckling is not experienced within the ascending branch of the response. The resulting moment-curvature and moment-compressive strain (compressive strain

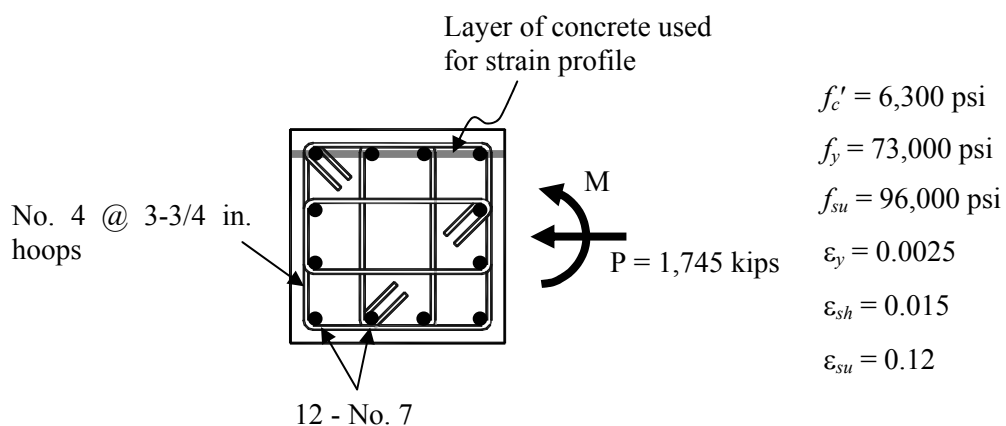


**Figure B.2 Details of Column S24-2UT**

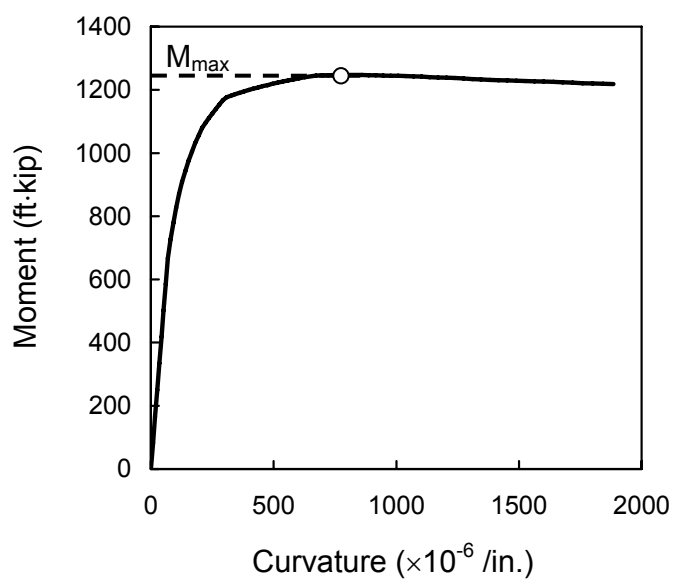


**Figure B.3 Moment-Curvature Relationship**

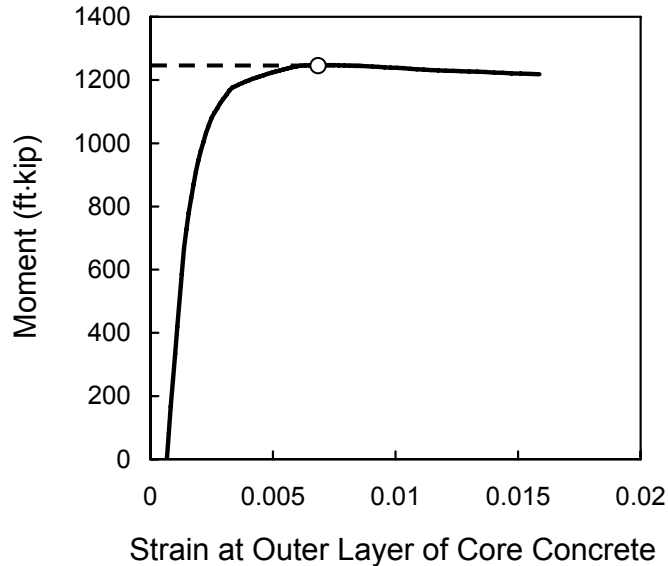


**Figure B.4 Moment-Compressive Strain Relationship**

at the outer layer of the confined core) relationships are shown in Figures B.3 and B.4.

### **B.3 STEPS (2) - (3): CONSTRUCTION OF MOMENT AND STRAIN DIAGRAMS ALONG COLUMN HEIGHT**

Following the assumptions described in Step (2), a moment diagram is constructed using the maximum moment ( $M_{max}$ ) from the sectional analysis (Figure B.3). Using the moment-compressive strain relationship (Figure B.4) and the bending moment diagram (Figure B.5(b)), the compressive strain profile along the length of specimen S24-2UT is generated (Figure B.5(c)).

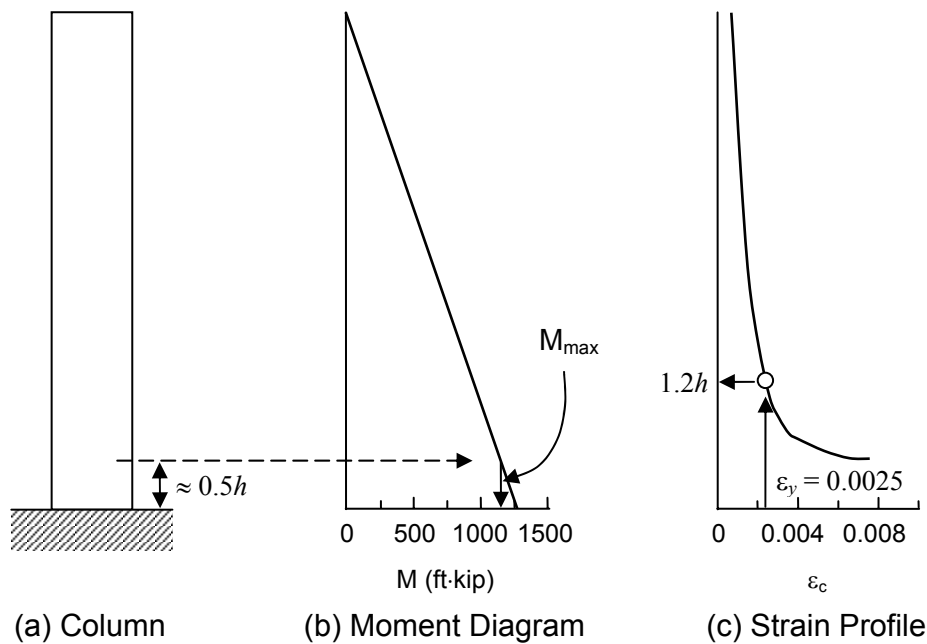


**Figure B.5 Construction of Moment Diagram and Strain Profile**

#### **B.4 STEPS (4) - (5): ESTIMATION OF LOCATION ALONG COLUMN HEIGHT CORRESPONDING TO YIELD STRAIN OF REINFORCING BAR AND PLASTIC HINGE LENGTH**

Based on the strain profile constructed (Figure B.5(c)), it is possible to identify the distance from the support to the section where the compressive strain of core concrete (or strain in compression steel) is equal to the yield strain of longitudinal reinforcement ( $\varepsilon_y$ ). By subtracting  $0.25h$  from this distance, the plastic hinge length ( $l_p = 1.2h - 0.25h = 0.95h$ ) of specimen S24-2UT can be estimated.

## APPENDIX C

### Computer Program Source

```
parameter (err_allow=0.001)
character ctemp(15)*1,infile*15,outfile*15
character momfile*15,drifile*15
common /input/ h,b,hc,bc,ys(10),As(10),rAs
common /concrete/ fcu,Ec,nc,hlayer,ec0un,ec85un,ec50un
common /steel/ Fys,Fus,Es,Esha,e_ha,e_ul,ns,As1,Ds1
common /steel_2/ Fy_h,E_h,A_h,D_h,s_h,nh,rNo_h(10),Deg_h(10)
c Failure Indicators
common /index/ ictype,ispall,ispall2,i2sD,irev,ibuc,irup,ibur
common /analysis/ rP0Pn,ipd,islip,ishhear,H0,rL_prov
real*8 ref(20)
real y(300)
real phi,for_tot,mom_tot,mom_max,mom_pre,P0

c ****
c generating file names
write(*,1000)
read(*,'(15a1)') (ctemp(i),i=1,15)
1000 format (/ ' enter input file name (15 chars. max)')

open(1,file="temp.txt")
write(1,'(15a1)') (ctemp(i),i=1,15)
do i=1,20
    if(ctemp(i) .eq. ".") then
        leng = i-1
        exit
    endif
enddo
ctemp(leng+2) = "m"
ctemp(leng+3) = "o"
ctemp(leng+4) = "m"
write(1,'(15a1)') (ctemp(i),i=1,leng+4)
ctemp(leng+2) = "d"
ctemp(leng+3) = "r"
ctemp(leng+4) = "i"
write(1,'(15a1)') (ctemp(i),i=1,leng+4)

open(unit=1,position="rewind",file="temp.txt")

read(1,'(a15)') infile
read(1,'(a15)') momfile
read(1,'(a15)') drifile
open(5,file = infile)
open(7,file = momfile)
open(8,file = drifile)

c ****
call InputData(i_in,i_out)
```

```

Asall = 0.
do i = 1,ns
    Asall = Asall + As(i)
enddo
rAs = Asall / (b*h)

rLhx = 0.
rLhy = 0.
do i = 1,nh
    rLhx = rLhx + rNo_h(i) * sind(90-Deg_h(i))*bc
    rLhy = rLhy + rNo_h(i) * sind(Deg_h(i))*hc
enddo
rLh = rLhx + rLhy
V_h = A_h * rLh
rou_v = V_h / (s_h*hc*bc)

Pn = 0.85*fcu* (b*h-Asall) + Fys*Asall
Pn = -1.*Pn
P0 = rP0Pn * Pn
H_story = 2 * H0

c ****
c generation of stress-stain curves of materials
call Curve_Concrete(ecc,fcc)
call Curve_Buckling(fs_max)
call Curve_Buckling1

ref(10) = abs(ecc)
ref(11) = abs(fs_max)

c ****
c output the information
print*, "Strains of Unconfined Concrete", ec0un, ec85un, ec50un
write(*,4000) ispec
4000 format(1x,"ispec"=",i10)
write(*,4100) rou_v*100
4100 format(1x,"Volumetric ratio (%)"=",f10.4)
write(*,4200) fcu/0.1450377
4200 format(1x,"Concrete strength (MPa)"=",f10.4)
write(*,4300) P0/Pn, P0*4448.222/1000.
4300 format(1x,"Axial load"=",f10.4," * Pn ",f10.4,"(kN)")

if(ibuc .eq. 1) then
    print*, "Buckling" OK"
else
    print*, "Buckling" NOT!!! considered -----
endif
if(ipd .eq. 1) then
    print*, "P-delta" OK"
else
    print*, "P-delta" NOT!!! considered -----
endif
if(islip .eq. 1) then
    print*, "Bar slip" OK"
else
    print*, "Bar slip" NOT!!! considered -----
endif

```

```

        if(ishear .eq. 1) then
            print*, "Shear          OK"
        else
            print*, "Shear          NOT!!! considered -----"
        endif
        print*, "*****"
c      ****
c      initialization
phi_inc_pre = 10000
mom_tot_pre = -10000

ierr         = 1
esb_pre      = -10000
nc=300
mom_max     = 0.
mom_pre      = 0.
write(7,1500)
1500  format(1x,           specimen_id", "           curvature",
+                  "           moment", "           top_conc_strain",
+                  "           top_bar_strain", "   bottom_bar_strain",
+                  "           top_bar_stress", "   bottom_bar_stress",
+                  "           top_conc_core_strain", " top_conc_core_stress",
+                  "           neutral_axis"      )
+
hlayer = h/nc
y(1)   = hlayer/2.
c      distance from the bottom fiber to the centroid of each layer
do i = 2,nc
    y(i)   = y(i-1) + hlayer
enddo

c      ****
c      calculate a centroid of section
c      ****
asi      = 0.
as_tot   = 0.

do i = 1,ns
    asi     = asi+As(i)*ys(i)*(Es/Ec-1)
    as_tot = as_tot+As(i)*(Es/Ec-1)
enddo
y_cen   = (b*h**2/2.+ asi)/(b*h + as_tot)

c      ****
c      calculate a pure axial capacity for the confined section
c      ****
Pgross = fcu*(h*b)+Fys*as_tot
Pcore  = fcu*(hc*bc)+Fys*as_tot
if(abs(P0).ge.Pcore) then
    print*, "*****"
    print*, " The axial force is too large"
    print*, "*****"
    print*, " - Pgross=", Pgross
    print*, " - Pcore =", Pcore
    print*, " - P0     =", -P0
    stop
endif

```

```

c      calculate the axial capacity of bars
Pbar   = Fys*as_tot

c ****
c find a pure axial strain corresponing to the given force
c ****
TOL     = 10**(-10.)
iMax    = 30
jMax    = 10
e_inc   = 10**(-4.)
Fconv   = 3
Phi     = 0.
c       = 10**5

c      get the corresponding strain wihich is closer to xu
x1      = -0.005
xu      = 0
econv_l= (xu-x1)/10.
econv_u= (xu-x1)/10.

c      reduce the lower bound
i       = 1
100    e_ct   = xl
e_cb   = xl
call InternalForce(e_ct,e_cb,y,y_cen,for_tot,mom_tot,ref)

z1      = P0-for_tot
if(abs(z1) .le. TOL) goto 200
if( ((abs(z1-zl_pre).le.Fconv).and.(zl*zl_pre.gt.0)).or.
+ (i.eq.1) ) then
    i       = i+1
    zl_pre = zl
    xl0   = xl
    zl0   = zl
    xl     = xl+econv_l
    goto 100
endif

c      check the validity of the lower bound
econv_l= econv_l/jMax
x1      = xl0+econv_l
110    e_ct   = xl
e_cb   = xl
call InternalForce(e_ct,e_cb,y,y_cen,for_tot,mom_tot,ref)

z1      = P0-for_tot
if(abs(z1).le.TOL) goto 200

if((abs(zl-zl0).le.Fconv) .and. (zl*zl0.gt.0)) then
    zl_pre = zl
    xl     = xl+econv_l
    if(xl .le. xl0 + econv_l*jMax) goto 110
else
    xl     = xl-econv_l
    zl     = zl_pre
endif

c      reduce the upper bound

```

```

120      i      = 1
      e_ct   = xu
      e_cb   = xu
      call InternalForce(e_ct,e_cb,y,y_cen,for_tot,mom_tot,ref)

      zu     = P0-for_tot
      if(abs(zu) .le. TOL) goto 200
      if( ((abs(zu-zu_pre).le.Fconv) .and. (zu*zu_pre.gt.0)).or.
+ (i.eq.1) ) then
          i      = i+1
          zu_pre = zu
          xu0    = xu
          zu0    = zu
          xu     = xu-econv_u
          goto 120
      endif

c      check the validity of the upper bound
      econv_u= econv_u/jMax
      xu     = xu0-econv_u
130      e_ct   = xu
      e_cb   = xu
      call InternalForce(e_ct,e_cb,y,y_cen,for_tot,mom_tot,ref)

      zu     = P0-for_tot
      if(abs(zu) .le. TOL) goto 200
      if((abs(zu-zu0).le.Fconv) .and. (zu*zu0.gt.0)) then
          zu_pre = zu
          xu     = xu-econv_u
          if(xu .ge. xu0 + econv_u*jMax) goto 130
      else
          xu     = xu + econv_u
          zu     = zu_pre
      endif

c      use a bisection method
c      get the corresponding strain which is closer to xu
140      x     = xl + (xu-xl)/2.
      e_ct   = x
      e_cb   = x
      call InternalForce(e_ct,e_cb,y,y_cen,for_tot,mom_tot,ref)

      z     = P0-for_tot
      if((abs(z).le.TOL) .or. (abs(xu-xl).le.TOL)) goto 200

      if(zu*z .lt. 0) then
          xl     = x
          zl     = z
      else
          if(zl*z .lt. 0) then
              xu     = x
              zu     = z
          else
              z_pre  = zu
              econv_u= (xu-xl)/100.
              x     = xu-econv_u
              e_ct   = x
              e_cb   = x

```

```

call InternalForce(e_ct,e_cb,y,y_cen,for_tot,mom_tot,ref)

z      = P0-for_tot
if(abs(z).le.TOL) goto 200
if(z*z_pre.lt.0) then
    xl      = x
    xu      = x+econv_u
    zl      = z
    zu      = z_pre
else
    z_pre  = z
    x      = x-econv_u
    if(x.lt.xl) then
        print*, "*****"
        print*, "          Error Occurs"
        print*, "*****"
        stop
    else
        goto 150
    endif
endif
endif
endif
i      = i+1
if(i.le.iMax) goto 140
200   e0_c  = e_ct

temp   = 10**7
if(i_out .eq. 0) then
c       output in unit of (kip and kip.ft)
c       write(7,3000) ispec,phi*10**6,mom_tot/12,-e_ct,ref(1),
+                   ref(2),ref(3),ref(4),ref(5),ref(6),temp
+       else
c       output in unit of (kN and kN.m)
c       call UnitTo_MPamm(phi,for_tot,mom_tot,P0)
c       write(7,3000) ispec,phi*10**6,mom_tot/10**6,-e_ct,ref(1),
+                   ref(2),ref(3)/0.1450377,ref(4)/0.1450377,
+                   ref(5),ref(6)/0.1450377,temp
+       call UnitTo_kipin(phi,for_tot,mom_tot,P0)
endif

phi_pre     = phi
phi_pre2    = phi_pre-100

write(*,2000)
2000  format(1x,"Calculation of strain for a pure axial force")
write(*,2010) e0_c
2010  format(1x,"      e0_c=",f19.10)
print*, "      P0=",P0
print*, "      For_tot=",for_tot
write(*,2020) P0-for_tot
2020  format(1x," P0-for_tot=",f19.10)
write(*,2030) mom_tot
2030  format(1x,"      mom_tot=",f19.10)
write(*,*)

fs_com_pre  = ref(3)
fs_ten_pre  = ref(4)

```

```

c ****
c esimate the optimum c
c e_ct = concrete strain at top fiber
c e_bt = concrete strain at bottom fiber
c ****
c TOL = 10**(-6.)
iMax = 30
jMax = 10
e_inc = 10**(-4.)
Fconv = 3
e_ct = e0_c

300 continue

e_inc = e_inc*1.02
e_ct = e_ct-e_inc
print*,e_ct

c since the only considered phi is positive
c get the corresponding strain which is closer to xl
310 xl = phi_pre*h + e_ct
if(ispall.eq.3) then
    xl = xl-.5
    ispall = 10
endif
if(i2sD .eq. 2) then
    xl = xl-.5
    i2sD = 3
endif

xu = xl+1
econv_l=(xu-xl)/jMax
econv_u=(xu-xl)/jMax

c reduce the lower bound
i = 1
320 e_cb = xl
call InternalForce(e_ct,e_cb,y,y_cen,for_tot,mom_tot,ref)

zl = P0-for_tot
if(abs(zl).le.TOL) then
    x = xl
    z = zl
    goto 400
endif
if( ((abs(zl-zl_pre).le.Fconv).and.(zl*zl_pre.gt.0)).or.(i.eq.1) ) then
    i = i+1
    zl_pre = zl
    xl0 = xl
    zl0 = zl
    xl = xl+econv_l
    goto 320
endif

c check the validity of the lower bound
econv_l = econv_l/jMax
xl = xl0+econv_l

```

```

330      e_cb     = xl
      call InternalForce(e_ct,e_cb,y,y_cen,for_tot,mom_tot,ref)

      zl      = P0-for_tot
      if(abs(zl).le.TOL) then
          x      = xl
          z      = zl
          goto 400
      endif
      if((abs(zl-zl0).le.Fconv).and.(zl*zl0.gt.0)) then
          zl_pre = zl
          xl     = xl+econv_l
          if(xl.le.xl0+econv_l*jMax) goto 330
      else
          xl     = xl-econv_l
          zl     = zl_pre
      endif

      c      reduce the upper bound
      i      = 1
340      e_cb     = xu
      call InternalForce(e_ct,e_cb,y,y_cen,for_tot,mom_tot,ref)

      zu      = P0-for_tot
      if(abs(zu).le.TOL) then
          x      = xu
          z      = zu
          goto 400
      endif
      if( ((abs(zu-zu_pre).le.Fconv).and.(zu*zu_pre.gt.0)).or.(i.eq.1) ) then
          i      = i+1
          zu_pre = zu
          xu0    = xu
          zu0    = zu
          xu     = xu-econv_u
          goto 340
      endif

      c      check the validity of the upper bound
      econv_u      = econv_u/jMax
      xu          = xu0-econv_u
350      e_cb     = xu
      call InternalForce(e_ct,e_cb,y,y_cen,for_tot,mom_tot,ref)

      zu      = P0-for_tot
      if(abs(zu).le.TOL) then
          x      = xu
          z      = zu
          goto 400
      endif
      if((abs(zu-zu0).le.Fconv).and.(zu*zu0.gt.0)) then
          zu_pre = zu
          xu     = xu-econv_u
          if(xu.ge.xu0-econv_u*jMax) goto 350
      else
          xu     = xu+econv_u
          zu     = zu_pre
      endif

```

```

c      use a bisection method
c      get the corresponding strain which is closer to xl
c      i      = 1
360    x      = xl+(xu-xl)/2.
e_cb   = x
call InternalForce(e_ct,e_cb,y,y_cen,for_tot,mom_tot,ref)

z      = P0-for_tot
if(abs(z).le.TOL) goto 400

if(zl*z.lt.0) then
  xu     = x
else
  if(zu*z.lt.0) then
    xl     = x
    zl     = z
  else
    z_pre  = zl
    econv_l=(xu-xl)/100.
    x     = xl+econv_l
    e_cb   = x
  Call InternalForce(e_ct,e_cb,y,y_cen,for_tot,mom_tot,ref)

  z      = P0-for_tot
  if(abs(z) .le. TOL) goto 400
  if(z*z_pre .lt. 0) then
    xu     = x
    xl     = x-econv_l
    zu     = z
    zl     = z_pre
  else
    z_pre  = z
    x     = x+econv_l
    if(x .lt. xu) then
c          fail to find the neutral axis
          goto 400
    else
      goto 370
    endif
  endif
endif
endif
380    i      = i+1
if(i .le. iMax) goto 360

400    e_cb   = x
phi   = (e_cb-e_ct)/h
c      since phi should be increasing (RE-EFFECTIVE ON 05-19-2004)
esb   = ref(4)

if(phi.le.phi_pre .or. esb.le.esb_pre) then
  if(ierr .gt. 30) then
    ifail  = 1
    goto 900
  endif
  print*,ierr
  e_ct   = e_ct - 2*e_inc

```

```

        if(ierr .gt. 20) e_ct      = e_ct - 10*e_inc
        ierr   = ierr + 1
        goto 300
    endif

    if(abs(for_tot-P0) .lt. .01) then
        if(mom_tot .gt. mom_max) then
            mom_max      = mom_tot
        elseif(abs(mom_tot-mom_pre)/mom_pre .gt. 1.3) then
            goto 900
        endif

        if(i_out.eq.0 .and. mom_tot.gt.0) then
            c          output in unit of (kip, kip.ft, /in x 10**6)
            write(7,3000) ispec,phi*10**6,mom_tot/12,
            -e_ct,ref(1),ref(2),ref(3),ref(4),ref(5),ref(6),-e_ct/phi
            format(1x,i20,1x,20(f20.6,1x))
        elseif(mom_tot .gt. 0) then
            c          output in unit of (kN, kN.m, and /mm x 10**6)
            call UnitTo_MPamm(phi,for_tot,mom_tot,P0)
            write(7,3000) ispec,phi*10**6,mom_tot/10**6,-e_ct,ref(1),
            ref(2),ref(3)/0.1450377,ref(4)/0.1450377,
            ref(5),ref(6)/0.1450377,-e_ct/phi
            call UnitTo_kipin(phi,for_tot,mom_tot,P0)
        endif

        c          termination of program
        if(mom_tot .lt. mom_max) then
            if(i2sD .eq. 1) i2sD = 2
        else
            mom_max      = mom_tot
        endif

        if(ispall.eq.2) ispall=3

        if(mom_tot .lt. 0.1*mom_max) then
            ifail  = 3
            print*, " Flexural failure"
            goto 900
        endif

        tmp     = 1.25 - rP0Pn
        if(abs(ref(1)-ref(2)) .gt. tmp*e_ul) then
            ifail  = 4
            print*, " Low-cycle fatigue failure occurred"
            goto 900
        endif

        if(abs(ref(2)) .gt. e_ul) then
            ifail  = 5
            print*, " Rupture of bars occurred"
            goto 900
        endif

        if(abs(ref(1)).gt.Fys/Es .and. abs(ref(3)).lt.0.2*Fys) then
            ifail  = 5
            print*, " Buckling failure occurred"
            goto 900
    endif

```

```

        endif

        ierr          = 1
        phi_pre       = phi
        phi_inc       = phi - phi_pre
        mom_pre       = mom_tot
    else
        if(ierr.gt.30) then
            ifail   = 2
            goto 900
        endif
        print*,ierr
        e_ct      = e_ct - 2*e_inc
        if(ierr.gt.20) e_ct  = e_ct - 10*e_inc
        ierr      = ierr + 1
    endif

c    initializations
phi_inc_pre  = phi_inc
esb_pre       = esb
goto 300

900  rewind(7)
PRINT*,H0,h
call UnitTo_MPamm(phi,for_tot,mom_tot,P0)
Pn = Pn * 4448.222
PRINT*,H0,h
call def_MAIN(ispec,P0,Pn,rou_v,i_out,disp_y,disp80,ecc)
close(7)
close(8)

stop
end

```

```

subroutine InputData(i_in,i_out)
character*72 title
common /input/ h,b,hc,bc,ys(10),As(10),rAs
common /concrete/ fcu,Ec,nc,hlayer,ec0un,ec85un,ec50un
common /steel/ Fys,Fus,Es,Esha,e_ha,e_ul,ns,As1,Ds1
common /steel_2/ Fy_h,E_h,A_h,D_h,s_h,nt,rNo_h(10),Deg_h(10)
common /index/ ictype,ispall,ispall2,i2sD,irev,ibuc,irup,ibur
common /analysis/ rP0Pn,ipd,islip,ishhear,H0,rL_prov
integer i_in,i_out

      read(5,1000) title
1000  format(a72)
      read(5,*) i_in,i_out
c      input and outout units: 0 -> kip and in / non-0 -> MPa and mm
      read(5,*) ictype,ispall,i2sD
      print*,-----
      if(ictype.eq. 1) print*," Concrete model: Park"
      if(ictype.eq. 2) print*," Concrete model: Sheikh and Uzumeri"
      if(ictype.eq. 3) print*," Concrete model: Mander"
      if(ictype.eq. 4) print*," Concrete model: Saatcioglu 1999"
      if(ictype.eq. 5) print*," Concrete model: Paultre 2003"
      print*,-----

c **** DESCRIPTION OF CONCRETE CROSS-SECTION ****
c
c      read(5,*) h,b,fcu,Ec
c      if(Ec.eq.0) then
c          if(i_in .ne. 0) fcu = fcu*0.1450377
c      c      for all range of concrete (Carrasquillo)
c          Ec = (40000*sqrt(fcu*1000)+1000000)/1000.
c          if(i_in .ne. 0) then
c              fcu = fcu/0.1450377
c              Ec = Ec/0.1450377
c          endif
c      endif
c
c **** DESCRIPTION OF LONGITUDINAL REINFORCEMENTS ****
c      initialization of ys(ns)
c
do i=1,10
      ys(i) = 0.
      As(i) = 0.
enddo

      read(5,*) Ds1,As1,Fys,Fus,Es,Esha,e_ha,e_ul
      if((i_in.eq.0).and.(Es.eq.0)) Es = 29600.
      if((i_in.ne.0).and.(Es.eq.0)) Es = 29600./0.1450377
      if(Esha.eq.0) Esha = Es/20.
      if(e_ha.eq.0) e_ha = 0.01
      if(e_ul.eq.0) e_ul = 0.3

      read(5,*) ns,(ys(i),As(i),i=1,ns)

c **** sorts the layers of steel so that extreme tenile layer is
c      sorts the layers of steel so that extreme tenile layer is
c      the first layer      and extreme compression layer is the last.

```

```

c ****
c if(ns .le. 1) goto 100
do 100 j = 1,ns-1
    kk = ns-j
    do 100 i = 1,kk
        if(ys(i) .le. ys(i+1)) goto 100
        dumy   = ys(i)
        duma   = As(i)
        ys(i)  = ys(i+1)
        As(i)  = As(i+1)
        ys(i+1)= dumy
        As(i+1)= duma
100     continue

c ****
c DESCRIPTION OF HOOPS
c Area, spacing and length of hoop on a section
c ****
read(5,*) D_h,A_h,Fy_h,E_h
if((i_in.eq.0) .and. (E_h.eq.0)) E_h = 29600.
if((i_in.ne.0) .and. (E_h.eq.0)) E_h = 29600./0.1450377
read(5,*) s_h,nt
do i = 1,nt
    read(5,*) rNo_h(i),Deg_h(i)
c Degree of hoop is measured from x-axis
enddo

c confined section
hc      = ys(ns)-ys(1)+Ds1+D_h
bc      = b-2*ys(1)+Ds1+D_h

c read the analysis parameters
read(5,*) rP0Pn,ibuc,ipd,islip,ishear
c ibuc   = 1; Buckling considered in the analysis
c ipd    = 1; P-delta effect considered
c islip  = 1; bar slip effect considered
read(5,*) H0,rL_prov
call Conc_Collins_un

c transform the units into the basic units (kip and inch)
if(i_in.ne.0) call UnitTo_kipin(phi,for_tot,mom_tot,P0)

return
end

```

```

subroutine InternalForce(e_ct,e_cb,y,y_cen,for_tot,mom_tot,ref)
common /input/ h,b,hc,bc,ys(10),As(10),rAs
common /concrete/ fcu,Ec,nc,hlayer,ec0un,ec85un,ec50un
common /steel/ Fys,Fus,Es,Esha,e_ha,e_ul,ns,As1,Ds1
common /steel_2/ Fy_h,E_h,A_h,D_h,s_h,nh,rNo_h(10),Deg_h(10)
common /index/ ictype,ispall,ispall2,i2sD,irev,ibuc,irup,ibur
common /analysis/ rP0Pn,ipd,islip,ishhear,H0,rL_prov
real y(300)
real*8 e_c(300),e_s(10),fc(300),fs(10),e_tmp
real*8 fun,fcon,funl
real phi,for_tot,mom_c,mom_s,mom_tot
real*8 ref(20)
CC assume a cover concrete spalls when a cover strain reaches -0.0025
parameter (ec_spall = -0.0025)

phi=-(e_ct-e_cb)/h
if(phi.ne.0) then
    c      = -e_ct/phi
    e_cen = phi*(h-c-y_cen)
else
    c      = 10**5
    e_cen = e_ct
endif

c ****
c strain & stress distribution
c ****
do 100 i=1,nc
    e_c(i) = e_cen-phi*(y(i)-y_cen)
100 continue
do 110 i=1,ns
    e_s(i) = e_cen-phi*(ys(i)-y_cen)
    if(abs(e_s(i)) .gt. Fys/Es) e_s(i) = e_s(i)*2
110 continue

CC y_con_upper = UPPER BOUNDARY OF CONFINED SECTION
CC y_con_lower = LOWER BOUNDARY OF CONFINED SECTION
y_con_upper=hc+(h-hc)/2.
y_con_lower=(h-hc)/2.

ecc      = ref(10)

do 200 i = 1,nc
    temp     = A_h
    A_h      = 0.03
    e_tmp   = e_c(i)
    if(ictype.eq.1) call Conc_Park(e_tmp,funl)
    if(ictype.eq.2) call Conc_ShUz(e_tmp,funl,c)
    if(ictype.eq.3) call Conc_Mander(e_tmp,funl)
    if(ictype.eq.4) call Conc_Saatcioglu99(e_tmp,funl)
    if(ictype.eq.5) call Conc_Paultre03(e_tmp,funl)

    if(e_c(i) .lt. -0.002) e_tmp = 0.5*(e_c(i)+0.002) - 0.002
    if(ictype.eq.1) call Conc_Park(e_tmp,fun)
    if(ictype.eq.2) call Conc_ShUz(e_tmp,fun,c)
    if(ictype.eq.3) call Conc_Mander(e_tmp,fun)
    if(ictype.eq.4) call Conc_Saatcioglu99(e_tmp,fun)
    if(ictype.eq.5) call Conc_Paultre03(e_tmp,fun)

```

```

A_h      = temp

if(ictype.eq.1) call Conc_Park(e_c(i),fcon)
if(ictype.eq.2) call Conc_ShUz(e_c(i),fcon,c)
if(ictype.eq.3) call Conc_Mander(e_c(i),fcon)
if(ictype.eq.4) call Conc_Saaticoglu99(e_c(i),fcon)
if(ictype.eq.5) call Conc_Paultre03(e_c(i),fcon)

if(fun1 .lt. fcon) fun1      = fcon

if((y(i).gt.y_con_upper) .or. (y(i).lt.y_con_lower)) then
    fc(i)  = fun1
else
    fc(i)  = ( fun1*(b-bc)+fcon*bc )/b
endif
c     gathering information
    if(i .eq. jcore) then
        ref(18)      = fun1
        ref(19)      = fun
        ref(20)      = fcon
    endif
200   continue

do 210 i=1,ns
c         call Steel_Bilinear(e_s(i),fs(i))
c         call Steel_Hardening(e_s(i),fs(i))
210   continue

CC     to prevent the change of buckling spacing
rnum   = As(ns) / As1
if(rP0Pn .lt. 0.3 .and. (rNo_h(1)+rNo_h(2))/2/rnum .gt. 0.7) then
    i2SD = 1
elseif(abs(e_s(ns)) .gt. ecc) then
    i2SD = 10
endif

c     ns = layer of the outmost compression bars
if(ibuc.eq.1) then
    call Steel_Buckling(e_s(ns),fs(ns))
    fs_max = ref(11)
endif

c ****
c axial force calculation
c ****
for_c=0.
for_s=0.

do 300 i=1,nc
    for_c  = for_c+hlayer*b*fc(i)
300   continue
do 310 i=1,ns
    for_s  = for_s+As(i)*fs(i)
310   continue
for_tot= for_c+for_s

c ****
c moment calculation

```

```

c      ****
mom_c=0.
mom_s=0.

do 400 i=1,nc
      mom_c = mom_c+hlayer*b*fc(i)*(y_cen-y(i))
400  continue
do 410 i=1,ns
      mom_s = mom_s+As(i)*fs(i)*(y_cen-ys(i))
410  continue
mom_tot= mom_c+mom_s

do i = nc,1,-1
      if(y(i).lt.y_con_upper) then
          jcore = i
          exit
      endif
enddo
jcore34      = 1/4.* (nc+2*jcore+1)
ref(1) = e_s(ns)
ref(2) = e_s(1)
ref(3) = fs(ns)
ref(4) = fs(1)
ref(5) = e_c(jcore)
ref(6) = fc(jcore)
ref(7) = e_c(jcore34)
ref(8) = e_c(nc)
ref(9) = fc(nc)

return
end

```

```

subroutine def_MAIN(ispec,P0,Pn,rou_v,i_out,disp_y,disp80,ecc)
common /input/ h,b,nc,bc,ys(10),As(10),rAs
common /concrete/ fcu,Ec,nc,hlayer,ec0un,ec85un,ec50un
common /steel/ Fys,Fus,Es,Esha,e_ha,e_ul,ns,As1,Ds1
common /steel_2/ Fy_h,E_h,A_h,D_h,s_h,nt,rNo_h(10),Deg_h(10)
common /index/ ictype,ispall,ispall2,i2sD,irev,ibuc,irup,ibur
common /analysis/ rP0Pn,ipd,islip,ishhear,H0,rL_prov
parameter (n_lay=300)
parameter (err_tol=0.1)
parameter (r_loss=0.8)
parameter (r_gain=0.75)

real mom(500),phi(500),es_b(500),fs_b(500)
real e_core(500),f_core(500),c(500)
real load(500),disp(500)
real yphi_mo(n_lay+1),yphi_pd(n_lay+1)
real yM_mo(n_lay+1),yM_pd(n_lay+1)
real def_mo(n_lay+1),def_pd(n_lay+1),def_sh(n_lay+1),def_slip
real H0,rmom60,rmom80,phi60,mom_max,Lp,Lp_pre
real phi_tot(500),temp(20)
open(unit=7,position="rewind")
*****  

c N(newton) into kN
Paxial = -P0/1000
Pcap   = -Pn/1000
print*, "Height of Specimen =",H0
print*, "Aspect Ratio      =",H0/h
print*, "Axial Load(kN)    =",Paxial

c *****  

c read MOMENT-CURVATURE data
do i = 1,500
    mom(i)  = 0.
    phi(i)  = 0.
    es_b(i) = 0.
    fs_b(i) = 0.
    e_core(i)= 0.
    f_core(i)= 0.
    c(i)    = 0.
enddo

i          = 0
ierr      = 0
mom_max= 0.
phi_max= 0.

read(7,*)
100  read(7,*,err=200) temp1, phi(i),mom(i) ,temp4,temp5,
     +      es_b(i),temp7 ,fs_b(i),e_core(i),f_core(i),c(i)
c CURVATURE values have a unit of (x10**(-6)) radian
c to transform it into unit radian, (10^6) has to be multiplied.
c MOMENT values have a unit of kN.m
c to transform it into kN.mm, (1000) has to be multiplied.
if(i_out .eq. 0) then
    phi(i) = phi(i)*0.03936996
    mom(i) = (mom(i)*12)*4448.222*25.4/(10**6)
    fs_b(i)= fs_b(i)/0.1450377
    f_core(i)      = f_core(i)/0.1450377

```

```

c(i) = c(i)/0.03936996
endif

phi_end= phi(i)
if(mom(i) .ge. mom_max) then
    mom_max = mom(i)
    phi_max = phi(i)
endif

if(i .le. 500) then
    i = i + 1
    goto 100
endif

200   imax = i - 1
phi_cri = phi_end
do i = 2,500
    if(phi(i) .eq. 0 .and. mom(i) .eq. 0) then
        mom(i) = 0.
        phi(i) = 10**10
        exit
    endif
enddo

c ****
c calculate EI_lin
rmom60 = r_gain * mom_max
do i = 1,imax
    if(mom(i) .ge. rmom60) then
        if(mom(i) .ne. mom(i-1)) then
            phi60 = (phi(i)-phi(i-1)) / (mom(i)-mom(i-1)) *
+                               (rmom60-mom(i-1)) + phi(i-1)
        else
            phi60 = phi(i)
        endif
        exit
    endif
enddo
EI_lin = rmom60 / phi60
phi_y = phi60 / r_gain
print*,phi_y

c ****
write(8,*) "h      =",h
write(8,*) "H_story  =",H0*2
write(8,*) "H_tip    =",H0
write(8,*) "Aspect R =",H0/h
write(8,*) "P0      =",Paxial
write(8,*) "Pn      =",Pcap
write(8,*)
write(8,1000)
write(8,1100)
1000  format(1x, "      disp(mm)", "      shear(kN)",
+           "      D_mo(mm)", "      D_slip(mm)",
+           "      D_sh(mm)", "      D_pd(mm)",
+           "      c(mm)", "      Mbase(kN.mm)",
+           "      M_mo(kN.mm)", "      M_pd(kN.mm)",
+           "      phi0_mo", "      phi0_pd",

```

```

+
+           "      iter.#", "      Lp/h",
+           "      rL_stub/h"      )    0.0",
+           "      0.0", "      0.0",
+           "      0.0", "      0.0",
+           "      0.0", "      0.0",
+           "      0.0", "      0.0",
+           "      0.0", "      0.0",
+           "      0.0", "      0.0",
+           "      0", "      0.0"  )
c      initializing data
do i=1,n_lay+1
    yphi_pd(i) = 0.
    yM_pd(i)   = 0.
    def_mo(i)   = 0.
    def_pd(i)   = 0.
    def_sh(i)   = 0.
enddo

def_shear      = 0.
def_slip       = 0.
def_mo_pre     = 0.
def_pd_pre     = 0.
def_shear_pre  = 0.
def_slip_pre   = 0.
def_tip        = 0.
def_tip_pre    = 0.

phi_inc        = phi_max/100.
phi0_mo        = phi_inc
phi0_pd        = 0.
phi0_pre       = 0.

rload_max      = 0.
Bshear_max     = 0.
Bshear_pre     = 0.
slope_slip     = 0.
slope_slip_pre = 10**10
yM0_max        = 0.
Lp              = 0.
Lp_pre          = 0.
dis_duc         = 0.

itry            = 1
jtry            = 1
rK_pre          = 10**10
iK_opt          = 1

c      ****
c      FLEXURAL DEFLECTION FROM MOMENT DISTRIBUTION
300  call def_moment(mom,phi,n_lay,phi_max,mom_max,EI_lin,phi_y,
+                   n0,rL_stub,ypsi_mo,ypsi_pd,yM_pd,phi0_mo,phi0_pd,
+                   yM_mo,yM0_max,def_mo,Lp,Lp_pre,phi_cri,
+                   f_core,e_core,c,def_sh,ecc,e_c_tot,c_tot)

if(def_mo(1).ge.def_mo_pre) then
    def_mo_pre= def_mo(1)
else

```

```

        def_mo(1) = def_mo_pre
    endif

    phi0 = yphi_mo(n0) + yphi_pd(n0)
    do i = 1,imax
        if(phi(i) .ge. phi0) then
            c0 = (c(i)-c(i-1)) / (phi(i)-phi(i-1)) *
+                (phi0-phi(i-1)) + c(i-1)
            exit
        endif
    enddo

    yMb           = yM_mo(n_lay+1)
    yMb           = yMb * 1000.

c     BAR SLIP DEFLECTION
    if(islip .eq. 1) then
        call def_barslip(phi,phi0_mo,phi0_pd,es_b,fs_b,c0,fs_b0,
+                           rot_slip,rLe,rLsh,bar_ext,bar_slip,U_end)
        def_slip = (H0 - rL_stub) * rot_slip
    endif

    if(def_slip .lt. def_slip_pre) then
        def_slip = def_slip_pre
    else
        def_slip_pre = def_slip
    endif

c     SHEAR DEFLECTION
    if(ishear .eq. 1) then
        def_shear      = 0.
        do i = 1,n_lay+1
            def_shear = def_shear + def_sh(i)
        enddo

        if(def_shear .lt. def_shear_pre) then
            def_shear = def_shear_pre
        else
            def_shear_pre = def_shear
        endif
    endif

c     FLEXURAL DEFLECTION FROM P-DELTA EFFECT
    if(ipd .eq. 1) then
        call def_pdelta(Paxial,H0,mom,phi,n_lay,rL_stub,yphi_pd,
+                           yM_pd,def_mo,def_slip,def_shear)
    endif
    phi0 = yphi_mo(n0) + yphi_pd(n0)

c     ****
c     check convergency and output the results
    def_tip       = def_mo(1) + def_slip + def_shear

    yMb           = yM_mo(n_lay+1)
    yMb           = yMb * 1000.

    if(ipd .eq. 1) then

```

```

        Bshear = (yMb-Paxial*def_tip) / H0
elseif(ipd .eq. 0) then
    Bshear = yMb / H0
endif
if(Bshear_max .lt. Bshear) Bshear_max = Bshear

    if(ipd .eq. 1 .and. abs(def_tip-def_pre) .ge. err_tol
+ .and. itry .lt. 10) then
        def_pre = def_tip
        itry   = itry + 1
        goto 300
    endif

    if(def_tip .ne. def_tip_pre) then
        rK      = (Bshear - Bshear_pre) / (def_tip - def_tip_pre)
    else
        rK      = 10**10
    endif

    if(iK_opt .eq. 1 .and. rK .gt. rK_pre) then
        jtry = jtry + 1
    elseif(phi0 .gt. phi0_pre .and. Bshear .gt. 0) then
        write(8,2000) def_tip,Bshear,def_mo(1),def_slip,def_shear,
+           def_pd(1),c0,yMb/1000,yM_mo(n0),yM_pd(n0),
+           yphi_mo(n0),yphi_pd(n0),real(itry),Lp/h,rL_stub/h,
+           phi0,e_c_tot,ecc,c_tot/h
2000      format(2x,30(f15.4,1x))

c          iteration
        itry             = 1
        jtry             = 1

        Lp_pre            = Lp
        phi0_pre          = phi0
        Bshear_pre        = Bshear
        def_tip_pre       = def_tip
        rot_slip_pre      = rot_slip
        slope_slip_pre    = slope_slip
        rK_pre            = rK
        if(rK .le. 0) iK_opt = 2
    else
        jtry = jtry + 1
    endif

c ****
phi0_mo= phi0_mo + phi_inc
phi_inc = 1.1 * phi_inc
if(phi0 .le. phi_end .and. Bshear .gt. 0 .and. jtry .le. 30) then
    goto 300
endif
print*, "===="
print*,jtry
c ****
c ductility calculation
c calculation of curvature ductility
c calculate phi_p80
rmom80 = r_loss * mom_max

```

```

iopt    = 1
phi_cri= 0.
do i = 1,imax
    if(mom(i) .ge. rmom80) then
        if(mom(i)-mom(i+1) .ne. 0 .and. mom(i+1) .gt. 0) then
            phi80  = (phi(i)-phi(i+1))/(mom(i)-mom(i+1)) *
+                      (rmom80-mom(i+1)) + phi(i+1)
        else
            phi80  = phi(i)
        endif
    endif
enddo

if(phi80 .gt. phi_end)      phi80 = phi_end
if(phi80 .lt. 0)             phi80 = phi_end
curv_duct = phi80/phi_y

c ****
c calculation of displacement ductility
c calculate disp_p80
c read lateral load-displacement data
print*
print*, "Calculation of Ductility factors"
rewind(8)
do i = 1,500
    load(i)      = 0.
    disp(i)       = 0.
    phi_tot(i)   = 0.
enddo

i      = 1
rload_max     = 0.
disp_max      = 0.
read(8,*)
read(8,*)
read(8,*)
read(8,*)
read(8,*)
read(8,*)
read(8,*)
read(8,*)
read(8,*)
500  read(8,*,err=600) disp(i),load(i),(temp(j),j=1,8),tmp1,tmp2
phi_tot(i)   = tmp1 + tmp2
if(load(i) .ge. rload_max) then
    rload_max   = load(i)
endif
if(disp(i) .ge. disp_max) then
    disp_max    = disp(i)
endif
if(i.le.500) then
    i = i + 1
    goto 500
endif

600  rload60= r_gain * rload_max
rload80= r_loss * rload_max

```

```

do i = 2,500
    if(load(i) .ge. rload60) then
        if(load(i) .ne. load(i-1)) then
            disp60 = (disp(i)-disp(i-1))/(load(i)-load(i-1)) *
+                               (rload60-load(i-1)) + disp(i-1)
        else
            disp60 = disp(i)
        endif
        exit
    endif
enddo
disp_y = disp60*rload_max/rload60

do i = 1,500
    if(load(i) .ge. rload80) then
        if(load(i) .ne. load(i+1) .and. load(i+1) .gt. 0) then
            disp80 = (disp(i)-disp(i+1))/(load(i)-load(i+1)) *
+                               (rload80-load(i+1)) + disp(i+1)
+           phi80_1=(phi_tot(i)-phi_tot(i+1))/(load(i)-load(i+1))* 
+                               (rload80-load(i+1)) + phi_tot(i+1)
        else
            disp80 = disp(i)
            phi80_1= phi_tot(i)
        endif
        if(phi_tot(i+1) .gt. phi80) exit
    endif
enddo
if(disp80 .gt. disp_max)    disp80 = disp_max
displ_duct      = disp80/disp_y
curv_duct1      = phi80_1/phi_y

print*, "-----"
print*, " curvature ductility = ", curv_duct
print*, " curvature ductility1 = ", curv_duct1
print*, "displacement ductility = ", displ_duct
print*, "-----"
return
end

```

```

subroutine def_moment(mom,phi,n_lay,phi_max,mom_max,EI_lin,phi_y,
+                      n0,rL_stub,yphi_mo,yphi_pd,yM_pd,phi0_mo,phi0_pd,
+                      yM_mo,yM0_max,def_mo,Lp,Lp_pre,phi_cri,
+                      f_core,e_core,c,def_sh,e_c_tot,c_tot)

common /input/ h,b,nc,bc,ys(10),As(10),rAs
common /steel/ Fys,Fus,Es,Esha,e_ha,e_ul,ns,As1,Ds1
common /analysis/ rP0Pn,ipd,islip,ishear,H0,rL_prov
real mom(500),phi(500)
real y(n_lay+1),yM_mo(n_lay+1),yM_pd(n_lay+1)
real yphi_mo(n_lay+1),yphi_pd(n_lay+1)
real def_mo(n_lay),phi0_mo,phi0_pd,yM0_mo,yM0_pd
real H0,Hlayer,Lp,Lp_pre,phi_max,mom_max
real rL_stub
real f_core(500),e_core(500),c(500),def_sh(n_lay+1)

c ****
c stub effect: the hinge region develops at the distance of rL_stub
c                  away from the column base
rL_stub      = 0.25 * h

n0           = n_lay * (H0 - rL_stub) / H0 + 1
phi0_pd     = yphi_pd(n0)
yM0_pd      = yM_pd(n0)

c find yM0_mo at the hinge region (the above stub confined region)
phi0_tot = phi0_mo + phi0_pd
do i = 1,500
    if(phi(i) .ge. phi0_tot) then
        yM0_tot = (mom(i) - mom(i-1)) / (phi(i) - phi(i-1)) *
+                   (phi0_tot - phi(i-1)) + mom(i-1)
        e_c_tot = (e_core(i)-e_core(i-1)) / (phi(i)-phi(i-1)) *
+                   (phi0_tot - phi(i-1)) + e_core(i-1)
        e_c_tot = -1.0 * e_c_tot
        c_tot = (c(i) - c(i-1)) / (phi(i) - phi(i-1)) *
+                   (phi0_tot - phi(i-1)) + c(i-1)
        exit
    endif
enddo

if(yM0_max .lt. yM0_tot) then
    yM0_max= yM0_tot
endif

yM0_mo = yM0_tot

c ****
c assign position of layer from tip and the corresponding moment
Hlayer       = H0/n_lay
y(1)         = 0.
yM_mo(1)    = 0.
do i = 2,n_lay+1
    y(i)     = y(i-1) + Hlayer
    yM_mo(i)= yM0_mo / (H0 - rL_stub) * y(i)
enddo

c ****
c assign curvature to each layer

```

```

c      has to be considered the consumed moment due to the P-delta effect
jstat= 1
do i = 2,n0
    yM_tot = yM_mo(i)
    do j = jstat,500
        if(mom(j) .gt. yM_tot) then
            yphi_tot      = (phi(j)-phi(j-1)) / (mom(j)-mom(j-1)) *
+                               (yM_tot-mom(j-1)) + phi(j-1)
            yphi_mo(i)    = yphi_tot + yphi_pd(i)
+
c      assign shear deformation to each layer
        f_c      = (f_core(j)-f_core(j-1)) / (mom(j)-mom(j-1)) *
+
+                               (yM_tot-mom(j-1)) + f_core(j-1)
+
+                               e_c      = (e_core(j)-e_core(j-1)) / (mom(j)-mom(j-1)) *
+
+                               (yM_tot-mom(j-1)) + e_core(j-1)
+
+                               c_c      = (c(j)-c(j-1)) / (mom(j)-mom(j-1)) *
+
+                               (yM_tot-mom(j-1)) + c(j-1)
+
+                               Ecsec   = f_c / e_c
+                               Geff    = Ecsec / (2*1.3)
+                               Aeff    = b * c_c
+                               V       = yM0_tot * 10**6 / H0
+                               def_sh(i)=V * Hlayer / (Geff * Aeff)
+
+                               jstat   = j - 1
+                               goto 100
+
+                               endif
+
+                               enddo
100    continue
+                               enddo
+
c      strengthened region due to stub effect
do i = n0+1,n_lay+1
    yphi_mo(i) = yM_mo(i) / EI_lin
enddo
+
c      ****
c      plastic hinge behavior
tmp = (0.3*rP0Pn + rAs - 0.06)
if(tmp .lt. 0) tmp = 0.
Lp_full= tmp*H0 + 0.25*h
if(Lp_full .lt. 0.25*h) Lp_full = 0.25*h
+
Lp = 0.
curv_duc     = phi0_tot / phi_y
+
if(curv_duc .gt. 1)  then
    Lp      = Lp_full
elseif(H0/h .le. 4 .and. c_c .lt. h) then
    Lp      = (ys(ns)-ys(1))
endif
if(Lp .lt. Lp_pre)  Lp      = Lp_pre
+
y_p = H0 - (Lp + rL_stub)
do i = 1, n_lay+1
    if(y(i) .ge. y_p) exit
enddo
i_p    = i

```

```

c      put the plastic hinge over the length of Lp
c      from the distance of rL_stub away from the column stub
if(Lp .gt. 0) then
    do i = n0,i_p,-1
        yphi_mo(i) = phi0_mo + phi0_pd
    enddo
endif

c ****
c calculate the deflection of a column
do i = 1,n_lay
    def_mo(i) = 0.
    do j = i,n_lay+1
        def_mo(i) = def_mo(i) +
+           ( yphi_mo(j) * (y(j) - y(i)) +
+           yphi_mo(j+1) * (y(j+1) - y(i)) ) /2. *
+           Hlayer / (10**6)
    enddo
enddo

return
end

```

```

      subroutine def_barslip(phi,phi0_mo,phi0_pd,es_b,fs_b,c0,fs_b0,
+                                rot_slip,rLe,rLsh,bar_ext,bar_slip,U_end)
c   ASSUMPTION: BAR SLIP DOES NOT OCCUR. Only bar extension is considered.
c   that is, rLe + rLsh < rLbar, provided
c   common /input/ h,b,nc,bc,ys(10),As(10),rAs
c   common /concrete/ fcu,Ec,nc,hlayer,ec0un,ec85un,ec50un
c   common /steel/ Fys,Fus,Es,Esha,e_ha,e_ul,ns,As1,Ds1
c   common /analysis/ rP0Pn,ipd,islip,ishhear,H0,rL_prov
c   real phi(500),es_b(500),fs_b(500)

c   ****
c   find M0 at the base
do i = 1,500
    phi0_tot = phi0_mo + phi0_pd
    if(phi(i) .ge. phi0_tot) then
        if(phi(i) .ne. phi(i-1)) then
            fs_b0 = (fs_b(i)-fs_b(i-1)) / (phi(i)-phi(i-1)) *
+                               (phi0_tot-phi(i-1)) + fs_b(i-1)
+            es_b0 = (es_b(i)-es_b(i-1)) / (phi(i)-phi(i-1)) *
+                               (phi0_tot-phi(i-1)) + es_b(i-1)
        else
            fs_b0 = (fs_b(i)+fs_b(i-1))/2.
            es_b0 = (es_b(i)+es_b(i-1))/2.
        endif
        exit
    endif
enddo
IF(es_b0 .gt. e_ul/4) RETURN

if(fs_b0 .lt. 0) then
    bar_ext      = 0.
    bar_slip     = 0.
    rot_slip     = 0.
    return
endif

c   ****
c   Bar stress distribution
c   elastic region
rLd      = 440.* As1 * Fys / (3.* Ds1 * sqrt(fcu) * 400)
if(rLd .lt. 300) rLd = 300.
Ue       = Fys * Ds1 / (4. * rLd)
if(fs_b0 .lt. Fys) then
    rLe      = fs_b0 * Ds1 / (4.* Ue)
else
    rLe      = Fys * Ds1 / (4.* Ue)
endif

c   yield plateau
Uf       = 5.* sqrt(fcu/27.6)
rLyi     = 0.
if(fs_b0 .gt. Fys .and. fs_b0 .lt. 1.01*Fys) then
    rLyi = (fs_b0 - Fys) * Ds1 / (4.* Uf)
elseif(fs_b0 .gt. 1.01*Fys) then
    rLyi = (0.01* Fys) * Ds1 / (4.* Uf)
endif

c   strain hardening region

```

```

rLsh = 0
if(fs_b0 .gt. 1.01*Fys) rLsh = (fs_b0 - Fys) * Ds1 / (4.* Uf)

c ****
c BAR SLIP
c Bar Slippage
rLe_prov = rL_prov - (rLy_i + rLsh)
if(rLe_prov .ge. rLe) then
    U_end = 0.
else
    if(fs_b0 .lt. Fys) then
        U_end = (fs_b0 * Ds1) / (4.* rLe_prov)
    else
        U_end = (Fys * Ds1) / (4.* rLe_prov)
    endif
endif
U_u = (20 - Ds1 / 4.) * sqrt(fcu/30.)
delta_1 = sqrt(30./fcu)
bar_slip = delta_1 * (U_end/U_u)**2.5

if(U_end .ge. U_u) then
    print*, ****
    print*, "ERROR MESSAGE"
    print*, "Bar slippage is larger than considered in the program"
    print*, ****
    stop
endif
c Bar Extension
if(Bar_slip .ne. 0) rLe = rLe_prov
if(fs_b0 .le. Fys) then
    e_s = fs_b0 / Es
    ext_el = 0.5 * e_s * rLe
    ext_yi = 0.
    ext_sh = 0.
elseif(fs_b0 .le. 1.01*Fys) then
    e_yi = Fys / Es
    ext_el = 0.5 * e_yi * rLe
    ext_yi = 0.5 * (e_s + e_yi) * rLy_i
    ext_sh = 0.
else
    e_yi = Fys / Es
    ext_el = 0.5 * e_yi * rLe
    ext_yi = 0.5 * (e_s + e_yi) * rLy_i
    ext_sh = 0.5 * (e_s + e_yi) * rLsh
endif

bar_ext = ext_el + ext_yi + ext_sh
ext_non = ext_yi + ext_sh

c ****
c tip deflection
if(c0 .ge. h-ys(1)) then
    rot_slip = 0.
else
    rot_slip = (bar_ext + bar_slip) / (ys(ns) - c0 )
endif
return
end

```

```

      subroutine def_pdelta(Paxial,H0,mom,phi,n_lay,rL_stub,yphi_pd,
+                                yM_pd,def_mo,def_slip,def_shear)
      parameter (err_tol=0.001)
      real mom(500),phi(500)
      real y(n_lay+1),yM_pd(n_lay+1),yphi_pd(n_lay+1)
      real def_mo(n_lay),def_slip
      real H0,Hlayer

      ****
      C assign the position of layer from base and the corresponding moment
      C due to P-delta effect
      Hlayer = H0/n_lay
      y(1) = 0.
      yM_pd(1)= 0.
      def_tip= def_mo(1) + def_slip + def_shear
      do i = 2,n_lay+1
          y(i) = y(i-1) + Hlayer
          def_slip_i = def_slip *
+            ( (H0-rL_stub-y(i)) / (H0-rL_stub) )
          if(def_slip_i .lt. 0) then def_slip_i = 0.
          def_shear_i = def_shear *
+            ( (H0-y(i)) / H0 )
          def_lay= def_mo(i) + def_slip_i + def_shear_i
          yM_pd(i)= Paxial * (def_tip-def_lay) / 1000.
      enddo

      ****
      C assign the curvature to each layer
      jstat = 1
      do i = 2,n_lay+1
          do j = jstat,500
              if(mom(j) .ge. yM_pd(i)) then
                  if(mom(j) .ne. mom(j-1)) then
                      yphi_pd(i) = (phi(j)-phi(j-1))/(mom(j)-mom(j-1)) *
+                        (yM_pd(i)-mom(j-1)) + phi(j-1)
                  else
                      yphi_pd(i) = phi(j-1)
                  endif
                  jstat = j-1
                  goto 200
              endif
          enddo
      200  continue
      1000 format(1x,i4,10f15.4)
      enddo

      return
      end

```

```

subroutine Conc_Collins_un
common /concrete/ fcu,Ec,nc,hlayer,ec0un,ec85un,ec50un
real n,k

c      unit: ksi, inch
c ****
c      use Collins HSC Model for ec0 and ec50u
n          = 0.8 + fcu*1000/2500.
k          = 0.67 + fcu*1000/9000.
if(k.lt.1.) k = 1.
ec0          = fcu/Ec*n/ (n-1)
ec0un  = ec0
etemp  = ec0
idex   = 0
50      dum          = etemp/ec0
Fratio = n*dum/(n-1+dum** (n*k))
if(idex .eq. 0 .and. Fratio .gt. 0.85) then
    etemp0 = etemp
    Fratio0= Fratio
    etemp  = etemp + 0.00001
    goto 50
elseif(idex .eq. 0) then
    ec85un = (etemp-etemp0)/(Fratio-Fratio0)*(.85-Fratio0)+etemp0
    idex   = 1
endif
if(idex .eq. 1 .and. Fratio .gt. 0.5) then
    etemp0 = etemp
    Fratio0= Fratio
    etemp  = etemp + 0.00001
    goto 50
elseif(idex .eq. 1) then
    ec50un = (etemp-etemp0)/(Fratio-Fratio0)*(0.5-Fratio0)+etemp0
endif
c ****
return
end

```

```

c      Scott, Park and Priestley (1982)
subroutine Conc_Park(e_c,fc)
common /input/ h,b,hc,bc,ys(10),As(10),rAs
common /concrete/ fcu,Ec,nc,hlayer,ec0un,ec85un,ec50un
common /steel/ Fys,Fus,Es,Esha,e_ha,e_ul,ns,As1,Ds1
common /steel_2/ Fy_h,E_h,A_h,D_h,s_h,nh,rNo_h(10),Deg_h(10)
real*8 e_c(1),fc(1)
real K

hc_outer = ys(ns)-ys(1)+Ds1+2*D_h
bc_outer = b-2*ys(1)+Ds1+2*D_h

C      TENSILE STRENGTH OF CONCRETE
fcr = 7.5*sqrt(fcu*1000)/1000

C      COMPRESSIVE STRENGTH OF CONCRETE
Vshx = 0.
Vshy = 0.
do i = 1,nh
    Vshx = Vshx + A_h*rNo_h(i) * sind(90-Deg_h(i))*bc
    Vshy = Vshy + A_h*rNo_h(i) * sind(Deg_h(i))*hc
enddo
Vsh = Vshx + Vshy
ROUs = Vsh/(s_h*hc_outer*bc_outer)

K = 1+ROUs*Fys/fcu
ec0 = 0.002*K

e_50u = (3+0.002*fcu*1000)/(fcu*1000-1000)
e_50h = 3/4.*ROUs*sqrt(bc_outer/s_h)
Zm = 0.5/(e_50u+e_50h-ec0)

c ****
do 100 i = 1,1
    fc(i) = 0.
    if(e_c(i).le.0) then
        if(e_c(i).gt.-ec0) then
            fc(i) = -K*fcu*( 2* (-e_c(i))/ec0-(-e_c(i))/ec0)**2 )
        else
            fc(i) = -K*fcu*( 1-Zm* ( (-e_c(i))-ec0) )
            if(fc(i).gt.-0.2*K*fcu) fc(i) = -0.2*K*fcu
        endif
    elseif(e_c(i).gt.0) then
c      CONCRETE TENSION INCLUDED -> CRACKS ARE INTRODUCED
        fc(i) = Ec*e_c(i)
        if(fc(i).gt.fcr) fc(i) = 0.
    endif
100  continue
c ****
return
end

```

```

c      SHEIKH AND UZUMERI (1982)
subroutine Conc_ShUz(e_c,fc,c_neutral)
common /input/ h,b,hc,bc,ys(10),As(10),rAs
common /concrete/ fcu,Ec,nc,hlayer,ec0un,ec85un,ec50un
common /steel/ Fys,Fus,Es,Esha,e_ha,e_ul,ns,As1,Ds1
common /steel_2/ Fy_h,E_h,A_h,D_h,s_h,nh,rNo_h(10),Deg_h(10)
real*8 e_c(1),fc(1)
real Ks,ROU

c_neutral=10**5
C_Sheikh      = (ys(ns)-ys(1))/(ns-1)

c      TENSILE STRENGTH OF CONCRETE
fcr      = 7.5*sqrt(fcu*1000)/1000

c      COMPRESSIVE STRENGTH OF CONCRETE
ec0      = ec0un
fcp      = 1.0*fcu

Vshx    = 0.
Vshy    = 0.
do I    = 1,nh
      Vshx = Vshx + A_h*rNo_h(i) * sind(90-Deg_h(i))*bc
      Vshy = Vshy + A_h*rNo_h(i) * sind(Deg_h(i))*hc
enddo
Vsh    = Vshx + Vshy
ROU   = Vsh/(s_h*hc*bc)

Asall  = 0.
do 100 i = 1,ns
      Asall = Asall+As(i)
100    continue

Pocc    = fcp*(hc*bc-Asall)
Ks      = 1.0 + 2.73*bc**2/Pocc *
+      ( (1-4*(ns-1)*C_Sheikh**2/(5.5*bc**2))*(1-s_h/(2*bc))**2 ) *
+      sqrt(ROU*Fy_h)
fcc    = Ks*fcp

es1    = 0.55*Ks*(fcu*1000)*10**(-6.)
if(c_neutral.ge.10**5) then
      es2 = 1 + ( 0.81/C_Sheikh*(1-5*(s_h/bc)**2) ) *
+      ROU*Fy_h*1000/sqrt(fcu*1000)
elseif(c_neutral.eq.0) then
      es2 = 10**5
else
      es2 = 1 + ( 0.81/C_Sheikh*(1-5*(s_h/bc)**2) +
+      0.25*sqrt(bc/c_neutral) ) * ROU*Fy_h*1000/sqrt(fcu*1000)
endif
es2 = es2*ec0
if(es1.gt.es2) es2 = es1

es85 = 0.225*ROU*sqrt(bc/s_h)+es2

c ****
do 200 i = 1,1
      fc(i) = 0.
      if(e_c(i).le.0) then

```

```

e_temp = -e_c(i)
if(e_temp.le.es1) then
    fc(i) = fcc * (2*(e_temp/es1)-(e_temp/es1)**2)
elseif(e_temp.gt.es1 .and. e_temp.le.es2) then
    fc(i) = fcc
elseif(e_temp.gt.es2) then
    fc(i) = fcc - (0.15*fcc)/(es85-es2)*(e_temp-es2)
    if(fc(i).lt.0.3*fcc) fc(i) = 0.3*fcc
endif
fc(i) = -fc(i)
elseif(e_c(i).gt.0) then
c      CONCRETE TENSION INCLUDED -> CRACKS ARE INTRODUCED
    fc(i) = Ec*e_c(i)
    if(fc(i).gt.fcr) fc(i) = 0.
endif
200  continue
c      ****
return
end

```

```

c      Mander, Priestley, and Park (1988)
c      subroutine Conc_Mander(e_c,fc)
c      common /input/ h,b,hc,bc,ys(10),As(10)
c      common /concrete/ fcu,Ec,nc,hlayer,ec0un,ec85un,ec50un
c      common /steel/ Fys,Fus,Es,Esha,e_ha,e_ul,ns,As1,Ds1
c      common /steel_2/ Fy_h,E_h,A_h,D_h,s_h,nh,rNo_h(10),Deg_h(10)
c      real*8 e_c(1),fc(1)
c      real ROU_cc,ke

c      TENSILE STRENGTH OF CONCRETE
c      fcr = 7.5*sqrt(fcu*1000)/1000

c      transform units into MPa and mm
c      call UnitTo_MPamm(0,0,0,0)
c      fcr = fcr/0.1450377

c      COMPRESSIVE STRENGTH OF CONCRETE
c      Asall = 0.
c      do i = 1,ns
c          Asall = Asall+As(i)
c      enddo
c      ROU_cc = Asall/(bc*hc)

c      ASSUME that every bars are restrained
c      wx_cl = (bc-Ds1-D_h) / (As(1)/As1) - Ds1
c      wy_cl = (ys(ns)-ys(1)) / (ns-1) - Ds1
c      s_cl = s_h-D_h

c      Ke =
c      + ( 1-( 2*(ns-1)*wy_cl**2 + 2*(As(1)/As1-1)*wx_cl**2 )/(6*bc*hc) )
c      + * (1-s_cl/(2*bc)) * (1-s_cl/(2*hc)) / (1-ROU_cc)

c      Ashx = 0.
c      Ashy = 0.
c      do i = 1,nh
c          Ashx = Ashx + A_h*rNo_h(i)*sind(90-Deg_h(i))
c          Ashy = Ashy + A_h*rNo_h(i)*sind(Deg_h(i))
c      enddo
c      lateral confining stress in y-direction
c      fl_y = Ashy/(s_h*bc)*Fy_h

c      fl_eff = fl_y*ke
c      VALID for equal confinement pressure for both directions
c      otherwise, chart tool shall be used for flx_eff/fcu and fly_eff/fcu
c      fcc = fcu*(-1.254+2.254*sqrt(1+7.94*fl_eff/fcu)-2*fl_eff/fcu)

c      ec0 = 0.002
c      ecc = ec0*(1+5*(fcc/fcu-1))

c      ****
c      do 200 i = 1,1
c          fc(i) = 0.
c          if(e_c(i).le.0) then
c              e_temp = -e_c(i)
c              temp = e_temp/ecc
c              Esec = fcc/ecc
c              r = Ec/(Ec-Esec)
c              fc(i) = fcc*temp*r/(r-1+temp**r)

```

```

        fc(i) = -fc(i)
c      elseif(e_c(i).gt.0) then
      CONCRETE TENSION INCLUDED -> CRACKS ARE INTRODUCED
          fc(i) = Ec*e_c(i)
              if(fc(i).gt.fcr) fc(i) = 0.
          endif
c      transform units into ksi; UnitTo_kipin does not have for fc(i)
          fc(i) = fc(i)*0.1450377
200    continue
c      ****
c      transform units into kip and in
call UnitTo_kipin(0,0,0,0)

      return
      end

```

```

c      Saatcioglu and Razi (1999)
subroutine Conc_Saatcioglu99(e_c,fc)
common /input/ h,b,hc,bc,ys(10),As(10),rAs
common /concrete/ fcu,Ec,nc,hlayer,ec0un,ec85un,ec50un
common /steel/ Fys,Fus,Es,Esha,e_ha,e_ul,ns,As1,Ds1
common /steel_2/ Fy_h,E_h,A_h,D_h,s_h,nh,rNo_h(10),Deg_h(10)
real*8 e_c(1),fc(1)
real ROU,k1,k2,kx2,ky2,k3,k4,K_Saatcio

c      TENSILE STRENGTH OF CONCRETE
fcr = 7.5*sqrt(fcu*1000)/1000
*****use Collins HSC Model for ec01 and ec085*****
c      use Collins HSC Model for ec01 and ec085
ec01 = ec0un
ec085 = ec85un
*****transform units into MPa and mm
call UnitTo_MPamm(0,0,0,0)
fcr=fcr/0.1450377

c      COMPRESSIVE STRENGTH OF CONCRETE
sx_1 = (bc-Ds1-D_h) / (As(1)/As1)
sy_1 = (ys(ns)-ys(1)) / (ns-1)

kx2 = 0.15*sqrt(bc**2/(s_h*sy_1))
if(kx2.gt.1.) kx2 = 1.
ky2 = 0.15*sqrt(hc**2/(s_h*sx_1))
if(ky2.gt.1.) ky2 = 1.
k2 = (kx2+ky2)/2.

fs_h = Fy_h

150   flx = 0.
fly = 0.
Ashx = 0.
Ashy = 0.
do i = 1,nh
    flx = flx + rNo_h(i)*A_h*fs_h*sind(90-Deg_h(i)) / (s_h*hc)
    fly = fly + rNo_h(i)*A_h*fs_h*sind(Deg_h(i)) / (s_h*bc)
    Ashx = Ashx + A_h*rNo_h(i)*sind(90-Deg_h(i))
    Ashy = Ashy + A_h*rNo_h(i)*sind(Deg_h(i))
enddo
Ash = Ashx+Ashy

c      ROU is NOT a volumetric ratio of ties
ROU = Ash/(s_h*(bc+hc))

flx_equi = kx2*flx
fly_equi = ky2*fly
fl_equi = (flx_equi*bc + fly_equi*hc) / (bc+hc)

k1=6.7*(fl_equi)**(-0.17)
fcc=fcu+k1*fl_equi

K_Saatcio=(k1*fl_equi)/fcu
k3=40./fcu
if(k3.gt.1) k3=1.

```

```

k4=Fy_h/500.
if(k4.lt.1) k4=1.

ec1 = ec01 * 6 * (fcc/fcu-0.83)
ec85 = 260*k3*ROU*ec1*(1+0.5*k2*(k4-1))+ec085
fs_h1= (ec1/2.)*k2 *E_h
if(fs_h1.gt.fy_h) fs_h1 = fy_h
if(abs(fs_h1-fs_h).gt.10**(-0.3)) then
    fs_h = fs_h1
    goto 150
endif

c ****
do 200 i=1,1
    fc(i)=0.
    if(e_c(i).le.0) then
        e_temp=-e_c(i)
        if(e_temp.le.ec1) then
            temp=e_temp/ec1
            Esec=fcc/ec1
            r=Ec/(Ec-Esec)
            fc(i)=fcc*temp*r/(r-1+temp**r)
        else
            fc(i)=fcc * (1-0.15/(ec85-ec1)*(e_temp-ec1))
            if(fc(i).lt.0.2*fcc) fc(i) = 0.2*fcc
        endif
        fc(i)=-fc(i)
    elseif(e_c(i).gt.0) then
c CONCRETE TENSION INCLUDED -> CRACKS ARE INTRODUCED
        fc(i)=Ec*e_c(i)
        if(fc(i).gt.fcr) fc(i)=0.
    endif
c transform units into ksi
    fc(i)=fc(i)*0.1450377
200 continue
c ****
c transform units into kip and in
call UnitTo_kipin(0,0,0,0)

return
end

```

```

c      Cusson and Paultre (1995)
c      subroutine Conc_Paultre97(e_c,fc)
c      common /input/ h,b,hc,bc,ys(10),As(10),rAs
c      common /concrete/ fcu,Ec,nc,hlayer,ec0un,ec85un,ec50un
c      common /steel/ Fys,Fus,Es,Esha,e_ha,e_ul,ns,As1,Ds1
c      common /steel_2/ Fy_h,E_h,A_h,D_h,s_h,nh,rNo_h(10),Deg_h(10)
c      real*8 e_c(1),fc(1)
c      real ROUc,Ke,k1,k2,kapa,kusai,kusai_cri,n

c      TENSILE STRENGTH OF CONCRETE
fcr = 7.5*sqrt(fcu*1000)/1000
c      ****
c      use Collins HSC Model for ec0
ec0          = ec0un
eC50U     = ec50un
c      ****

c      transform units into MPa and mm
call UnitTo_MPamm(0,0,0,0)
fcr = fcr/0.1450377

c      COMPRESSIVE STRENGTH OF CONCRETE
Asall = 0.
do 100 i = 1,ns
    Asall = Asall+As(i)
100 continue
ROUc = Asall/(bc*hc)
wx_cl = (bc-Ds1-D_h) / (As(1)/As1-1) - Ds1
wy_cl = (ys(ns)-ys(1)) / (ns-1) - Ds1
s_cl = s_h-D_h

Ke           =
+ ( 1 - 2*((As(1)/As1-1)*wx_cl**2 + (ns-1)*wy_cl**2)/(6*bc*hc) )
+ * ( 1 - s_cl/(2*bc) ) * ( 1 - s_cl/(2*hc) ) / (1-ROUc)

c      estimate the stress in the transverse steel
Ashx = 0.
Ashy = 0.
do i = 1,nh
    Ashx = Ashx + A_h*rNo_h(i)*sind(90-Deg_h(i))
    Ashy = Ashy + A_h*rNo_h(i)*sind(Deg_h(i))
    Vshx = Vshx + A_h*rNo_h(i) * sind(90-Deg_h(i))*bc
    Vshy = Vshy + A_h*rNo_h(i) * sind(Deg_h(i))*hc
enddo
Vsh = Vshx + Vshy
ROUs = Vsh/(s_h*hc*bc)
kapa = 2. / (ROUs*Ke)
kusai = kapa*fcu/Es - 0.01
kusai_cri = 0.528*sqrt(ec0)
if(kusai.lt.kusai_cri) then
    fhcc = fy_h
else
    temp1 = 0.5*Es*ec0
    temp2 = 3.225*kapa*fcu * ( kusai-sqrt(kusai**2-kusai_cri**2) )
    if(temp1.ge.temp2) then
        temp=temp1
    else
        temp=temp2

```

```

        endif
        if(fy_h.le.temp) then
            fhcc=fy_h
        else
            fhcc=temp
        endif
    endif

c      lateral confining stress
fl = fhcc/s_h * (Ashx+Ashy) / (bc+hc)
fl_eff = fl*Ke
fcc = fcu*( 1+2.353*(fl_eff/fcu)**0.7 )

ecc = ec0+0.277*(fl_eff/fcu)**1.7
eC50C = eC50U+0.15*(fl_eff/fcu)**1.1

ehcc = 0.5*ecc*(1-fl_eff/fcc)

c ****
do 200 i=1,1
    fc(i) = 0.
    if(e_c(i).le.0) then
        e_temp = -e_c(i)
        if(e_temp.le.ecc) then
            temp = e_temp/ecc
            Esec = fcc/ecc
            r = Ec/(Ec-Esec)
            fc(i) = fcc*temp*r/(r-1+temp**r)
        else
            k2 = 0.58+16*(fl_eff/fcu)**1.4
            k1 = log(0.5)/(eC50C-ecc)**k2
            fc(i) = fcc * exp(k1*(e_temp-ecc)**k2)
        endif
        fc(i) = -fc(i)
    elseif(e_c(i).gt.0) then
c      CONCRETE TENSION INCLUDED -> CRACKS ARE INTRODUCED
        fc(i) = Ec*e_c(i)
        if(fc(i).gt.fcr) fc(i) = 0.
    endif
c      transform units into ksi
        fc(i) = fc(i)*0.1450377
200  continue
c ****

c      transform units into kip and in
call UnitTo_kipin(0,0,0,0)

return
end

```

```

c      steel model: Strain Hardening Effect included
subroutine Steel_Hardening(e_s,fs)
common /steel/ Fys,Fus,Es,Esha,e_ha,e_ul,ns,As1,Ds1
common /steel_2/ Fy_h,E_h,A_h,D_h,s_h,nh,rNo_h(10),Deg_h(10)
      common /index/ ictype,ispall,ispall2,i2sD,irev,ibuc,irup,ibur
real*8 e_s(1),fs(1)
irup = 0

es_y = Fys/Es
p = Esha*(e_ul-e_ha) / (Fus-Fys)

do 100 i = 1,1
c   for compression curve
      temp = e_s(i)
      e_s(i) = dabs(e_s(i))
      fs(i) = Es*e_s(i)
      if((e_s(i) .gt. es_y) .and. (e_s(i) .le. e_ha)) then
          fs(i) = Fys + 0.01*Fys * (e_s(i) - es_y) / (e_ha - es_y)
c   STRAIN HARDENING
      elseif((e_s(i).gt.e_ha) .and. (e_s(i).lt.e_ul)) then
          fs(i) = Fus+(1.01*Fys-Fus)*((e_ul-e_s(i))/(e_ul-e_ha))**p
          if(fs(i).gt.Fus) fs(i) = Fus
      elseif(e_s(i).gt.e_ul) then
c   RUPTURE
          fs(i) = fus
          irup = 1
      endif
      if(e_s(i)*temp.lt.0) then
          e_s(i) = temp
          fs(i) = -fs(i)
      endif
100    continue

      return
end

```

```

subroutine Steel_Buckling(strain,stress)
real*8 strain,stress,rstrain,rstress
common /index/ ictype,ispall,ispall2,i2sD,irev,ibuc,irup,ibur
real dataStrain(50),dataStress(50)

c transfer a strain into a relative strain based on the yielding strain
rstrain = -strain

if(i2sD.lt.2) then
    open(12,file="CurveBuckling.out")
else
    open(12,file="CurveBuckling1.out")
endif
do 100 i = 1,50
    dataStrain(i) = 0.
    dataStress(i) = 0.
100 continue

read(12,*)
read(12,*) SD
read(12,*)
read(12,*)
temp1=-1.
temp2=-1.
do i=1,50
    read(12,*,err=999) dataStrain(i),dataStress(i)
    if(dataStrain(i).lt.temp1) then
        dataStrain(i)=temp1
        dataStress(i)=temp2
    else
        temp1=dataStrain(i)
        temp2=dataStress(i)
    endif
enddo
999 close(12)

do 500 i = 1,50
    if(rstrain.ge.datastrain(i)) iSTN0 = i
    if(rstrain.le.datastrain(i)) then
        iSTN1 = i
        goto 600
    endif
500 continue
600 if(iSTN0.ne.iSTN1) then
    if(datastrain(iSTN1)-datastrain(iSTN0).ne.0) then
        rstress = ( datastress(iSTN1)-datastress(iSTN0) ) /
+           ( datastrain(iSTN1)-datastrain(iSTN0) ) *
+           ( rstrain-datastrain(iSTN0) ) + datastress(iSTN0)
    else
        rstress = ( datastress(iSTN1)-datastress(iSTN0) ) / 2.
    endif
else
    rstress = datastress(iSTN0)
endif
stress = -rstress

return
end

```

```

subroutine Curve_Buckling(fs_max)
common /steel/ Fys,Fus,Es,Esha,e_ha,e_ul,ns,As1,Ds1
common /steel_2/ Fy_h,E_h,A_h,D_h,s_h,nh,rNo_h(10),Deg_h(10)

open(10,file="CurveBuckling.out")

sD      = s_h/Ds1
fs_max = 0.

        write(10,1000)
1000   format(1x,"           s/D",
+                  "           Ds1",
+                  "           s,hoop"  )
        write(10,3000) sD,Ds1,s_h
        write(10,*)
        write(10,2000)
2000   format(1x,"     strain_tot",
+                  "     stress",
+                  "     dis_lateral",
+                  "     stress"  )
        stress_buckle = Fys
        strain_buckle = stress_buckle / Es
        strain_inc    = strain_buckle / 2

c      strain_tot < strain_buckle
        strain_mat    = 0.
100    call Buckling_Material(strain_mat,stress)
        strain_tot    = strain_mat
        write(10,3000) strain_tot,stress
3000   format(1x,10e20.10)
        strain_mat    = strain_mat+strain_inc
        if(strain_mat.le.strain_buckle) goto 100

c      buckling initiates
        dis_lateral   = 0.
        dis_inc       = 0.05
200    stress0      = stress
        strain0       = strain_mat
        call Buckling_Geometry(dis_lateral,strain_geo,stress,sD)
        call Buckling_Material2(stress,strain_mat,stress0,strain0)
        strain_tot    = strain_mat + strain_geo
        if(strain_tot .gt. strain_tot_pre) then
            write(10,3000) strain_tot,stress,dis_lateral,stress
        endif
        strain_tot_pre= strain_tot

        dis_lateral   = dis_lateral + dis_inc
        if(abs(stress) .gt. fs_max) fs_max = abs(stress)
        if(dis_lateral.le.3 .and. stress.gt.0) goto 200

        close(10)
        return
end

```

```

subroutine Curve_Buckling1
common /steel/ Fys,Fus,Es,Esha,e_ha,e_ul,ns,As1,Ds1
common /steel_2/ Fy_h,E_h,A_h,D_h,s_h,nh,rNo_h(10),Deg_h(10)

open(10,file="CurveBuckling1.out")

call Buckling_Space(sD)

      write(10,1000)
1000  format(1x,"           s/D",
+                  "           Ds1",
+                  "           s,hoop"  )
      write(10,3000) sD,Ds1,s_h
      write(10,*)
      write(10,2000)
2000  format(1x,"     strain_tot",
+                  "     stress",
+                  "     dis_lateral",
+                  "     stress"  )
      stress_buckle=Fys
      strain_buckle=stress_buckle/Es
      strain_inc=strain_buckle/2

c      strain_tot < strain_buckle
      strain_mat=0.
100   call Buckling_Material(strain_mat,stress)
      strain_tot=strain_mat
      write(10,3000) strain_tot,stress
3000  format(1x,10e20.10)
      strain_mat=strain_mat+strain_inc
      if(strain_mat.le.strain_buckle) goto 100

c      buckling initiates
      dis_lateral=0.
      dis_inc=0.05
200   stress0=stress
      strain0=strain_mat
      call Buckling_Geometry(dis_lateral,strain_geo,stress,sD)
      call Buckling_Material2(stress,strain_mat,stress0,strain0)
      strain_tot=strain_mat+strain_geo
      write(10,3000) strain_tot,stress,dis_lateral,stress

      dis_lateral=dis_lateral+dis_inc
      if(dis_lateral.le.3 .and. stress.gt.0) goto 200

      close(10)
      return
      end

```

```

subroutine Buckling_Geometry(dis_lateral,strain_geo,stress,sD)
common /steel/ Fys,Fus,Es,Esha,e_ha,e_ul,ns,As1,Ds1
common /steel_2/ Fy_h,E_h,A_h,D_h,s_h,nh,rNo_h(10),Deg_h(10)
real L,k
L      = s_h

c   Relation between dis_lateral & axial force
k      = Fus/Fys

a      = 4*(k-1)**2 - 5
y04   = -0.45 * k**1.5 * (log(sD) - log(4.)) + k
if(y04 .gt. k) y04 = k
x1    = 0.04
y1    = y04
b     = y1 - a * 0.04

y2    = y1/1.5
x2    = (y2 - b)/a
a2    = a/2
b2    = y2 - a2*x2

x=dis_lateral/s_h
if(x.le.x1) then
    if(y1.gt.1) then
        stress = Fys * ( 1 + (y1-1) * sqrt(1-(x/x1-1)**2) )
    else
        stress = Fys * ( (y1-1)/x1*x + 1 )
    endif
elseif(x.gt.x1 .and. x.le.x2) then
    stress      = Fys * ( a*x + b )
elseif(x.gt.x2) then
    stress      = Fys * ( a2*x + b2 )
endif
if(stress .lt. 0.2*Fys) stress = 0.2*Fys

c   Relation between dis_lateral & mean axial strain
rot=6.9/sD**2-0.05
strain_geo   = (0.035*cos(rot)+rot)/(cos(rot)-0.035*rot) *
+ (dis_lateral/Ds1)
if(dis_lateral/Ds1*cos(rot).gt.1+strain_geo*rot) then
    strain_geo   = 1/(cos(rot)-0.07*rot) *
+ ( (0.07*cos(rot)+rot) * (dis_lateral/Ds1) - 0.035 )
    strain_geo   = abs(strain_geo)
endif

return
end

```

```

subroutine Buckling_Material(e_s,f_s)
common /steel/ Fys,Fus,Es,Esha,e_ha,e_ul,ns,As1,Ds1

e_y = Fys/Es
*****  

c      the following statements are NOT necessary
c      p = Esha*(e_ul-e_ha)/(Fus-Fys)
c      f_s = Es*e_s
c      if((e_s.gt.e_y) .and. (e_s.le.e_ha)) then
c          f_s = Fys
c      elseif((e_s.gt.e_ha) .and. (e_s.lt.e_ul)) then
c          f_s = Fus+(Fys-Fus)*((e_ul-e_s)/(e_ul-e_ha))**p
c          if(f_s.gt.Fus) f_s = Fus
c      endif
c *****

      return
      end

```

```

      subroutine Buckling_Material2(f_s,e_s,f_s0,e_s0)
c      stress input and strain output
c      common /steel/ Fys,Fus,Es,Esha,e_ha,e_ul,ns,As1,Ds1
      real e_s,f_s

      if(f_s.gt.1.05*Fus) then
      print*, "Error Code 1:Bar stress is higher than its ultime strength"
      stop
      endif

      e_y     = Fys/Es
      p       = Esha*(e_ul-e_ha)/(Fus-Fys)

      if(f_s .le. f_s0) then
      de_s    = (f_s-f_s0)/Es
      e_s     = e_s0+de_s
      istat   = -1
      else
      if(f_s .eq. Fys) e_s1 = e_ha
      if(f_s .gt. Fys .and. f_s .lt. Fus) then
      e_s1   = e_ha - 0.0001
      e_s1   = e_s1 + 0.0001
      100    f_trial = Fus+(Fys-Fus)*((e_ul-e_s1)/(e_ul-e_ha))**p
      if(f_trial.lt.f_s) goto 100
      else
      e_s     = e_ul*1.5
      endif
      if(istat .eq. 1) then
      e_s     = e_s1
      else
      de_s    = (f_s-f_s0)/Es
      e_s2   = e_s0+de_s
      if(e_s1 .gt. e_s2) then
      e_s     = e_s1
      istat = 1
      else
      e_s     = e_s2
      endif
      endif
      endif

      return
      end

```



# APPENDIX D

## ANALYTICAL METHOD TO ESTIMATE COLUMN BEHAVIOR: EXAMPLE

### D.1 INTRODUCTION

To illustrate the analytical method presented in Chapter 7, the details of the procedure to estimate concrete column behavior are provided. For this purpose, the lateral load-displacement relationship of specimen S24-2UT is estimated using the analytical method described in Chapter 7.

### D.2 SECTIONAL ANALYSIS

First step to generate the lateral load-displacement behavior of concrete columns is to obtain a moment-curvature relationship through sectional analysis. The details of specimen S24-2UT can be found in Figure B.2. Various constitutive models are used in this sectional analysis. The confined and unconfined concrete models proposed by Razvi and Saatcioglu (1999), the strain hardening model proposed by Mander et al. (1984), and the bar buckling model developed in this research (Chapter 6) are used. The use of these constitutive models in sectional analysis is illustrated in Figure D.1. The resulting stress-strain relationships for concrete and longitudinal reinforcement are illustrated in Figures D.2 and D.3, respectively. Figure D.4 shows the analytical estimation obtained for the moment-curvature relationship of specimen S24-2UT.

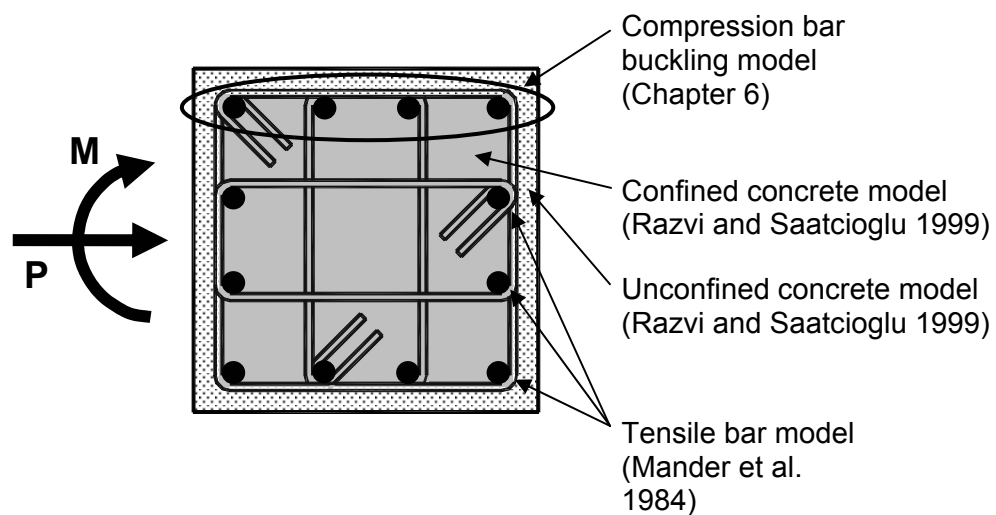


**Figure D.1 Constitutive Models used for Sectional Analysis**

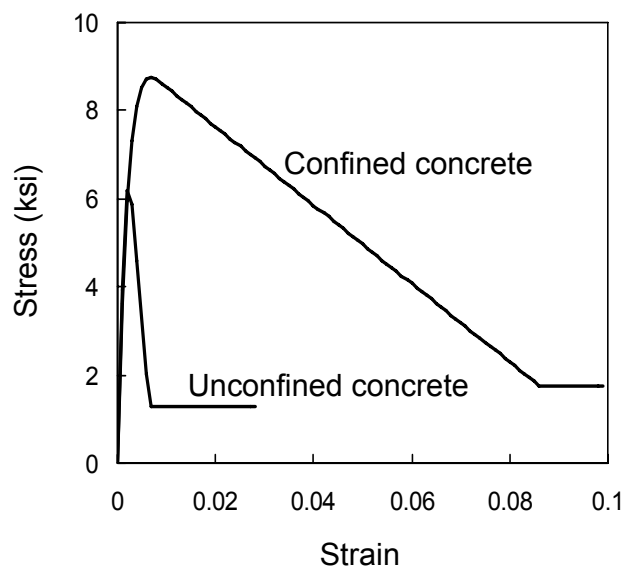


**Figure D.2 Concrete Stress-Strain Relationships (Razvi and Saatcioglu 1999)**

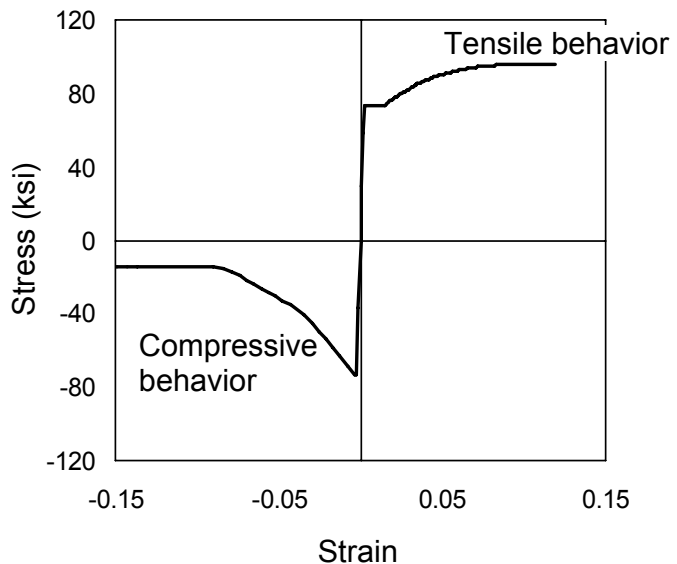


**Figure D.3 Stress-Strain Relationship for Longitudinal Reinforcement**

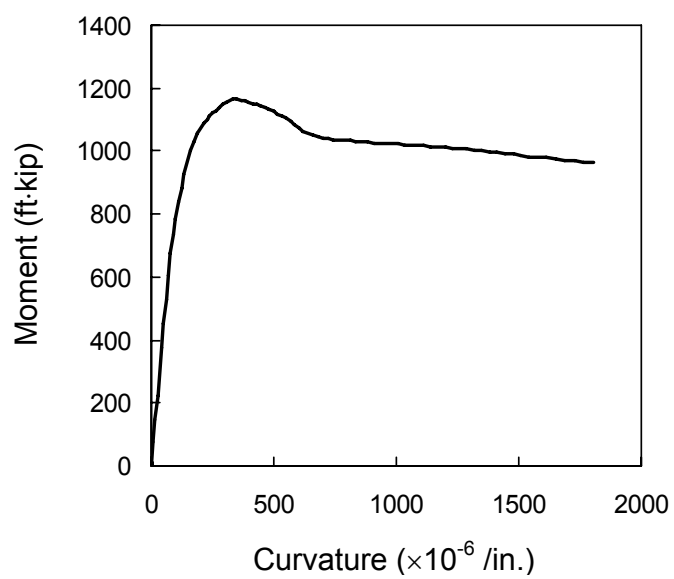


**Figure D.4 Moment-Curvature Relationship of Specimen S24-2UT**

### D.3 ANALYSIS OF MEMBER BEHAVIOR

Combining the moment-curvature relationship with the estimated plastic hinge length ( $l_p = 0.74h$ ), the flexural deformations of specimen S24-2UT can be estimated. Deformations stemming from reinforcing bar slip, shear and secondary moments have to be calculated to obtain the tip deflection of a cantilever concrete column. Since the deformations due to the secondary moments depend on the deflected shape of a column, iteration is required to get the total deformation (Figure 7.3). Lateral load corresponding to a given tip displacement can be obtained through the use of the following expression.

$$V = \frac{M_{base} - P \cdot \Delta}{L}$$

The estimated lateral load-displacement relationship for specimen S24-2UT is shown in Figure D.5.

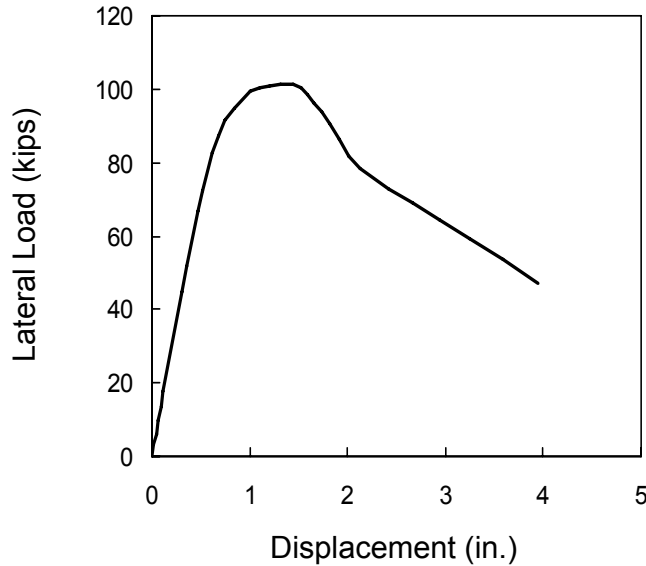


**Figure D.5 Lateral Load-Displacement Relationship of Specimen S24-2UT**

## APPENDIX E

### ESTIMATION OF DRIFT CAPACITY: EXAMPLE

#### E.1 APPLICATION OF EQUATION (7.27)

To illustrate the use of Equation (7.27), the drift capacity of a first story interior column (C1) in a typical 6-story reinforced concrete frame is estimated (Figure E.1). The factored column axial load can be estimated by considering the following load combinations:

- $1.2D + 0.5L$
- $1.2D + 0.5L + E$
- $0.9D + E$

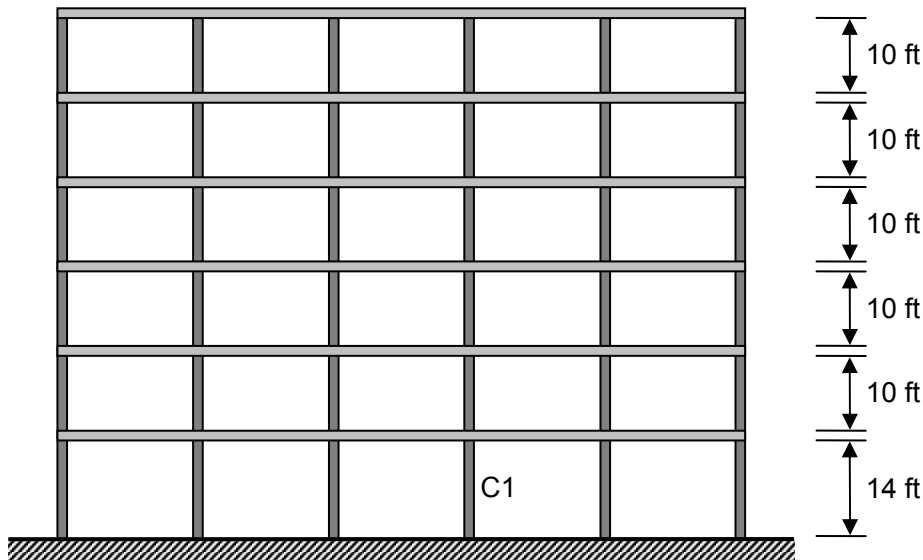


*Figure E.1 Configuration of Example Building*

Table E.1 contains an assumed maximum factored axial load for the interior column (C1) from load combinations where seismic forces and gravity loads are considered. The details of this interior column are provided in Figure E.2. Based on the details of this column, a  $P$ - $M$  interaction diagram for this column is constructed (Figure E.3). From the  $P$ - $M$  interaction curve, the nominal moment capacity corresponding to the given axial load can be obtained, which is 890 ft·kip in this case. Using this axial load and moment capacity values and the distance from zero moment to maximum moment, which is 7 ft ( $= 14/2$ ), the drift capacity of this column can be estimated using Equation (7.27).

$$\delta = 20 \times \frac{890 \text{ ft} \cdot \text{kip}}{900 \text{ kip}} \times \frac{1}{7 \text{ ft}} = 2.8\%$$

Alternatively, the drift capacity can be also estimated from the drift capacity-axial load curve, as shown in Figure E.4.

**Table E.1 Factored Axial Load for Column C1**

Column	Factored Axial Force (kips)
C1	900

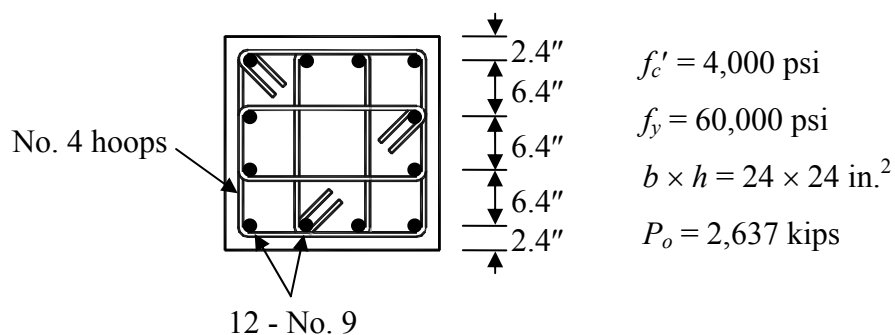


**Figure E.2 Column Details**

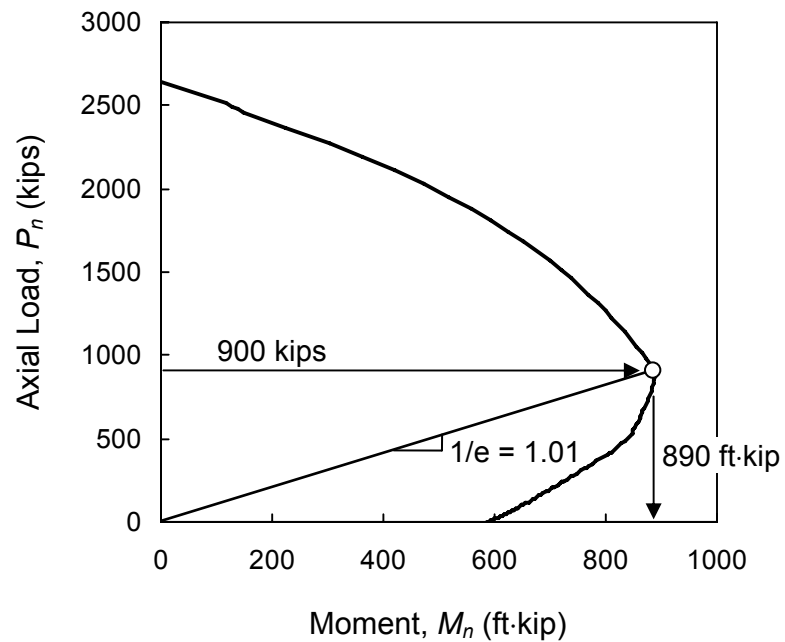


**Figure E.3 P-M Interaction Curve**

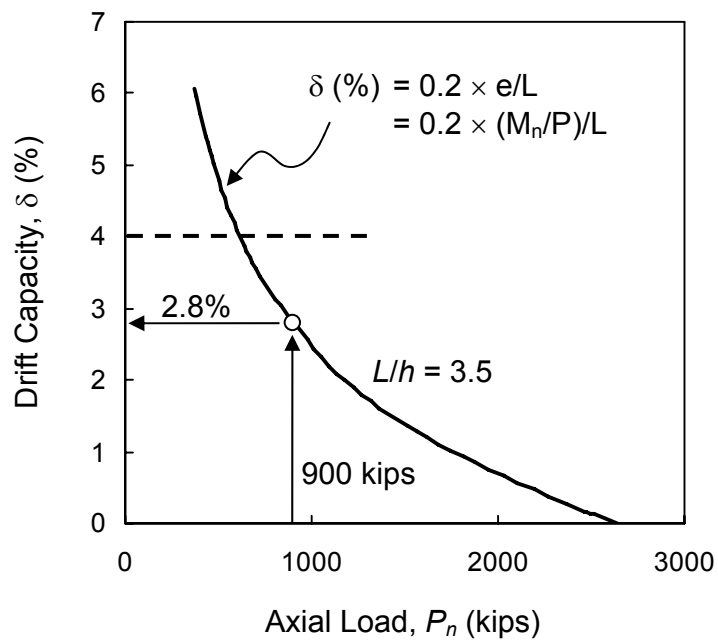


**Figure E.4 Drift Capacity-Axial Load Curve**

## **REFERENCES**

1. AASHTO (1995) "Standard Specifications for Highway Bridges, 16th Edition," American Association of State Highway and Transportation Officials.
2. ACI Committee 105 (1933) "Reinforced Concrete Column Investigation - Tentative Final Report," Journal of The American Concrete Institute, V. 29, No. 6, Feb., pp. 275-282.
3. ACI Committee 318 (1971) "Building Code Requirements for Reinforced Concrete (ACI 318-71)," American Concrete Institute, Detroit, Michigan, 78 pp.
4. ACI Committee 318 (1977) "Building Code Requirements for Reinforced Concrete (ACI 318-77)," American Concrete Institute, Detroit, Michigan, 103 pp.
5. ACI Committee 318 (1983) "Building Code Requirements for Reinforced Concrete (ACI 318-83)," American Concrete Institute, Detroit, Michigan, 102 pp.
6. ACI Committee 318 (1989) "Building Code Requirements for Reinforced Concrete and Commentary (ACI 318-89/ACI 318R-89)," American Concrete Institute, Detroit, Michigan, 351 pp.
7. ACI Committee 318 (2005) "Building Code Requirements for Reinforced Concrete and Commentary (ACI 318-05/ACI 318R-05)," American Concrete Institute, Detroit, Michigan, 423 pp.
8. ACI Innovation Task Group 1 (2001) "Acceptance Criteria for Moment Frames Based on Structural Testing and Commentary," ACI ITG/T1.1-01, Manual of Concrete Practice, 10 pp.
9. ACI-ASCE Committee 428 (1968) "Progress Report on Code Clauses for Limit Design," Journal of The American Concrete Institute, V. 65, No. 9, Sep., pp. 713-715.

10. Alsiwat, J.M. and Saatcioglu, M. (1992) "Reinforcement Anchorage Slip under Monotonic Loading," *Journal of Structural Engineering, ASCE*, V. 118, No. 9, Sep., pp. 2421-2438.
11. American Association of State Highway and Transportation Officials (1977) "Standard Specifications for Highway Bridges," Washington, D.C.
12. Ang, B.G., Priestley, M.J.N. and Park, R. (1981) "Ductility of Reinforced Concrete Bridge Piers under Seismic Loading," Research Report 81-3, Department of Civil Engineering, University of Canterbury, Christchurch, New Zealand, Feb., 109 pp.
13. Applied Technology Council. (1996) "Improved Seismic Design Criteria for California Bridges: Provisional Recommendations," ATC-32, Redwood City, California, 215 pp.
14. ASTM International (2003) "Standard Test Method for Compressive Strength of Cylindrical Concrete Specimens," ASTM C 39C/C 39M, 7 pp.
15. ASTM International (2003) "Standard Test Methods and Definitions for Mechanical Testing of Steel Products," ASTM A 370-03a, 49 pp.
16. Atalay, M.B. and Penzien, J. (1975) "The Seismic Behavior of Critical Regions of Reinforced Concrete Components as Influenced by Moment, Shear and Axial Force," Report No. EERC 75-19, University of California, Berkeley, Dec., 226 pp.
17. Azizinamini, A., Corley, W.G., and Johal, L.S. (1992) "Effects of Transverse Reinforcement on Seismic Performance of Columns," *ACI Structural Journal*, V. 89, No. 4, July-Aug., pp. 442-450.
18. Bae, S. and Bayrak, O. (2003) "Early Cover Spalling in High-Strength Concrete Columns," *Journal of Structural Engineering, ASCE*, V. 129, No. 3, Mar., pp. 314-323.
19. Bae, S. and Bayrak, O. (2003) "Stress Block Parameters for High-Strength Concrete Members," *ACI Structural Journal*, V. 100, No. 5, Sep.-Oct., pp. 626-636.
20. Baker, A.L.L. (1956) "Ultimate Load Theory Applied to the Design of Reinforced and Prestressed Concrete Frames," Concrete Publications Ltd., London.

21. Baker, A.L.L. and Amarakone, A.M.N. (1964) "Inelastic Hyperstatic Frame Analysis," Proceedings International Symposium on the Flexural Mechanics of Reinforced Concrete, ACI SP-12, Miami, pp. 85-142.
22. Bayrak, O. (1995) "High-Strength Concrete Columns subjected to Earthquake Type Loading," M.A.Sc. Thesis, Department of Civil Engineering, University of Toronto, Toronto, Ontario, 239 pp.
23. Bayrak, O. (1999) "Seismic Performance of Rectilinearly Confined High Strength Concrete Columns," Ph.D. dissertation, University of Toronto, Ontario, Canada, 339 pp.
24. Bayrak, O. and Sheikh, S.A. (1997) "High-Strength Concrete Columns under Simulated Earthquake Loading," ACI Structural Journal, V. 94, No. 6, Nov.-Dec., pp. 708-722.
25. Bayrak, O. and Sheikh, S.A. (1998) "Confinement Reinforcement Design Considerations for Ductile HSC Columns," Journal of Structural Engineering, ASCE, V. 124, No. 9, Sep., pp. 999-1010.
26. Bayrak, O. and Sheikh, S.A. (2001) "Plastic Hinge Analysis," Journal of Structural Engineering, ASCE, V. 127, No. 9, Sep., pp. 1092-1100.
27. Bresler, B. and Gilbert, P.H. (1961) "Tie Requirements for Reinforced Concrete Columns," Journal of The American Concrete Institute, V. 58, No. 5, Nov., pp. 555-570.
28. Caltrans (1986) "Bridge Design Specifications Manual," California Department of Transportation.
29. Chan, W.W.L. (1955) "The Ultimate Strength and Deformation of Hinges in Reinforced Concrete Frameworks," Magazine of Concrete Research, V. 7, No. 21, pp. 121-132.
30. Corley, W.G. (1966) "Rotational Capacity of Reinforced Concrete Beams," Journal of the Structural Division, ASCE, V. 92, No. ST5, Oct., pp. 121-146.
31. Cusson, D. and Paultre, P. (1995) "Stress-Strain Model for Confined High-Strength Concrete," Journal of Structural Engineering, ASCE, V. 121, No. 3, Mar., pp. 468-477.

32. Dhakal, R.P. and Maekawa, K. (2002) "Reinforcement Stability and Fracture of Cover Concrete in Reinforced Concrete Members," *Journal of Structural Engineering*, ASCE, V. 128, No. 10, Oct., pp. 1253-1262.
33. Ehsani, M.R. and Wight, J.K. (1990) "Confinement Steel Requirements for Connections in Ductile Frames," *Journal of Structural Engineering*, ASCE, V. 116, No. 3, Mar., pp. 751-767.
34. Federal Emergency Management Agency (2000) "Prestandard and Commentary for the Seismic Rehabilitation of Buildings," FEMA 356, Washington, DC.
35. Galeota, D., Giannatto, M.M. and Marino, R. (1996) "Seismic Resistance of High Strength Concrete Columns," Eleventh World Conference on Earthquake Engineering, Acapulco, Mexico, Disc 3, Paper No. 1390.
36. International Code Council (ICC) (2003) "International Building Code," Falls Church, VA.
37. International Conference of Building Officials (ICBO) (1997) "Uniform Building Code," Whittier, CA.
38. Kanda, M., Shirai, N., Adachi, H., and Sato, T. (1988) "Analytical Study on Elasto-Plastic Hysteretic Behaviors of Reinforced Concrete Members," *Transactions of the Japan Concrete Institute*, V. 10, pp. 257-264.
39. Kent, D.C. and Park R. (1971) "Flexural Members with Confined Concrete," *Journal of the Structural Division*, ASCE, V. 97, No. ST7, July, pp. 1969-1990.
40. Légeron, F. and Paultre, P. (2000) "Behavior of High-Strength Concrete Columns under Cyclic Flexure and Constant Axial Load," *ACI Structural Journal*, V. 97, No. 4, July-Aug., pp. 591-601.
41. Légeron, F. and Paultre, P. (2003) "Uniaxial Confinement Model for Normal- and High-Strength Concrete Columns," *Journal of Structural Engineering*, ASCE, V. 129, No. 2, Feb., pp. 241-252.
42. Lehman, D.E. and Moehle, J.P. (2000) "Seismic Performance of Well-Confining Concrete Bridge Columns," PEER Report 1998-01, College of Engineering, University of California, Berkeley, Dec., 286 pp.

43. Li, B. Park, R. and Tanaka, H. (1993) "Strength and Ductility of Reinforced Concrete Members and Frames Constructed using High Strength Concrete," Research Report 94-5, Department of Civil Engineering, University of Canterbury, Christchurch, New Zealand, May, 373 pp.
44. Mander, J.B., Priestley, M.J.N. and Park, R. (1984) "Seismic Design of Bridge Piers," Research Report 84-2, Department of Civil Engineering, University of Canterbury, Christchurch, New Zealand, Feb., 483 pp.
45. Mander, J.B., Priestley, M.J.N. and Park, R. (1988) "Theoretical Stress-Strain Model for Confined Concrete," Journal of Structural Engineering, ASCE, V. 114, No. 8, Aug., pp. 1804-1826.
46. Matamoros, A.B. and Sozen, M.A. (2003) "Drift Limits of High-Strength Concrete Columns subjected to Load Reversals," Journal of Structural Engineering, ASCE, V. 129, No. 3, Mar., pp. 297-313.
47. Mattock, A.H. (1964) "Rotational Capacity of Hinging Regions in Reinforced Concrete Beams," Proceedings International Symposium on the Flexural Mechanics of Reinforced Concrete, ACI SP-12, Miami, pp. 143-181.
48. Mattock, A.H. (1967) Discussion of "Rotational Capacity of Hinging Regions in Reinforced Concrete Beams," by Corley, W.G., Journal of the Structural Division, ASCE, V. 93, No. ST2, Apr., pp. 519-522.
49. Mau, S.T. (1990) "Effect of Tie Spacing on Inelastic Buckling of Reinforcing Bars," ACI Structural Journal, V. 87, No. 6, Nov.-Dec., pp. 671-677.
50. Mau, S.T. and El-Mabsout, M. (1989) "Inelastic Buckling of Reinforcing Bars," Journal of Engineering Mechanics, ASCE, V. 115, No. 1, Jan., pp. 1-17.
51. Mendis, P. (2001) "Plastic Hinge Lengths of Normal and High-Strength Concrete in Flexure," Advances in Structural Engineering, V. 4, No. 4, Oct., pp. 189-195.
52. Mieses, A.M. (2002) "Inelastic Buckling Behavior of Concrete Reinforcing Bars under Monotonic Uniaxial Compressive Loading," M.S. thesis, The University of Texas at Austin, 236 pp.
53. Mitchell, D. and Paultre, P. (1994) "Ductility and Overstrength in Seismic Design of Reinforced Concrete Structures," Canadian Journal of Civil Engineering, V. 21, No. 6, Dec., pp. 1049-1060.

54. Mo, Y.L. and Wang, S.J. (2000) "Seismic Behavior of RC Columns with Various Tie Configurations," *Journal of Structural Engineering*, ASCE, V. 126, No. 10, Oct., pp. 1122-1130.
55. Monti, G. and Nuti, C. (1992) "Nonlinear Cyclic Behavior of Reinforcing Bars Including Buckling," *Journal of Structural Engineering*, ASCE, V. 118, No. 12, Dec., pp. 3268-3284.
56. Muguruma, H., Watanabe, F. and Komuro, T. (1989) "Applicability of High Strength Concrete to Reinforced Concrete Ductile Column," *Transactions of the Japan Concrete Institute*, V. 11, pp. 309-316.
57. Ohno, T. and Nishioka, T. (1984) "An Experimental Study on Energy Absorption Capacity of Columns in Reinforced Concrete Structures," *Proceedings of the JSCE*, V. 1, No. 2, Oct., pp. 137-147.
58. Ozcebe, G. and Saatcioglu, M. (1987) "Confinement of Concrete Columns for Seismic Loading," *ACI Structural Journal*, V. 84, No. 4, July-Aug., pp. 308-315.
59. Papia, M. and Russo, G. (1989) "Compressive Concrete Strain at Buckling of Longitudinal Reinforcement," *Journal of Structural Engineering*, ASCE, V. 115, No. 2, Feb., pp. 382-397.
60. Papia, M., Russo, G. and Zingone, G. (1988) "Instability of Longitudinal Bars in RC Columns," *Journal of Structural Engineering*, ASCE, V. 114, No. 2, Feb., pp. 445-461.
61. Park, R and Leslie, P.D. (1977) "Curvature Ductility of Circular Reinforced Concrete Columns Confined by the ACI Sprial," *6<sup>th</sup> Australasian Conference on the Mechanics of Structures and Materials*, V. 1, Christchurch, New Zealand, Aug., pp. 342-349.
62. Park, R and Sampson, R.A. (1972) "Ductility of Reinforced Concrete Column Sections in Seismic Design," *Journal of American Concrete Institute, Proceedings* V. 69, No. 9, Sep., pp. 543-555.
63. Park, R. and Paulay, T. (1975) "Reinforced Concrete Structures," John Wiley and Sons, New York, 769 pp.
64. Park, R., Priestley, M.J.N. and Gill, W.D. (1982) "Ductility of Square-Confining Concrete Columns," *Journal of Structural Division*, ASCE, V. 108, No. ST4, Apr., pp. 929-950.

65. Paulay, T. and Priestley, M.J.N. (1992) "Seismic Design of Reinforced Concrete and Masonry Buildings," John Wiley and Sons, New York, 767 pp.
66. Paultre, P., Légeron, F. and Mongeau, D. (2001) "Influence of Concrete Strength and Transverse Reinforcement Yield Strength on Behavior of High-Strength Concrete Columns," ACI Structural Journal, V. 98, No. 4, July-Aug., pp. 490-501.
67. Popovics, S. (1973) "Numerical Approach to the Complete Stress-Strain Curve of Concrete," Cement and Concrete Research, V. 3, No. 5, Sep., pp583-599.
68. Priestley, M.J.N. and Park, R. (1987) "Strength and Ductility of Concrete Bridge Columns under Seismic Loading," ACI Structural Journal, V. 84, No. 1, Jan.-Feb., pp. 61-76.
69. Razvi, S. and Saatcioglu, M. (1999) "Confinement Model for High-Strength Concrete," Journal of Structural Engineering, ASCE, V. 125, No. 3, Mar., pp. 281-288.
70. Richart, F.E., Brandtzaeg, A. and Brown R.L. (1928) "A Study of the Failure of Concrete under Combined Compressive Stresses," Bulletin 185, University of Illinois Engineering Experimental Station, Urbana, Illinois, 104 pp.
71. Richart, F.E., Brandtzaeg, A. and Brown R.L. (1929) "Failure of Plain and Spirally Reinforced Concrete in Compression," Bulletin 190, University of Illinois Engineering Experimental Station, Urbana, Illinois, 74 pp.
72. Saatcioglu, M. and Grira, M. (1999) "Confinement of Reinforced Concrete Columns with Welded Reinforcement Grids," ACI Structural Journal, V. 96, No. 1, Jan.-Feb., pp. 29-39.
73. Saatcioglu, M. and Ozcebe, G.(1989) "Response of Reinforced Concrete Columns to Simulated Seismic Loading," ACI Structural Journal, V. 86, No. 1, Jan.-Feb., pp. 3-12.
74. Saatcioglu, M. and Razvi, S.R. (1992) "Strength and Ductility of Confined Concrete," Journal of Structural Engineering, ASCE, V. 118, No. 6, June, pp. 1590-1607.
75. Saatcioglu, M. and Razvi, S.R. (2002) "Displacement-Based Design of Reinforced Concrete Columns for Confinement," ACI Structural Journal, V. 99, No. 1, Jan.-Feb., pp. 3-11.

76. Saatcioglu, M., Salamat, A.H. and Razvi, S.R. (1995) "Confined Columns under Eccentric Loading," *Journal of Structural Engineering, ASCE*, V. 121, No. 11, Nov., pp. 1547-1556.
77. Sakai, K. and Sheikh, S.A. (1989) "What Do We Know about Confinement in Reinforced Concrete Columns? (A Critical Review of Previous Work and Code Provisions)," *ACI Structural Journal*, V. 86, No. 2, Mar.-Apr., pp. 192-207.
78. Sakai, Y., Hibi, J., Otani, S., and Aoyama, H. (1990) "Experimental Study on Flexural Behavior of Reinforced Concrete Columns Using High-Strength Concrete," *Transactions of the Japan Concrete Institute*, V. 12, pp. 323-330.
79. Scott, B.D., Park, R., and Priestley, M.J.N. (1982) "Stress-Strain Behavior of Concrete Confined by Overlapping Hoops at Low And High Strain Rates," *Journal of The American Concrete Institute*, V. 79, No. 1, Jan.-Feb., pp. 13-27
80. Scribner, C.F. (1986) "Reinforcement Buckling in Reinforced Concrete Flexural Members," *Journal of The American Concrete Institute*, V. 83, No. 6, Nov.-Dec., pp. 966-973.
81. Sheikh, S.A. and Khoury, S.S. (1993) "Confined Concrete Columns with Stubs," *ACI Structural Journal*, V. 90, No. 4, July-Aug., pp. 414-431.
82. Sheikh, S.A. and Khoury, S.S. (1997) "Performance-Based Approach for the Design of Confining Steel in Tied Columns," *ACI Structural Journal*, V. 94, No. 4, July-Aug., pp. 421-431.
83. Sheikh, S.A. and Uzumeri, S.M. (1982) "Analytical Model for Concrete Confinement in Tied Columns," *Journal of the Structural Division, ASCE*, V. 108, No. ST12, Dec., pp. 2703-2722.
84. Sheikh, S.A. and Yeh, C.C. (1992) "Analytical Moment-Curvature Relations for Tied Concrete Columns," *Journal of Structural Engineering, ASCE*, V. 118, No. 2, Feb., pp. 529-544.
85. Sheikh, S.A., Shah, D.V. and Khoury, S.S. (1994) "Confinement of High-Strength Concrete Columns," *ACI Structural Journal*, V. 91, No. 1, Jan.-Feb., pp. 100-111.
86. Soesianawati, M.T., Park, R. and Priestley, M.J.N. (1986) "Limited Ductility Design of Reinforced Concrete Columns," *Research Report 86-10*,

Department of Civil Engineering, University of Canterbury, Christchurch, New Zealand, Mar., 208 pp.

87. Standards Association of New Zealand. (1978) "Draft Code of Practice for the Design of Concrete Structures," DZ 3101, Wellington, New Zealand.
88. Standards Association of New Zealand. (1982) "New Zealand Standard Code of Practice for the Design of Concrete Structures," NZS 3101, Wellington, New Zealand.
89. Standards Association of New Zealand. (1995) "New Zealand Standard Code of Practice for the Design of Concrete Structures," NZS 3101, Wellington, New Zealand, 256 pp.
90. Sugano, S. (1996) "Seismic Behavior of Reinforced Concrete Columns which used Ultra-High-Strength Concrete," Eleventh World Conference on Earthquake Engineering, Acapulco, Mexico, Paper No. 1383.
91. Tanaka, H. and Park, R. (1990) "Effect of Lateral Confining Reinforcement on the Ductile Behavior of Reinforced Concrete Columns," Research Report 90-2, Department of Civil Engineering, University of Canterbury, Christchurch, New Zealand, June, 458 pp.
92. Thomsen, J. and Wallace, J. (1994) "Lateral Load Behavior of Reinforced Concrete Columns Constructed Using High-Strength Materials," ACI Structural Journal, Vol. 91, No. 5, Sep.-Oct., pp. 605-615.
93. Watson, S. and Park, R. (1989) "Design of Reinforced Concrete Frames of Limited Ductility," Research Report 89-04, Department of Civil Engineering, University of Canterbury, Christchurch, New Zealand, Jan., 232 pp.
94. Watson, S. and Park, R. (1994) "Simulated Seismic Load Tests on Reinforced Concrete Columns," Journal of Structural Engineering, ASCE, V. 120, No. 6, June, pp. 1825-1849.
95. Watson, S., Zahn, F.A. and Park, R. (1994) "Confining Reinforcement for Concrete Columns," Journal of Structural Engineering, ASCE, V. 120, No. 6, June, pp. 1798-1824.
96. Wehbe, N.I., Saiidi, M.S. and Sanders, D.H. (1997) "Effects of Confinement and Flares on the Seismic Performance of Reinforced Concrete Bridge Columns," Report No. CCEER-97-2, Engineering Research and Development Center, University of Nevada, Reno, Sep., 399 pp.

97. Xiao, Y. and Martirossyan, A. (1998) "Seismic Performance of High-Strength Concrete Columns," Journal of Structural Engineering, ASCE, Mar., pp. 241-251.
98. Yalcin, C. and Saatcioglu, M. (2000) "Inelastic Analysis of Reinforced Concrete Columns," Computers & Structures, V. 77, No. 5, July, pp. 539-555.
99. Zahn, F.A., Park, R. and Priestley, M.J.N. (1986) "Design of Reinforced Concrete Bridge Columns for Strength and Ductility," Research Report 86-7, Department of Civil Engineering, University of Canterbury, Christchurch, New Zealand, Mar., 330 pp.

## **Vita**

Sungjin Bae was born on January 14, 1973 in Masan, Korea, the son of Sangsul Bae and Kyoungsoon Lee. He attended Kyungsang High School in Masan, Korea and graduated in December 1990. After high school he enrolled in Hanyang University, Seoul, Korea and received Bachelor of Science degree in December 1997. He entered the Master's program at Hanyang University, Seoul, Korea in August 1998. After completing his Master's degree, he entered the Ph.D. program at The University of Texas at Austin in August 2000.

Permanent address: 16-5 Hoiwondong, Masan, Korea 630-040

This dissertation was typed by the author.